ОБЪЕДИНЕННЫЙ ИНСТИТУТ ЯДЕРНЫХ ИССЛЕДОВАНИЙ

Лаборатория высоких энергий

Эль-Наги
Ахмед Ахмед

УДК 539.I72.6/8
539.I7I.0I7
539.I2

ВЗАИМОДЕЙСТВИЕ П-МЕЗОНОВ, ПРОТОНОВ, ЯДЕР И НЕЙТРИНО С ЯДРАМИ ФОТОЭМУЛЬСИИ ПРИ ВЫСОКОЙ ЭНЕРГИИ

Специальность: 0I.04.I6 - физика ядра и элементарных частиц

Диссертация на соискание ученой степени доктора физико-математических наук

Дубна, I993 г.

ВВЕДЕНИЕ

Актуальность работы. Исследование адрон-нуклонного (hN), адрон-ядерного (hA), ядро-ядерного (AA) и нейтрино-ядерного (νA) взаимодействий важно для понимания природы процесса взаимодействия.

Множественное рождение частиц в hA столкновениях при высоких энергиях может послужить чувствительным тестом механизма множественного рождения в hN столкновениях. Можно использовать ядро, как анализатор пространственно-временной структуры процесса множественного рождения и провести разделение между различными теоретическими моделями элементарного акта. Изучение hA столкновений дает возможность также исследовать механизмы возбуждения ядра и дезинтеграции (фрагментации).

Преобладающий интерес при исследовании AA столкновений в области высоких энергий представляет поиск новых явлений или состояний, которые не могут иметь место в hN или в hA реакциях. Например, состояния со столь высокими плотностью вещества, давлением и температурой, что они не могут быть достигнуты в отдельных NN столкновениях. Из квантовой хромодинамики следует, что при температуре выше критической, около 250 МэВ, ядерная материя реализуется в форме кварк-глюонной плазмы с плотностью энергии $\epsilon \geq 1 - 3$ ГэВ/ФМ^3. Такие условия могут быть достигнуты в центральных AA столкновениях при высокой энергии.

Изучение множественности, углового и энергетического распределений и корреляций между ними в AA столкновениях прояснят ситуацию при отсутствии реалистичной картины взаимодействия. Такое исследование, к примеру, позволить сделать выбор между "когерентной" моделью, в которой множественное рождение происходит через промежуточный этап, и "некогерентной", когда рождение частиц и их материализация происходят внутри ядра-мишени.

Много теоретических моделей посвящено изучению процесса мультифрагментации. В некоторых моделях фрагментирующее ядро испытывает превращения через стадию теплового равновесия, в других эта стадия не рассматривается, фрагментирующее ядро раскаливается на части. Изучение фрагментации налетающего ядра в АА соударении помогает решить эту проблему.

Исследование угловых и энергетических фрагментов обоих сталкивающихся ядер дает возможность зарегистрировать эффект "бокового потока" ядерного вещества.

Изучение νA взаимодействий представляет адэкватный способ иследования пространственно-временных характеристик процесса множественного рождения частиц.

Принимая во внимание вышеизложенное, можно заключить, что выполненные в диссертации работы являются весьма актуальными.

Цель работы:

- исследование hN, hA, AA и νA взаимодействий для изучения природы множественного рождения; исследование фрагментации ядра-снаряда для нахождения механизма процесса фрагментации; опробование возможности образования кварк-глюонной плазмы; обнаружение и изучение характеристик коллективного "бокового потока" ядерной материи; оценка времени формирования при исследовании νA взаимодействий.

В диссертации автор защищает

1. Измерение характеристик вторичных частиц, испущенных при взаимодействии 50 ГэВ/с π^--мезонов и 69 ГэВ/с протонов с ядрами фотоэмульсии.

2. Исследование свойств и особенностей ядро-ядро взаимодействий при импульсе 4.5 АГэВ/с, исследование фрагментации ядер Ne^{22}, Mg^{24}, Si^{28},

наблюдение боковых потоков ядерной материи при столкновении ядер с ядрами фотоэмульсии, наблюдение адронного черенковского излучения.

3. Исследование взаимодействий нейтрино в фотоэмульсии, анализ с помощью двух вариантов каскадной модели, определение времени формирования адронов.

Научная новизна и практическая ценность работы состоит в том, что она содержит разнообразные точные и статистически надежные результаты по hA, AA, νN и νA взаимодействиям. Анализ этих результатов - хороший способ понять механизм ядерных взаимодействий при высокой энергии, в частности пространственно-временную эволюцию взаимодействия.

Изучение νA взаимодействия предствляет одно из самых ранних исследований в этой области. Это первые эмульсионные эксперименты, в которых проводилось экспонирование в FNAL пучком нейтрино с энергией 300 -400 ГэВ. Анализ данных позволил определить с достаточной точностью время формиривания адронов. Этот подход был применен к hA и AA взаимодействиям и таким образом сложилась единая широкомасштабная работа по вопросам времени формирования.

Изучение процесса мультифрагментации без всяких сомнений потверждает, что теоретические модели, использующие одну промежуточную возбужденную ядерную систему при определенной температуре противоречат эксперименту. Это результат очень важен при критической оценке моделей.

Результаты изучения фрагментации ядер оказываются полезны в применении к физике космических лучей при исследовании состава космических лучей и их каскада в атмосфере.

При исследовании эффекта бокового потока ядерного вещества в столкновениях ядер впервые обращено внимание на существование

дополнительных методических возможностей связанных с определением плоскости реакции столкновения. Показано, что боковые эффекты сильнее выражены в плоскости реакции. Сам факт наблюдения эффекта бокового потока побуждает думать, что аналогичный эффект должен иметь место вообще при столкновении макросистем, имеющих какую-либо микроструктуру.

При изучении кольцеобразных событий в центральных столкновениях ядер впервые были представлены статистически значимые и надежные результаты наблюдения черенковских адронных ливней.

Аппробация работы

Основные результаты диссертации были опубликованы в сообщениях ОИЯИ, препринтах ICTP и INFN (Италия), в научных журналах разных стран (России, Египта, Англии, Германии, Италии, Японии, США), в докладах на международных конференциях и семинарах, защищены авторскими свидетельствами.

Публикации

Материалы, изложенные в диссертации опубликованы в работах (Г.I / 1 - 12 / и / 17 - 18 /, (Г.II / 2 - 36,38,39,42,43,48,50,62,69-73/) и (Г.III / 5,6,20,21 /) выполненных автором в 1972 - 1992 г.г.

ОБЪЕДИНЕННЫЙ ИНСТИТУТ ЯДЕРНЫХ ИССЛЕДОВАНИЙ

Лаборатория Высоких Энергий

На правах рукописи

УДК 539.172.6/8

539.171.017

539.12

Эль-Наги

Ахмед Ахмед

Взаимодействие П-мезонов, протонов, ядер и нейтрино с ядрами фотоэмульсии при высокой энергии

Специальность: 01.04.16 - Физиика ядра и элементарных частиц

Диссертация на соискание ученной степени

доктора физико-математических наук

Дубна, 1993.

Joint Institute for Nuclear Research
Laboratory of High Energies

EL-NAGHY
Ahmed Ahmed

Interactions of π mesons, protons, nuclei and neutrino with emulsion nuclei at high energy

Specialization :01.04.06 - Physics of nucleus and elementary particles.

Dissertation Submitted for Obtaining the degree of doctor of Science in Physico - mathematical science.

DUBNA ,1993.

Contents

INTRODUCTION.

The vitality of the work.The investigations of :hadron - nucleon (hN), hadron - nucleus (hA),nucleus-nucleus (AA) and neutrino - nucleus (νA) interactions are fundamental for understanding the nature of the interaction process.

The multiparticle production in hA collisions at high energies provides a senstive test for the mechanism of multiparticle production in hN collisions. It may be possible to use nuclei as analyzers of the space - time structure of the multiple production process and to discriminate between different theoretical models of the elementary act. In addition to this,one can study the nucleus excitation and disintegration (fragmentation) mechanism.

The main dominant goal of investigating AA collisions at high energy is searching for new phenomena which may not occur in hN and hA reactions. Many years ago,theorists speculated about the existence of novel states of nuclear matter. These states require high pressure,high temperature and high density, and can not be reached in a single NN collision. Collisions between nuclei at high energy may create finite volume of high density hadronic matter. The lattice quantum chromodynamics (QCD) suggests that above a critical temperature of about 250 MeV the hadronic state of nuclear matter is changed into a new phase consisting of deconfined quarks and gluons,quark - gluon plasma(QGP) with energy density $\mathcal{E} > \mathcal{E}_c \simeq 1 - 3$ GeV/fm^3.Such conditions could be reached in central nucleus - nucleus collisions at high energy

The study of multiplicity,angular,and energy characteristics of emitted particles in AA collisions and the correlations between them will shed light on the mechanism of interaction. This is of

main importance especially in absence of reliable scheme of calculation. Such study will distinguish mainly between "coherent models" in which the multiparticle production occurs via an intermediate step,and the "incoherent models" in which the created particles are directly produced and become physical inside the target nucleus.

Many theoretical models have been devoted to the study of the multifragmention process. In some models,the prefragment nucleus heats up and then condensates into droplets. Other statistical approaches try to explain the multifragmentation process without any reference to thermal equilibrium i.e. as shattering of the prefragment nucleus into many pieces. The study of projectile fragmentation in AA collisions will help to solve this problem.

The investigation of angular and energy characteristics of projectile and target fragments enables one to detect and study the "collective sideward flow" of nuclear matter.

The study of νA interactions represents an adequate tool for studying the space-time characteristics of the multiparticle production process.

Considering all the above mentioned factors the study of hN,hA,AA, and νA interactions is a very vital problem.

The aims of this work are: to study hN,hA,AA and νA interactions to understand the nature of multiparticle production. Also to investigate the projectile fragments to find the acceptable mechanism of multifragmentation process. One of the main aims is to check the possibility of formation of QGP and to study the characteristics of collective sideward flow of nuclear matter.In addition to this, to investigate νA interactions to

estimate the hadron formation time.

In the dissertation the author defends :

I. The characteristics of secondary charged particles emitted in interactions of 50 GeV/c π^- mesons and 69 GeV/c protons with emulsion.

II. Investigation of regularities and pecularities of nucleus-nucleus interactions at 4.5 A GeV/c,the study of fragmentation of Ne^{22}, Mg^{24},Si^{28} nuclei,the observation of sideward flow of nuclear matter in collisions of nuclei with emulsion,and the observation of hadronic Cherenkov radiation.

III. The study of neutrino charged current interactions with emulsion,the analysis of experimental data using two variants of the cascade model and estimation of hadron formation time.

The scientific novelty and practical value. This work includes a comprehensive,through, and statistically significant results from hN,hA,AA,νN, and νhA interactions. The study of these results provides precise tool to understand the mechanism of high energy nuclear interactions,especially the space - time evolution of the interacting system.

The study of νA interactions represents one of the early investigations in this field. It is the first emulsion experiment in which stacks were exposed to Fermilab neutrino beam at energy (300 - 400)GeV. The physical analysis of the experimental data enabled us to determine with sufficient accuracy the formation time of hadrons. Moreover, in the dissertation this question (formation time) was followed in hA and AA interactions.Thus ,the present thesis is a unique work which gives a wide account for the principle of formation time and its estimation using various

interactions such as γA,hA and AA.

The study of the multifragmentation process,had shown without doubt,that theoretical models assuming one intermediate excited nuclear system at certain temperature is in conflict with the present analysis. This conclusive result is very important to exclude such models. The results of studying projectile and target fragmentation is of great benefit to cosmic ray physicists who investigate the nuclear composition of cosmic rays and their cascade in the atmosphere.

This work is the first one which attracts the attension of high energy physicists to the importance of reaction plane determination. It had been shown that the sideward effect is better seen in the reaction plane.

It is the first time in which a claim was made that any macroscopic system,consisting of microscopic constituents should display the sideward flow of nuclear matter during the collision process.

It is the first time to report on statistically significant observation of Cherenkov hadronic jets, in high multiplicity central interactions of (4.1 - 4.5)A GeV/c Ne^{22} +Ag(Br) and Si^{28} + Ag(Br) collisions.These jets are consistent with a new mechanism of hadron emission as a consequence of Cherenkov gluon radiation.

The digestion of works. The basic results of the dissertation were published in JINR communications, ICTP (International Centre for Theoretical Physics) reports, and reprints of INFN (National Institute of Nuclear Physics) in ITALY. They were published,also, in international journals of different

countries (Russia,Egypt,England,Germany,Italy,Japan and USA).

Publications: The materials presented in the dissertation are published in references:(chapter I /1 - 12/ and /17,18/), (chapter II /2-36/,/38,39/,/42,43/,/48,50/,/62/,/69 - 73/) and (chapter III /5,6/,/20,21/) which were carried out by the author in the period of 1975 - 1992.

CHAPTER I.CHARACTERISTICS OF SECONDARY CHARGED PARTICLES EMITTED IN INTERACTIONS OF 50 GeV/c Π^- MESONS AND 69 GeV/c PROTONS WITH EMULSION

I.1. INTRODUCTION. The data discussed in this chapter are based on two experiments/1-12/. In the first one, emulsions were exposed to 50 GeV/c π^- mesons and in the second one to 69 GeV/c protons. Irradiations were carried out using beams of the accelerator of the Institute of High Energy Physics (IHEP),Serpukhov(RUSSIA). Emulsion pellicles of the type Br-2 and size 20 cm x 10 cm x 600 μm (undeveloped emulsion) were used.Along the track scanning was carried out. For the calculation of the inelastic mean free path,λ_{in} ,the following types of events were excluded :(i) Stars with single relativistic track deflected by less than 7 mrad (mostly due to elastic scattering),(ii) electron - positron pairs on the beam tracks and (iii) knock - out electrons.

Comparing the values of the mean free path of the inelastic interactions of protons with those of pions, one can conclude that there is no big difference between the proton and the pion inelastic interaction cross-section in emulsion at the energy range 4 - 300 GeV. From the Br-2 emulsion composition and applying the $A^{2/3}$dependence of cross-section on the atomic weight A,a value for the mean free path λ_{in} amounting to 35.9 cm is calculated.

There is a slight difference between some of the experimentally obtained values of λ_{in} and that calculated from the emulsion

composition considering the $A^{2/3}$ dependenceof the cross-section. The insight of the dependence of the average multiplicity of charged secondary shower particles, $\langle n_{ch} \rangle$,on the energy of center of mass of nucleon - nucleon collisions S, led to the formula: $\langle n_{ch} \rangle = a + b\,(\ln S) + c\,(\ln S)^2$ .....(1)
This relation is consistent with the multiperipheral models /e.g.13/ and Feynman's scaling /14/.

The high energy physicists used the normalized multiplicity $R = \langle n_s \rangle / \langle n_{ch} \rangle$ for comparison with predictions of various models. Table 1 represents the values of R obtained at different energies. From this table it is seen that R slowly increases with energy and reaches to approximately a constant value (R ~ 1.8) after 69 GeV.

Table 1 . The values of R at different beam energies

E(GeV)	$R=\langle n_s \rangle / \langle n_{ch} \rangle$
6.2	1.27+0.02
8.4	1.29+0.24
16.0	1.24+0.12
28.0	1.40+0.12
67.0	1.53+0.40
69.0	1.43+0.12
69.0	1.59+0.11
200.0	1.72+0.03
200.0	1.62+0.66
300.0	1.72+0.03
300.0	1.65+0.10
400.0	1.83+0.07
1000.0	1.79+0.26
3000.0	1.83+0.30

In the study of proton-nucleus interactions, the average number of collisions of the incident particle inside the target nucleus, ν, is a very important factor and is given by,

$$\nu = A\ \sigma_{PP} / \sigma_{PA} \quad \text{.....(2)}$$

where σ_{PP} and σ_{PA} are the inelastic cross-sections for PP and P-nucleus interactions respectively. The value of ν, from equation(2), was used to calculate R according to the prediction of energy flux cascade model (EFCM)/15/, and the coherent production tube model (CPTM)/16/. The calculated values of R are compared with the corresponding experimental values in Table 2. Our data agree with the predictions of EFCM, moreover it is consistent with ν=1 for PP interactions.

Table.2 The values of R_{cal}, calculated according to EFCM and to CPTM compared to our data of R_{exp}.

Momentum (GeV/c)	R_{exp}	R_{cal}	
		EFCM	CPTM
8.4	1.29+0.24	1.5	1.75
69.0	1.43+0.12		

Fig.1 illustrates the dependence of the dispersion of the shower particles multiplicity, $D = [\langle n_s^2 \rangle - \langle n_s \rangle^2]^{1/2}$, on the average multiplicity $\langle n_s \rangle$, for P - emulsion inelastic

interactions (line I). Line II ,was obtained for PP interactions/12/. It is seen that the intersection part increases from -0.58 in PP collisions to -0.02 in P - nucleus interactions,while the slopes are not changed.

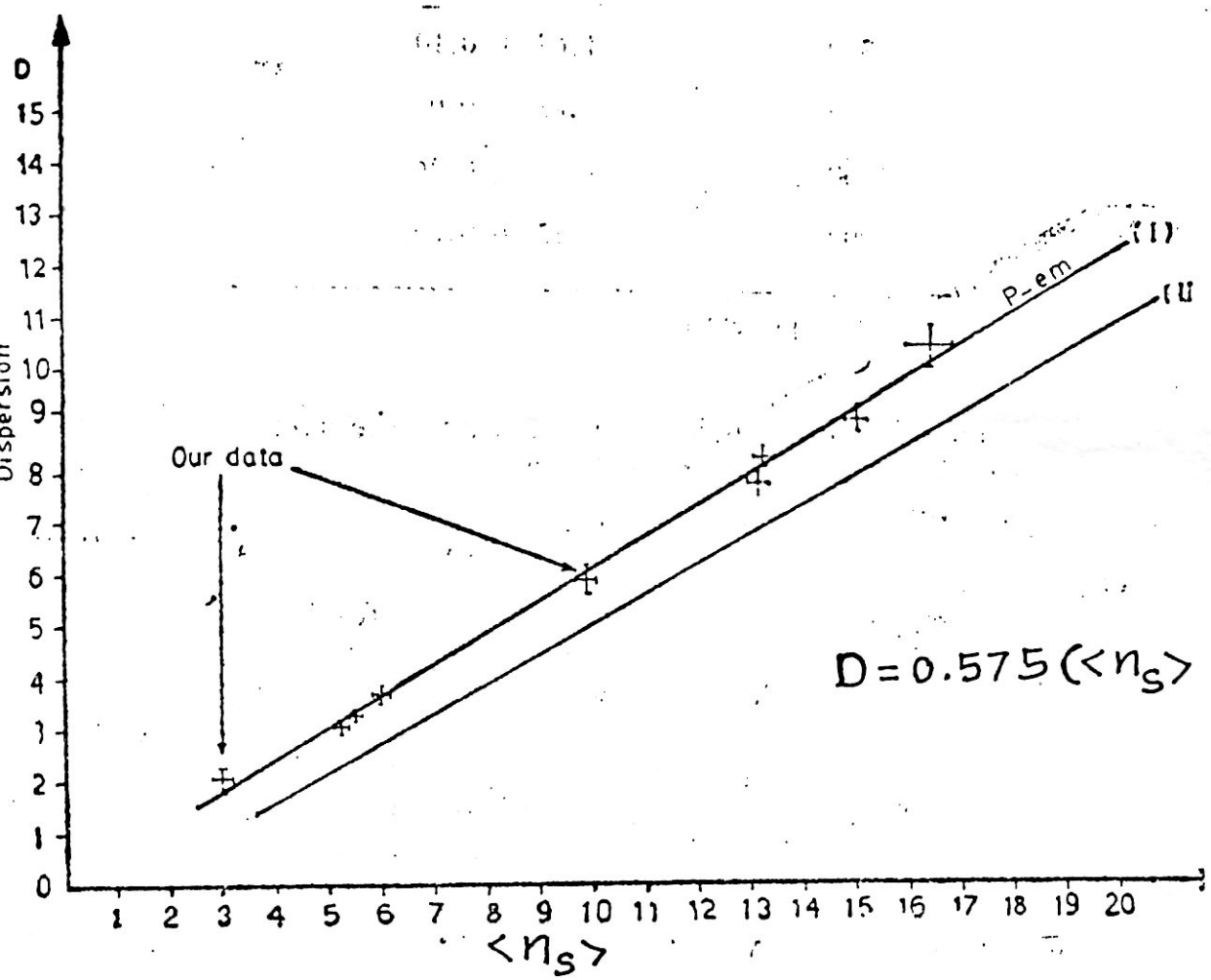

Fig.1 The disper sion D ersusns for collisions of proton with emulsion (I) and pr with proton (II). The solid lines represent the fitting of experimental data

The n_s - distributions are compared with the predictions of KNO scaling/12/,which can be tested in either of the two following relations:

$$\sigma_n / \sigma_{in} = \langle n_s \rangle^{-1} \psi (n_s / \langle n_s \rangle \quad \ldots\ldots\ldots\ldots\ldots\ldots (3)$$

or $$\langle n_s^q \rangle = C_q \langle n_s \rangle^q \quad \ldots\ldots\ldots\ldots\ldots\ldots\ldots\ldots\ldots (4)$$

where $\langle n_s \rangle^q = (1/\sigma_{in}) \sum_{n=1} n_s^q \sigma_n / \sigma_{in}$ is the qth momen of the multiplicity distribution for q=2,3,4.....; σ_n is the partial cross-section for producing n_s charged particles and σ_{in} is the total inelastic cross-section (excluding coherent events). ψ and C_q are energy independent functions.

Fig 2 shows that our experimental data lie on a universal curve fitted by the emperical formula /12/.

$\psi(z)=(3.42\ z + 14.34\ z^3 - 1.06\ z^5 + 0.09\ z^7) \exp(-3.28\ z)$....(5)

where $z= n_s/\langle n_s \rangle$. Furthermore, Table 3 lists the experimental values of the ratio $\langle n_q \rangle / \langle n^q \rangle = C_q$ for q=2 - 5. The values of C_q are approximately constant over the energy range from 6 to 200 GeV for q=2,3 and 4

Table.3 The values of scaling moments C_q for P-emulsion interactions.

Momentum (GeV/c)	q=2	q=3	q=4	q=5
6	1.37+0.07	2.27+0.12	4.33+0.36	9.18+0.91
8.4	1.40+0.08	2.32+0.13	4.32+0.40	8.90+0.90
20.5	1.34+0.03	2.39+0.08	3.93+0.42	7.82+0.85
27.0	1.33+0.05	2.11+0.25	3.82+0.61	7.67+1.60
69.0	1.38+0.01	2.34+0.09	4.63+0.43	10.31+0.74
200.0	1.26+0.06	1.95+0.11	3.46+0.23	6.84+0.52

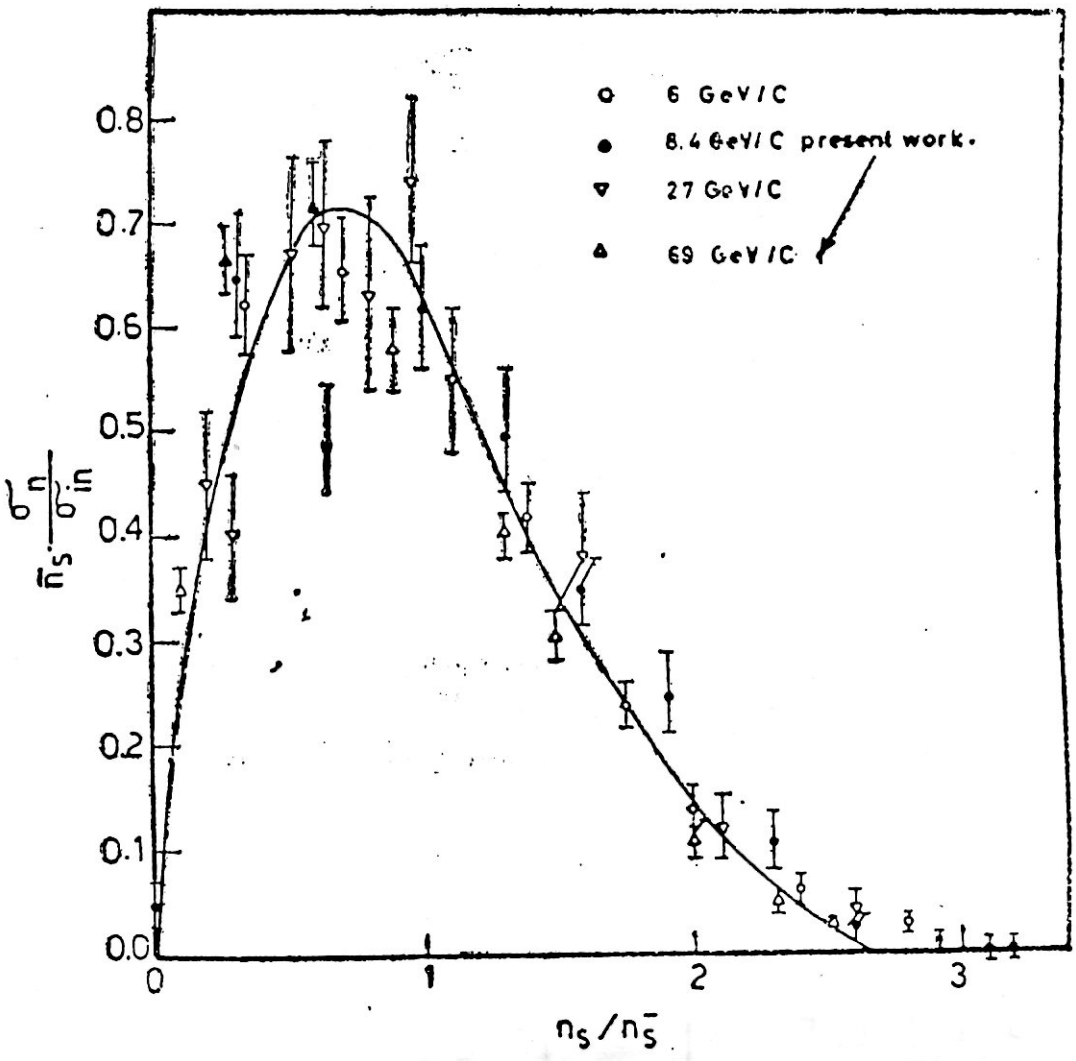

Fig. 2 $\bar{n}_s \frac{\sigma n}{\sigma in}$ versus $n_s/\bar{n}_s$ for interactions of protons with emulsion at 6, 8.4, 27 and 69 GeV/C. The solid line is drawn according to equation (6).

I.2. Angular Distribution of Shower Particles Emitted in Proton-Nucleon Interactions.

Figure 3 presents the angular distributions of the emitted charged secondaries in case of P - n and P - P interactions, respectively, for different groups of multiplicity. The transformation of the laboratory angular distribution into the center- of- mass system of the two colliding nucleons was done considering all of the secondaries as

pions,each with a P_t value equal to $\langle P_t \rangle$ = 0.4 GeV/c. The values of the asymmetry parameter [$a=(N_F - N_B)/(N_F + N_B)$] for each group of multiplicity in case of Pn ,PP,and P-nucleon are given on the figures. It is clear that the asymmetry in the forward direction decreases with the increase of the multiplicity of the given interaction.

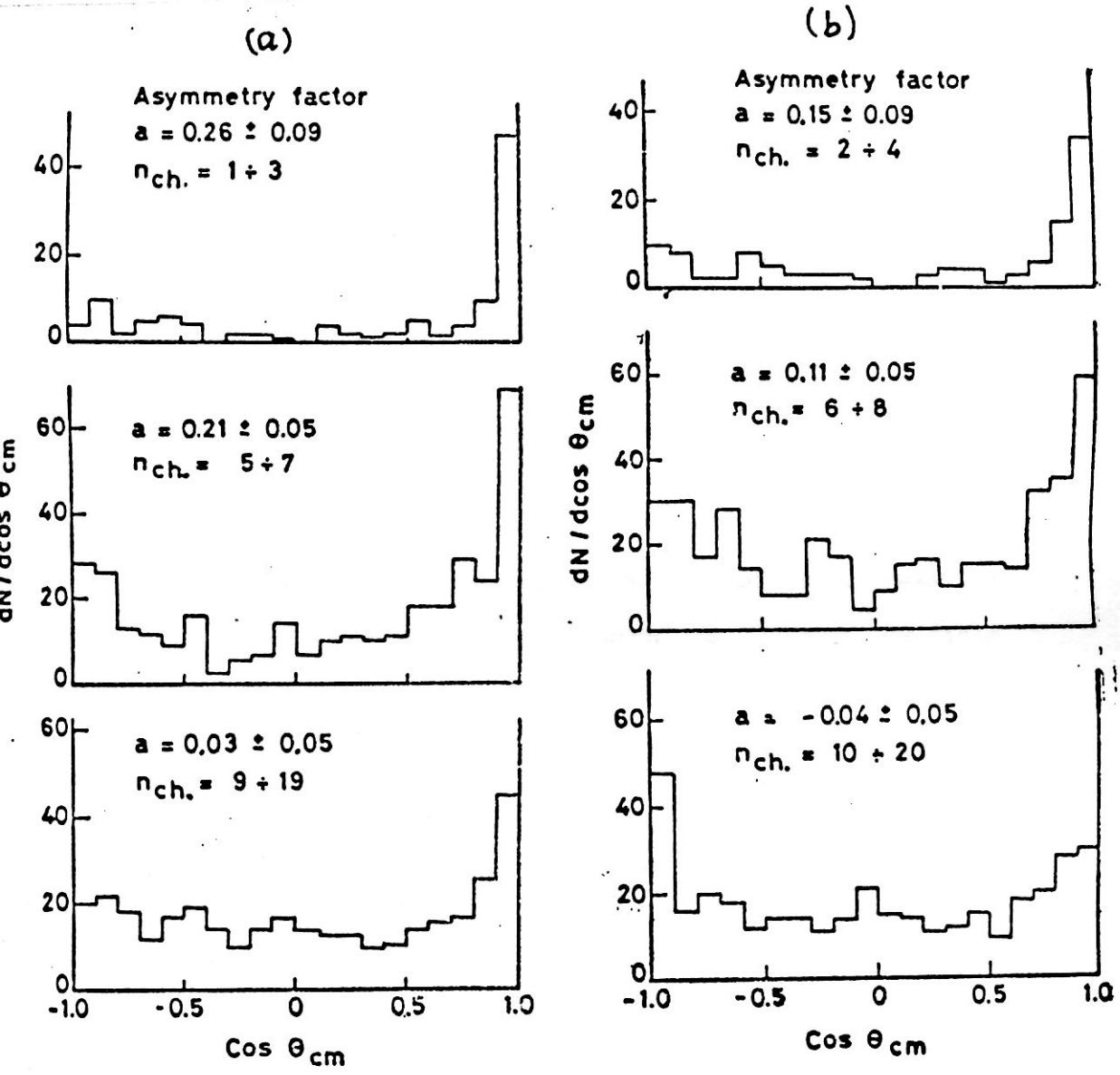

Fig.3a Angular distribution of different multiplicities of charged secondaries emitted in the cm system of p-n collisions at 69.0 GeV/c laboratory momentum

Fig.3b Angular distribution of different multiplicities of charged secondaries emitted in the cm system of p-p interactions at 69.0 GeV/c laboratory momentum

I.3. Emission of ^{8}Li Fragments in Interactions of 69 GeV/c protons with Ag(Br) Nuclei.

Out of 2338 inelastic interactions of 69 GeV/c protons with Br-2 nuclear emulsion 21 hammer tracks and 9 decays of $^{8}Be_{4}$ were detected. For the events in which these phenomena were observed,measurements of multiplicities and angles of all types of particle tracks were measured accurately.

The emission cross-section of different fragments is very sensitive to the incident energy in the range E< 2 GeV. In this energy region the cross-section increases dramatically with the incident particle energy. At E>2 GeV the cross-section σ_f increases very slowly and reaches to a plateau at 5 GeV. The production ratio of ^{8}Li in P - emulsion interactions at 69 GeV/c is 1.2%.

The charge distribution of the emitted fragments was studied and the probability of emission of a fragment with charge Z_f decreases with Z_f at a given energy . The probability of emission of two or more fragments increases with the incident particle energy.

Figure 4 shows the angular distribution of emitted fragments of ^{8}Li and ^{8}Be . The forward asymmetry is noticed in this distribution which is distinguished from the isotropic angular distribution of b-tracks. The F/B ratio for b-tracks equals 1.2+o.5 while it is 2.2+0.5 for Li and Be fragments. This anisotropy is strong and can not be explained by the motion of the residual nucleus.

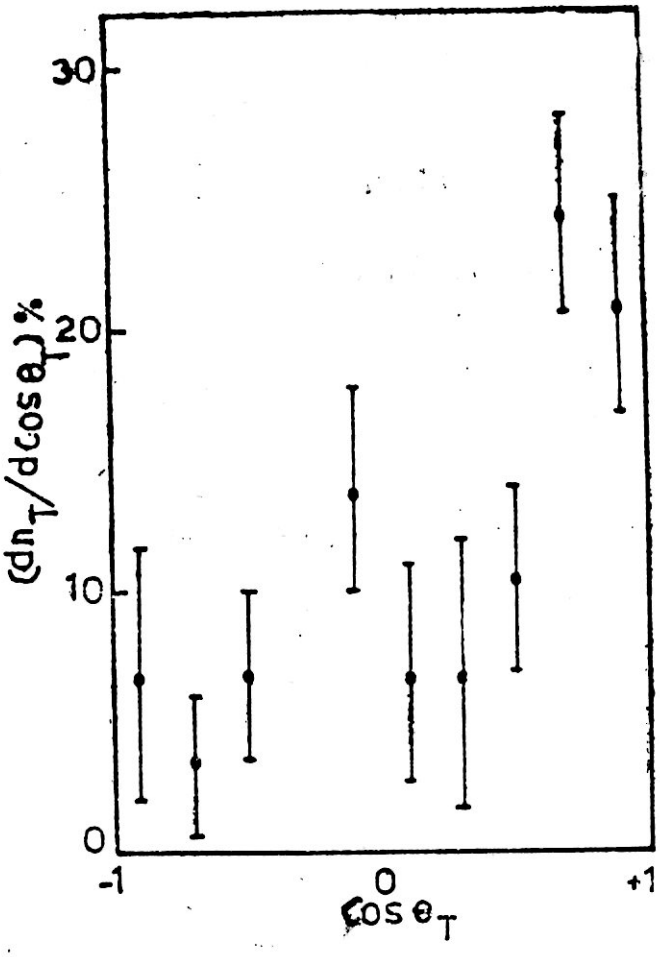

Fig. 4. The angular distribution of hammer tracks.

Figure 5 shows the experimental energy distribution of the emitted fragments as well as the fitting of this distribution with the well known evaporation formula/11/. From the figure it is seen that the evaporation curve can describe the experimental data. The fitting parameters resulting from our data are the potential V=15 MeV,the temperature T=14 MeV and the velocity of the emitting source v=0.01c.

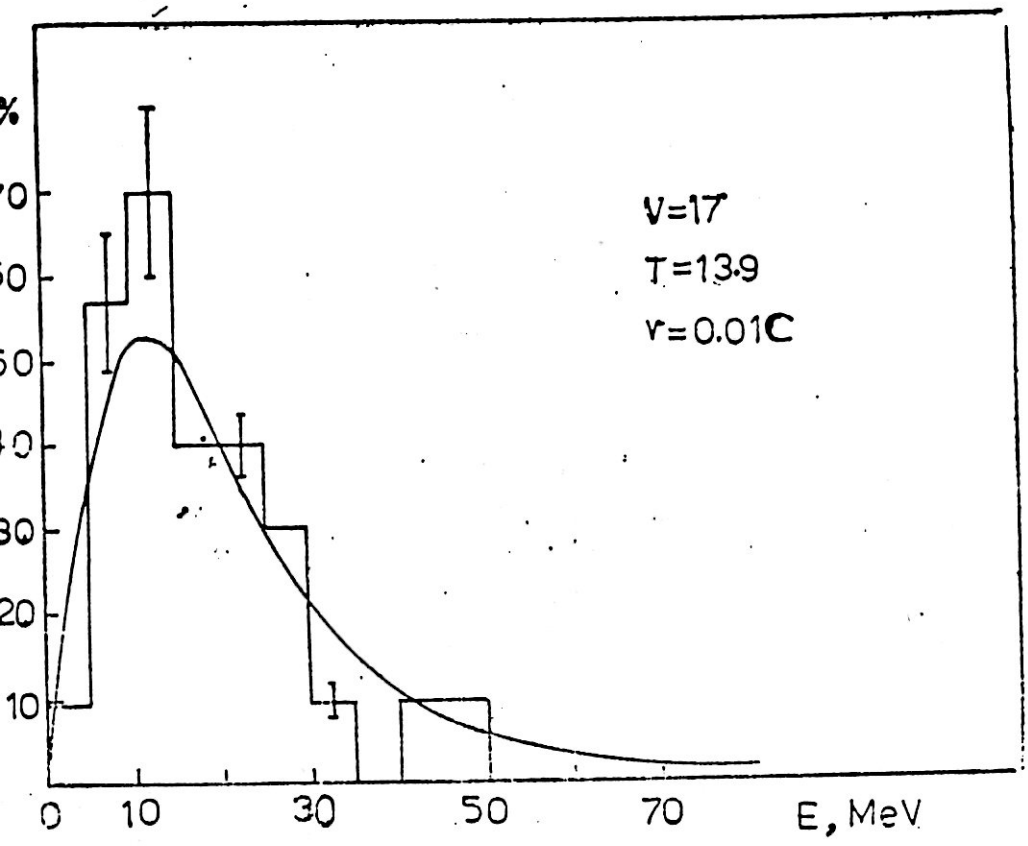

g. 5. **The energy distribution of hammer tracks and the fitting of this distribution.**

I.4. Central Collisions of Fast Particles with Ag(Br) Nuclei.

This section deals mainly with two points:(i) the multiparticle production process in these extreme central collisions and (i) the disintegration of residual nucleus. These processes were discussed in details in our works/7,8,10,17,18/, and the second point will be discussed in details in Section II.9,II.12 and II.13.

The analysis of different multiplicities shows that $\langle n_g \rangle$ is strongly dependent on the target mass number A_T and is weakly dependent on the projectile mass number A_P whereas $\langle n_s \rangle$ is vice versa. To estimate these dependences, we investigated the relation:

$$\langle n_i \rangle (A_{j1}) / \langle n_i \rangle (A_{j2}) = [A_{j1}/A_{j2}]^{\alpha_{ij}} \quad \ldots\ldots (7)$$

where i denotes s or g particles and j stands for projectile P or target T. Using the experimental data in equation (7) one may get : $\alpha_{sp} = 0.62 \pm 0.03$, $\alpha_{gp} = 0.11 \pm 0.01$ and $\alpha_{gT} = 0.62 \pm 0.03$ To calculate α_{sT} , the proton and heavy ion data were studied separately and the obtained values are $\alpha_{sT} = 0.11 \pm 0.01$ for protons and $\alpha_{sT} = 0.36 \pm 0.03$ for heavy ions. Thus for central collisions of protons in emulsion we have $\langle n_s \rangle = \text{const.} A_T^{0.11}$ whereas $\langle n_g \rangle = \text{const.} A_T^{0.62}$, in case of heavy ions $\langle n_s \rangle = \text{const.} A_P^{0.62} A_T^{0.36}$ and $\langle n_g \rangle = \text{const.} A_P^{0.11} A_T^{0.62}$.

The analysis of experimental data in central P-emulsion collisions and PP ones led to the conclusion that the incident particle, after the first collision, interacts with next target nucleons with a measurable cross-section.

I.5. Energy and Angular Distributions of Secondary Charged Particles from Interactions of 50 GeV/c π^- mesons with Nuclei.

Nuclear emulsions were exposed in a strong pulsed magnetic field at the IHEP(Serpukhov) accelerator. This technique enables one to obtain fairly reliable information on the momenta and charges of the produced particles while retaining the well known advantage of the emulsion technique that slow particles can be reliably detected and identified. The experimental material

examined here consists of 536 inelastic interactions of π^- mesons with nuclei (π^- A events) in which the momenta of about 3000 particles were measured. These events do not include those of quasinucleon type (π^-N events). The latter (242 events) are investigated separately and compared with π^- A events. Elastic scattering and coherent production reactions on nuclei were excluded.

Figure 6 shows distributions in longitudinal rapidity $Y=(1/2)\ \ln\ [(E+P_L)/(E-P_L)]$ in the laboratory system for π^+ and π^- from π^-N interactions and from π^-A collisions with $n_h<6$ and $n_h> 7$. At the same time, the distributions in Fig.6 are also distributions in the C.M.system of the colliding pion and intranuclear nucleon : the "shift" to the latter is effected by simple transformation $Y^*= Y- \cosh^- \gamma_c$, where γ_c is the Lorentz factor connecting the two reference systems. The angular distributions in the latter system for π^+ and π^- from the same groups of interactions are shown in Fig.7. From figures 6 and 7 one may conclude that :

As the number of intranuclear collisions increases, the longitudinal distributions shift steadily toward the lower rapidities and larger angles θ^*. This shift is especially marked in the n_g dependences of the average characteristics of the distributions (Figs.8a and 8c). In the "pion-nucleon" C.M.system, the longitudinal distributions for π^-N collisions are highly asymmetric in the forward direction; for π^-A events with $n_h < 6$ the distributions are approximately symmetric in this reference

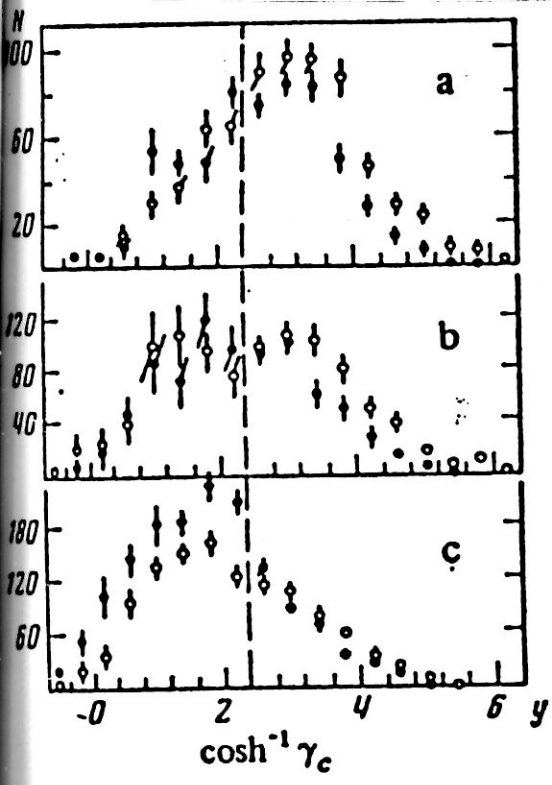

FIG. 6. Distributions in longitudinal rapidity y of π^- (open circles) and π^+ (black circles) mesons from $\pi^- N$ interactions (a) and $\pi^- A$ interactions with $n_h \leqslant 6$ (b) and $n_h \geqslant 7$ (c).

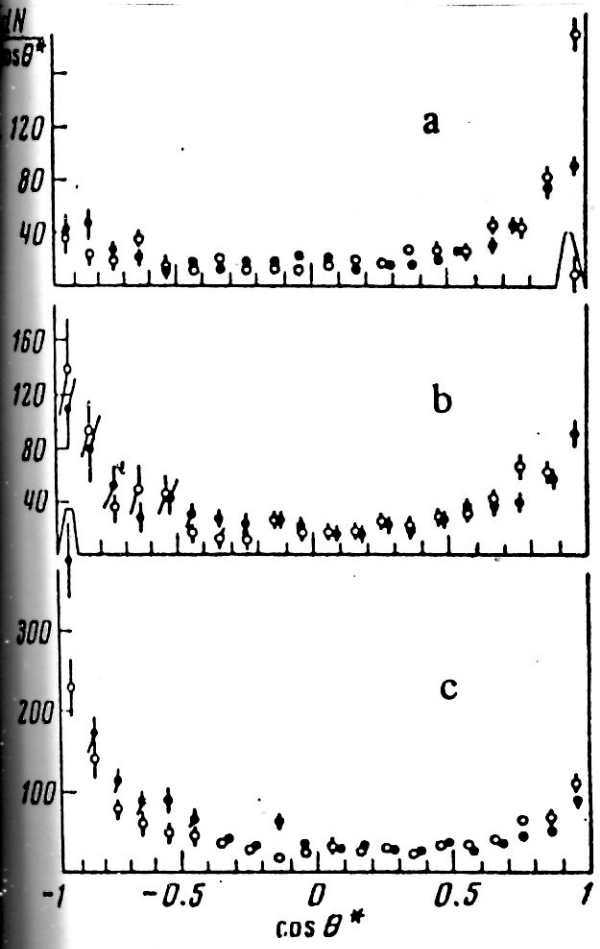

FIG. 7. Angular distributions of π^- and π^+ mesons in the c.m. system of the colliding pion and intranuclear nucleon from $\pi^- N$ interactions (a) and $\pi^- A$ interactions with $n_h \leqslant 6$ (b) and $n_h \geqslant 7$ (c). The notation is the same as in Fig. 6.

system; and for events of $n_h > 7$ the distributions are highly asymmetric backward. The shift of the spectra is less marked in the projectile fragmentation region and is more marked in the target fragmentation region. It is cleary evident that the shapes of the rapidity spectra change as the number of intranuclear collisions increases, because of the more rapid increase in the number of slow particles.

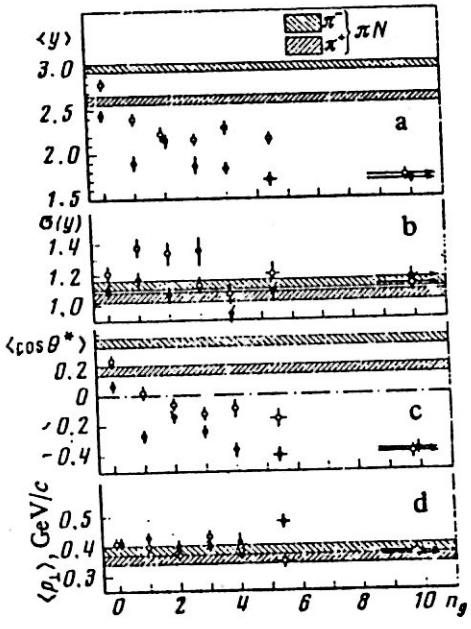

FIG. 8. n_g dependences of the average rapidity $\langle y \rangle$ (a), the standard deviation of the y distribution (b), the average $\langle \cos\theta^* \rangle$ (c), and the average transverse momentum $\langle p_\perp \rangle$ (d) for π^- and π^+ mesons from $\pi^- A$ interactions. The notation is the same as in Fig. The hatched bands are confidence intervals for the corresponding quantities from $\pi^- N$ events.

Figure 8b shows that the widths of the Y distributions are approximately independent of the number of slow particles which is usually identified with the number of intranuclear collisions, for both π^- and π^+ mesons.

Also , it is noted that as n_g increases the magnitude of the shifts of the centers of longitudinal distributions decreases; thisindicates that n_g (or n_h) is most likely a nonlinear function of the number of intranuclear collisions.

In all the groups of collisions, except possibly for events in which n_g is exceptionally large, there are more π^- mesons with large Y (small θ^*) than π^+ mesons. This is the well known leading - particle effect, which is characteristic of the elementary hadron - nucleon collision events. The numbers of high energy ($\geq$ 0.1 P_o) π^- and π^+mesons per collisions are plotted in Fig.9 versus the pion energy in the Laboratory system.

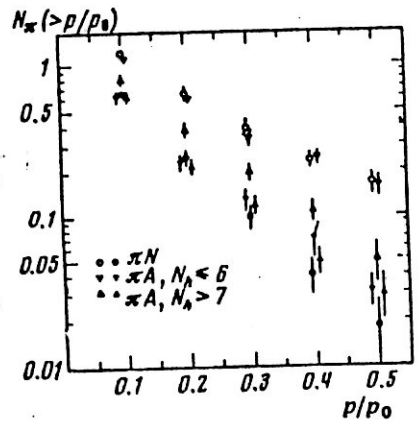

FIG. 9. Number of fast π^- (open points) and π^+ (black points) mesons per event from $\pi^- N$ and $\pi^- A$ collisions vs p/p_0.

I.6. Associated Multiplicities in Interactions of Negative Pions with Emulsion Nuclei at 50 GeV/c.

The data in this section is based on 536 π^- nucleus (π^-A) events, induced by π^- mesons at 50 GeV/c in a strong pulsed magnetic field. The experimental material does not include quasi-nucleon interactions,elastic interactions, or coherent particle production on nuclei. For comparison with the π^-A events,242 π^-N events are also studied.

We considered the average multiplicities ⟨n(a)⟩ of secondary particles in the inclusive reactions,

$$\pi^- + \text{nucleus} \text{ ---- } \pi_1 + a + \text{anything else}$$

$$\pi^- + \text{nucleon} \text{ ---- } \pi_1 + a + \text{anything else}$$

as functions of the different characteristics of the inclusive π_1 meson (a = π_2^-, π_2^+ and all s,g,b,h particles).

Figures 10 and 11 show how the average multiplicities⟨n_π-⟩ and ⟨n_π+⟩ associated with the emission of inclusive π^- (Fig.10) and π^+ (Fig.11) depend on the transverse momentum of the latter.

The data in the intervals $\Delta Y < 1.2$ and $\Delta Y > 1.2$show that the decrease of ⟨n_π- ⟩ is characteristic mainly for the second interval. This indicates a long-range character of the correlations and is characteristic of both π^-A and π^-N events.

A more detailed picture of the compensation of the transverse momentum of the inclusive particle can be obtained by comparing the associated multiplicities of particles emitted in two intervals of azimuthal angle between a pair: that is ,$\varepsilon < \pi/2$ (i.e. into the same azimuthal hemisphere with the given inclusive

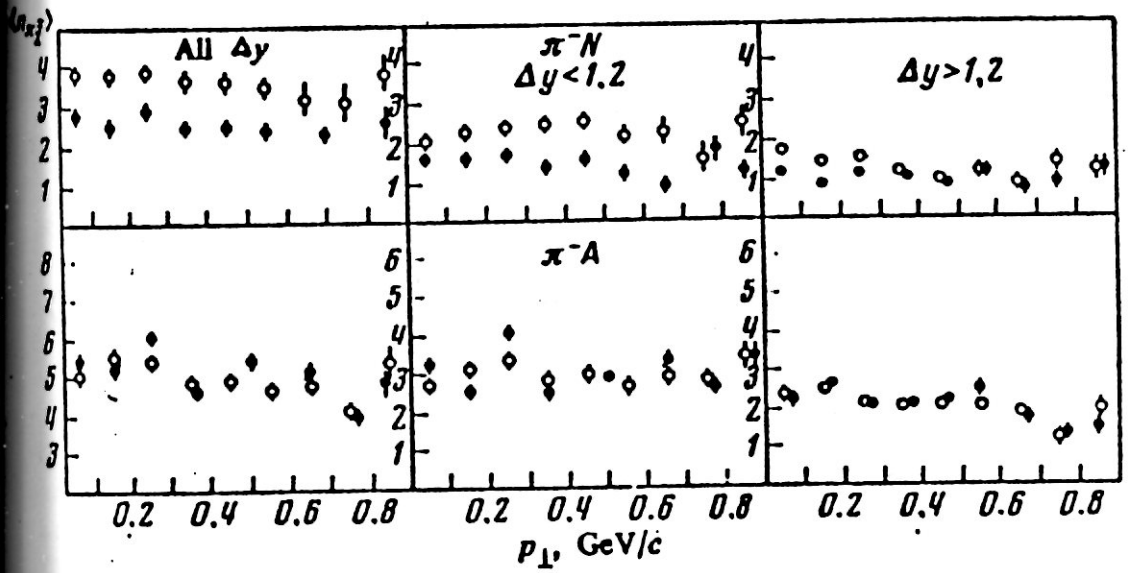

FIG. 10 $\langle n_{\pi_2^-} \rangle$ (open circles) and $\langle n_{\pi_2^+} \rangle$ (solid circles) as functions of π_1^+ transverse momentum in the reactions $\pi^- A \to \pi_1^+ + \pi_2^\mp + \ldots$ and $\pi^- N \to \pi_1^+ + \pi_2^\mp + \ldots$.

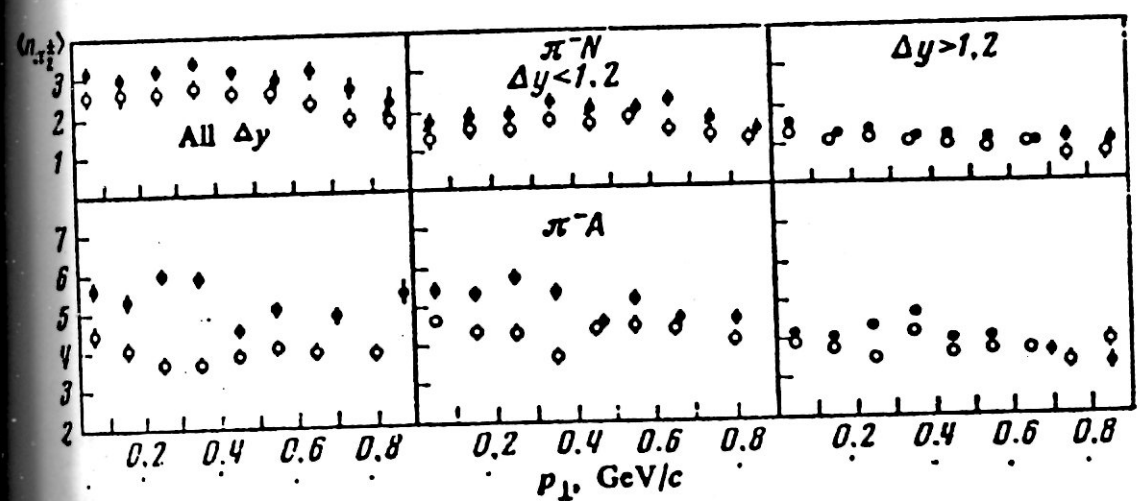

FIG. 11. $\langle n_{\pi_2^-} \rangle$ (open circles) and $\langle n_{\pi_2^+} \rangle$ (solid circles) as functions of π_1^- transverse momentum in the reactions $\pi^- A \to \pi_1^- + \pi_2^\mp + \ldots$ and $\pi^- N \to \pi_1^- + \pi_2^\mp + \ldots$.

pion) and $\varepsilon_{12} > \pi/2$ (into the oppsite hemisphere). For example, Fig.12 shows the dependence of $\langle n_{\pi^-} \rangle$ and $\langle n_{\pi^+} \rangle$ on P_t (as in Fig.10) for the different regions of ΔY and ε_{12}. The following features are cleary seen.

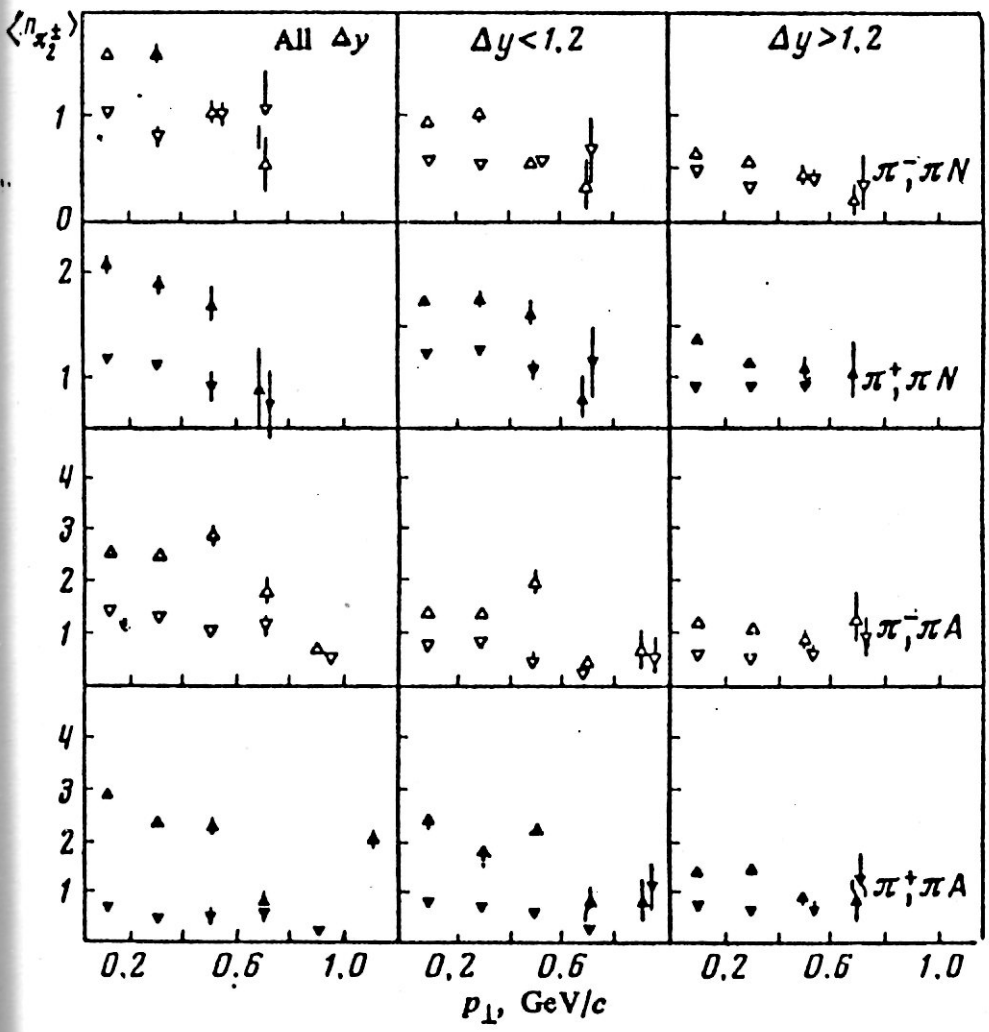

FIG. 12. Dependence of $\langle n_{\pi_2^-} \rangle$ with $\varepsilon_{12} < \pi/2(\Delta)$ and $\varepsilon_{12} > \pi/2(\nabla)$ and of $\langle n_{\pi_2^+} \rangle$ with $\varepsilon_{12} < \pi/2(\blacktriangle)$ and $\varepsilon_{12} > \pi/2(\blacktriangledown)$ on transverse momentum of the inclusive π_1^- meson in the reactions $\pi^- A \to \pi_1^- + \pi_2^{\mp} + \ldots$ and $\pi^- N \to \pi_1^- + \pi_2^{\mp} + \ldots$.

a) the number of particles emitted at ($\varepsilon_{12} > \pi/2$) to the inclusive particle depends weakly on the transverse momentum for $P_t < 1$ GeV/c whereas the number of particles with $\varepsilon_{12} < 90^{\circ}$ decreases substantially as P_t increases. This indicates the validity of models of hadron - nucleus collisions where the production mechanism resembles an elementary act.

b) Within the limits of quite large statistical errors the noted effects do not depend on the charge signs of the considered pion pairs and are approximately identical in π^-A and π^-N collisions.

Figures 13 and 14 show the dependence of the associated multiplicities on the longitudinal rapidity of the given inclusive π^+meson. Considerable correlation is indicated,different for the two regions $\Delta Y < 1.2$ and $\Delta Y > 1.2$ but qualitatively identical for π^-N and π^-A collisions.

From the study of analogous dependences in PP collisions it is known that there are strong constraints due to the conservation of longitudinal momentum and energy (accounting, in particular, for the sharp decrease of $< n_\pi >$ at large absolute rapidities in the C.M.System of PP collisions). In hadron-nucleus collisions these constraints can be strongly "suppressed" by a cascade mechanism of multiplication.Figures 11 and 12 show that this does not occur; the reduction of $< n_\pi >$ at the edges of the rapidity scale is of the same order as in an elementary event

Figure 15 shows the dependence of $< n_s - 1 >$,$< n_g >$ and $< n_b >$ on the laboratory momentum ($P_{l.s}$),transverse momentum ($P_{t\ l.s.}$) and

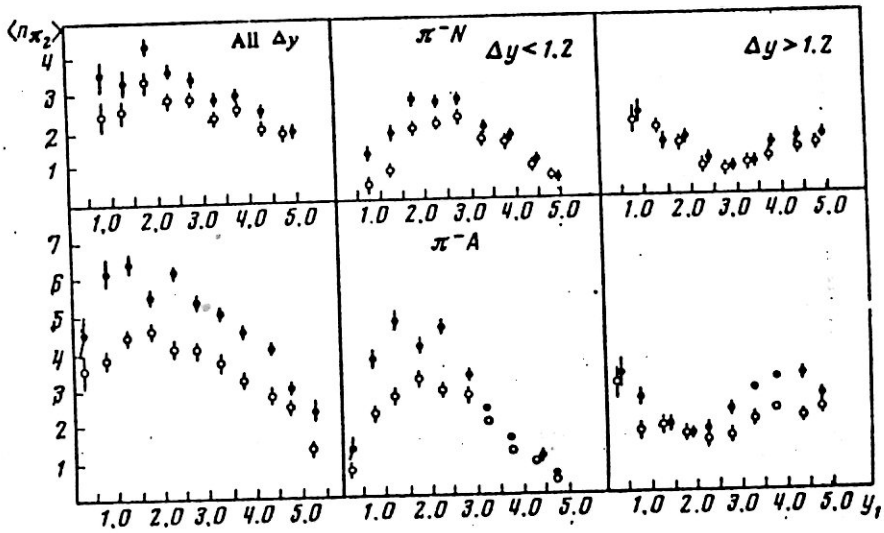

FIG.13. Dependence of $\langle n_{\pi_2^-} \rangle$ (open circles) and of $\langle n_{\pi_2^+} \rangle$ (solid circles) on the rapidity of the π_1^- meson in the reactions $\pi^- A \to \pi_1^- + \pi_2^{\mp} + \ldots$ and $\pi^- N \to \pi_1^- + \pi_2^{\mp} + \ldots$.

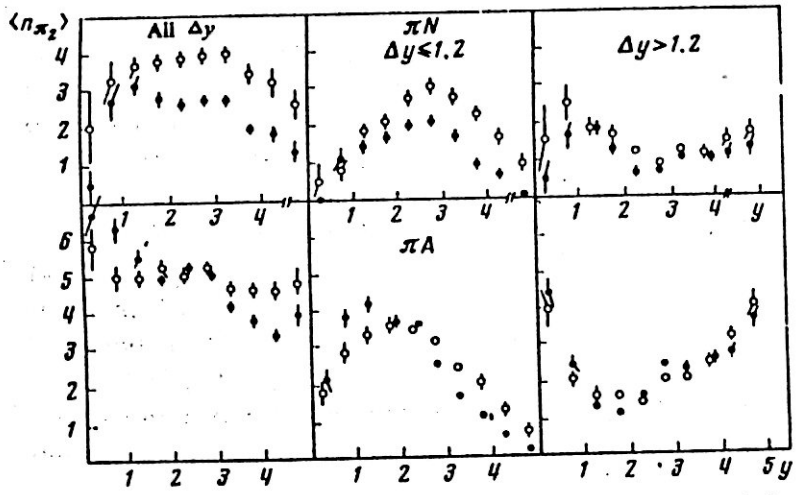

FIG.14. Dependence of $\langle n_{\pi_2^-} \rangle$ (open circles) and of $\langle n_{\pi_2^+} \rangle$ (solid circles) on the rapidity of the π_2^+ meson in the reactions $\pi^- A \to \pi_1^+ + \pi_2^{\mp} + \ldots$ and $\pi^- N \to \pi_1^+ + \pi_2^{\mp} + \ldots$.

on the four momentum transfer $\Delta^2_{l.s.}$ of the leading π^- meson. With increasing $P_{l.s.}$ the multiplicity $\langle n_s - 1 \rangle$ is seen to decrease very rapidly (more rapidly than for $\pi^- N$ collisions), while $\langle n_b \rangle$ and $\langle n_g \rangle$ vary very weakly . With increasing $P_{tl.s.}$ or $\Delta^2_{l.s}$ in $\pi^- A$ collisions a somewhat weaker growth occurs in the number of shower particles, for $\pi^- N$ collisions there is no appreciable dependence in the considered interval. All these properties of the multiplicities associated with the leading particle appear to be easily explained by the models of weak intranuclear interaction of produced fast particles. However, the fact that for an identical momentum loss of the leading particle ($P_o - P$ or Δ^2) the multiplicity of shower particles in $\pi^- A$ collisions considerably exceeds that for $\pi^- N$ shows that the target nucleus is not simply a spectator of the multiple production process.

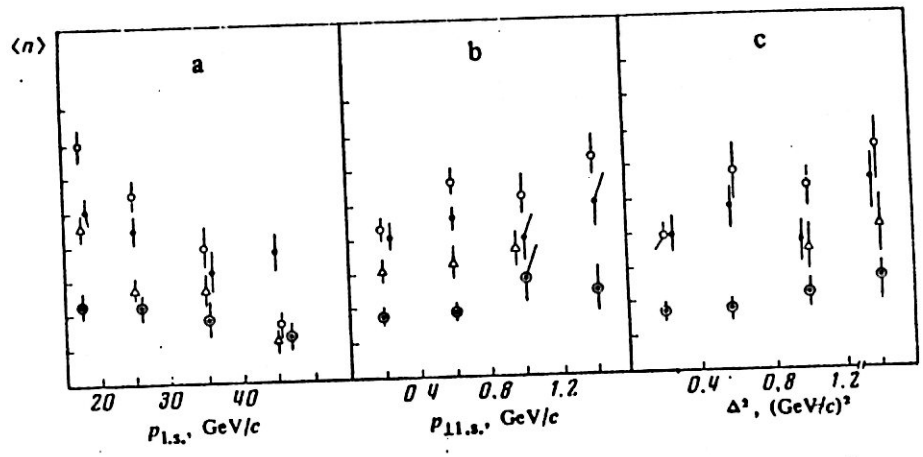

FIG. 15 Dependence of $\langle n_s - 1 \rangle$ (○), $\langle n_g \rangle$ (⊙), and $\langle n_b \rangle$ (●) on characteristics of the "leading" π^- meson in a $\pi^- A$ collisions: momentum (a), transverse momentum (b), and square of lost 4-momentum (c). Also, analogously in the case of $\langle n_s - 1 \rangle$ for $\pi^- N$ collisions (Δ).

REFERENCES OF CHAPTER I.

1. O.E.Badawy et al.,Abstracts of Contributed Papers in the Sixth Int.Conf. on High Energy Phys. and Nucl.Structure,Santa Fe Los Alamos, USA,June 1975,P.325-326.

2. V.G.Voinov et al.,Comm.of JINR,PI-9217,Dubna,1975; Pisma v JETP,22,56,1975 (in russian).

3. V.G.Voinov et al.,preprint Lebedev physical Institute,Russian Academy of Science,No.106,Moscow 1976; 18th Int.Conf.on High Energy Phys.,Tbilisi,1976,No.A6-445,P.45 ;Yadernia Fizika,25,1003,1977 [Sov.J.Nucl.Phys.25(5),533,1977.

4. V.G.Voinov et al.,preprint Lebedev physical Institute,Russian Academy of Science,No.105,Moscow 1976;Yadernia Fizika,25,782,1977 (in Russian),[Sov.J.Nucl.Phys.25(4),416,1977.

5. V.G.Voinov et al.,preprint Lebedev physical Institute,Russian Academy of Science,No.104,Moscow 1976.

6. V.G.Voinov et al.,preprint Lebedev physical Institute,Russian Academy of Science,No.159,Moscow 1976.

7. G.A.Salamov et al.,Comm.of JINR PI-10724,Dubna 1977;Yadernia Fizika 27,1008,1978 [Sov.J.Nucl.Phys.27(4),533,1978].

8. O.Akhrorov et al.,Comm.of JINR PI-9963,Dubna 1976 .

9.O.E.Badawy et al., Egypt. J.Phys., 7(2),53,1976;
Bulg.J.Phys.V,1,1978.

10. B.P.Bannik et al.,Comm. of JINR PI-10762 Dubna 1977;
Z.Phys.A284,283,1978.

11. M.EL-Nadi et al .,Egypt.J.Phys.14(2),137,1983.

12. M.EL-Nadi et al .,Egypt.J.Phys.14(2),149,1983.

13. C.E.D.Tar,Phys.Rev. D3,128(1971)

14. Y.Baudinet-Robinet et al.,Nucl.Phys.32,452,1962.

15. K.Gottfried,Phys.Rev.Lett.32,957,1974.

16. A.Dar and I.Vary ,Phys.Rev.D6,2412,1972.

17. A.El-Naghy et al.,J.Phys.Soc.JAPAN,58,741,1989 suppl.

18. M.EL-Nadi et al.,Z.Phys.A310,301,1983.

Chapter II

Some Regularities and Pecularities of Nucleus-Nucleus Interactions at 4.5 A GeV/C

II.1. Introduction: What are the goals of investigating nucleus-nucleus collisions at high energy? There is one clearly dominant goal searching for new phenomena which do not occur in pp or pA reactions. Already many years ago, scientists speculated about the existence of complex states of nuclear matter, states which may have occurred during the creation of the universe and perhaps still occur in supernova explosions or in neutron stars/1/. These states require high pressure, high temperature and a large baryon density, and cannot be reached in a single pp collision. But perhaps there is a way to reproduce these conditions in the laboratory by colliding beams of heavy ions at high energy. What scientists visualized as states of higher complexity may in fact turn out to be states of a more fundamental nature than the normal states of nuclear matter, i.e. of nuclei. Lattice quantum chromodynamics (QCD) predicts that, under the quoted conditions, a deconfinement phase transition will take place: nuclear matter (thought to be composed of separate nucleons) will melt into a quark-gluon plasma (QGP).

Many people believe that the experimental proof of such a phase transition will be almost as important a test for QCD as finding the W or Z was for the theory of electroweak interactions. According to recent theoretical estimates, the necessary temperature and pressure or baryon density can indeed be reached in nucleus-nucleus collisions at c.m. energies perhaps as low as a few GeV per nucleon-nucleon collision. This explains the excitment and the remarkable activation of interest for nucleus-nucleus collisions which has brought together again nuclear physicists, astrophysicists and particle physicists, in the last years.

The goal of this chapter is to review some of the experimental results from 4.5 A GeV/c nucleus-nucleus

collision, using emulsion technique and to compare them with pp and pA data, and with theoretical predictions or expectations. Since there may be hints of new phenomena but there is no convincing proof yet, the comparisons serve the purpose of showing to which level "old physics" can explain the data.

After briefly surveying the sources of the experimental information and presenting a typical experimental procedure, this chapter will discuss: the multiplicity characteristics, theoretical calculations of n_s-distribution comparison with the cascade evaporation model, angular characteristics and correlations, central collision and complete destruction of heavy nuclei, fragmentation of beam nuclei, sideward flow of nuclear matter and formation of hadronic and baryonic clusters in central nucleus-nucleus collisions.

II.2. Sources of the data. Most of the data on nucleus-nucleus collisions, used in this chapter, are at energies of the Dubna synchrophasotron i.e. at 4.1-4.5 A GeV/c. Scaning, measurements of emulsion plates and analysis of data were carried out either by the emulsion collaboration (including the author) or by the author individually. Some works were carried out in the cities of Cairo and Sohag (Egypt), the others in: Dubna, Moscow, Leningrad, Tashkent, Alma-Ata, Dushanbe, Gatchina , Rostov on Don, Tbilisi and Yerevan (USSR), Bucharest (Romania), Rez and Kosice (Czechoslovakia), Krakov (Poland), Ulan-Bator (Mongolia). The details may be found in/2-35/. The beams used are: H, H^2, He^3, He^4, C^{12}, O^{16}, Ne^{22}, Mg^{24} and Si^{28}.

II.3. Typical experimental procedure. Stacks of Br-2 nuclear emulsions were exposed to 4.5A GeV/c (e.g) Mg^{24} beam at the Dubna synchrophastron. The stacks consisted of 48 pellicles having dimensions of 20 Cm X 10 Cm X 600 μm (undeveloped emulsion). The intensity of irradiation was

10^4 particles/cm^2 and the beam diameter was about 1 cm. Along the track double scanning was carried out, fast in the forward and slow in the backward direction. The scanned beam tracks were further examined by measuring the delta-electron density on each of them to exclude the tracks having charge less than the beam particle charge. The one-prong events with an emission angle of secondary particle track less than three degrees and without visible tracks from excitation or disintegration of the target nucleus were excluded. These events were considered to be elastic scattaring. The secondary particles are classified into three classes. The first class consists of black particles track "b" having a range $L \lesssim 3$ mm in emulsion which corresponds to proton kinetic energy of < 26 MeV, Table 1 presents the kinetic energy of different black particles.

Table (1): The kinetic energy for different black track particles with L<3 mm.

Particle	Kinetic energy T MeV
T^1	T < 12 MeV
K	T < 20 MeV
H^1	T < 27 MeV
He^4	T < 105 MeV
Li	T < 184 MeV
Be	T < 210 MeV

The second class includes grey particle tracks "g" having relative ionization I* (=I/Io)>1.4 and L>3 mm which corresponds to a proton kinetic energy from 26 to 400 MeV. Where I is the particle track ionization and I_o is the ionization of a shower track in the narrow forward cone of an opening angle of 3°. Table 2 shows the kinetic energy of several grey particles. The "b" and/or "g" particle tracks are called heavy ionizing particle track "h".

Table (2): The kinetic energy for different grey track particles with L>3 mm, I* > 1.4.

Particle	Kinetic energy T MeV
π	$12 \lesssim T \lesssim 60$ MeV
K	$20 \lesssim T \lesssim 212$ MeV
H^1	$27 \lesssim T \lesssim 400$ MeV
H^2	$27 \lesssim T \lesssim 800$ MeV
He^4	$105 \lesssim T \lesssim 1600$ MeV

The third class is the shower particle tracks "s" having I* < 1.4 and $\Theta > 5°$. Tracks of this type but with an emission angle < 5° were further subjected to rigorous multiple scattering measurements for momentum determination and consequently for separating produced pions from single charged projectile fragments (protons, deutrons and tritons/35-38/. Table 3 presents the kinetic energy for some shower particles.

Table (3): The kinetic energy for different shower track particles..

Particle	Kinetic energy T MeV
π	> 60 MeV
K	> 212 MeV
H^1	> 400 MeV
H^2	> 800 MeV
H^4_e	>1600 MeV

(v) The multicharged Z > 2 PF are subdivided into Z = 2,3.... Z_b fragments according to the measured delta-electron and/or gap density. Thus, all particles were adequately divided into PF of Z = 1-Z_b, target fragments (TF), i.e. h particles, and the generated s particles. The total charge of the PF, $Z^* = \sum_i n_i Z_i$, was calculated

in each star, where n_i, is the number of fragments of charge Z_i in an event. For each track we obtained from measurements: (a) the polar angle Θ, i.e. the space angle between the direction of the beam and that of the given track and (b) the azimuthal angle Φ, i.e. the angle between the projection of the given track in the plane normal to the beam and the direciton perpendicular to the beam in this plane (in an anticlockwise direction).

II.4. **Total Inelastic cross-section.** With the total scanned length measured and the corresponding number of inelastic interactions counted, the nuclear, interaction mean free path of the beam nucleus in emulsion can be calculated. Table 4 presents the values of λ_B for different projectiles most of them at 4.5A GeV/c. The mean free path λ_B of a projectile nucleus in emulsion is given by:

$$\frac{1}{\lambda_B} = \sum_i n_i \sigma_{Bi} \quad \ldots\ldots\ldots \quad (1)$$

where n_i is the composition of the nuclear component i in emulsion and σ_{Bi} is the interaction cross-section between the projectile nucleus and the i th target nucleus. Equation 1 implies that $1/\lambda_B$ is a quadratic function of $A_B^{1/3}$. For comparison of the data in table 4, Fig. 1 shows a plot of $1/\lambda_B$ aganist $A_B^{2/3}$. The points are an obvious good fit to straight line $1/\lambda_B = (0.029 \pm 0.009). \pm (0.008 \pm 0.002) A_B^{2/3}$.

A similar result has been obtained at 2.1 GeV/c ref/36/. The reaction cross-section for a high energy heavy ion incident on a complex target nucleus has been extensively studied. An emperical geometrical formula first proposed by Bradt and Peters/37/

$$\sigma_{BT} = \pi r_o^2 (A_B^{1/3} + A_T^{1/3} - b)^2 \quad \ldots\ldots\ldots \quad (2)$$

where σ_{BT} is the reaction cross-section of the beam nucleus with the target one, A_B and A_T are the mass numbers of the beam and target nuclei respectively, b is an overlapping parameter.

Table (4). The mean free path λ_B for different projectiles

Beam nucleus	λ_B cm	Ref.
H^2	26.9 ± 0.6	9
H_e^3	23.7 ± 0.7	38
H^4	19.5 ± 0.3	39
C^{12}	13.7 ± 0.1	9
N^{14}*	13.1 ± 0.5	40
O^{16}	13.0 ± 0.5	41
N_e^{22}	9.92± 0.3	42
M_g^{24}	10.2 ± 0.6	50
S_i^{28}	8.7 ± 0.3	43
F_e^{56}	7.4 ± 1.4	44

* at 2.1 A GeV/C.

Fig. 2 represents the relation between $\sqrt{1/\lambda_B}$ and $(A_B^{1/3} + A_T^{1/3})$, where A_T (=70) is the effective mass number of the average emulsion nucleus. The points are the experimental data of Table 4. These points are fitted well by the expression $(1/\lambda_B)^{1/2} = (-0.191 \pm 0.040) + (0.072 \pm 0.007)(A_B^{1/3} + A_T^{1/3})$. To deduce the parameters b and r_o we adopted the following scheme: $1/\lambda_B = \sum n_i \sigma_i$, where n_i is the number of ith atoms per cubic centimeter and σ_i is the corresponding C.S.

$$\sigma_{Bi} = \pi r_o^2 (A_B^{1/3} + A_i^{1/3} - b)^2.$$

This gives a system of equations in b and r_o. The best solutions for these equations are r_o = 1.44 ± 0.01 fm and b= 1.22 ± 0.02.

It has been argued in literature that the overlapping parameter b can be parameterized in terms of A_B and A_T. Thus equation 2 can be rewritten in the form.

$$\sigma_{BT} = \pi r_o^2 [A_B^{1/3} + A_T^{1/3} - \beta (A_B^{-1/3} + A_T^{-1/3})]^2 \quad \ldots\ldots (3)$$

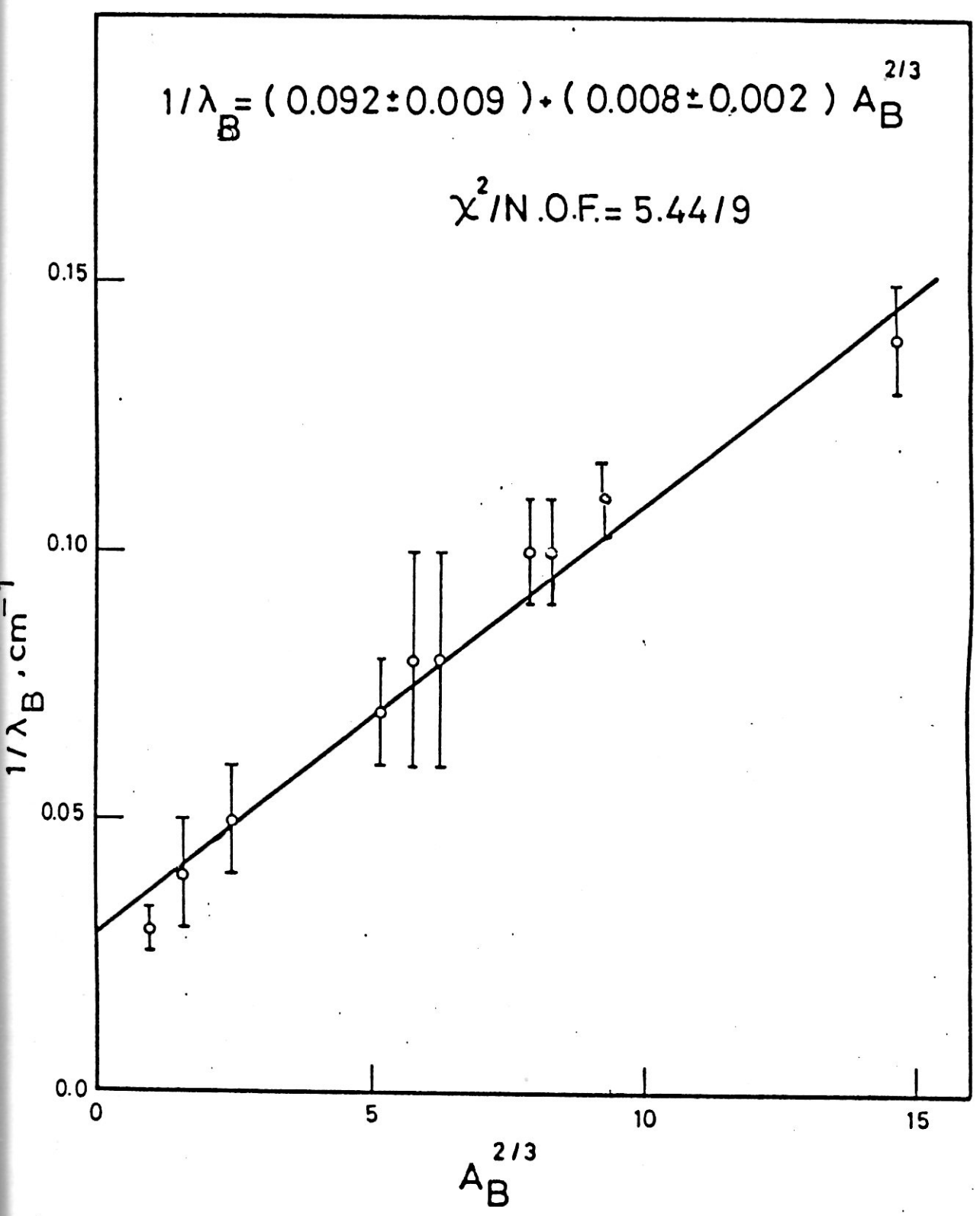

Fig.(1): The inverse of the inelastic mean free path $1/\lambda_B$ plotted against $A_B^{2/3}$ where A_B is the incident projectile mass number.

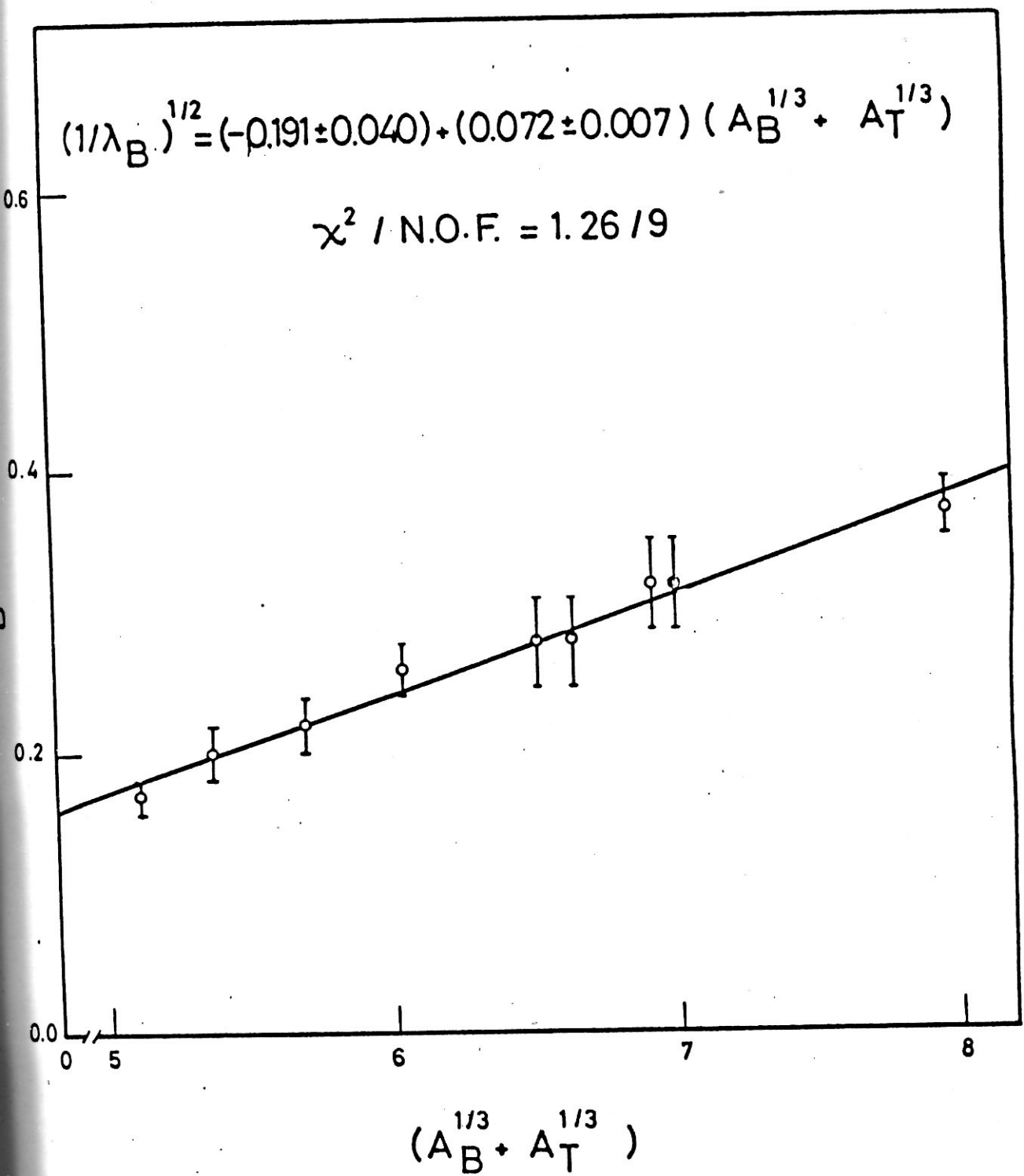

Fig.(2): The dependence of $\sqrt{1/\lambda_B}$ on $(A_B^{1/3} / A_T^{1/3})$ where A_B and A_T are the mass numbers of the colliding nuclei.

The previous procedure gave $r_o = 1.30 \pm 0.01$ fm and $\beta = 0.80 \pm 0.02$.

These results show that the interaction cross-sections of nuclei are essentially independent of the incident energy in the few GeV region. The interaction cross sections of nuclei are successfully explained by the geometrical cross section including an overlapping parameter. This Parameter depends on the size of the interacting nuclei.

II.5. **The multiplicity characteristics.** The multiplicity characteristics provide a valuable tool to investigate the mechanism of nucleus-nucleus interaction. In the present section, we study the n_s-, n_g- and n_b- distributions and their average values. A trial is made to regenerate theoretically the n_s-distribution using a geometrical picture of the nucleus-nucleus collision. A comparison is made with the superposition model/45/ using the relation between the dispersion and the average multiplicity. A direct comparison is carried out between experimental data and the cascade evaporation model CEM/6,7/.

It is widely believed that the inclusive nucleus-nucleus data can be explained within the framework of superposition models/45/. It is expected that in nucleus-nucleus collisions the distribution of s-particles will be wider than the corresponding one in hadron-nucleus interactions. This is due to the large variations of the impact parameters, several superposition models/45/ predicted that the ratio of the dispersion $D(=\sqrt{\langle n_s^2 \rangle - \langle n_s \rangle^2})$, to the average multiplicity of shower particles, $\langle n_s \rangle$, is about twice the corresponding ratio for proton-nucleus interactions. The shaded area represents the prediction of the superposition models ($D/\langle n_s \rangle = 0.8 - 1.3$) depending upon the model. The experimental points are data from different projectile and target at various energies/46/. One can observe the universaltiy of $D/\langle n_s \rangle$ ratio which

The previous procedure gave $r_o = 1.30 \pm 0.01$ fm and $\beta = 0.80 \pm 0.02$.

These results show that the interaction cross-sections of nuclei are essentially independent of the incident energy in the few GeV region. The interaction cross sections of nuclei are successfully explained by the geometrical cross section including an overlapping parameter. This Parameter depends on the size of the interacting nuclei.

II.5. **The multiplicity characteristics.** The multiplicity characteristics provide a valuable tool to investigate the mechanism of nucleus-nucleus interaction. In the present section, we study the n_s-, n_g- and n_b- distributions and their average values. A trial is made to regenerate theoretically the n_s-distribution using a geometrical picture of the nucleus-nucleus collision. A comparison is made with the superposition model/45/ using the relation between the dispersion and the average multiplicity. A direct comparison is carried out between experimental data and the cascade evaporation model CEM/6,7/.

It is widely believed that the inclusive nucleus-nucleus data can be explained within the framework of superposition models/45/. It is expected that in nucleus-nucleus collisions the distribution of s-particles will be wider than the corresponding one in hadron-nucleus interactions. This is due to the large variations of the impact parameters, several superposition models/45/ predicted that the ratio of the dispersion $D(=\sqrt{\langle n_s^2 \rangle - \langle n_s \rangle^2})$, to the average multiplicity of shower particles, $\langle n_s \rangle$, is about twice the corresponding ratio for proton-nucleus interactions. The shaded area represents the prediction of the superposition models ($D/\langle n_s \rangle = 0.8 - 1.3$) depending upon the model. The experimental points are data from different projectile and target at various energies/46/. One can observe the universaltiy of $D/\langle n_s \rangle$ ratio which

is independent of the incident energy, projectile and target masses. A similar universality was reported for proton-nucleus collisions[47]. From Fig. 3 one may conclude that the superposition models are consistent with the experimental data of nucleus nucleus interactions.

To investigate the dependence of the average multiplicity $\langle n_s \rangle$ on the mass number of the beam nucleus A_B, we consider the reactions shown in Table 5. In these reactins, the momentum per incident nucleon is constant and it equals to 4.5 GeV/c.

Table (5). The everage multiplicities $\langle n_s \rangle$ for reactions of different projectiles with emulsion at 4.5 A GeV/c.

Projectile	$\langle n_s \rangle$	Ref.
H	1.60 ± 0.10	
H^4	3.40 ± 0.10	48
C^{12}	7.60 ± 0.20	
N_e^{22}	10.53 ± 0.05	49
M_g^{24}	11.00 ± 0.60	50

The experiments were carried out under the same conditions. Fig.4 shows the dependence of the average multiplicity $\langle n_s \rangle$ on the mass number of the beam nucleus A_B. The points are the experimental data while the continuous line is the result of fitting by the relation $\langle n_s \rangle = K A_B^{\alpha}$. The results of fitting gave that K=1.55 $\pm$ 0.28 and $\alpha = 0.62 \pm 0.02$. This result agrees with the fact that the interaction cross section is proportional to $A_B^{2/3}$ and does not contradict the superposition models.

It is more convenient to study the dependence of the average multiplicity $\langle n_s \rangle$ on the average number of interacting projectile nucleons $\langle \nu \rangle = A_B \sigma_{P_T} \sigma_{B_T}$ where σ_{P_T} is the reaction cross section of protons with the

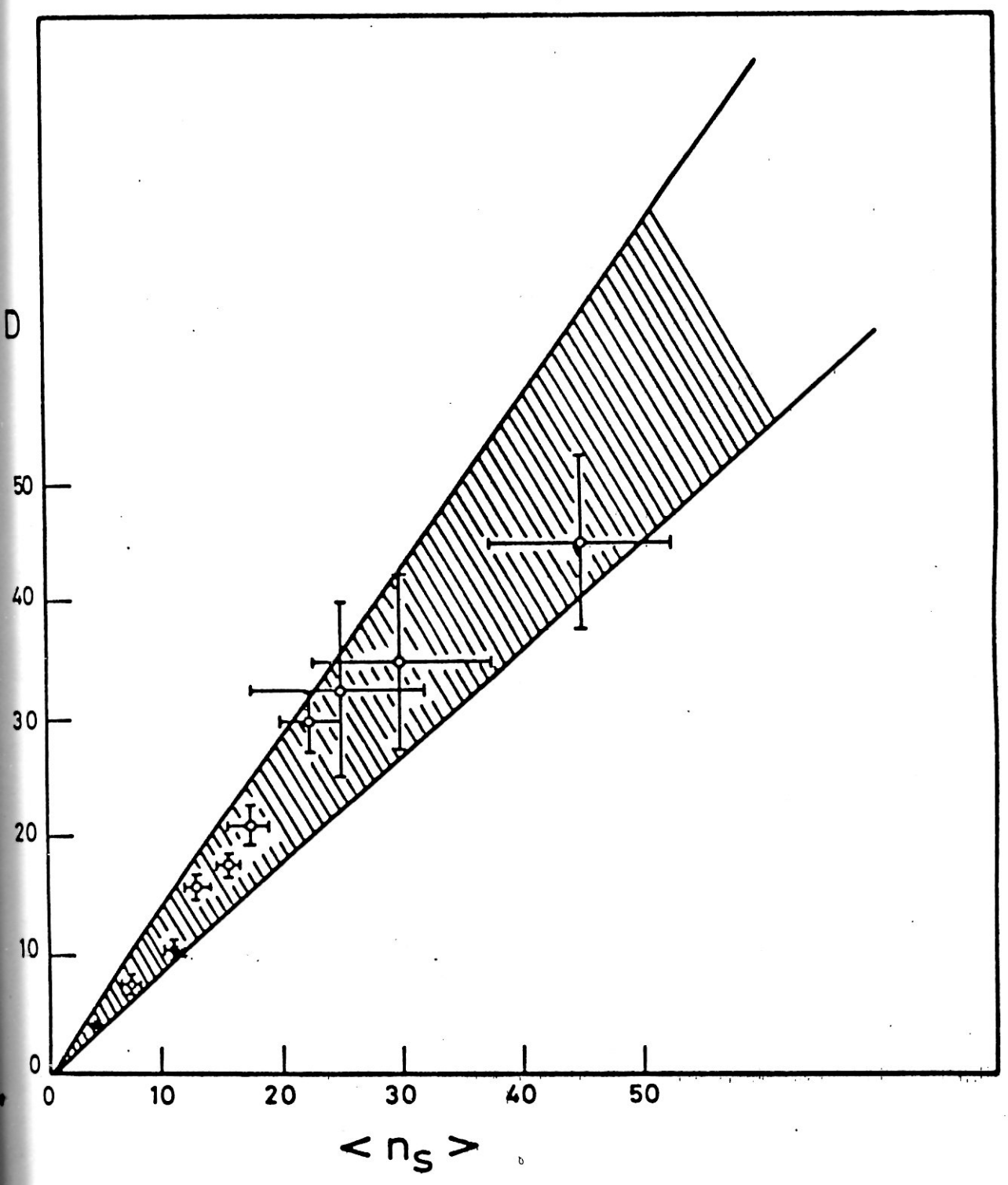

Fig. (3): The dependence of D on $< n_s >$. The shaded area are due to superposition models /45/. The points are experimental data.

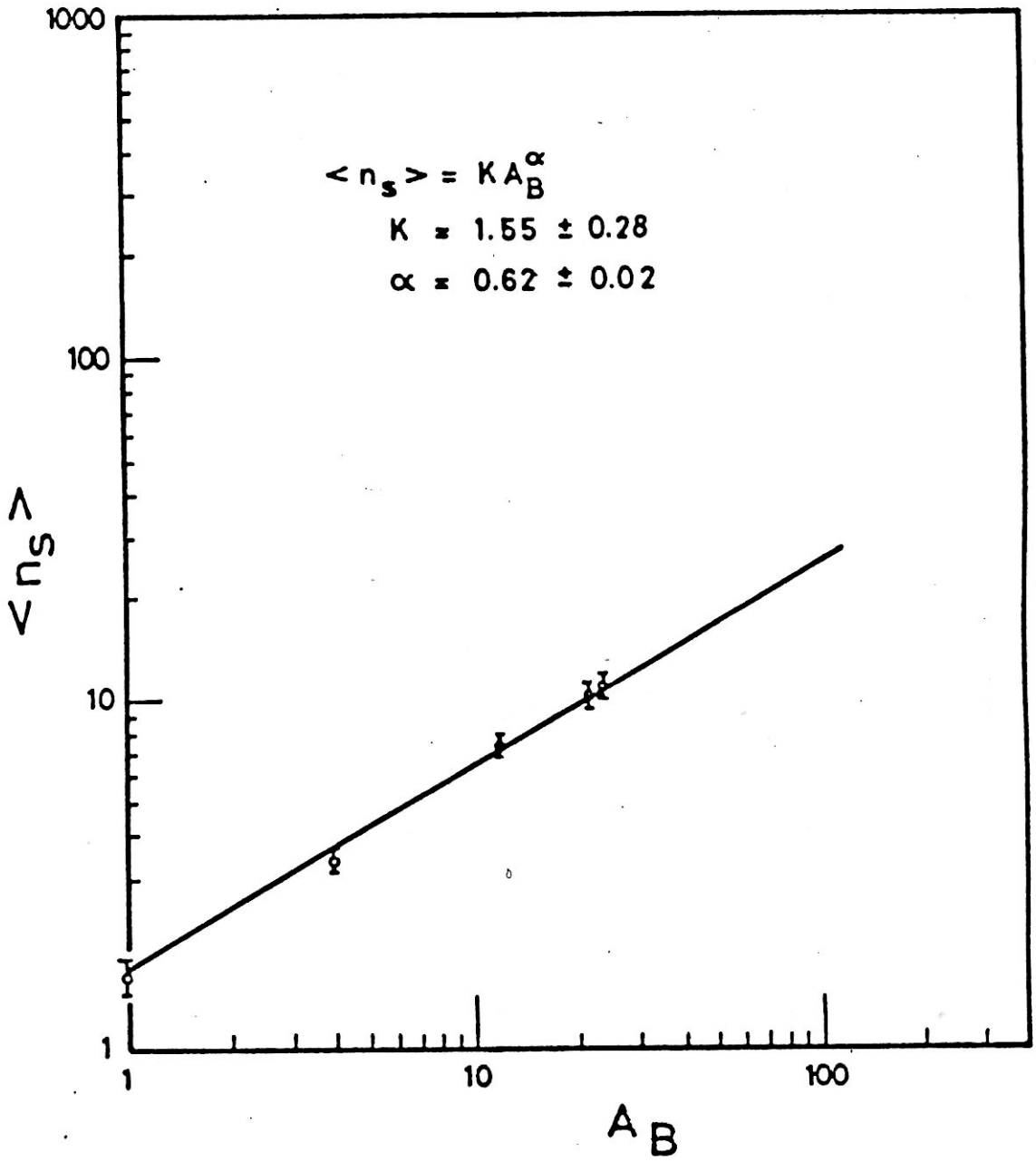

Fig. (4): The average multiplicity of s-particles as a function of the projectile mass number A_B in nucleus-nucleus interactions at 4.5 A GeV/c.

target nucleus and $\sigma_{A_BA_T}$ is reaction cross section of the beam nucleus A_B with the target one A_T, both at the same energy per nucleon. In Fig. 5, we present the average multiplicity $\langle n_s \rangle$ versus the average number of interacting projectile nucleons $\langle \nu \rangle$. The experimental points are fitted by the relation $\langle n_s \rangle = a + b \langle \nu \rangle$, where a and b were found to be (0.69 ± 0.03) and (0.96 ± 0.08) respectively. This shows the close similarity between the nucleus-nucleus interactions and the hadron-nucelus ones.

It is worth-while to study the dependence of the average multiplicity on the number of interacting protons and/or nucleons from the projectile and target nuclei. First we study the average multiplicity $\langle n_s \rangle$ as a function of R,

$$R = (Z_B A_T^{2/3} + Z_T A_B^{2/3}) / (A_B^{1/3} + A_T^{1/3})^2 \quad \ldots\ldots (4)$$

Where R is some geometrically determined number of interacting protons from the projectile and target nuclei, Z_B and A_B are the charge and mass nubmers of the beam nucleus, Z_T and A_T are the same for the target nucleus. Fig. 6 shows the dependence of the average multiplicity $\langle n_s \rangle$ on the number of interacting protons R for the data of Table 5. The experimental points were fitted by the relation $\langle n_s \rangle = KR^{\alpha}$. The values obtained from the fitting are given in Table 6. Fig. 6 and Table 6 show that $\langle n_s \rangle$ increases in proportion to R. It should be noted that the denominator in 4 is proportinal to the interaction cross section in the hard spheres model without overlap. It would be more accurate if one considers the overlap of nucles and their curvature, i.e. the relation 4 is modified to:

$$R = (Z_B A_T^{2/3} + Z_T A_B^{2/3}) / (A_B^{1/3} + A_T^{1/3} - b)^2 \quad \ldots (5)$$

This modification removes the linearity of $\langle n_s \rangle$ versus R and the exponent becomes greater than before.

Similarly, we study the dependence of the average multiplicity $\langle n_s \rangle$ on the number of interacting nucleons from both nuclei. Thus we define R_A as:

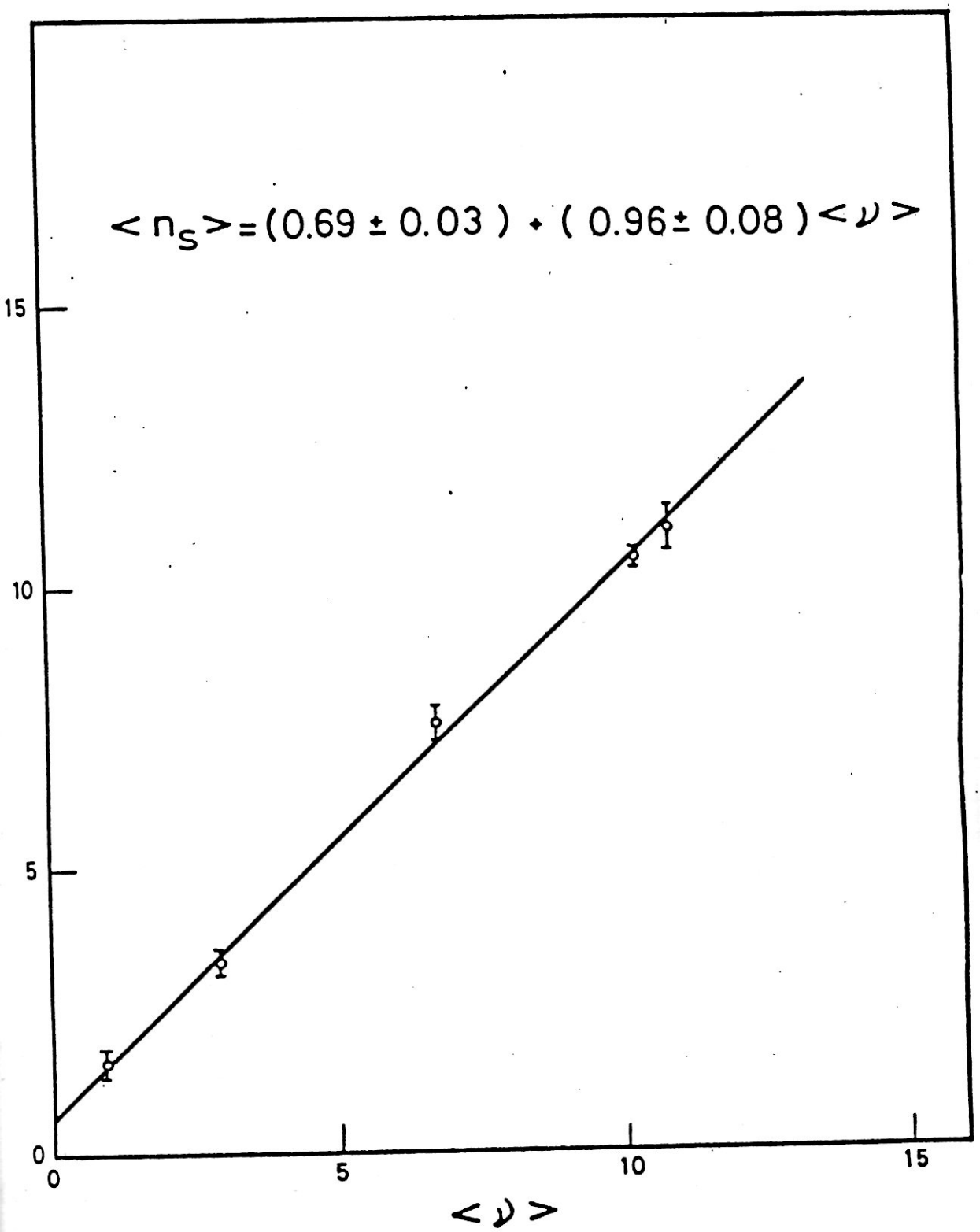

Fig.(5) The average multiplicity $< n_s >$ as a function of the average number of interacting projectile nucleons $< \nu >$ in nucleus - nucleus interactions at 4.5 A GeV/c.

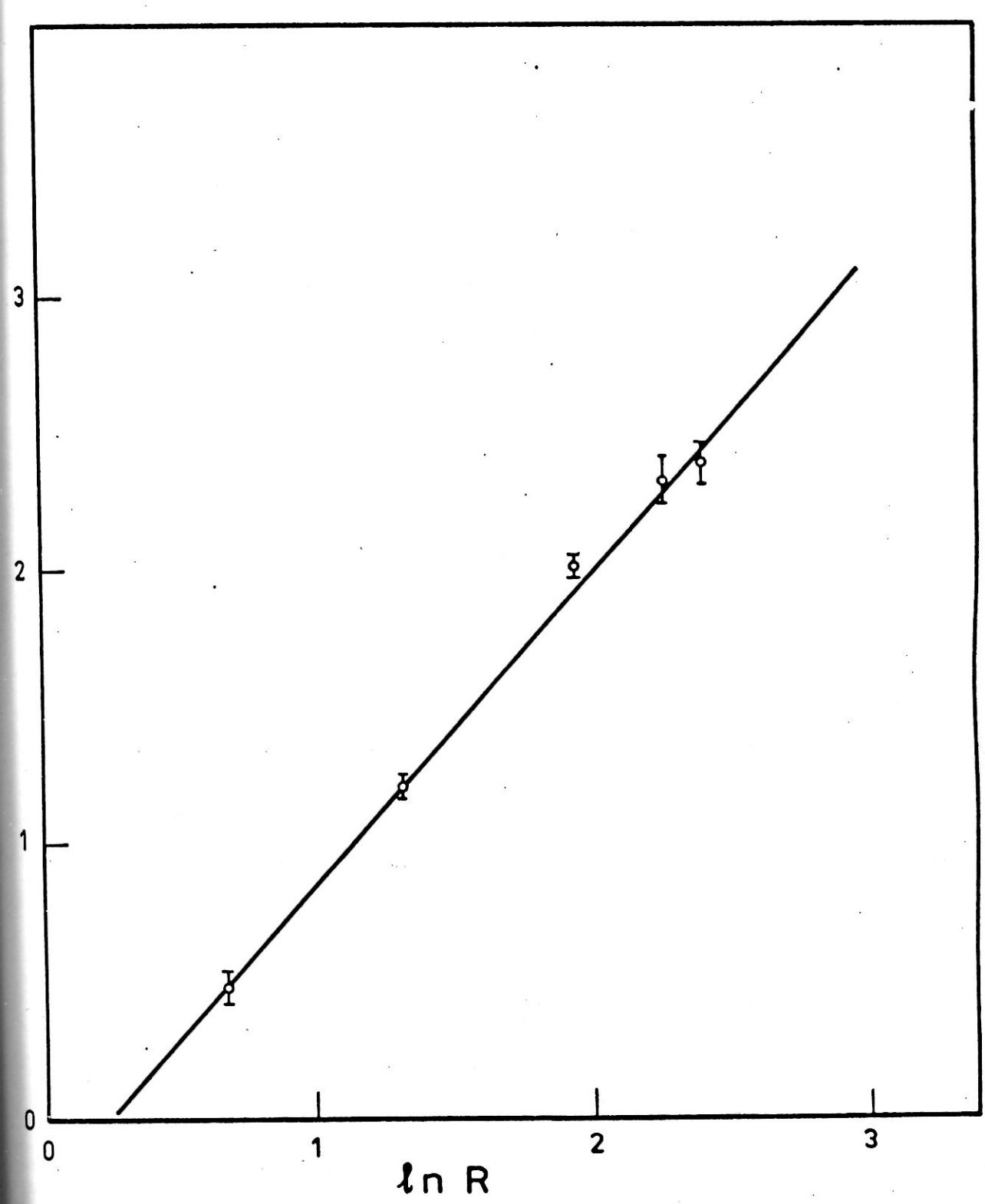

Fig.(6): The dependence of the average multiplicity $\langle n_s \rangle$ on the number of interacting protons from both nuclei.

$$R_A = (A_B A_T^{2/3} + A_T A_B^{2/3}) / (A_B^{1/3} + A_T^{1/3})^2 \qquad (6)$$

Where R_A is some geometrically determined number of interacting nucleons from both interacting nuclei. Fig. 7 shows the average multiplicity $\langle n_s \rangle$ versus the number of interacting nucleons R_A, the experimental points are fitted by relations $\langle n_s \rangle = KR^{\alpha}$. The results of fitting is given in Table 6.

Table (6). Results of approximation of the dependence of $\langle n_s \rangle$ on R_A in accordance with equation $\langle n_s \rangle = KR^{\alpha}$ for charged paticles.

R from relation	α	K
(5)	1.16 ± 0.03	0.74 ± 0.04
(6)	0.80 ± 0.06	0.85 ± 0.06

Let us study the dependence of the average multiplicity $\langle n_s \rangle \sim (\bar{A})^{\alpha}$, where $\bar{A}$ is defined as:

$$(A_B^{1/3} + A_T^{1/3})^3 \qquad (7)$$

$$\bar{A} = (A_B^{1/3} + A_T^{1/3} - b)^3 \qquad (8)$$

$$[(A_B^{1/3} + A_T^{1/3} - b_o (A_B^{1/3} - A_T^{1/3})]^3 \qquad (9)$$

This definition of A originates from simple geometrical models of interaction of nuclei. Fig. 8 shows the dependence of the average multiplicity $\langle n_s \rangle$ on $\bar{A}$. The results of fitting by the relation $\langle n_s \rangle \sim (\bar{A})^{\alpha}$ are given in Table 7.

Table (7). Results of approximation of the dependence of $\langle n_s \rangle$ on A in accordance with equation $\langle n_s \rangle \sim (\bar{A})^{\alpha}$ for charged particles.

A is taken from relation	α
(7)	2.06 ± 0.06
(8)	1.65 ± 0.04
(9)	1.93 ± 0.05

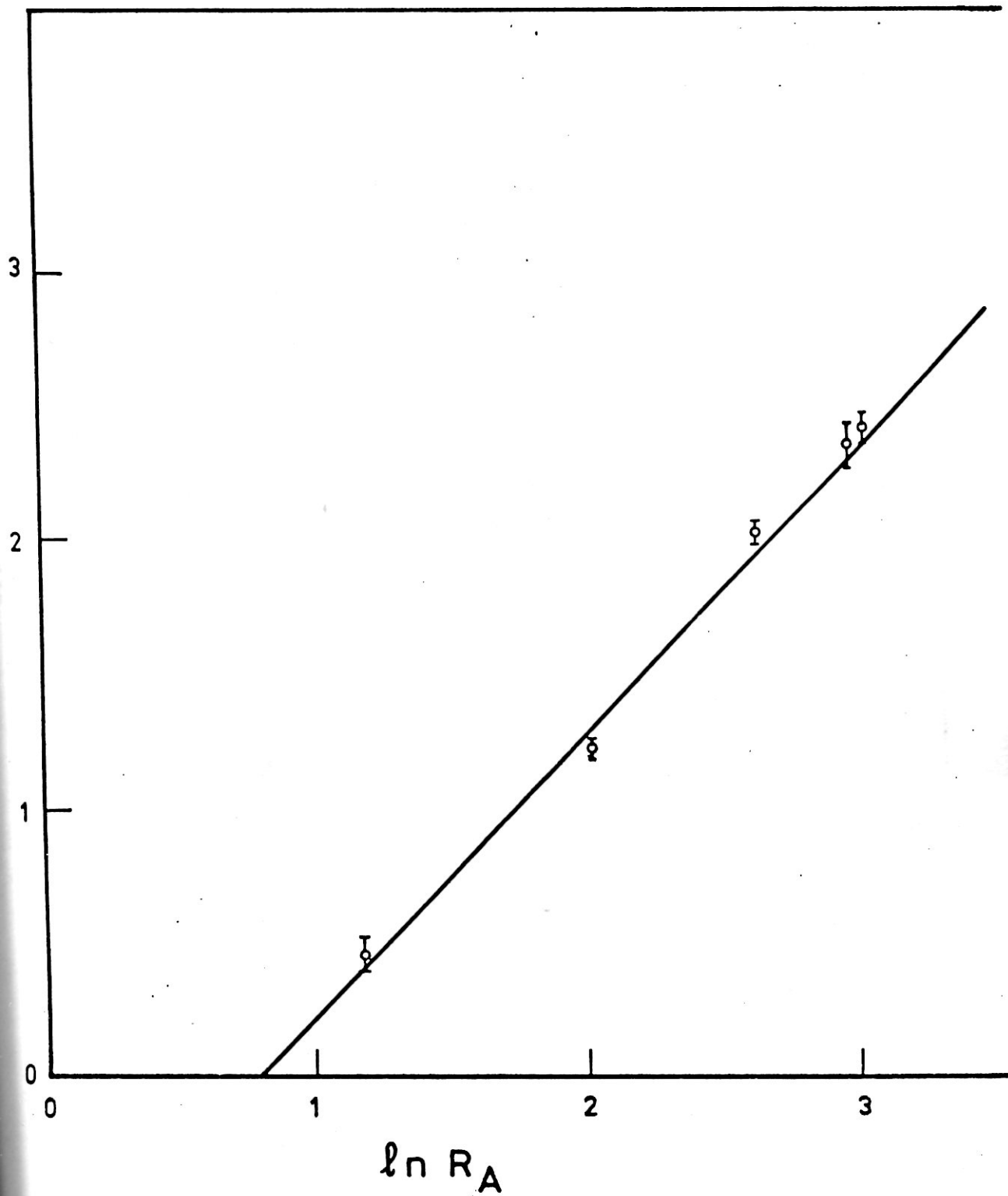

Fig.(7) The dependence of the average multiplicity $< n_s >$ on the number of interacting nucleons R_A from both nuclei.

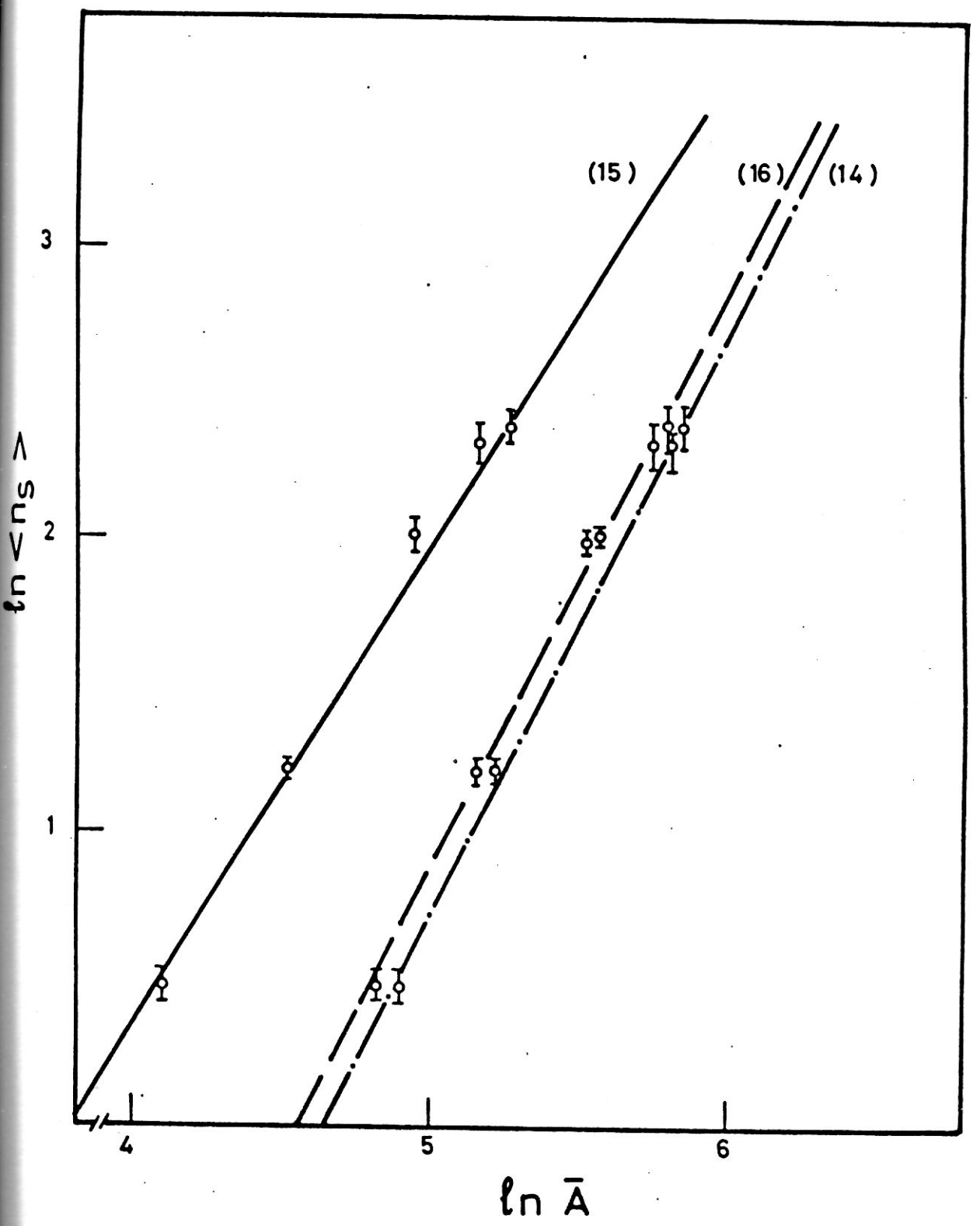

Fig.(8): The dependence of the average multiplicity $\langle n_s \rangle$ on the man numbers of the colliding nuclei, where $\bar{A}$ is some geometerically determined parameter which is proportional to the masses of the interacting nuclei.

The investigation of the mean free path of different nuclei in emulsion has shown that the interaction cross section of nucleus-nucleus interactions is independent of energy in the range of few GeV per nucleon. The cross sections of nuclei are will fitted by the geometrical formulae with an overlapping paramter. The overlapping parameter depends on the mass numbers of the interacting nuclei,

The systematic study of the multiplicity characteristics and their regularities had proved the validity of the incoherent superposition models. The nucleus-nucleus interactions at a few GeV/c per nucleon can be viewed as a chain of hadron nucleus collisions at the same energy per nucleon.

II.6. Calculation of n_s distribution using geometrical picture. When a relativistic heavy ion projectile collides with a target nucleus there should be during a primary fast stage a localization of the interaction to overlapping domain of target and projectile undisturbed. The surface energy and dissipation of compressional well as reabsorption of pions and nucleons emitted from the primary interaction region will excite these remnants. This idea leads to the separation of the nucleons in the system into participants and spectators with respect to the fast interaction stage. The model assumes that the two nuclei sweep out cylindrical cuts through each other. The average internal kinetic energy per nucleon is much higher than the binding energy per nucleon. The velocity regions near the target and projectile will contain contribution from spectator decay which are not treated by the fireball model. Also, the expanding fireball nucleons may in part coalesce to form clusters. The model is formally described, by assuming spherical nuclei, with radii equal to $R = r_o\ A^{1/3}$ fm. Where $r_o = 1.36$, and straight trajectories. One can calculate as a function

of impact parameter b the number of participant nucleons from the target N_t and projectile N_p calculating the volume of intersection of a sphere and a cylinder. This geometrical concept is shown in Fig. 9. The number of participating nucleons is given by the relation(10); where Z_i and A_i are the charge number and mass number of the target or projectile nucleus.

$$N(b)=\sum_i \left(\frac{Z_i}{A_i}\right)N_i(b) \quad ,i=t,p \text{ ------ ..... } (10)$$

One can calculate the velocity of the center of mass of the participant nucleon in the Laboratory system

$$\beta_{C.M}= P_{Lab}/E_{Lab}=\frac{N_p[t_p(t_p+2m)]^{1/2}}{(N_p+N_t)m+N_p t_p} \quad \text{----} \quad (11)$$

where P_{Lab} is the momentum of the system in the Lab, E_{Lab} is the total energy (kinetic energy + mass) of the system in the Lab, t_p is the projectile incident kinetic energy per nucleon, and m is the mass of a bound nucleon, taken to be 0.931 GeV.
The total energy in the center of mass of the fireball is written as

$$E_{C.M}=(E^2_{Lab}-P^2_{Lab})^{1/2}= [(N_p+N_t)^2m^2+2N_pN_tmt_p]^{1/2} \text{ ----------} (12)$$

where N_p, N_t are the numbers of nucleons from the projectile and target respectively and m is the nucleon rest mass.

Consider a high energy nucleus-nucleus collision at impact parameter b in the C.M. system the projectile is assumed to sweep a cylinderical cut inside the target nucleus so the number of participating nucleons of the target as a function of the impact parameter involves the calculation of the volume of intersection of a ssphere and a cylender, this problem is solved by J. Gosset et al./51/.

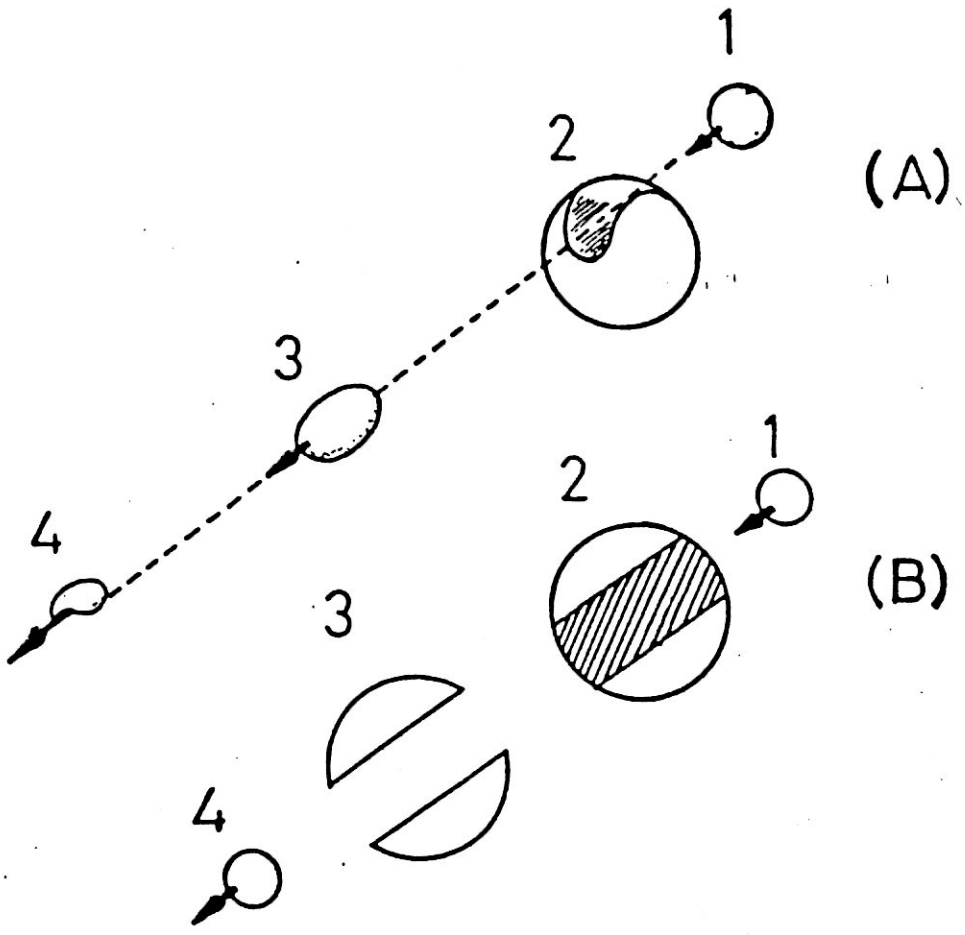

Fig.9. In the framework of fireball model, the target and projectile are assumed to make clean cylindrical cuts through each other leaving a target spectator residue, and if the impact parameter is large enough also a projectile spectator. The fireball is made up from the participant nucleons which are mutually swept out in the primary interaction. A- peripheral collision and B-Central collision (1- projectile, 2-target, 3-target spectators, 4-fireball and participant region which is dashed).

Let $N_p(b)$ and $N_t(b)$ be the number of participating nucleons from the projectile and target at impact parameter b, so that the square of the center of mass energy S(b) is written as in the form.

$$S(b) = [N_p(b)]^2 m^2 + 2N_p(b) N_t(b) mE \qquad (13)$$

where E is the total energy/nucleon of the projectile in the Lab. system, $E = \sqrt{p^2 + m^2}$, p(=4.5 GeV/c) is the momentum and m is the free nucleon rest mass, m=0.938 GeV.

Now we show how to determine $N_t(b)$ and $N_p(b)$/52,53/

These values depend on ν & β where $\nu = \frac{R_p}{R_p+R_t}$, $\beta = \frac{b}{R_p + R_t}$ where R_p and R_t are the projectile and target radii ($R_p = r_o A_p^{1/3}$, $R_t = r_o . A_t^{1/3}$). r_o =1.36 and A_p , A_t are the mass numbers of the projectile and target respectively.

$$N_p(b) = A_p F(\nu, \beta) \qquad N_t(b) = A_t F(\nu, \beta) \qquad (14)$$

where F is dimensionless function specifying the relative sizes of the two nuclei. The dimensionless variable specifies the impact parameter b. The variables ν, β range from zero to one these limits define a square with unit side in the space of ν and β as shown in Fig. 10, the following are approximate formulas for F. in the four sectors of the square indicated in Fig. 10.

1- If 0.5 and

$$F_I = [1-(1-\mu^2)^{3/2}][1-(\beta/\nu)^2]^{1/2} \qquad (15)$$

2- If $\nu \geq 0.5$ and $\beta \geq 2\nu - 1$.

$$F_{II} = \frac{3}{4}(1-\nu)^{1/2}\left(\frac{1-\beta}{\nu}\right)^2 - \frac{1}{8}\left(\frac{3(1-\nu)^{1/2}}{\mu} - \frac{[1-(1-\mu^2)^{3/2}][1-(1-\mu)^2]^{1/2}}{\mu^3}\right) \times \left(\frac{1-\beta}{\nu}\right)^3 \qquad (16)$$

3- If $\nu \leq 0.5$ and $\beta \geq 1-2\nu$.

$$F_{III} = \frac{3}{4}(1-\nu)^{1/2}\left(\frac{1-\beta}{\nu}\right)^2 - \frac{1}{8}[3(1-\nu)^{1/2}-1]\left(\frac{1-\beta}{\nu}\right)^3 \qquad (17)$$

4- If $\nu < 0.5$ and $\beta < 1-2\nu$.

$$F_{IV} = 1 \qquad (18)$$

The abbreviation $\mu = \frac{1}{\nu - 1} = \frac{R_t}{R_p}$ has been used, the four sectors correspond to the following situations.

1- A cylinderical hole is gouged in the nucleus A_p which is larger than A_t.

2- A cylinderical channel is gouged in A_p, with a radius smaller than that of A_p.

3- A cylindrical channel is gouged in A_p with a radius larger that that of A_p.

4- All of A_p is obliterated by A_t, whose radius is larger than that of A_p.

The above approximate expressions for F are based on solutions for a number of limiting situations, when analytical expressions can be derived, e.g. close to the edges of the square in Fig. 10.

In the present calculation it is assumed that the multiplicity distribution depends only on the square of the center of mass energy, S, so the multiplicity distribution of the shower particies in nucleus-nucleus collision at impact parameter b has the same form as that obtained from nucleon-nucleon collision at the same value of S(b), and has the following Gaussian probability distribution function.

$$P(n_s,b)=\frac{1}{\sqrt{2\Pi D(b)}}\, e^{-[n_s-\bar{n}_s(b)]^2/2D^2(b)} \qquad \text{----------(19)}$$

where

$$\bar{n}_s(b)= 1.291\, S(b)^{0.29} \qquad \text{----------} \qquad (20)$$

and

$$D(b)= 0.6(\bar{n}_s(b)-1) \qquad \text{----------} \qquad (21)$$

where $n_s(b)$ is the average number of showers produced at impact parameter b and it is taken from pp data at the same value of s (b).

Equations (19,20) are well tested (experimentally) relations/15,54/.

The scheme of calculations is as follows:

(1) The kind of interacting nuclei e.g. the projectile is He^3 (A_p=3) or C^{12}(A_p=12) and the target is A_g emulsion nucleus (A_t=108).

(2) The parameter ν is defined and the parameter β is varied from 0 to 1. At each value of β (each value of b), the number $N_p(b)$ and $N_t(b)$ are calculated according to equations (14) and (15) to (18). Thus S (b) is calculated from equation (13). Consequently $n_s(b)$ and D(b) are calculated respectively from equations (20) and (21).

(3) The multiplicity distribution P (n_s,b) at certain impact parameter b is calculated from (19).

(4) The total multiplicity distribution of shower particles from these two interacting nuclei is obtained by integrating P (n_s,b) over all possible values of impact parameter b o b R_p+R_t

$$P(n_s,t)=\int_{.}^{R_p+R_t} P(n_s,b)2\Pi bdb \Big/ \int_{.}^{R_p+R_t} 2\Pi bdb \quad ,(t=Ag,Br,....) \text{---} (22)$$

(5) The net multiplicity distributions of ^{3}He-Emulsion and C^{12}-emulsion are calculated by repeating steps (1) to (4) for all emulsion nuclei and summing over all nuclei taking into consideration a statistical weight factor for each nucleus $W_{t,i}= n_i \sigma_i / \sum n_i \sigma_i$ where n_i is the number of i th atom/c.c and σ_i is the interaction inelastic cross section of ^{3}He and C^{12} with the i th emulsion nucleus which is calculated from Bradt-Peters equation.

$$\sigma_i = \sigma_{pti} = \Pi r_0^2 (A_p^{1/3} + A_t^{1/3} - \Delta)^2 \text{ ---------- } (23)$$

Where Δ is the overlap parameter [Δ =1.56 - 0.2 ($A_p^{1/3} + A_t^{1/3}$)]. Thus the net multiplicity distribution of shower particles for ^{3}He and C^{12} with emulsion at 4.5 A GeV/c is given by

$$P(n_s)=\sum P(n_s,t)\, W_{ti} \quad \text{such that} \quad \sum W_{ti} = 1 \text{ ------} (24)$$

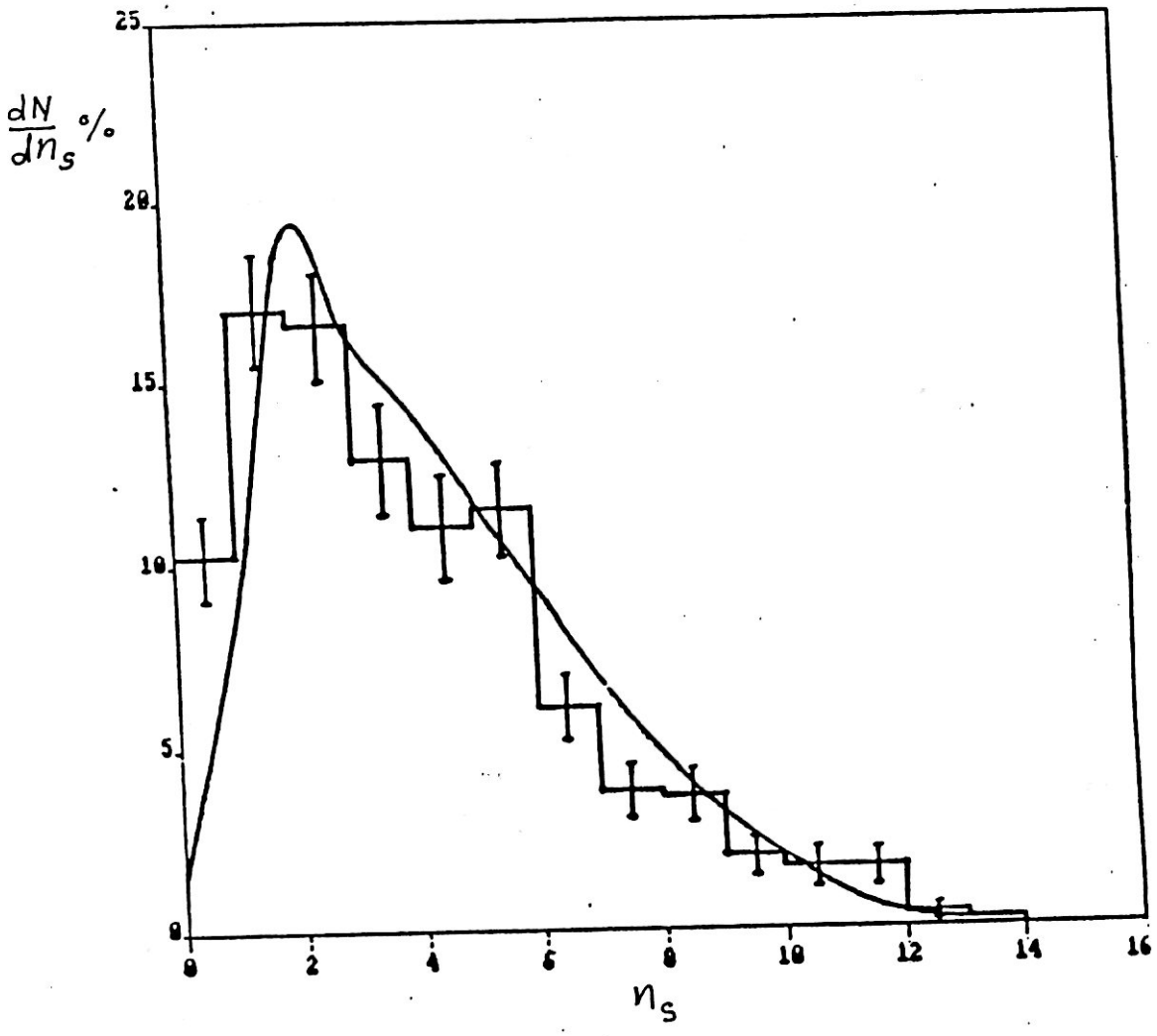

Fig. 11

The net multiplicity distribution of shower particles produced in 4.5 A GeV/c ^{3}He-emulsion interactions. The histogram is the experimental data while the curve is the theoretical calculations Both distributions are normalized to 100 .

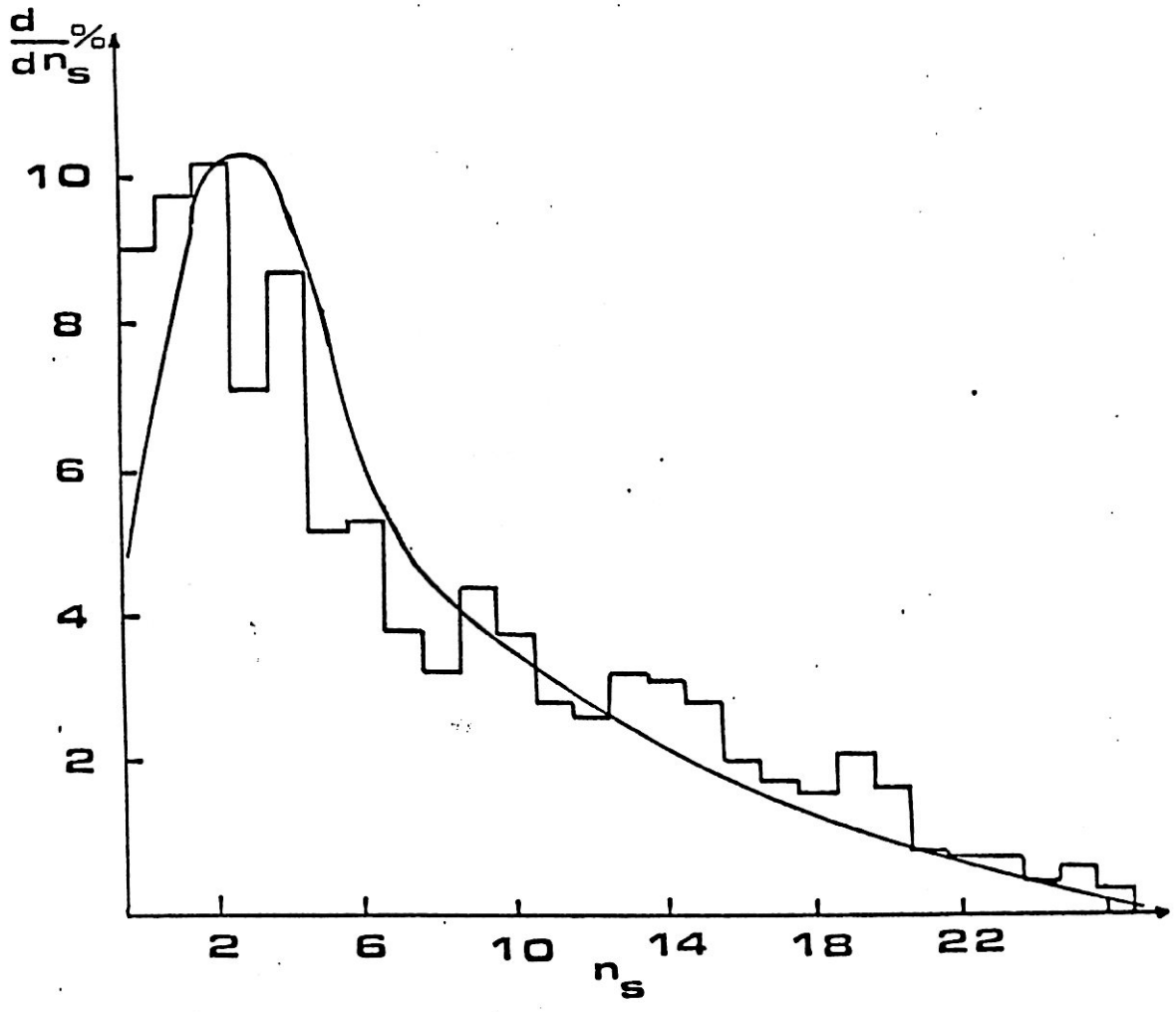

Fig. 12. Shower particle multiplicity distribution produced in ^{12}C - emulsion interactions at 4.2 GeV/c/nucleon . The histogram is the experimental data and the curve is the theoretical calculations.

Moreover in any step in which the probability is calculated we make sure that the total probability should be equal to unity.

A comparison of experimental n_s-distribution with the theoretically calculated one is shown in Figs. 11, 12. The histograms are the experimental data and the curves are the corresponding calculated multiplicity distribution of shower particles. The agreement between experimental data and theoretical calculations is good. This confirms that the nucleus-nucleus and nucleon-nucleus interactions are superposition of nucleon-nucleon interactions.

II.7. Comparison with the cascade evaporation model (CEM. In this section, we concentrate our attention to the comparison between the theoretical calculations of CEM and the experimental data of C^{12} + Em collisions at 4.5A GeV/c.

II.7.1. The cascading-evaporation model. The general physical features of this model remind us with the collision of two gas coulds. Each of the colliding nuclei in its own reference frame is treated as a Fermi gas of nucleons in the potential well $V(r)=B + P_F^2/2m$, where m is the mass of a free nucleon, B is the average binding energy of a nucleon inside a nucleus which nearly equals 7 MeV. The nuclear nucleons have a momentum distribution $W(p)dp \sim p^2 dp$, $0 \leq P \leq P_F \simeq P_F(r)$, isotropic in the momentum space. The maximum value of the local Fermi momentum $P_F(r)$ is expressed in terms of the nuclear density $\rho(r)$, $P_F(r) = \hbar [3\pi^2 \rho(r)]^{1/3}$, which is an approximation of two-parameter Fermi distributions with their parameters extracted from electron elastic scattering experiments. This distribution cuts off at a distance R, where $\rho(R)/\rho(0) = 0.01$. It is also supposed that for A nucleons inside the nucleus the distance between them is not smaller than $2r_c$, where r_c = 0.4 fm is the radius of

the nucleon core.

It was sugggested that the incident nucleus nucleon in the laboratory system can be considered as independent particle characterized by four-vector space-time $(\vec{r},t)$ and four-vector momentum effective mass $m_{eff} = \sqrt{E^2-P^2}=m-V(r)$. This is also valid for the target nucleus but in the coordinate system of the projectile.

The approximation of the independent particle with effective mass allows one to use the relativistic kinematics taking into consideration, in particular, the effect of relativistic compression and the symmetry of the problem with respect to the colliding nuclei. In fact, this is one of the basic assumptions of our model which turns the interaction of two complex systems to the interaction between their constitutents.

The dynamic of the interaction was followed in time with the help of the Monte-Carlo method. The model takes into consideration the interaction between nucleons of the two nuclei, also interaction of the cascading particles with the nucleons of both target and projectile. The incident particle can interact with any target nucleon which it can see in a cylinder of cross-sectional area $\pi(r_{int}+\lambda)^2$, where λ is the De Broglie wave length, r_{int} equals nearly the double value of the strong interaction range. Usually this value in the cascading calculation is taken to be 1.3 fm. Thus the probability of scattering on the k <u>th</u> nucleon, traversing without interaction (k-1) nucleons, is given by the binomial distribution

$$\omega_k = \sum_{i=1}^{k-1} (1-q_i)\, q_k$$

where the partial probability q_i (i=1,2,.....) is expresed in terms of interaction cross-section on the <u>ith</u> nucleon, σ_i.

$$q_i = \sigma_i / \pi (r_{int} + \lambda)^2$$

The time evolution of the interacting system is traced, At a fixed time t all possible collisions are raffled from which, is chosen, that which is realized before the others i.e. $t = \min(t_i)$, and the system is moved towards a new moment $t \rightarrow t + \Delta t$. Thus, for two particle collision the reaction characteristics are raffled and for nucleons the obeying of Pauli principle is checked.

The cascading stage ends when the interacting nuclei are separated by a distance such that their potential do not overlap further and all cascading particles are emitted from the nuclei or absorbed by them. The estimation of the residual nucleons in the potential well and their isotopic constitution gives the mass and charge number of the residual excited nucleus. The excitation energy is determined by the energy of the absorbed particles and "holes", which are formed as a result of intranuclear cascading. The momentum of the residual nucleus is deduced from the momentum conservation which was applied, in the course of calculation, at every act of particle collision. The next behaviour of the residual excited nucleus is described in the frame of the statistical equilibrium theory. The calculation of this evaporation stage is carried out by the Monte Carlo method, in this case the density parameter of the excited state is always a = A/10 MeV.

It is worth-while to mention that the generalization of the cascading-evaporation model to the interaction of complex nuclei, does not need any further parameter.

II.7.2. <u>Multiplicity of secondary particles</u>. Table 8 presents the experimental and the calculated, according to the cascading - evaporation model, average muliplicities of secondary particles in ^{12}C-Em interactions at 50 GeV/c for various groups of events, namely, those with $N_h > 6$ and $N_h \geq 28$. In table 9 the mean multiplicities in ^{12}C A interactions are compared to those for PA, dA and α A interactions /2/ at the same energy per incident nucleon. From these data it follows that:

Table (8). Average multiplicities of different secondary particles for ^{12}C A interactions in comparison with predictions of the cascading-evaporation model.

Type of events		Particle type $\langle n_s \rangle$	$\langle n_g \rangle$	$\langle n_b \rangle$
All events	theoretical	7.39	5.30	5.29
	experimental	7.65±0.24	6.12±0.28	4.41±0.17
$N_h > 6$	theoretical	11.54	10.21	9.91
	experimental	11.78±0.39	11.37±0.43	7.83±0.25
$N_h \geq 28$	theoretical	18.61	20.61	14.09
	experimental	18.61±0.74	22.29±0.82	11.12±0.48

Table (9). Comparison of the average multiplicities for interactions of different projectiles with emulsion at 4.5 GeV/C per nucleon.

	Pa	dA	αA	^{12}C A
$\langle n_s \rangle$	1.6±0.1	3.2±0.1	4.4±0.1	8.1±0.3
$\langle n_g \rangle$	3.6±0.1	2.3±0.1	4.7±0.2	6.1±0.3
$\langle n_b \rangle$	5.7±0.2	5.7±0.2	5.3±0.2	4.4±0.2

(i) The mean multiplicity of relativistic s particles increases fastly with increasing the atomic number of the projectile nucleus A_{proj}. In this case the number of grey tracks significantly rises. The number of the slow target fragments (b particles) decreases weakly with increasing A_{proj}.

(ii) The experimental values of the average multiplicities for particles well agree with the theoretically calculated values. For the g particles the agreement is satisfactory for all groups of events whereas for b particles, the calculated values are markedly different from the experimental data. This deviation is due to the fact that the used evaporation calculation for describing the decay of the excited nucleus is very rough especially in case of light nuclei and as seen from table 8 the calculated average values of b-particles are overestimated.

A more sensitive character for nucleus-nucleus interaction is the correlation between multiplicities of different types of particles. As seen from figs./13,14/ where the correlations $\langle N_h(n_s)\rangle$ and $\langle n_s(N_h)\rangle$ are presented, the cascade evaporation model reproduces the experimental data. It is worthy to mention that, like in hadron-nucleus interactions, these correlations can be approximated by a linear dependences with positive slopes.

It is interesting to study the dependence of the multiplicity of secondary particles on the number of nucleons, in the projectile-nucleus, interacting with the target. It is possible to estimate roughly this number knowing the total charge of non-interacting particles (fragments) in the carbon nucleus:

$Z^* = \sum N_i Z_i$, where N_i is the number of projectile fragments with charge Z_i and summation is made over all such fragments. The number of interacting nucleons of the projectile-nucleus, on the average, equals to $n._{int} = 12. - 2Z^*$.

Figure 15 shows the dependece of the mean multiplicities of secondary particles on n_{int} (and on Z^*). One can see that they increase abruptly with increasing n_{int} (with decreasing Z^*. The increasing of $\langle n\rangle$ with n_{int} is nearly linear one. In this case $\langle n\rangle/n_{int}$=const which shows evidence for an approximate validity of the assumption that nucleus-nucleus interactions at energy equal to a few GeV/ nucleon can be,

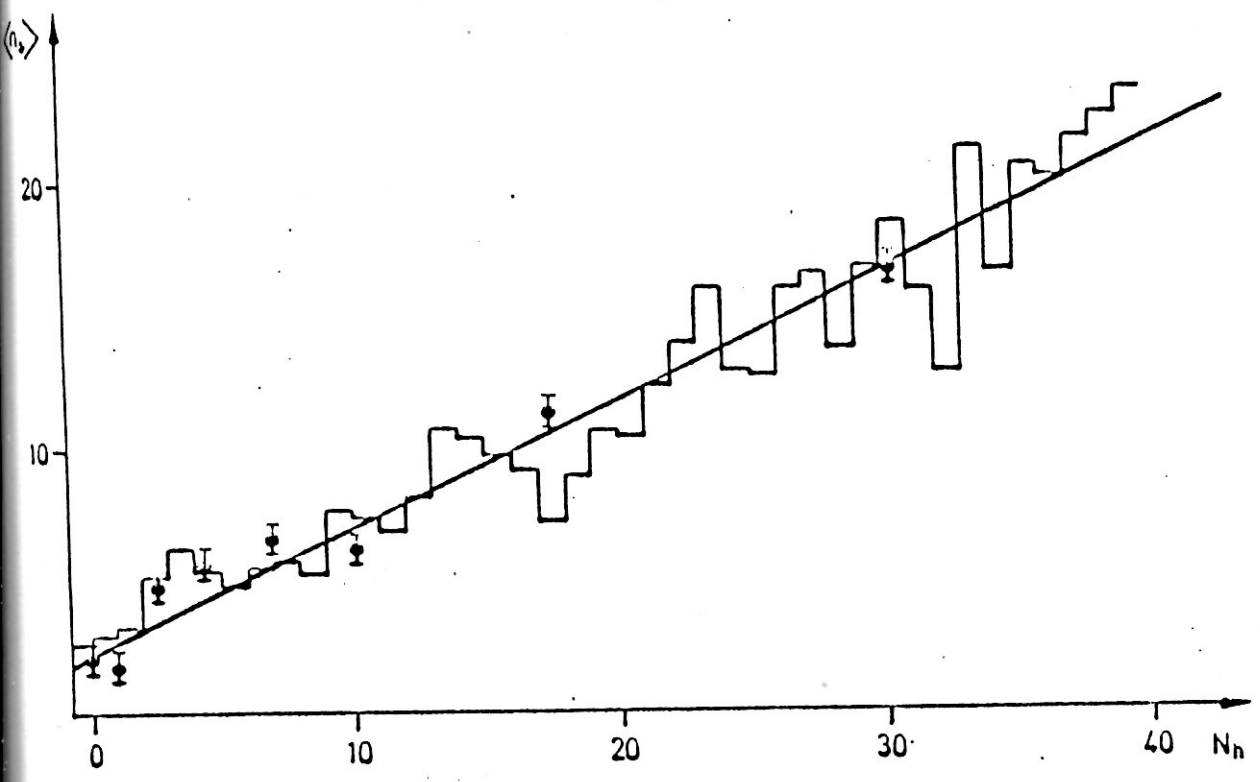

Fig.13 The dependence of the average multiplicity of shower particles on the number of target fragments (h-particles), the histogram represents the theoretical prediction of the cascading-evaporation model and the straight line ($\langle n_s \rangle = (1.96 \pm 0.13) + (0.49 \pm 0.02) N_h$) is the result of fitting the experimental data to a linear relation

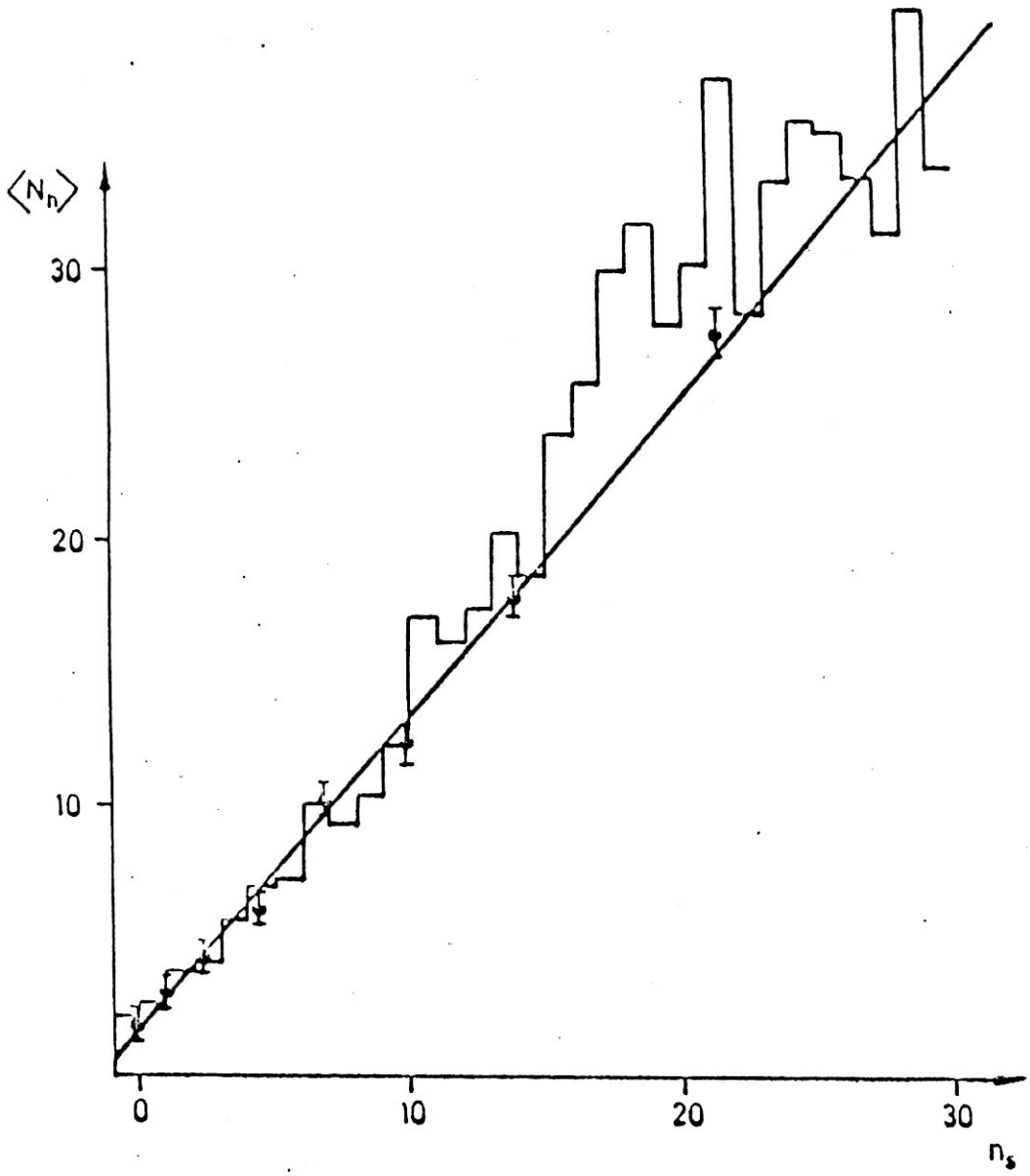

Fig. 14. The dependence of the average multiplicity of h-particles on the number of s-particles, the histogram is the prediction of the cascading-evaporation model and the straight line ($\langle N_h \rangle = (1.70 \pm 0.18) + (1.20 \pm 0.04) n_s$) is the result of fitting the experimental points to a linear relation

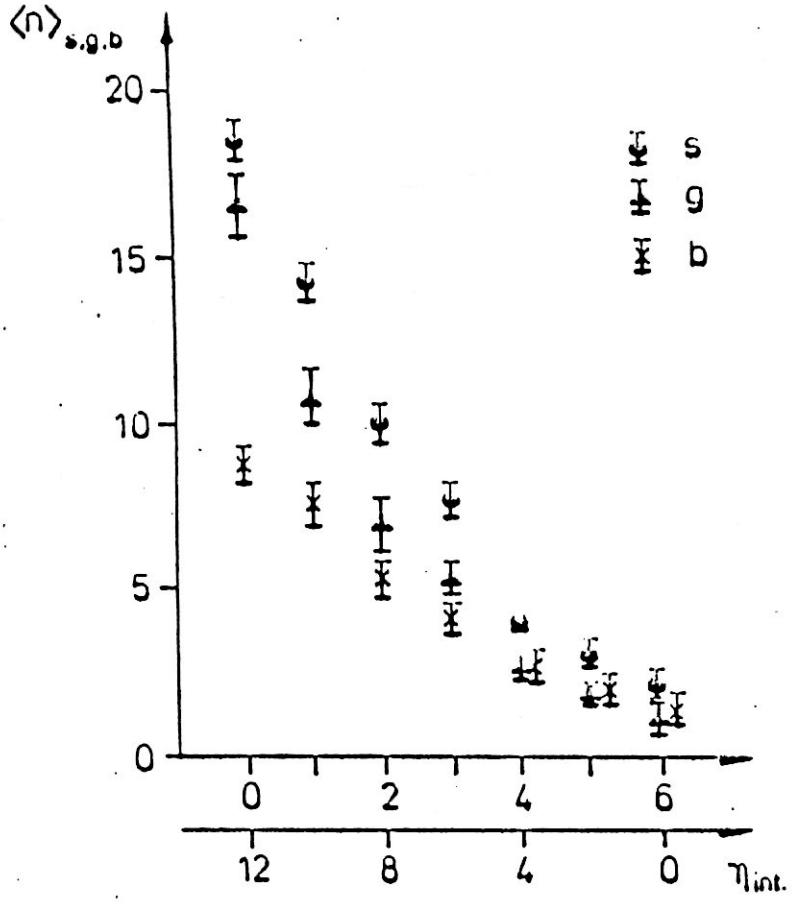

Fig. 15 The average multiplicity values of secondaries versus η_{int} and

to a first rough approximation, considered as a superposition of nucleon-nucleus collisions.

It is evident that, despite the roughness of the definition n_{int} (or Z^*) is a convenient experimental character to classify nuclear-nuclear interactions and degrees of their periphere: interactions with small Z^* (large n_{int}) are naturally considered to be "central" collisions, and events large Z^* (small n_{int}) to be "peripheral" nuclear collisions, with large impact parameter.

II.7.3. **Angular distribution.** The angular distributions of black, grey and shower particles, emitted in ^{12}C-Em interactins, are shown in fig. 16 in comparison with the corresponding calculated distributions. All distributions are normalized to unit area, the statistics of the experimental data nearly equals the theoretically generated events. The analysis of these distributions leads us to conclude that

(i) The angular distributions of the target fragments, for all groups of ^{12}C A interactions, are well reproduced by the cascading-evaporation model calculations. It is to be noted that the angular distributions of b and g particles show no peculiarity or peaks which can be explained by mechanisms of nuclear shock wave type. This is true for all groups of ^{12}C A interactions even the central one.

(ii) The experimental angular distribution of ς particles is consistent with the theoretically calculated one except the first interval, at small angles, where a contribution from the projectile singly charged fragments gave an increasing in the experimental value.

(iii) Comparing the angular distributions of b,g and s particles in ^{12}C A interactions with the corresponding distributions for collisions of P,d, α with emulsion nuclei

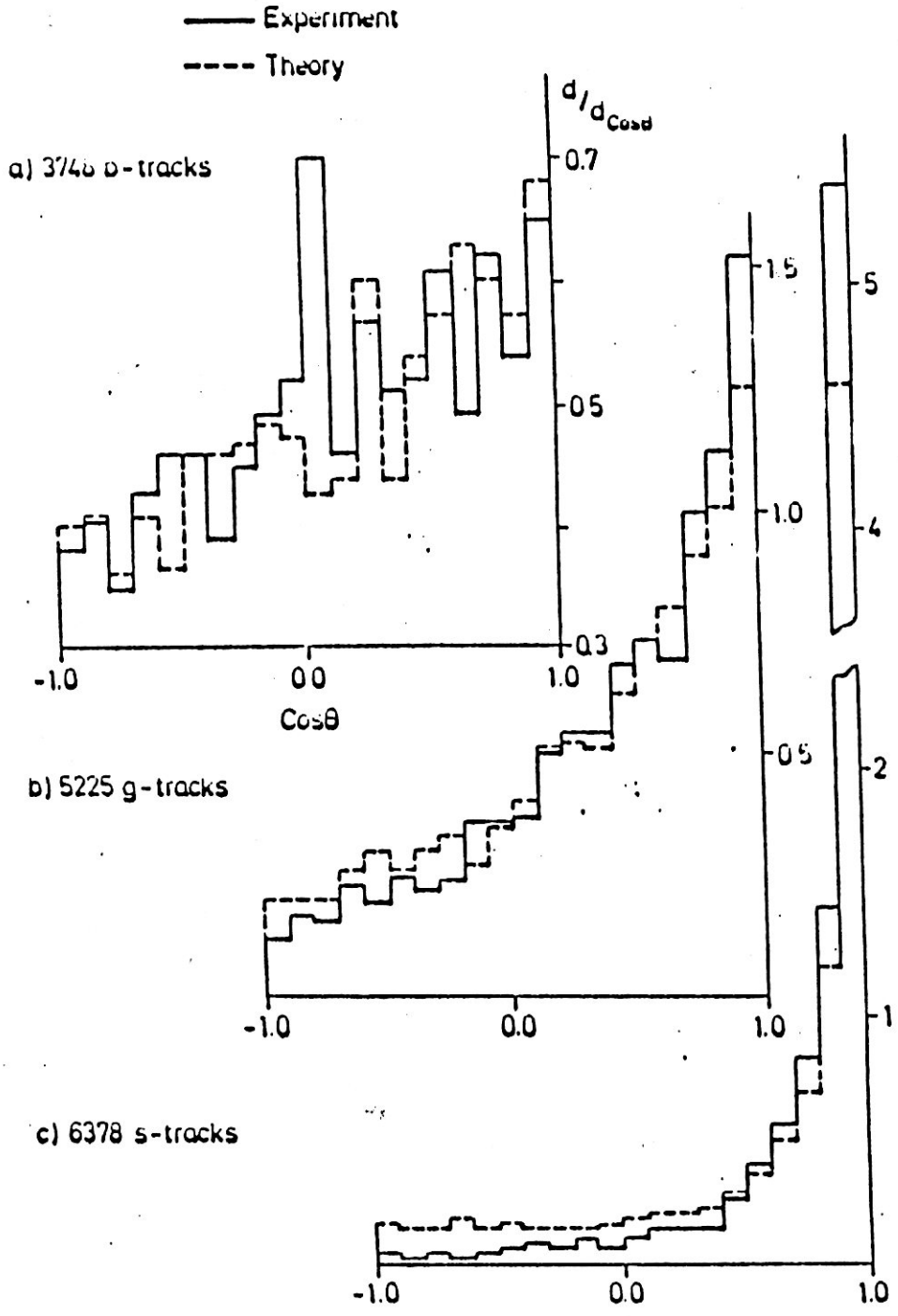

Fig. 16. The angular distributions of different secondary particles for ^{12}C-Em interactions at 4.5 GeV/c nucleon in comparison with the calculations of the cascading evaporation model

/2/, it was observed that, within experimental errors, these distributions are independent on A_{proj}.

I. In 90% of ^{12}C inelastic interactions, fragments of the projectile nucleus were observed.

2. The average multiplicities of secondary particles per interacting nucleon of the incident nucleus are identical for interactions of d, α and ^{12}C with emulsion nuclei.

3. Experimental results show that increasing the mass number of the incident nucleus from A_{proj} = 2 to A_{proj}=12, the global mechanism of interaction does not change. Within experimental errors the cacasding-evaporation model describes very well the general characteristics of the nucleus-nucleus interaction at momentum up to 4.5 GeV/C per nucleon.

II.8. Study of correlation between the secondary particles produced in inelastic collisions of relativistic nuclei with emulsion.

The purpose of the present section is to study two-particle correlations between various types of secondary charged particles from inelastic collisions of relativistic carbon nuclein[momentum 4.5 (GeV/C)/ nucleon] with nuclei of nuclear emulsion. The combined experimental material analyzed in the present work consists of 1001 cases of inelastic interaction of ^{12}C nuclein with nuclear emulsion nuclei. These events were found by double scanning along the track and were selected for measurements without discrimination.

We give the results of study of two-particle correlations between the spatial emission angles θ of the secondary particles, carried out by means of correlation functions; we discuss the correlations in the transverse plane of the collision (between the azimuthal angles φ), finally we give a brief resume of the results of the work.

II.8.1. Correlations between polar emission angles of particles. To study correlations between the angles θ of various types of secondary particles from carbon-emulsion (^{12}CEm) interactions we used the device of two-particle correlation functions. This method is very sensitive, in particular, to the possible appearance of a preferential emission of fragment particles of the target at definite angles in interaction events, which was expected in the model of nuclear shock waves.

We write the two-particle correlation functions

$$C_2(z_1, z_2) = \frac{1}{\sigma_{in}} \frac{d^2\sigma}{dz_1 dz_2} - \frac{1}{\sigma_{in}} \frac{d\sigma}{dz_1} \frac{d\sigma}{dz_2} \qquad (25)$$

and

$$R_2(z_1, z_2) = \sigma_{in} \frac{d^2\sigma}{dz_1 dz_2} \Big/ \frac{d\sigma}{dz_1} \frac{d\sigma}{dz_2} - 1 \qquad (26)$$

$$\sigma_{in}^{-1}(d\sigma/dz) = N_{ev}^{-1}(\Delta n/\Delta z), \quad \sigma_{in}^{-1}(d^2\sigma/dz_1 dz_2) = N_{ev}^{-1}(\Delta n_{12}/\Delta z_1 \Delta z_2),$$

ev

N_{ev} is the number of inelastic events, Δn is the number of particles in the interval Δz, Δn_{12} is the number of pairs of particles with variables z1 and z_2 respectively in the intervals Δz_1 and Δz_2 (thus, σ_{in} is the cross section for nucleus-nucleus collision with production of charged particles $\sigma_{in} = \sigma_{prod}$). The functions 25 and 26 were calculated in the complete set of ^{12}CEm interactions in various groups of stars for strongly ionizing (h) and relativistic (s) secondary particles. In a separate analysis of gray (g) and black (b) particles ($n_g + n_b = n_h$) we used geometrical corrections, since the exact separation of h particles into g and b was carried out only for dip angles of the analyzed tracks in the emulsion <30°. As the variable z in the Eqs. (25) and (26) we used cos θ for h particles and $\ln \operatorname{tg}(\theta/2)$ (the pseudorapidity) for s particles. We note that the fragments of the incident

nucleus were not included in the analysis; singly charged fragments were excluded from the s particles, and multiply charged fragments from the h particles.

It is well known that the inhomogeneity of the collision ensemble considered (presence of a spectrum of multiplicities, dependence of the single-particle spectra $d\sigma/dz$ on the multiplicity, distributions in impact parameters, and so forth) leads to strong pseudocorrelations (C_2, $R_2 \neq 0$), and therefore for each studied ensemble or subensemble of events we generated by the Monte Carlo method corresponding ensembles of random stars in accordance with the model of independent emission of particles (IEM), we recall that the distributions in multiplicity and the dependence of $d\sigma/dz$ on n were accurately reporoduced for each real ensemble of events.

In Fig. 17 we have shown values of the functions C_2 and R_2 for values of the arguments $z_2 = z_1$ (the diagonal of the correlation matrix, which provides information on the presence or absence of short-range correlations) of h particles from ^{12}CEm collisions with various total charges Z of noninteracting fragments of the incident nucleus in the final state $Z^* = 0, 1, \ldots 6$). There are convincing reasons for use of Z^* as the quantity which classified (on the average) nucleus-nucleus collisions on the basis of the impact parameter-small corresponds to small impact parameters (central collisions), and large Z^* correspond to large impact parameters (peripheral collisions). We have shown also the values of C_{20} and R_{20} calculated in the corresponding ensembles of generated events.

As can be seen from the data of Fig. 17 the correlation functions C_2 and R_2 are consistent within experimental error with the values calculated on the assumption of independent emission of h particles in the collisions considered. This is valid for any of the subgroups of events considered by us, any sets of the arguments z_1

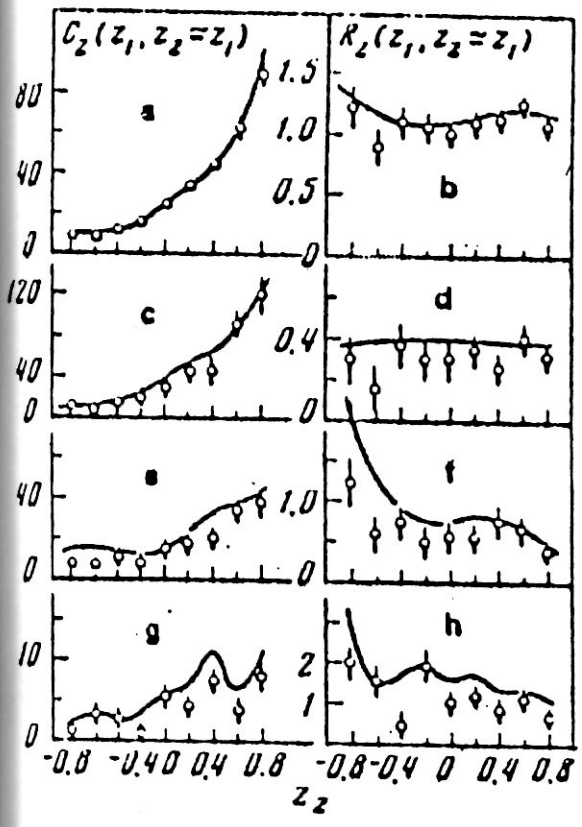

FIG. 17. Correlation functions $C_2(z_1, z_2 \simeq z_1$ and $R_2(z_1, z_2 \approx z_1)$ ($z = \cos\theta$) for h particles from ^{12}CEm interactions (a, b) and subgroups of events with $Z^* = 0, 1$ (c, d), $Z^* = 2, 3$ (e, f), and $Z^* = 4$–6 (g, h). The curves are calculations according to the independent emission model.

and Z_2, and individually for g and b particles (not shown). Thus, in carbon-nucleus collisions at 4.5 GeV/C per nucleon no correlations are observed between the angles of emission of strongly ionizing particles; in particular, we did not observe any tendency to preferential emission of fragments of the target nucleus at a definite angle as expected if the mechanism of nuclear shock wave production is realized. Of course, it is not excluded that this mechanism is realized. Of course, it is not excluded that this mechanism is realized with a small cross section or does not lead to production of an expressed Mach cone for the nuclei and collision energies considered.

Conclusions similar to those drawn in analysis of Fig. 17 follow also from consideration of other arguments of the correlation functions 25 and 26 (not shown).

In Fig. 18 we have shown values of C_2 and R_2 for the arguments $Z_2 \simeq Z_1$ and $(2, Z_2)$ of shower particle from the complete set of ^{12}CEm interactins, together with calculated values C_{20} and R_{20} from the IEM. It can be seen that, as in the case of h particles, no excess of C_2 (R_2) over C_{20} (R_{20}) for s paricles is observed.

It is of interest to compare data on two-particle correlaitons in nucleus-nucleus and hadron-nucleus (hA) or hadron-nucleon (hN) interactions at similar average multiplicities of shower particles (we note that the shapes of the distributions in multiplicity in all three classes of interactions are similar). The average multiplicity $\langle n_s \rangle = 7.8 \pm 0.2$ ^{12}CEm collisins at $p_0 = 4.5$ GeV/c per nucleon corresponds to a pA collision at $p_0 = 50$ GeV/c and to a pN collision at $p_0 = 200$ GeV/c. The existing data indicate that in pN and pA collisions at these energies C_2 (R_2) is guaranteed to be greater than C_{20} (R_{20}). This indicates existence of correlations which are dynamic (in the sense of being short-range). The absence of such

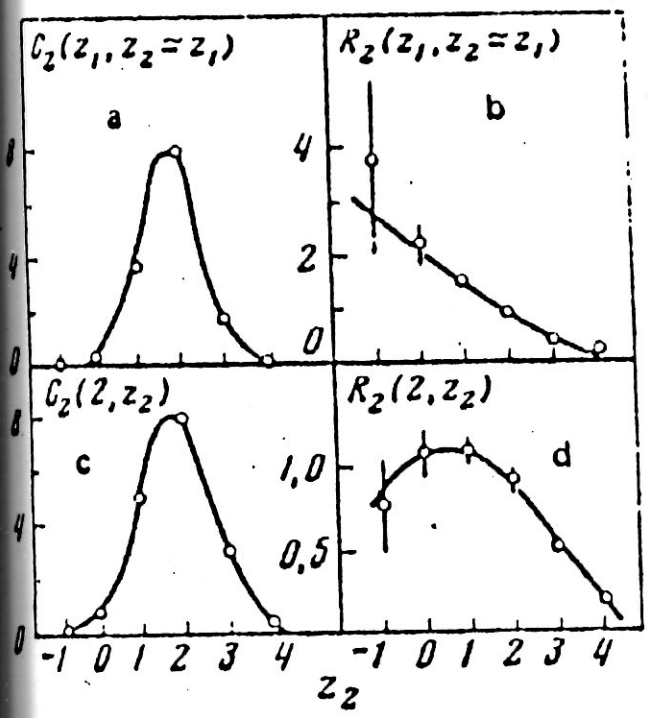

FIG. 18. Correlation functions $C_2(z_1, z_2 \approx z_1)$ (a), $R_2(z_1 z_2 \approx z_1)$ (b), $C_2(2, z_2)$ (c), and $R_2(2, z_2)$ (d), ($z = \ln \operatorname{ctg}(\theta/2)$) for s particles from ^{12}CEm collisions. The curves are calculations according to the IEM.

correlations (or their extreme attenuation) in nucleus-nucleus collisions may indicate a difference of the particle production mechanisms in these classes of interactions. We shall dwell in more detail on this difference in the next section in discussion of the difference in the azimuthal correlaitons.

II.8.2. Azimuthal correlations. To study the correlation links between secondary particles in the transverse plane of the collision we used the following quantities:

a) the azimuthal asymmetry coefficient

$$\mathcal{A} = \left(\int_{\pi/2}^{\pi} f(\varepsilon)\,d\varepsilon - \int_{0}^{\pi/2} f(\varepsilon)\,d\varepsilon \right) \Big/ \int_{0}^{\pi} f(\varepsilon)\,d\varepsilon, \qquad (27)$$

where $\varepsilon \equiv \varepsilon_{ij} = \arccos\left(\vec{p}_{\perp i} \cdot \vec{p}_{\perp j} / p_{\perp i} p_{\perp j}\right)$ is the angle between the transverse momentum vectors $p_\perp$ of the secondary particles i and j, $0 \leqslant \varepsilon \leqslant \pi$; $\cos\varepsilon_{ij} = \cos(\varphi_i - \varphi_j)$;

b) the azimuthal collinearity coefficient

$$\mathcal{B} = \left(\int_{0}^{\pi/4} f(\varepsilon)\,d\varepsilon + \int_{3\pi/4}^{\pi} f(\varepsilon)\,d\varepsilon - \int_{\pi/4}^{3\pi/4} f(\varepsilon)\,d\varepsilon \right) \Big/ \int_{0}^{\pi} f(\varepsilon)\,d\varepsilon; \qquad \ldots (28)$$

c) the distribution and average value of the angle between the directions of preferential emission of two groups of particles from a single collision in the transverse plane (the angle between the resultant vectors composed of unit vectors directed along the transverse momenta of each particle of the two groups):

$$\Phi_{kl} = \arccos\{(a_k a_l + b_k b_l)\,[(a_k^2 + b_k^2)(a_l^2 + b_l^2)]^{-1/2}\},$$

$$a_k = \sum_i \cos\varphi_i, \quad b_k = \sum_i \sin\varphi_i, \quad a_l = \sum_j \cos\varphi_j, \quad b_l = \sum_j \sin\varphi_j, \qquad \ldots (29)$$

$$i = 1, 2, \ldots, n_k;\ j = 1, 2, \ldots, n_l;\ n_k, n_l \geqslant 1.$$

If the emission of the particles is independent and there is azimuthal isotropy, the expectation values of the quantities A, B, $\Phi_{kl} - \pi/2$ and $\langle\Phi_{kl}\rangle - \pi/2$ ($\langle\Phi_{kl}\rangle = \Sigma\Phi_{kl}/N_{st}$), where N_{st} is the number of events in the ensemble studied, are equal to zero.

If the particles i and j are of the same type (for example, s particles), we shall speak of intragroup correlations; if they are different (for example, s and h particles or s particles from different kinematic regions of the interaction on the longitudinal rapidity scale) we shall speak of intergroup correlations. The coefficients A and B can characterize both these and other correlations, but the angle (Φ_{kl}) determines only the intergroup effects.

Let us turn to analysis of the experimental data.

In Table 10, we have given the values of A and B for particle pairs of a signle type. The asymmetry coefficients A are equal to zero within experimental error (except perhaps for the fragments of the ^{12}C nucleus); the values of the coefficients B indicate existence of a weak collinearity of the transverse momentum vectors of the particles, which is most noticeable for fragments of ^{12}C. Analysis of these data permits the following conclusions to be drawn.

A. The essential absence of azimuthal correlations between s particles indicates that the mechanism of their production in ^{12}CM interactions in a certain sense differs from that in hN and hA collisions. In fact, in emssion of particles from a "single" decaying object" (as in hadron-hadron collisions) the kinematics of the decay (conservation of the transverse momentum) requires substantially nonzero positive values of the asymmetry coefficient $A \simeq 1/n$, where n is the total number of particles from decay of this object (for hN and hA collisions $n \simeq 1.5n_s$). For hN interactions with multiplicities close to those observed

in the ensembles and subensembles of ^{12}CEm collisions studied by us, the values of A agree with expectation values of the order 0.1; the same situation exists also for hA collisions. The data of table 10 indicate that s particles from ^{12}CEm interacions at energy of several GeV/nucleon cannot be considered emitted from a "single" object similar to that realized in an elementary hh collision event. The zero values of A for s particles can easily be understood if we assume that these particles are produced in several independent subcollisions and (or) have undegone substantial rescattering inside the target nucleus. Thus, the data on correlations convincingly support models of the superposition type at the primary energies considered; however, application of purely collective models (such as the hydrodynamical theory, the collective tube model,[4] the one-fireball model[5]) to description of the production of particles in nucleus-nucleus collisions in the moderate energy region is unjustified in the light of the data which have been presented. This conclusion is in good agreement also with the results of a comparative analysis of longitudinal correlations.

B. The tendency to coplanarity of the momenta of the fragments of the ^{12}C incident nucleus may indicate that the residual light nucleus after the collision has an angular momentum (is rotating). Another, trivial interpretation of the inequality B > 0 (Table 10)- that conservation of transverse momentum is "responsible" - is unsatisfactory, since here A $\lesssim$ 0 (action of the conservation law leads simultaneously to A>0 and B>0, while A $\simeq 1/n$ > B $\simeq 1/n^2$). It should be mentioned, of course that the statistical reliability of the collinearity of the transverse momenta of the ^{12}C fragments is poor, so that it is desirable to confirm this effect with better statistics.

Table (10). Coefficients A and B for particles of the same type (intragroup correlations).

Type of particle	A	B
particles	-0.002 ± 0.005	0.014 ± 0.005
particles	0.007 ± 0.004	0.009 ± 0.004
ngly charged fragments of projectile	-0.055 ± 0.036	0.110 ± 0.036
ubly charged fragments of projectile	-0.207 ± 0.064	0.122 ± 0.064

Table (11) lists some numerical data on the coefficients A,B, and the average values $(\Phi_{hl}) - \pi/2$ for cases of intergroup correlations. Let us analyze these data.

1. Fragments of the incident nucleus turn out to be uncorrelated with other particles (shower and highly ionizing particles) (lines 1-4 of Table (11). This lack of correlation is retained for any impact parameters (data for subgroups of events with $z^* 1,2,2,3, \geq 4$). This result is quite natural from the point of view of most models of nucleus-nucleus interactions, in which the fragmentation of the incident and target nuclei and poinization are considered as isolated (independent).

2. Distinct and assured correlations exist between s and h particles; these particles reveal a tendency to be emitted on different sides in the transverse plane of the collision. It is possible that these correlations depend on the angle of emission of the s particles; in any case s particles with $\theta > \pi/2$ are already uncorrelated with h particles (line 6 of Table 11). No dependence of the correlations on the emission angle of the h particles is observed (not shown). The described correlations in Fig. 19, which show the Φ_{kl} distributions for different subgroups of ^{12}CEm collisions, are especially evident.

Table (11). Characteristics of intergroup correlations in ^{12}CEm interactions.

No.	Group k	Group l	A	B	$\langle\Phi_{kl}\rangle-\pi/2$
1	Singly charged fragments of ^{12}C.	S	0.011±0.011	0.011±0.011	0.037±0.036
2	Ditto	h	0.007±0.010	0.007±0.010	0.020±0.039
3	Doubly charged fragments of ^{12}C	S	-0.023±0.010	-0.006±0.022	0.073±0.046
4	Ditto	h	0.063±0.028	-0.035±0.028	0.073±0.050
5	S_1	h	0.021±0.003	0.005±0.003	0.267±0.031
6	$S_2 < 0$	h	0.002±0.012	0.019±0.012	0.019±0.062
7	S 0< < 1	h	0.022±0.005	-0.005±0.005	0.168±0.040
8	S 1< < 2	h	0.020±0.004	-0.001±0.004	0.181±0.036
9	S > 2	h	0.025±0.005	0.010±0.005	0.193±0.033
		Events with Z* =0.1			
10	S	h	0.016±0.004	0.002±0.004	0.280±0.056
		Events with Z =2.3			
11	S	h	0.029±0.006	0.000±0.006	0.213±0.058
		Events with Z > 4			
12	S	h	0.041±0.011	0.011±0.011	0.288±0.018

Correlations of the type described can be the consequence of the fact that AA collisions are a superposition of more elementary hA (or hh) collisions, in each of which there is an obvious tendency not to emit s and g particles (produced particles and recoil protons) in the transverse plane, which is required by the conservation of transverse momentum. This assumption corrsponds qualitatively to the observed decrease (Table 11) ofAwith increase of the number of subcollision (decrease of Z*) with simultaneous independence (or weak dependence) of $\langle \Phi_{kl} \rangle$ on Z^* (Table 11, Fig.19). Actually an increase of the number of subcollisions, on the other hand, leads to a decrease in the average correlation between s and h particles as a consequence of the increase of the relative contribution of sh pairs from different subcollisions, but on the other hand it decreases the errors in determination of the directions of the predominant emission of s and h groups, as a result of the increase of multiplicity of the various particles with decrease of Z*. These circumstances, which compensate each other, can lead to a weak dependence (independence) of $\langle \Phi_{sh} \rangle$ on Z* of course, quantitative calculations are necessary for high reliability.

II.8.3. Conclusion. We shall give a brief resume of the results of the present work.

1. A search was carried out for pair correlations between different forms of secondary particles from inelastic interactions of carbon nuclei at momentum - 4.5 GeV/C per nucleon with emulsion nuclei.

2. No dynamical pair correlations were observed between the polar emission angles of all types of particles. The absence of such correlations for fragments of the target nucleus indicates that collective phenomena such as a simple nuclear shock wave produced in formation of an

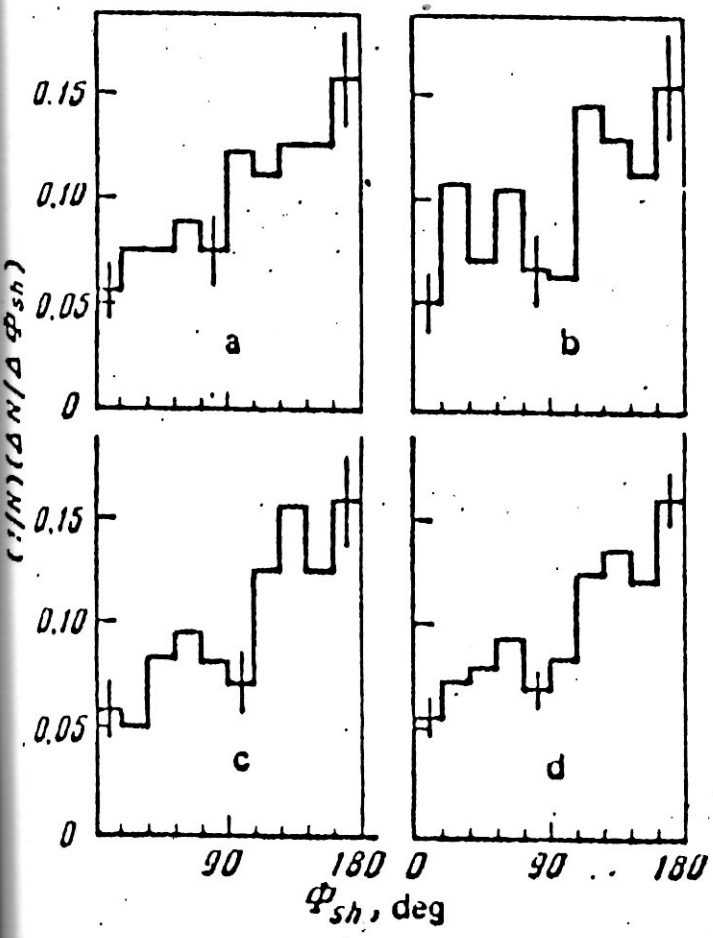

FIG. 19. Distributions in Φ_{sh} for carbon-nucleus collisions for $Z^* = 0, 1$ (a), $Z^* = 2, 3$ (b), $Z^* \geq 4$ (c), all ^{12}CEm (d).

expressed Mach cone do not occur with an appreciable cross section in collisions of light nuclei with nuclei at energies of several GeV/nucleon.

3. Correlations between particles in the transverse plane of nucleus-nucleus interactions have been observed and qualitatively analyzed.

4. It has been shown that models of nucleus-nucleus collision which assume identity of the particle-production mechanisms in collisions of nuclei and hadrons with a large effetive energy (mass) qualitatively are inconsistent with data on azimuhal correlations at primary momenta of several GeV/c per nucleon, while, for example, in pN collisions at 200 GeV/c there is an absolute majority of them (~ 0.9).

By such an object we understand only a system whose decay into secondary particles is controled by the conservation laws, this is not necessarily a physical formation such as a resonance or fireball.

Models in which an A A collision is identified in any sense with an hh collision with a high effective energy in the c.m.s.

II.9. <u>Catastrophic destruction of Ag (Br) and Pb nuclei induced by 4.5 A GeV/C ions</u>. The study of the phenomena of complete destruction of heavy target nuclei is very interesting. This interest stems from the fact that most of these interaction are due to centeral collisions. The centeral collisions provide a nuique opportunity to investigate the consequences of nuclear compression, such as hydrodynamical effects. Also, one can study the mechanism of multiparticle production. In addition, there is a good possibility to obtain valuable informations on the excitation and consequent decay of residual target nucleus.

The investigation of complete destruction of heavy target nuclei began in 1958 at the laboratory of high energies at the Joint Institute of Nuclear Research in Dubna/55/. A detailed and systematic study of this phenomenon was carried out in/50/. In this work the criterion (N_h>28) was used to select events of complete destruction of Ag (Br) nuclei. It was found that this condition corresponds to the destruction of the target nucleus nearly to individual nucleons without a measurable residual nucleus. Since then, this criterion is used to select the events of the complete destruction of Ag (Br).

Nowadays, there are a huge amount of data concerning the study of this phenomena. Different beam nuclei at various energies have been used in the experiments. There are two main directions for the interpretation of the experimental results of complete destruction. The first direction considers such events as a tail in the multiplicity distribution which can be accounted for by the cascade evaporation process inside the target nucleus. The second one implies a one-step like process which occurs due to the collectivity of the target nucleons together.

In the present section, we study complete destruction ($N_h \geqslant 28$) of Ag (Br) emulsion nuclei induced by 4.5 A GeV/c nuclei. We are trying to shed light on the preferable mechanism of the complete destruction phenomena by studying the probability of occurence, the multiplicity distributions and their correlations with the characteristics of the interacting nuclei.

II.9.1. <u>The probability of complete destruction of Ag (Br) nuclei</u>. In the present work, the probability of complete destruction of Ag (Br) emulsion nuclei P is defined as the ratio between the number of evetns of ($N_h \geqslant 28$) to the total nubmer of inelastic interactions of the

incident particle with Ag(Br) nuclei. It is interesting to study the probability P as a function of the energy of the particle and its mass number A_B. Table 12 presents the probability P as a function of the energy of the incident particle and its mass number A_B. To study the dependence of the probability P on the energy of the incident particle we consider the proton data in Table 12. One can observe that the probability P is independent of the energy of the incident proton in the interval 5-300 GeV and its average value is 0.026 ± 0.003.

Fig. 20 taken from Table 12 illustrates the dependence of the probability P on A_B for various beam nuclei, all at momentum 4.5 GeV/c per nucelon. It is seen that the probability P increases linearly with $A_B^{2/3}$ up to the carbon nucleus starting form $A_B = 12$ the probability P seems to reach to a plateau. The values of P, predicted by the cascade evaporation model, are larger than the corresponding experimental values. Moreover, the behaviour of P versus A_B in the experiment does not agree with the calculations of the cascade evaporation model.

II.9.2. <u>The multiplicity characteristics of shower particles</u>. Table 13 presents the average multiplicities of s-particles emitted in events of ($N_h \geq 28$) from different reactions at 4.5 GeV/C per nucleon. It is interesting to study the dependence of the average multiplicity of shower particles $\langle n_s \rangle$ on the mass number of the beam nucleus A_B.

Table (12). The probability of complete destructiuon of Ag(Br) nuclei by different projectiles at various energies.

The projectile	Momentum GeV/c	Probability of complete destruction	
		Experiment	CEM
P	4.5	.010± .002	0.0012
Protons	7.1	.020± .004	
	8.4	.040± .006	
	9.6	.030± .006	
	23.4	.030± .007	
	69	.030± .008	
	200	.020± .002	
	300	.030± .006	
d^2	9	.030± .005	0.03
H_e^4	18	.060± .010	0.05
C^{12}	54	.190± .023	0.28
N_e^{22}	99	.190± .010	0.31
Mg^{24}	108	.220± .033	0.32

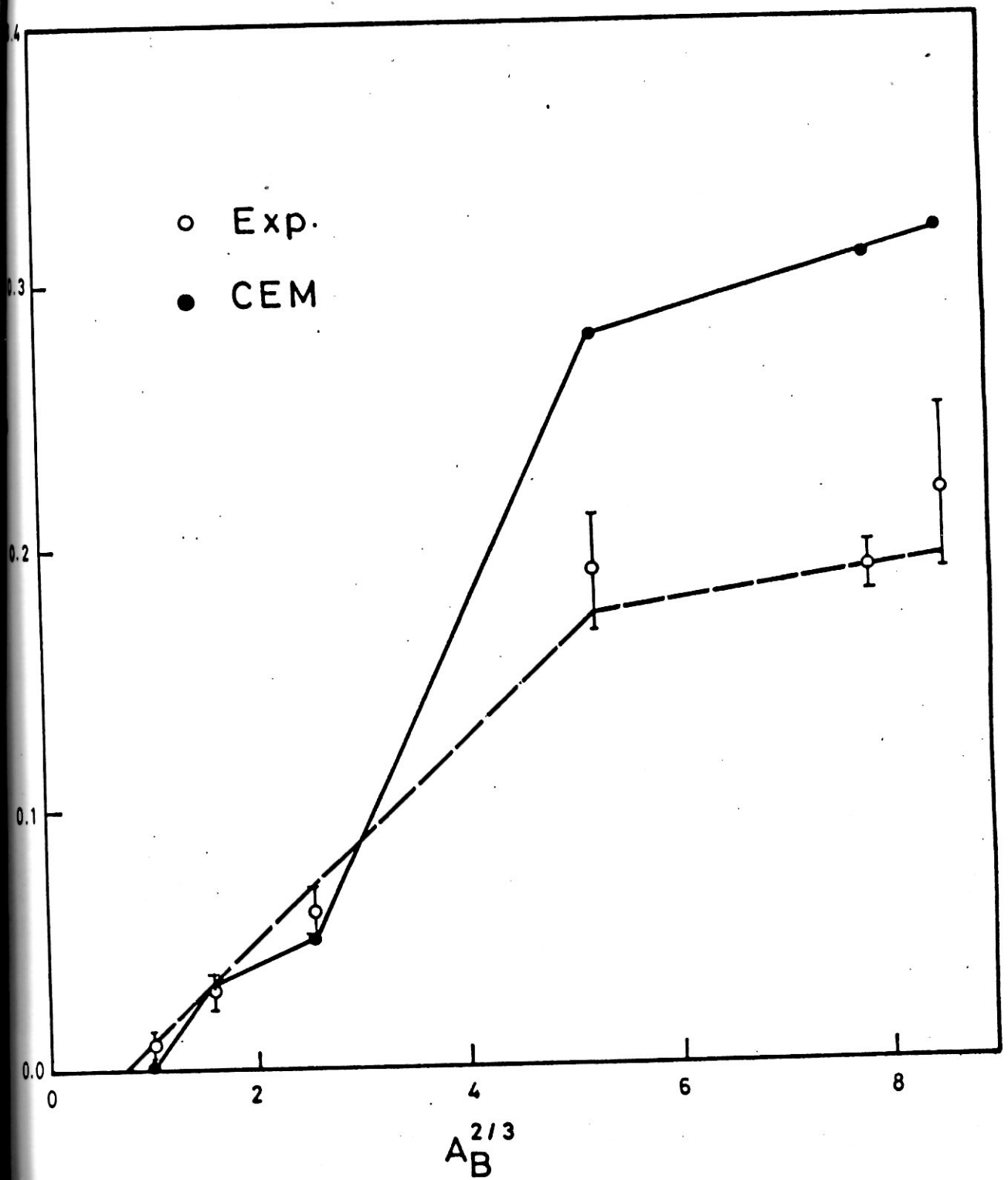

Fig.(2.20): The probability of complete destruction P as a function of the mass number of the beam nucleus at momentum 4.5 GeV/c per nucleon. The dashed line is drawn to guide the eye.

Table (13). The average number of shower particles $\langle n_s \rangle$ as a function of the number of interacting nucleons R_A from both of the colliding nuclei.

The projectile nucleus	$\langle n_s \rangle$	Number of interacting nuclens from both nuclei
H_e^4	9.4±0.4	5.48
C^{12}	18.8±0.7	15.85
O^{16}	25.1±1.1	18.58
Ne^{22}	27.7±0.3	22.10
Mg^{24}	28.8±0.8	23.15
Si^{28}	28.8±0.8	

Fig. 21 shows the relation between $\langle n_s \rangle$ and A_B for complete destruction events from interactions of H_e^4, C^{12}, O^{16}, N_e^{22} and Mg^{24} with emulsion at momentum 4.5 A GeV/C. The experimental points were fitted to the relations $\langle n_s \rangle = KA_B^{\alpha}$. The straight line represents the result of the fitting. The value of α was found to be $0.64 \pm .05$ and that of K equals 3.92 ± 0.4. This result shows that $\langle n_s \rangle$ is strongly dependent on the mass number of the projectile nucleus A_B. The $\langle n_s \rangle$ increases proportional to the geometrical cross-section of the beam nucleus. To study the dependence of the average multiplicity $\langle n_s \rangle$ on the mass number of the target, we have compared He^4 + Ag(Br) with He^4 + pb reactions. The comparison give a value of the exponent equals to 0.36 ± 0.03. Thus in the complete destruction events from the heavy ion interactions the $\langle n_s \rangle \sim A_B^{0.63} \cdot A_T^{0.36}$. This result will be more elaborated in the further analysis.

According to ref./50/, the number of interacting nucleons from the projectile and target nuclei can be given by

$$R_A = (A_B A_T^{2/3} + A_T A_B^{2/3}) / (A_B^{1/3} + A_T^{1/3})2 \qquad (30)$$

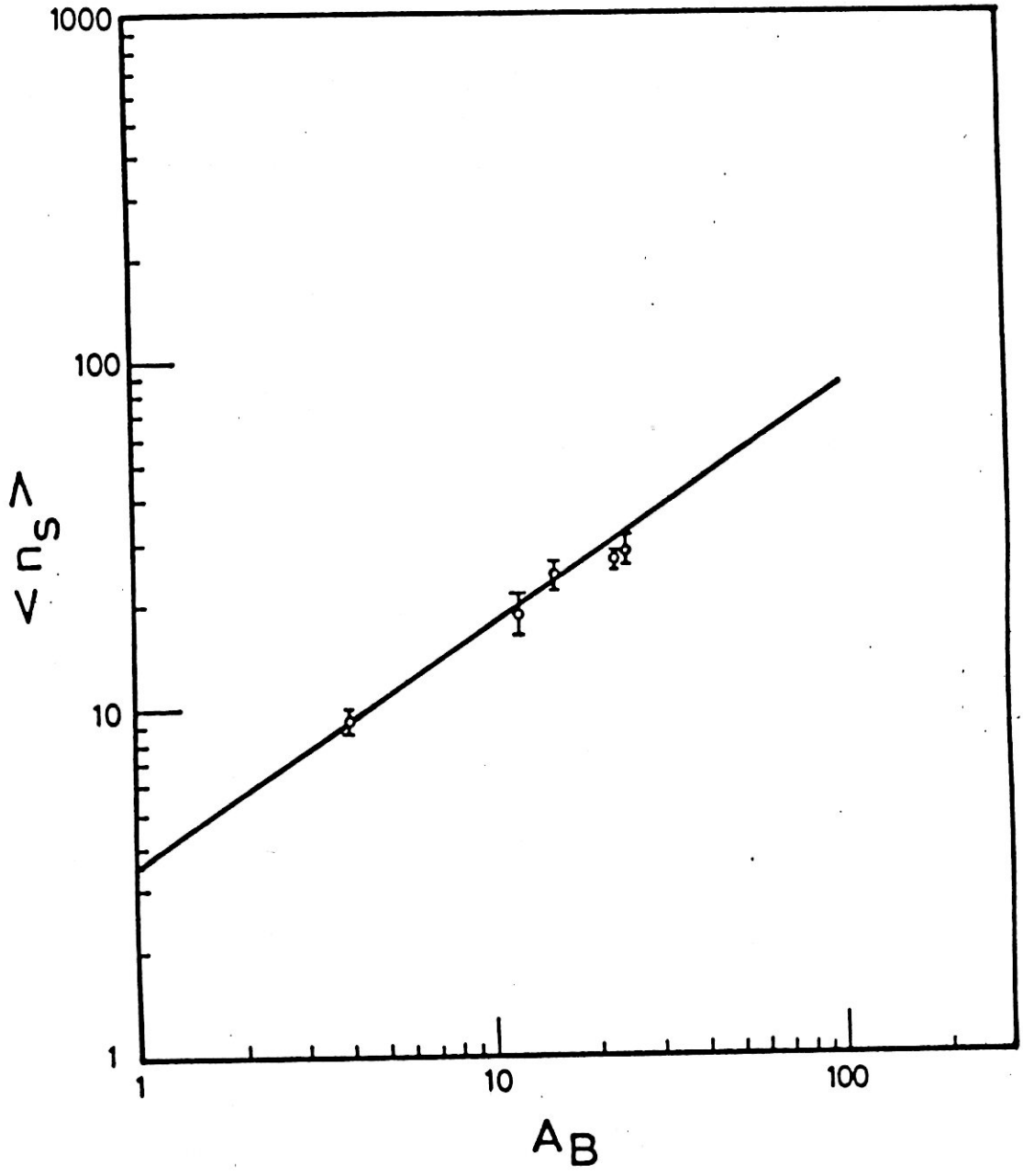

Fig.(21): The average multiplicity $\langle n_s \rangle$ as a function of the projectile mass number A_B in complete destruction at 4.5 A GeV/c.

where A_B and A_T are the mass numbers of the projectile and target respectively. Fig. 22 illustrates the $\langle n_s \rangle$ versus R_A. The experimental data are will fitted by the relation $\langle n_s \rangle = K R_A^{\alpha}$, where $\alpha = .78 \pm 0.07$ and $K = 2.45 \pm 0.22$

To explain the number of shower particles produced in the complete destruction events, we adopt a simple geometrical model. To calculate the number of participating protons from the target. We assume that one has to take into account all protons from the target which lie in the cylinder cut by the projectile. Approximate length of this cylinder equals the diameter of the target nucleus $2R_T$, the cross-sectional area of which is πR_B^2 therefore its volume equals $2R_T \pi R_T^2$. Dividing this volume by that of the target nucleus $\frac{4}{3} \pi R_T^3$ and multipling by Z_T. We obtain the number of participant protons equal $Z_B + \frac{3}{2} Z_T (A_B/A_T)^{2/3}$. This geometrical model was used to calulate the total free energy in the center of mass system E_f. The value of E_f is given by:

$$E_f = [M_B + M_T)^2 + 2M_T E_B^k]^{\frac{1}{2}} - (M_B + M_T) \qquad (31)$$

where M_B and E_B^k are the rest mass and the kinetic energy of the projectile in the laboratory system. In this case the effective mass of the trget, $M_T = \frac{3}{2} A_B^{2/3} A_T^{1/3} m$, is the mass of the cylinder cut in the target by the projectile at impact parameter b=0, where m is the nucleon rest mass. The calculated values of total free energy E_f are presented in Table 14. A strong correlation between these values and those of $\langle n_s \rangle$ is observed. The average multiplicity of showers $\langle n_s \rangle$ increases regularly with E_f.

The values of $\langle n_s \rangle$ drawn versus the calculated values of E_f in Fig. 23. The experimental data were fitted to the formula:

$$\langle n_s \rangle = A + B \mathrm{Ln}\, E_f + C\, (\mathrm{Ln}\, E_f)^2$$

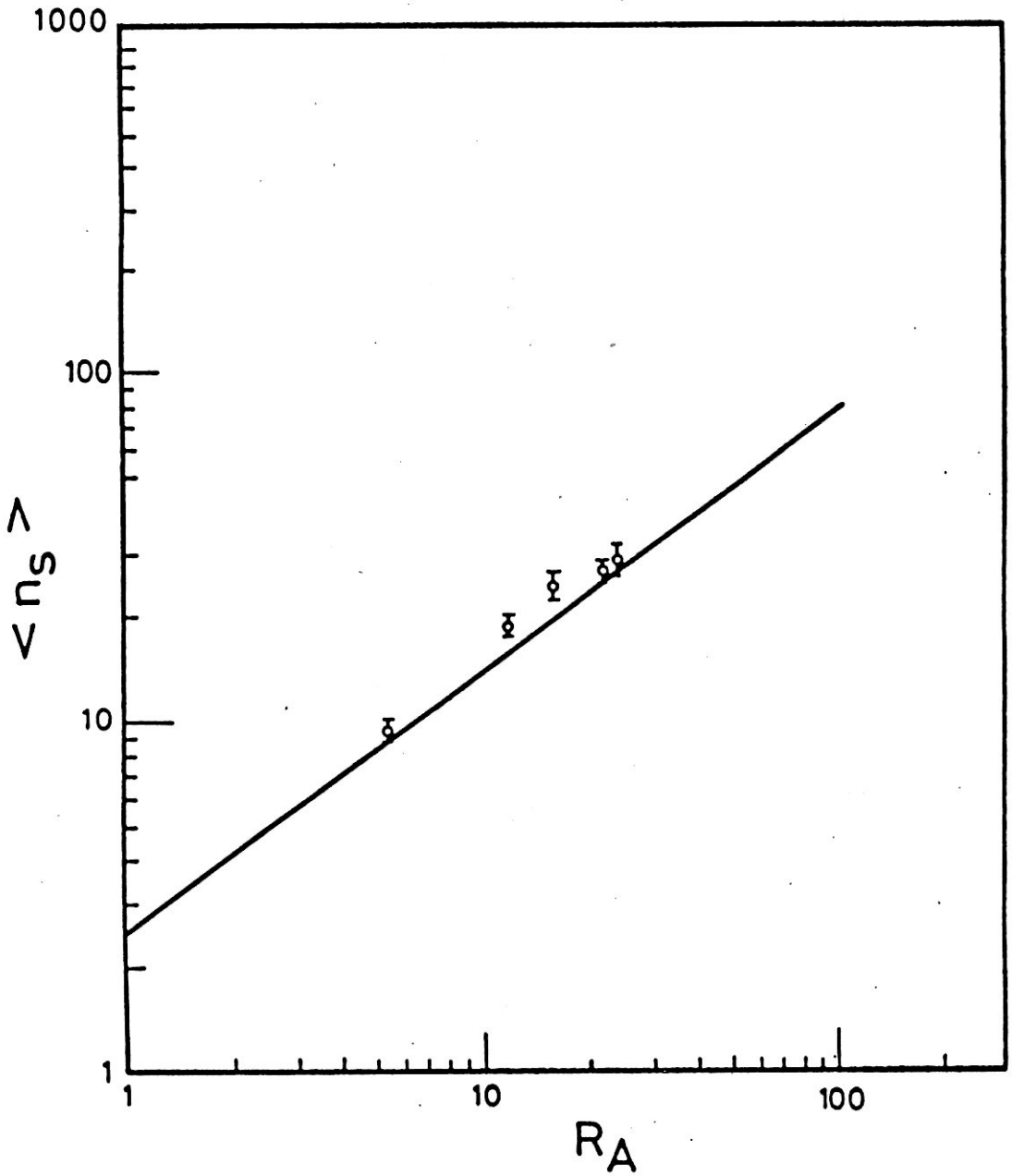

Fig. (22): The average multiplicity $\langle n_s \rangle$ as a function of the number of interacting nucleons R_A in complete destruction at 4.5 A GeV/c.

Table (14). Characteristics of complete destruction events.

P+Ag (Br) 4.5 GeV/C	P+Ag(Br) 7.1 GeV/C	P+Ag(Br) 6.9 GeV/C	d^2+Ag(Br) 4.5 GeV/C/N	He^4+Ag(Br) 4.5 GeV/C/N	C^{12}+Ag(Br) 4.5 GeV/C/N	O^{16}+Ag(Br) 4.5 GeV/C/N	^{24}Mg-Ag(Br) 4.5 GeV/C/N
$\langle n_s \rangle$ 1.16±0.5	3.4±0.4	19.1±1.0	2.8±0.2	9.5±0.2	18.6±0.7	25.1±1.1	28.8±0.8
$\langle n_g \rangle$ 11.3±0.6	11.3±0.7	14.2±0.8	16.4±0.2	19.1±0.4	22.5±0.8	26.1±1.1	25.0±0.6
$\langle n_b \rangle$ 18.3±0.9	18.9±0.8	15.8±0.5	16.2±0.3	14.4±0.3	11.9±0.5	11.9±0.5	13.0±0.4
E_f 2.7	4.1	23.1	4.5	9.2	23.7	33.	47.

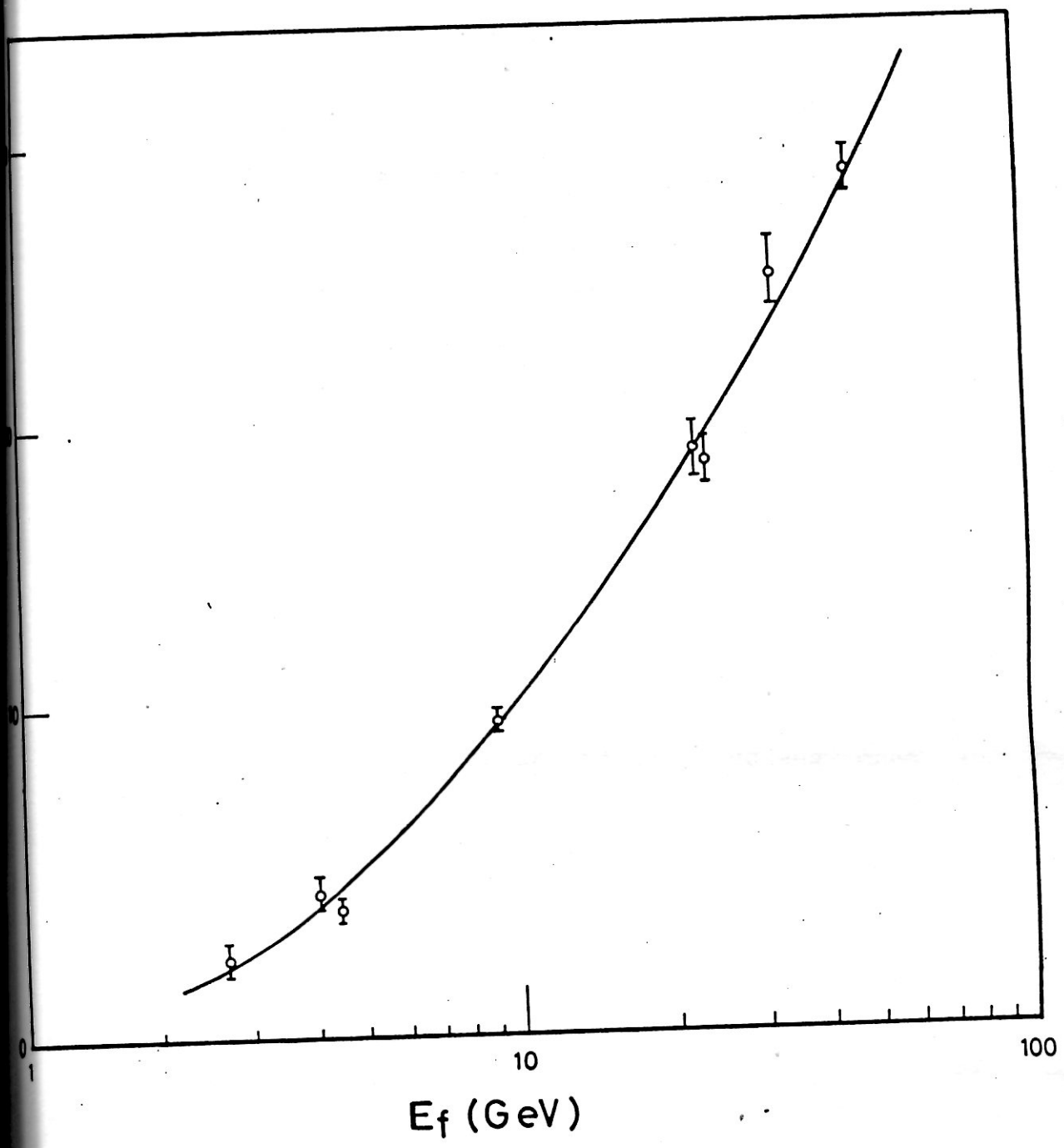

Fig. (2.3): The average multiplicity $\langle n_s \rangle$ versus the free energy E_f. The curve represent the relation $\langle n_s \rangle = (-1.97 \pm 0.1) + (1.07 \pm 0.004) \ln E_f + (1.79$ $0.19) (\ln E_f)^2$.

The obtained values of A, B and C : $A = -1.97 \pm 0.01$ $B = 1.07 \pm 0.004$ $C = 1.79 \pm 0.19$ respectively this a universal relation for this central collisions in the interaction of hadrons and heavy ions with juclei.

According to ref. 50 the authors had shown that at nearly zero impact parameter the n_s-distribution should be a poisson one for thermodynamic fireball and a wide range of dynamical models. It is interesting to compare the experimental n_s-distribution with the poisson one $P(n_s) = \frac{\langle n_s \rangle^{n_s} e^{xp} - \langle n_s \rangle}{n_s!}$ where $\langle n_s \rangle$ is the average multiplicity of showers in the present experiment. Fig.24 shows a good agreement between the experimental data and the poisson distribution. In Fig. (24), we also show a universal distribution of shower particles from P-emulsion collisions, at all impact parameters rescaled for our $\langle n_s \rangle$ and the total number of events. The comparison of the distributions shown in Fig. 24 indicates that the n_s-distribution from nucleus-nucleus collisions at small impact parameter is narrower than p-nucleus ones and deviates from KNO scalling. At small impact parameter the n_s-distribution is typically a poisson one.

II.9.3. <u>The multiplicity characteristic of grey particles</u>. The main characteristic of complete destruction events is the emission of unusually large number of grey particels. The grey particles are thought to be cascade particles or recoil nucleons. In the simple model proposed by us to give an account for the $\langle n_s \rangle$, one can make estimation of the average number of grey particles $\langle n_g \rangle$. The number of protons in the cylinder cut by the projectile in the target is given by:

$$Z_B + Z_T \cdot \frac{3}{2} (A_B/A_T)^{2/3}$$

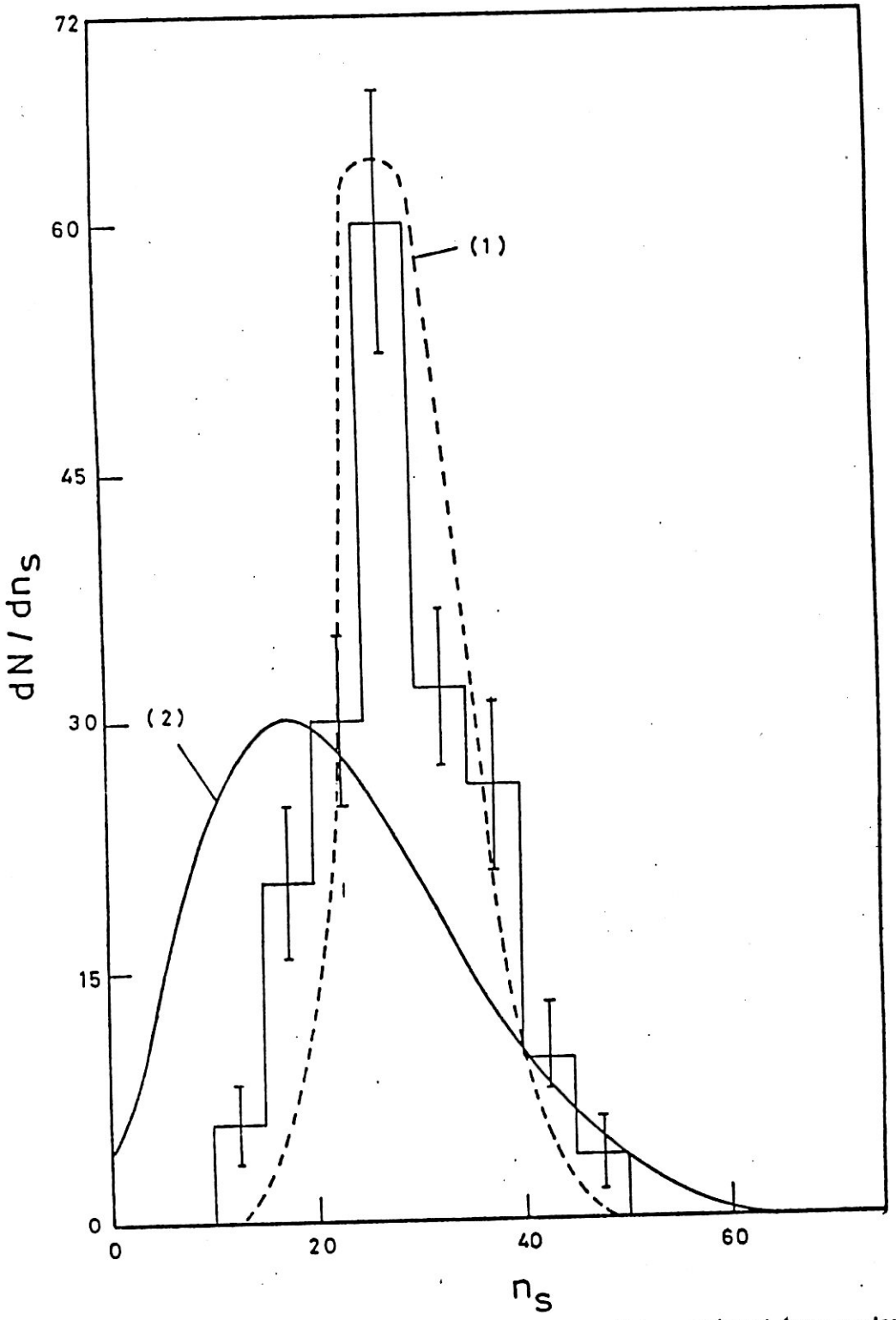

Fig.(24): The n_s - multiplicity distribution of particles emitted from central collision and having $I/I_o<1.4$, corresponding to proton energy >400 MeV. Curve (1) is the Poission distribution with $<n>=28.8$. Curve (2) is universal multiplicity distribution of p-nucleus which is rescaled to our $<n_s>$

In the present case this amounts to 37 which is much greater than the experimental $\langle n_g \rangle$ (=25.0 $\pm$ 0.6). However, the $\langle n_g \rangle$ is much greater than the prediction of the cascade evaporation model. Table 15 and Fig. 25 shows the dependence of $\langle n_g \rangle$ on the mass number of the incident nucleus A_B. The experimental points were fitted by the relation $\langle n_g \rangle = K_1 A^{\alpha}$. The results of fitting gave that $\alpha = 0.14 \pm 03$. It has been argued in the literature that $\langle n_g \rangle$ is a measure of the number of interacting nucleons. Fig. 26 and Table 15 presents the average grey particles $\langle n_g \rangle$ as a function of the number of interacting nucleons from both of the colliding nuclei. The data were fitted by the relation $\langle n_g \rangle = K_2 R^{\alpha}$, where α was found to be equal to 0.17 $\pm$ 0.04.

Table (15). The average number of grey particles $\langle n_g \rangle$ as a function of the number of interacting nucleons R_A from both of the colliding nuclei.

The projectile nucleus	$\langle n_g \rangle$	Number of interacting nucleons
H_e^4	19.8±1.4	5.48
C^{12}	22.3±0.8	15.85
O^{16}	26.2±1.1	18.58
N_e^{22}	24.3±0.3	22.10
M_g^{24}	25.0±0.6	23.15

In ref. 56, the authors claim that they observe a KNO-type scaling in the multiplicity distribution of medium energy protons emitted in central M_g^{24}-Ag(Br) interactions at 4.5 A GeV/c Fig. 27 shows the n_g-distribution for our complete destruction events. The curve is the universal distribution claimed in ref. 56, rescaled for our $\langle n_g \rangle$ and normalized to the same area. Our data contradict the results of the paper 56. The n_g-distribution seems to follow a poisson like one.

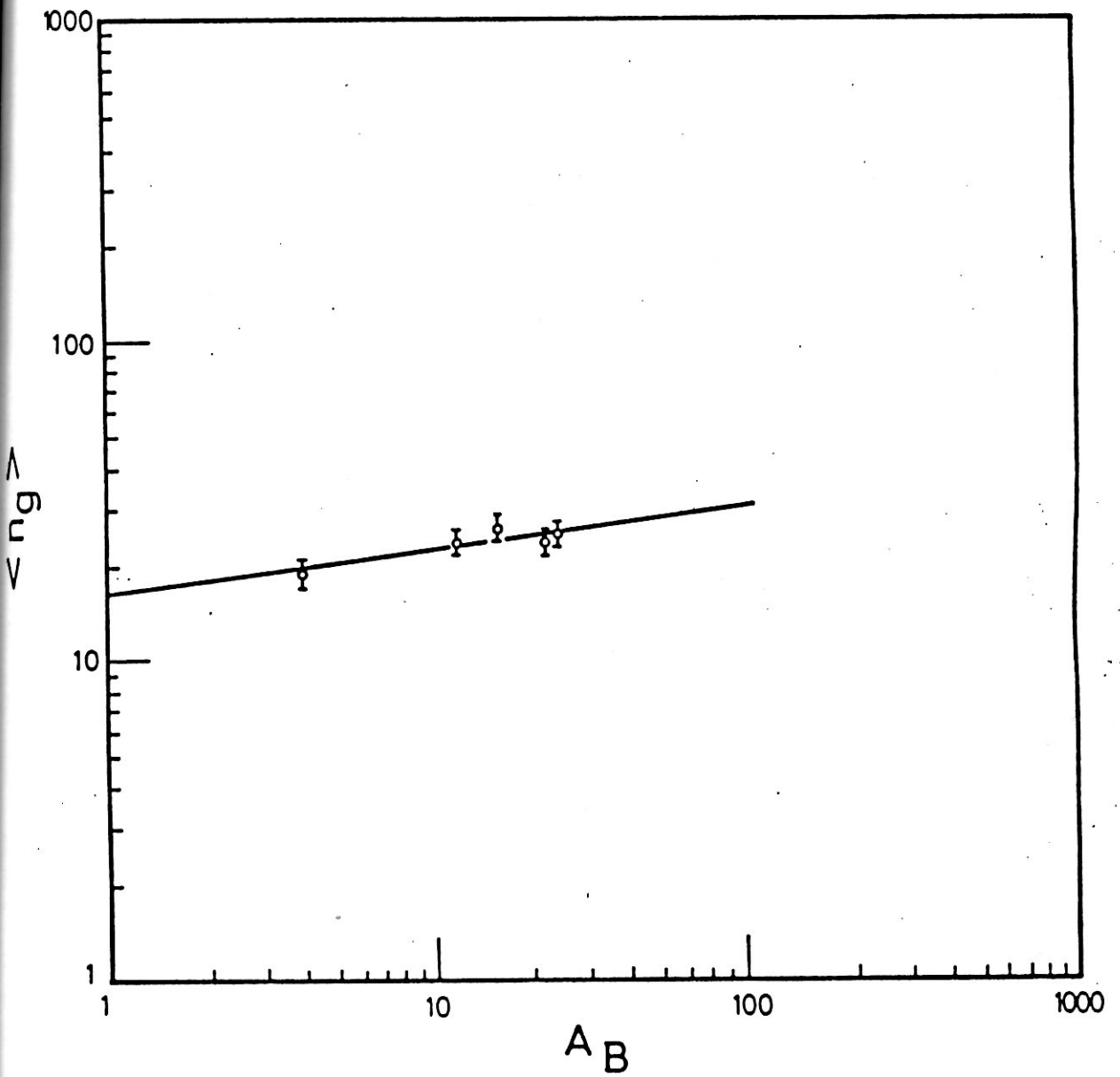

Fig.(25): The average multiplicity $\langle n_g \rangle$ as a function of the projectile mass number A_B in complete destruction at 4.5 A GeV/c.

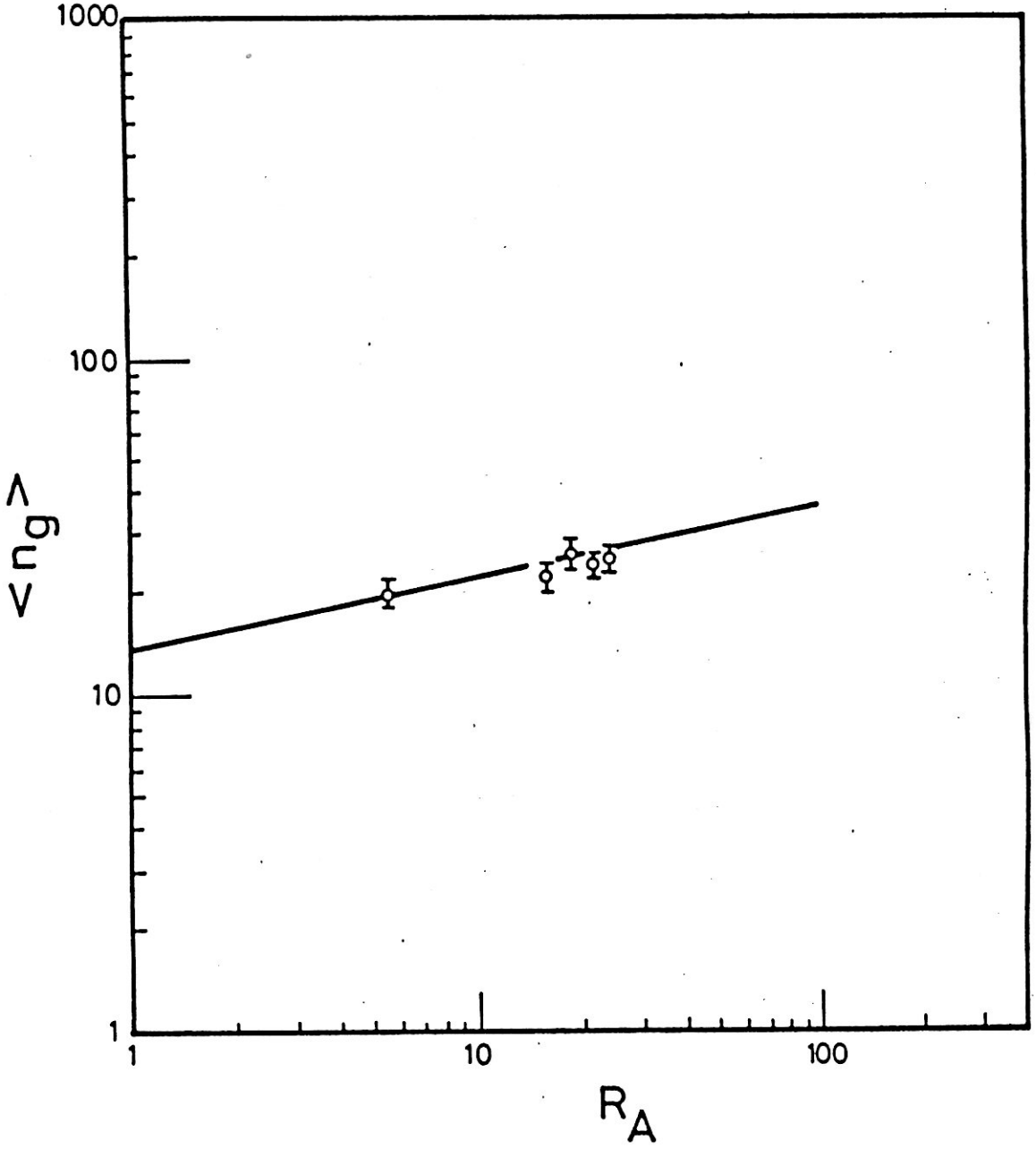

Fig.(26): The average multiplicity $\langle n_g \rangle$ as a function of the number of interacting nucleons R_A in complete destruction at 4.5 GeV/c.

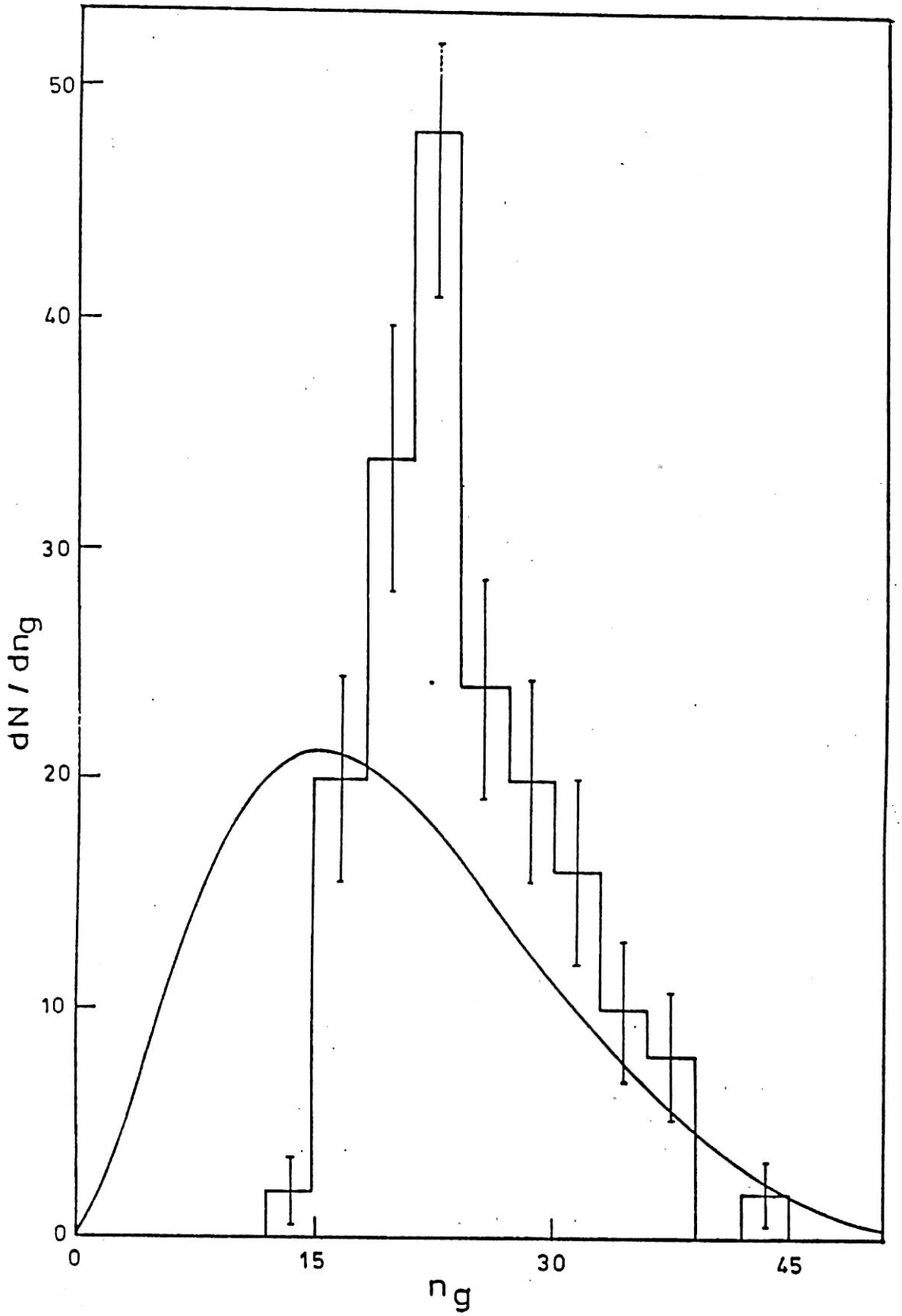

Fig. (27): The n_g - multiplicity distribution of particles emitted from central collisions and having $I^* > 1.4$. The curve is a universal multiplicity distribution[49] of nucleus-nucleus collisions which is rescaled to our $< n_g >$.

II.9.4. The multiplicity characteristic of black particles. Fig. 28 displays the n_b-distribution from Mg^{24}-Ag(Br) complete destruction events. A piosson like distibution is observed which significantly differs from n_b-distribution at all impact parameters.

The average multiplicity of black particles $\langle n_b \rangle$ which is a possible measure of the exitation energy of the residual nucleus is not sensitive to the variation of the incident energy and the beam nucleus. This fact is reflected in Fig.29, where the relation between $\langle n_b \rangle$ and A_B is fitted by the power law $\langle n_b \rangle = KA_B^{\alpha}$, α was found to be 0.040 ± 0.002 which is very small value.

II.9.5. Conclusions. The study of complete destruction of Ag (Br) nuclei i.e. events of $N_h \geq 28$ shown that:

1. The probability of complete destruction events is nearly independent of the incident energy and it increases linearly with $A_B^{2/3}$ up to $A_B=12$ where it becomes constant.

2. The $\langle n_s \rangle$ is proportional to A_B and A_T by the relations $\langle n_s \rangle \sim A_B^{0.63} . A_T^{0.36}$.

3. The $\langle n_s \rangle$ is proportional to the number of interacting nucleons R_A from both nuclei by the relation:

$$\langle n_s \rangle = 2.45 \pm 0.22) R_A^{(0.78 \pm 0.07)}$$

4. A model was put to explain the $\langle n_s \rangle$ values obtained in these events. It was found that $\langle n_s \rangle$ is proportional to the free energy in the CMS of the interacting particles by the relation:

$$\langle n_s \rangle = (-1.97 \pm .01) + (1.07 \pm .01) \mathrm{Ln}\, E_f + (1.79 \pm .19)(\mathrm{Ln} F_f)^2$$

5. The n_s-distribution is a poisson like one.

6. The average number of g-particles is greater than the prediction of the cascade evaporation model.

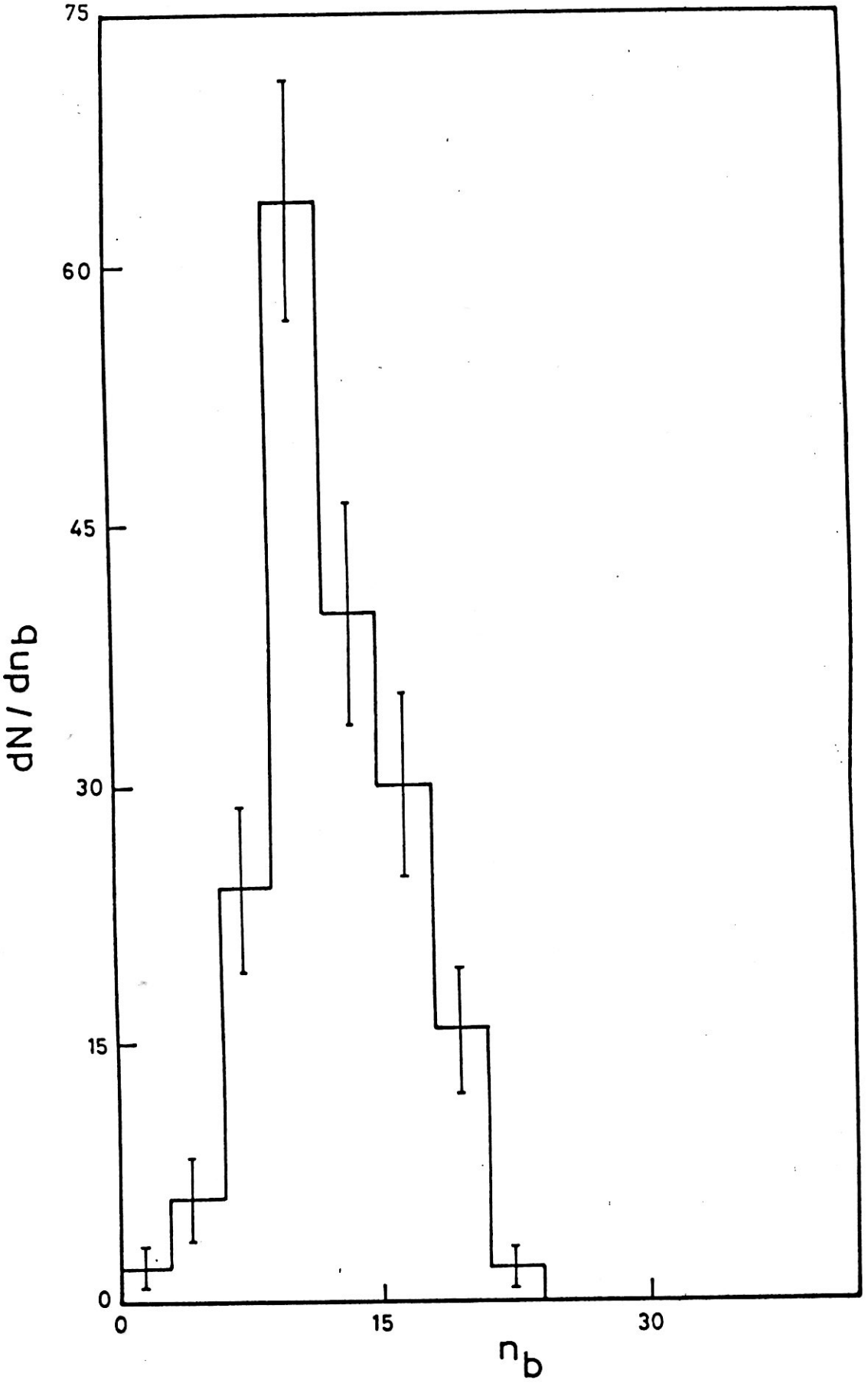

Fig. (28) The n_b -multiblicity distribution of particles emitted from central collisions.

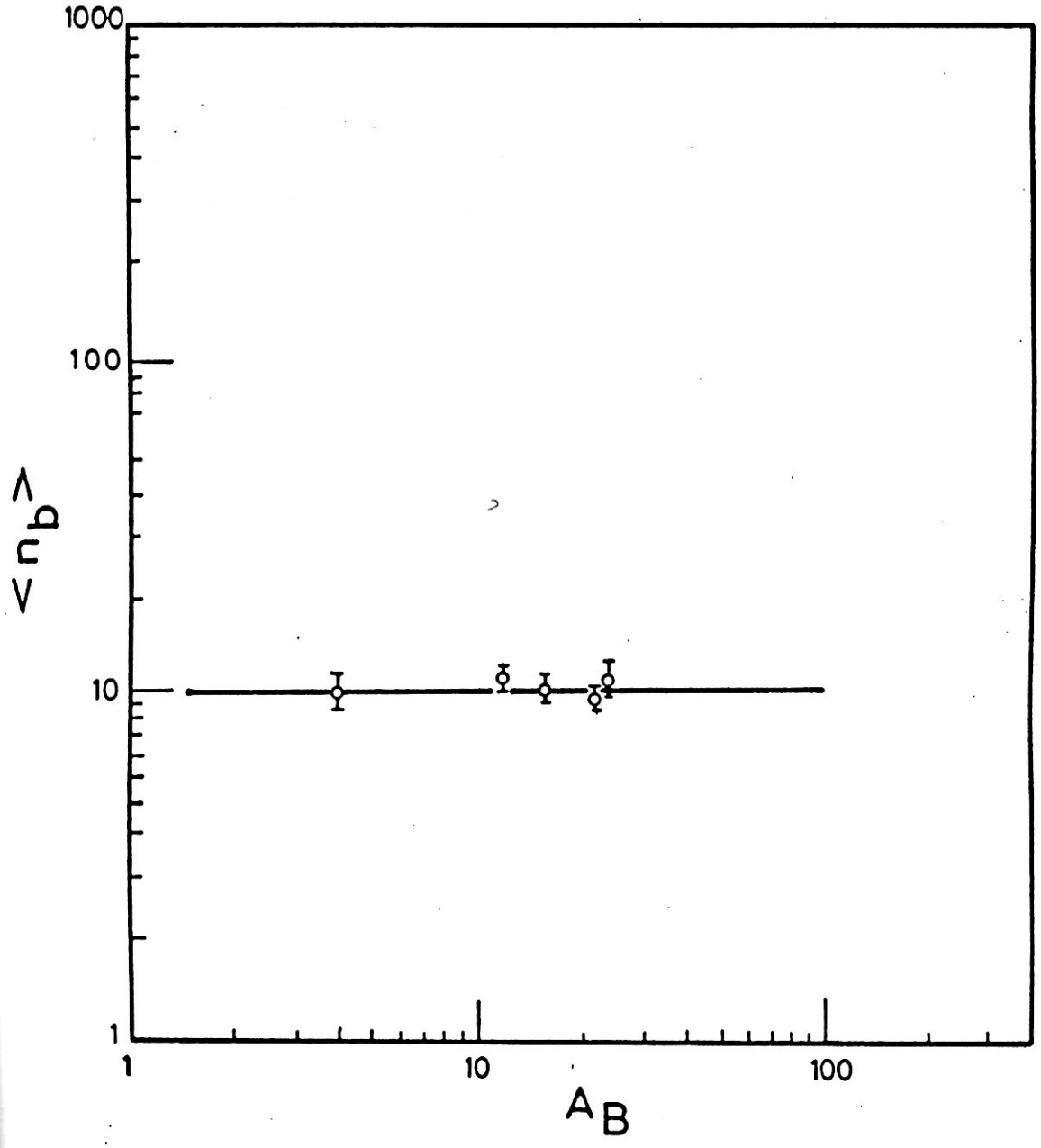

Fig. (29): The average multiplicity $\langle n_b \rangle$ as a function of the mass number A_B. The solid line represent the relation $\langle n_b \rangle = K A_B^{\alpha}$

7. The $\langle n_g \rangle$ is related to the mass number of the beam nucleus by the relation

$$\langle n_g \rangle \sim A_B^{0.14 \pm 0.01},$$

$$\langle n_g \rangle \sim R_A^{0.17 \pm 0.04}$$

where R_A is the average number of interacting nucleons.

8. The n_b-distribution is independent of any of the considered variables.

II.10. Fragmentation of Ne^{22}, Mg^{24} and Si^{28} in emulsion at 4.1-4.5 A GeV/c.

II.10.1. Introduction. In nucleus-nucleus collisions, the nucleons in the overlap region are called participants. The remaining nucleons are spectators. Large impact parameters lead to "gentle" reactions while small ones give "violent" interactions. The spectators are the prefragments which further decay into fragments. The mechanism of this process is still a matter of debate. Fragmentation is one of the historical and fundamental questions in high energy nuclear physics. The author of /57/ schematically distinguished three main mechanisms for the fragmentation of $A \geq 200$ prefragment nucleus: the first mechanism is spallation which leads to one fragment of mass near that of the prefragment nucleus, the second one is fission which gives two heavy fragments, each of mass close to half the prefragment nucleus mass. Multifragmentation is the third mechanism which provides several fragments. In /58/ the fragmentation processes are divided according to the temperature, T, of prefragment nucleus as follows: at $T \leq 5$ MeV the mass yield distribution is localized near the minimal and maximal masses corresponding to single nucleons and residual nuclei.

At $T \simeq 5\text{-}7$ MeV the mass distribution has a U-shaped form which indicates the multifragmentation threshold. At $T>7$ the inclusive mass yield distribution becomes a monotonously decreasing function, the steepness of which increases with increasing T.

Many theoretical models have been devoted to the study of the multifragmentation process/57/. In some models, the prefragment nucleus heats up and then condensates into droplets/23/. In others, it simply evaporates the fragments sequentially /23/ . In /23/ , the fragments are statistically emitted from an intermediate excited nuclear system. Other statistical approaches/ 57/ try to explain the multifragmentation without any reference to thermal equilibrium, i.e. as shattering of the prefragment nucleus into many pieces. A detailed description of different multifragmentation models is given in the review articles /57,58/ .

To study the mechanism of multifragmentation, a huge number of experiments has been carried out. These experiments dealt with heavy target nucleus fragmentation induced by energetic protons and ions The use of heavy ion beams has an important experimental advantage: one can study the fragments produced by the disintegration of the projectile nucleus. The fragments of the projectile nucleus are fast, distinguishable and can be easily measured in detectors and/or spectrometers while the target fragments are slow, difficult to be measured and often fragmentation experiments gave one-particle inclusive measurements, e.g. the charge $d\sigma/dz$ or mass $d\sigma/dA$ yield of the fragments. Various models predicted nearly the same form of $d\sigma/dz$ and $d\sigma/dA$. Thus, these data turned out to be inconclusive with respect to various models.

In the present experiment all projectile fragments (PFs) were recorded, and their charges and emission angles

were measured. Thus, we have exclusive data which enable one to study different types of fragment distribution, correlations and comparison with theoretical models. It is of particular interest to test whether fragments are emitted from one source at a single excitation energy.

In the present study, two samples of 4.1A GeV/c ^{22}Ne-emulsion collisions have been used. The first sample consists of 4307 events measured in this experiment (EXP) and the second one is 4976 events simulated in a computer by the cascade-evaporation model (CEM) under the same experimental conditions. Another two samples were used, each consists of 1000 events, of 4.5 A GeV/c Mg^{24}-and Si^{28}-emulsion collisions.

II.10.2. **Selection criteria**. We selected events having the total charge of PFs, $Z^*=Z_b$ i.e. those conserving the charge of the beam nucleus. Here we study the charge yield distribution for the projectile fragmentation, the fragment-fragment correlation and the relation between PFs and TFs. This enables us to distinguish between different theoretical models

II.10.3. **Results and discussion**. The multiplicity characteristics of the events selected from EXP and CEM are presented in Table 16. The value of $\langle n_s \rangle$, $\langle n_b \rangle$ in CEM are systematically higher than the corresponding values in EXP. Light and heavy PFs are produced in CEM more copiously than in EXP. The PFs of medium charge Z=4,6 are nearly absent in CEM. This can be explained by the fact that in CEM the light fragments are produced by evaportion and the heavy ones are just residual nuclei of the prefragment systems. Table 16 demonstrates that there is a great deviation between CEM and EXP in all average multiplicities of fragments. Table 17 shows the catalogue of 855 selected evetns, i.e. those having the total charge

Table 16. The multiplicity characteristics of the selected events of the total charge of PF, $Z^* = 10$, from EXP and CEM.

		EXP	CEM
$\langle n_s \rangle$		1.30±0.06	1.91±0.09
$\langle n_g \rangle$		0.96±0.06	1.46±0.10
$\langle n_h \rangle$		1.44±0.07	2.34±0.13
$\langle n_{Z=i} \rangle$, $i =$	1	0.99±0.05	1.59±0.11
	2	0.81±0.04	0.36±0.04
	3	0.02±0.01	0±0
	4	0.03±0.01	0.01±0.01
	5	0.04±0.01	0.01±0.01
	6	0.12±0.01	0.02±0.01
	7	0.15±0.01	0.02±0.01
	8	0.23±0.02	0.05±0.01
	9	0.10±0.01	0.12±0.01
	10	0.26±0.02	0.59±0.02

Table 17. The catalogue of the selected events. Different channels of fragmentation are ordered according to Z_{max}.

Fragmentation channel	Frequency	Fragmentation channel	Frequency
Ne	222	H + Be + B	2
H + F	82	5H + B	4
He + O	142	2B	1
2H + O	49	2H + 2He + Be	9
		4H + He + Be	5
H + He + N	102	3He + Be	4
3H + N	24	H + He + Li + Be	1
2H + He + C	54	3H + 2He + Li	7
2He + C	29	H + 3He + Li	4
4H + C	14	7H + Li	1
H + Li + C	2	H + 3Li	1
Be + C	1	5He	10
		2H + 4He	30
3H + He + B	14	4H + 3He	14
H + 2He + B	13	6H + 2He	5
		8H + He	3

of PFs, $Z^*=10$. One can see different channels of fragmentation ordered according to Z_{max} the charge of the heaviest PF emitted in an interaction. At the beginning one can observe the "gentle" spallation process in which one or two particles are evaporated from the prefragment nucleus leaving the residual nucleus which cools down forming a heavy fragment. This process is characterized by low excitation energy and temperature. On the contrary, at the end of the table one can notice a "violent" process in which the prefragment Ne^{22} nucleus has been destroyed into H and He fragments. Fig.30 shows the charge yield curve for fragment production from the ^{22}Ne, Mg^{24} and Si^{28} projectiles in the case of collision with emulsion. The distribution has a characteristic U shaped form. In the region of small Z, the curve decreases, then it rises for large values of Z. The number of target fragments N_h can be used as a measure of the "violence" of a collision. To demonstrate the correlation between PFs and N_h, Fig.31 shows the charge distribution of PFs for a sub-class of events of $N_h=1$ and $N_h=4$. In the former case a nearly symmetric U-shaped distribution is obtained which is connected with the "gentle" low temperature process. In the latter case the distribution decreases from light to heavier fragments. The class of $N_h=1$ events cannot be totally attributed to the "gentle" peripheral collisions. Fragments of small Z, in this class of events, are mostly the products of "non-peripheral" collisions between beam nucleus Ne^{22} and emulsion. In these events a target nucleon dives into the projectile nucleus destroying it into small fragments. The size of the largest fragment which can be formed from the projectile spectator nucleus decreased with decreasing the impact parameter. At $N_h=1$, fragments of large Z are the evaporation residues of peripheral collisions. Thus, light fragments (Z=1 and 2) are the products of either "gentle" evaporation or "violent" multifragmentation.

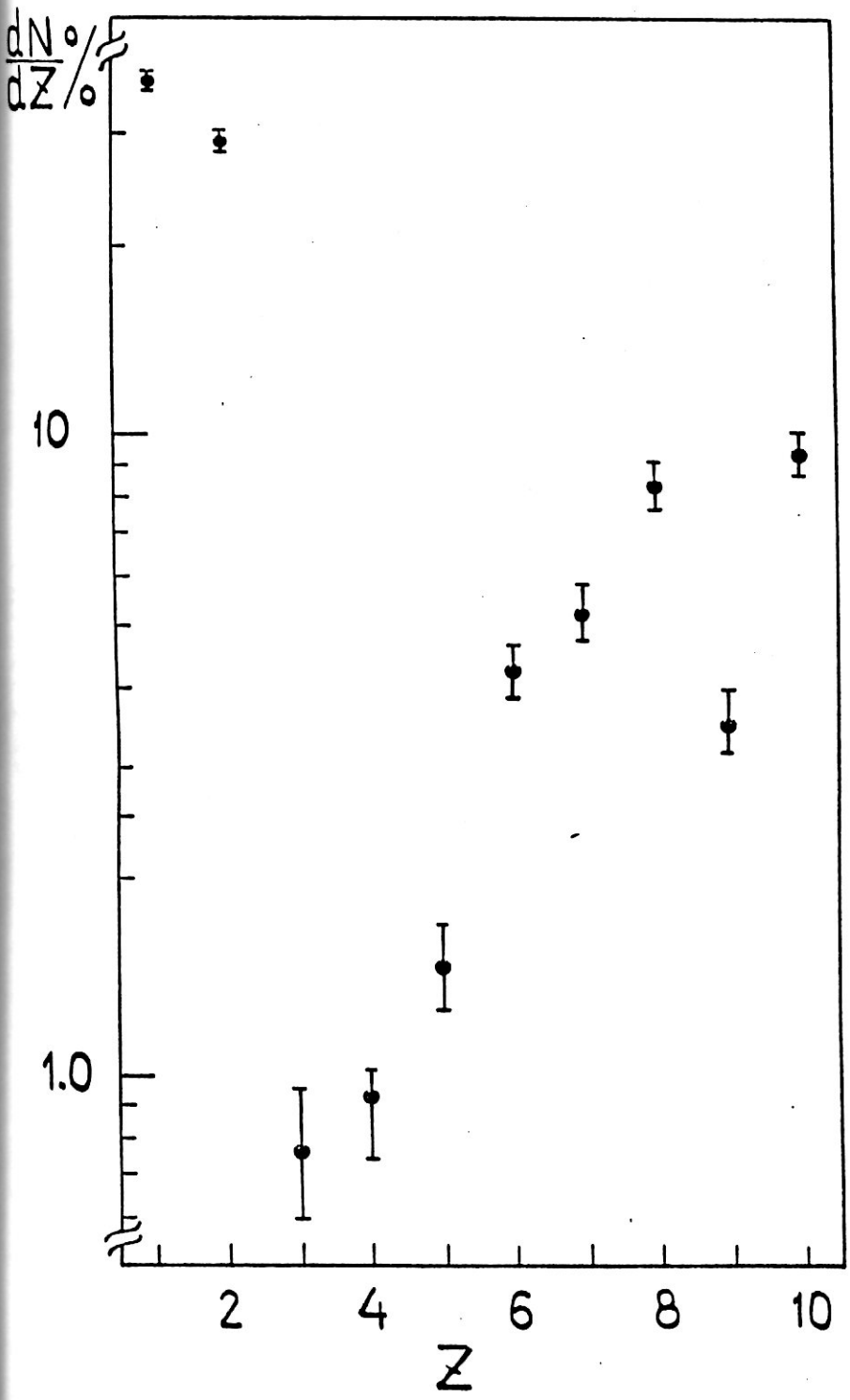

Fig. 30a. The charge yield distribution of PF from ^{22}Ne.

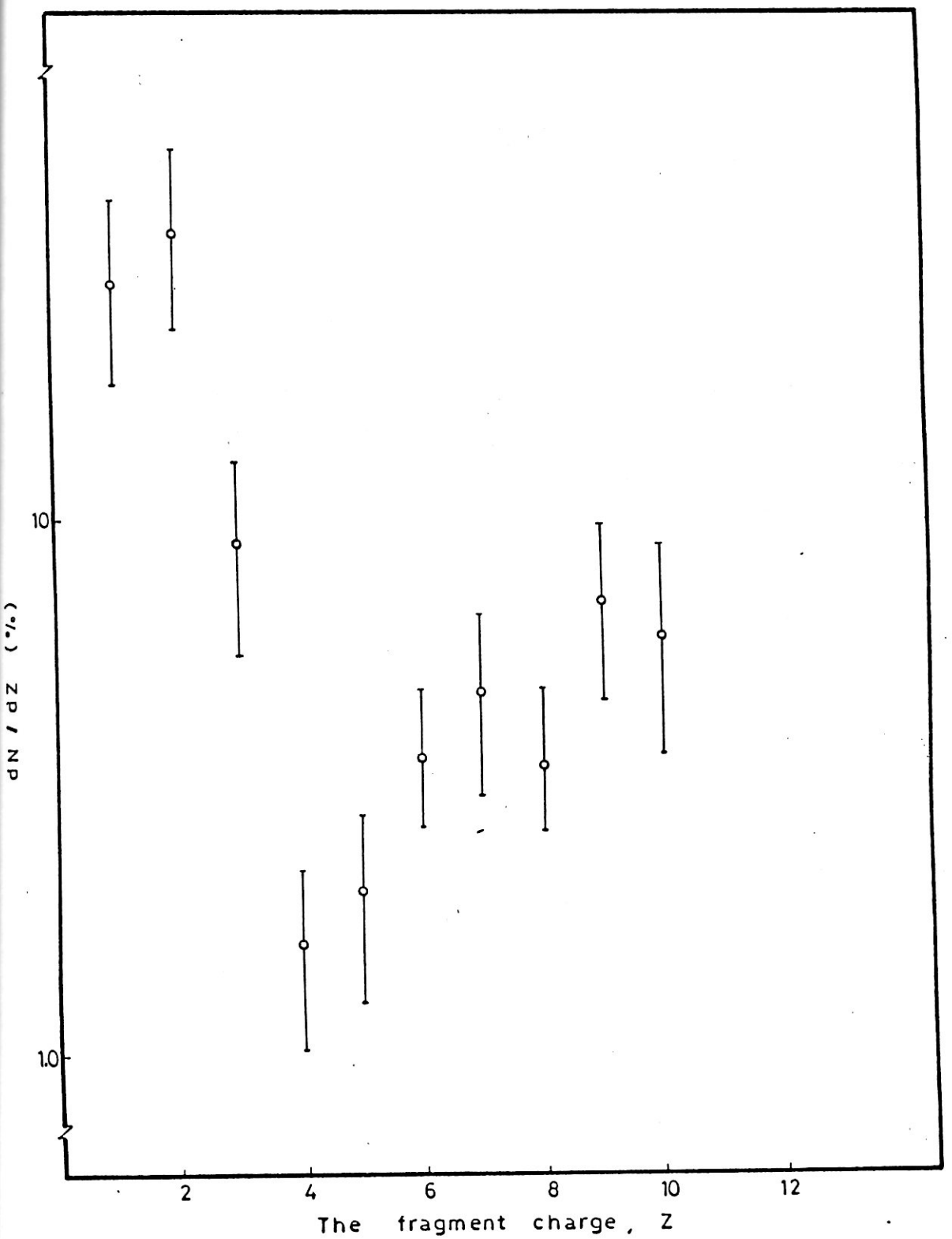

Figure 30.b. The charge yield distribution of projectile fragment from Mg^{24} fragmentation in emulsion at 4.5 A Gev/c $Z^* = Z_{beam}$.

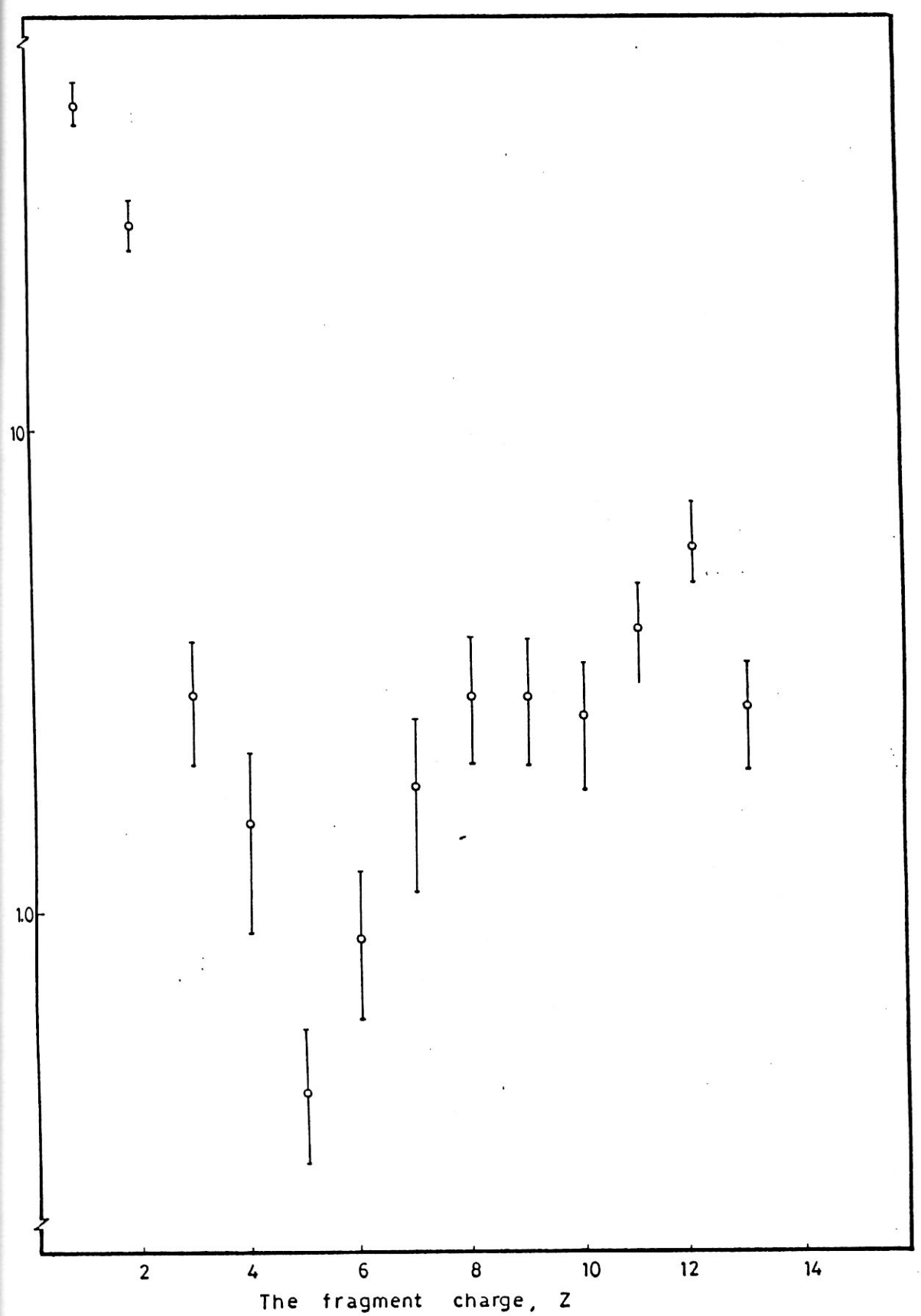

Figure 30. The charge yield distribution of projectile fragment from Si^{28} fragmentation in emulsion at 4.5 A Gev/c $Z^* = Z$ beam.

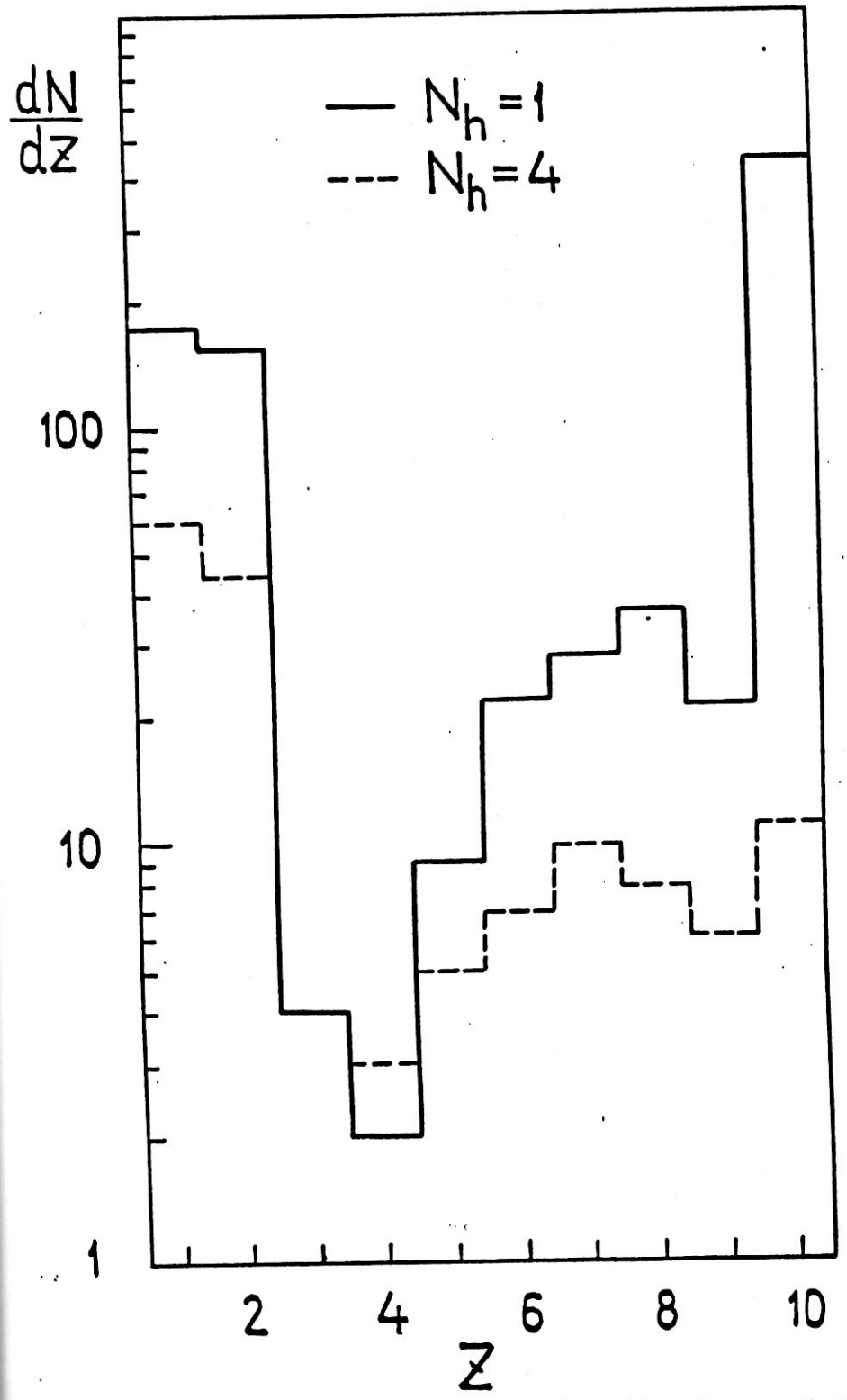

Fig. 31. The charge yield distributions of PF from N_h =1 (——) and N_h =4 (---) events (Ne^{22}).

The degree of "violence" of a collision can be characterized by the number of signly charged projectile fragments N_1. These fragments are from different sources: direct pick up during the intranuclear cascade, evaporation, and the smallest fragments of the multifragmentation process. In any of these cases the production rate should increase with the degree of "violence" of the collision or with the excitation energy of the emitting source. Table 18 shows the charge distribution of PFs as a function of N_1. Fig. 32 shows that the charge distribution takes the U-shaped from in the case of $N_1 \leq 2$ while it decreases for $N_1 \geq 3$. This behaviour is more pronounced in the class of $N_h=0$ events. Fig. 33 displays the charge distribution for $N_1 = 0$ and $N_1 \geq 4$ events. The transition from the U-shaped distribution to the monotonously decreasing one is more obvious in this case.

Another measure of the "violence" of a collision is Z_{max}, the charge of the largest PF emitted in the interaction. Table 19 shows the dependence of the charge distribution of PFs on Z_{max}. At large values of Z_{max}, i.e. "gentle" collisions, the charge distribution of PFs is a nearly symmetric U-shaped one. At low values of Z_{max}, i.e. "violent" collisions, the charge distribution is a decreasing function. These features are seen better in Fig. 34 where the charge distributions are presented for $Z_{max} \geq 6$ and Z_{max} events. The analysis of Figs. 30-40 and Tables 16-19 show that the inclusive charge yield distribution of fragments is a superposition of different mechanisms. One can at least distinguish two main classes of mechanisms gentle evaporation and violent multifragmentation. The authors of /59/ have interpreted the mass yield curve in the frame of liquid gas transition. The present analysis shows that this claim is not conclusive; singly and doubly charged fragments are obviously due to different mechanisms. The violence of

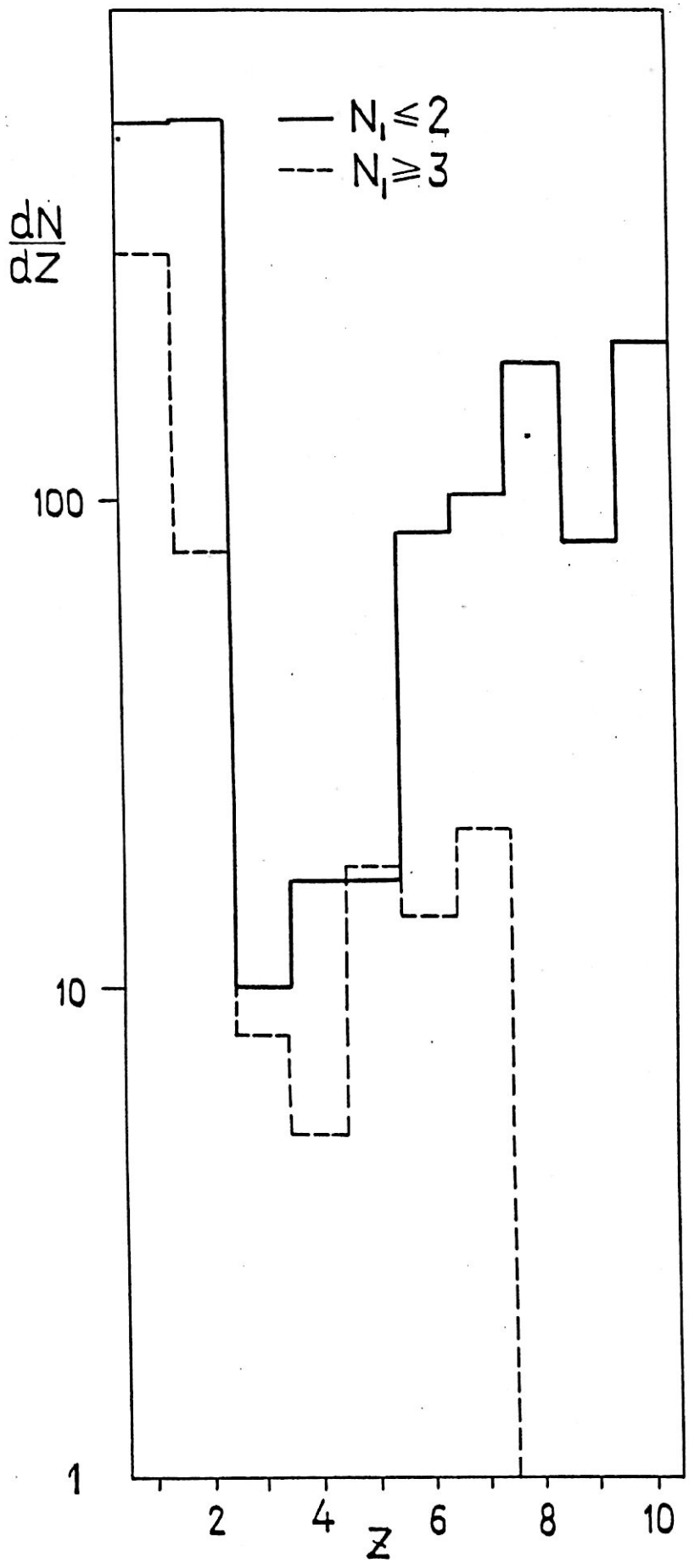

Fig. 32. The charge yield distribution of PF from events of $N_1 \leq 2$ (—) and $N_1 > 3$ (- - -)

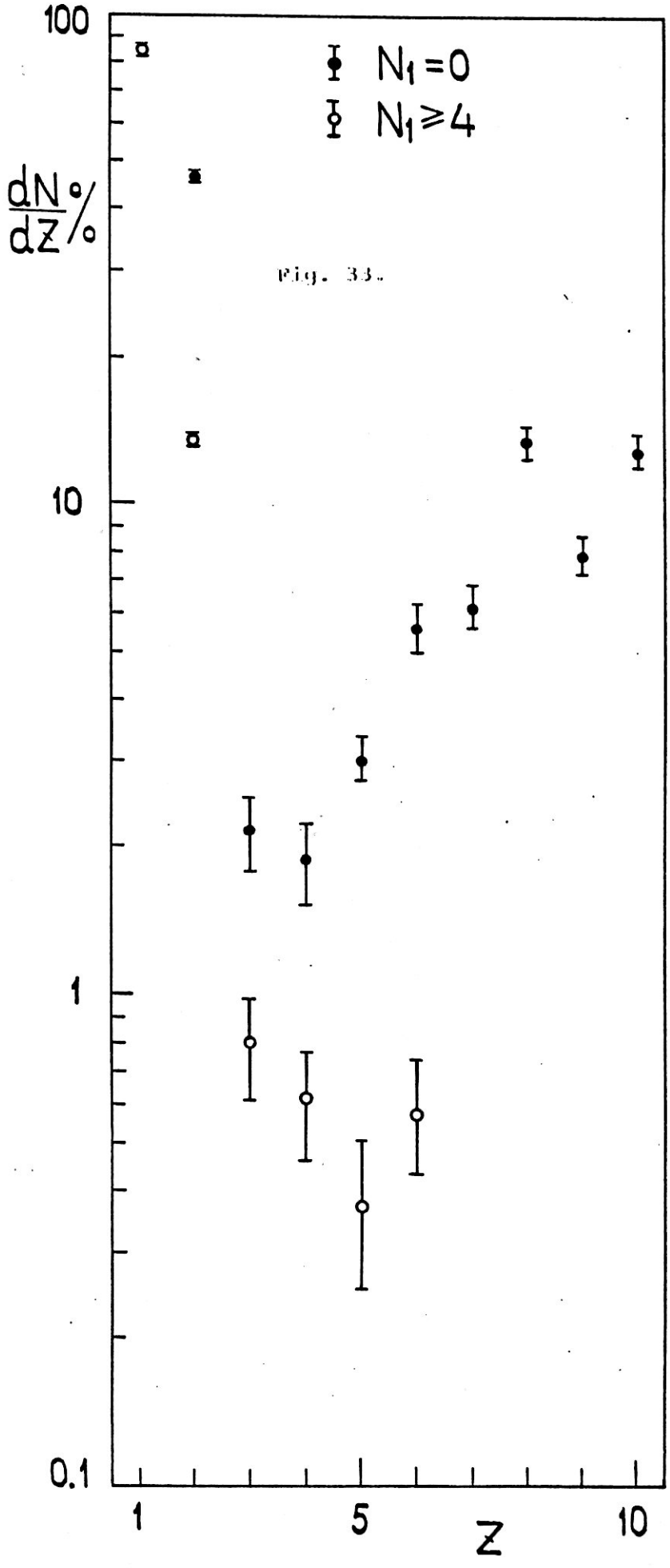

Fig. 33.

Table 18. The charge distribution of PF as a function of the number of singly charged PF

	N_1								
Z	0	1	2	3	4	5	6	7	8
1		207	284	135	132	20	30	7	24
2	262	141	192	28	47		10		3
3		10		7			1	1	
4	5	3	9		5				
5	2	15		14		4			
6	30	2	54		14				
7		102		24					
8	142		49						
9		82							
10	222								

Table 19. The dependence of the charge distribution of PF on Z_{max}.

	Z									
Z_{max}	1	2	3	4	5	6	7	8	9	10
2	180	225								
3	33	26	15							
4	39	36	1	19						
5	77	40		2	35					
6	176	112	2	1		100				
7	174	102					126			
8	98	142						191		
9	82								82	
10										222

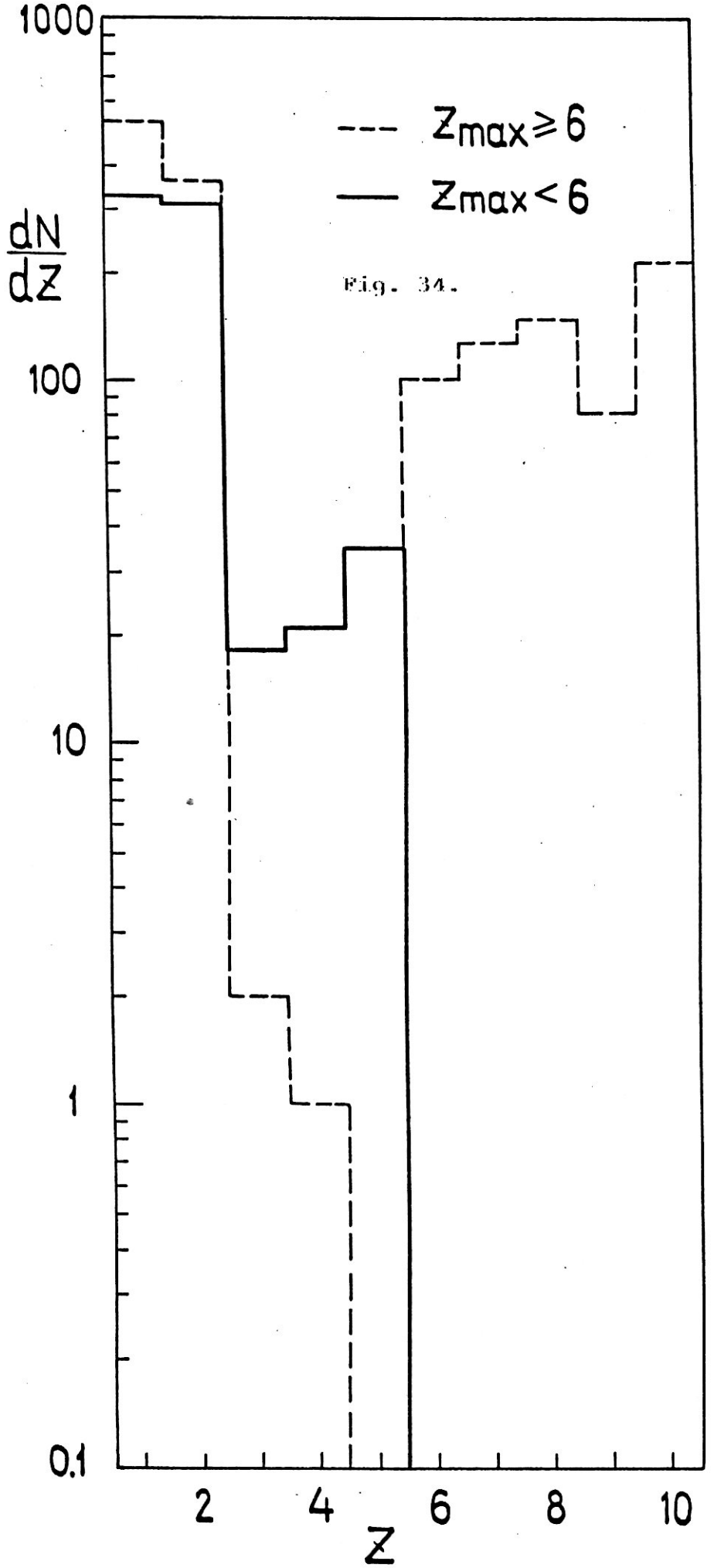

Fig. 34.

the interaction can be measured by the multiplicities of target fragment associated with a projectile fragment. Table 20 presents $\langle n_s \rangle$ and $\langle N_h \rangle$ as a function of the number of PFs. The first column represents the average number of PFs . The second column is the excitation energy per nucleon (in MeV) of the prefragment nucleus calculated according to the statistical model [58]. The third and fourth columns represent the average multiplicities of the associated s and h particles, respectively. The correlation between the multiplicities of PFs and TFs is clearly seen from Table 20 . The values of $\langle n_s \rangle$ and $\langle N_h \rangle$ increase systematically with N_{PF}.

The class of events of $N_h=0$, i.e. those without target fragmentation, were studied in detail for ^{12}C-emulsion collisions at 4.5 A GeV/c and at 2.1 A GeV . It is interesting to compare the present data with these results. The production frequency of events in ^{22}Ne-Em collisions as a function of Z_{max} is shown in Fig. 35 and Table 21 . It should be noted that the maximum probability is for events having $Z_{max}=2$. In the case of 4.5 A GeV/c ^{12}CEm collisions , the fraction of such events is (62±9) % of all $N_h=0$ events. For 4.1 A GeV/c ^{22}Ne-Em, the coressponding ratio is only (24±2)%. This experimental fact can be interpreted by two main reasons: (i) The ^{12}C nucleus is an even-even one of total zero spin, i.e. an α -cluster nucleus. (ii) The main channel of fragmentation is a two-particle one. In the case of ^{22}Ne-Em collisions, Ne $\longrightarrow$ He + O predominates, and both He and O are stable nuclei. The corresponding channel in ^{12}C-Em collisions is $^{12}C \longrightarrow$ He + Be, but is an unstable nucleus which directly decays into 2 He nuclei. In fact, the percentage of He for ^{12}C-Em collisions is (62±9)%. If this percentage is divided by two, it will be nearly equal to the corresponding value of ^{22}Ne-Em collisions.

Table 20 $\langle n_s \rangle$ and $\langle N_h \rangle$ as a function of the number of PF.

$\langle N_{PF} \rangle$	ε^*/A	$\langle n_s \rangle$	$\langle N_h \rangle$
1.51	5	0.64±0.08	1.94±0.18
3.35	7	1.82±0.15	2.69±0.31
5.47	15	2.44±0.38	3.19±0.61
7.62	18	2.81±0.97	4.04±1.38

Table 21. The production frequency in percentage of events in emulsion as a function of Z_{max}, the charge of the heaviest PF in an interaction.

	Z_{max}			
Beam	1	2	3	≥4
2.1*A* GeV ^{12}C	7±2	59±10	8±3	26±12
4.5*A* GeV ^{12}C	13±4	62±9	15±4	10±3
4.1*A* GeV ^{22}Ne	2±1	24±2	4±1	70±4

Table 22. The catalogue of the observed PF in events of $N_h = 0$ and $n_s = 0$ ordered according to Z_{max}.

Fragmentation channel	Frequency
Ne	3
H + F	18
He + O	56
2H + O	8
H + He + N	10
3H + N	3
2H + He + C	3
2He + C	6
4H + C	1
He + Li + B	1
H + 2He + B	3
3He + Be	2
2H + 2He + Be	1
2H + 4He	1
5He	4

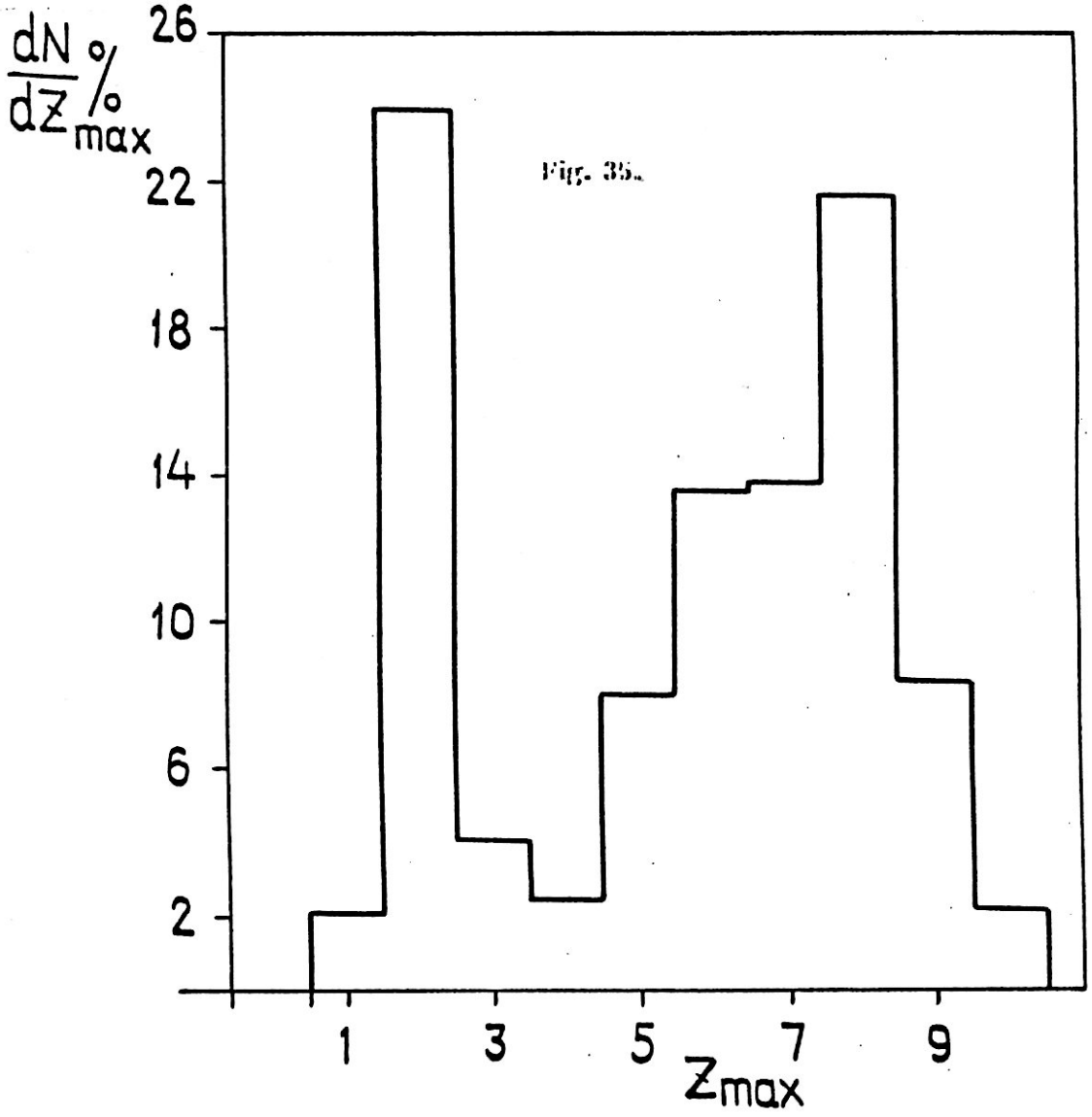

Fig. 35.

Table 21 shows that the production frequency of events in emulsion as a function of Z_{max} is independent of energy in the range of a few GeV/c per nucleon. It is remarkable that Z=2 and Z=8 are the first two magic numbers. This explains the peaks observed at these values in Fig.35. The results show that the nucler structure of the prefragment nucleus plays an important role in the fragmentation process. More "gentle" fragmentations of ^{22}Ne projectile nuclei are the events of $N_h=0$ and $n_s=0$, i.e. those without target fragmentation and generation of shower particles. Table 22 presents a catalogue of the observed PFs in the 120 events of $N_h=0$ and $n_s=0$ ordered according to Z_{max}. Out of them, the number of single and double-prong stars is 77 (64.2%). This shows a low excitation energy of the prefragment nucleus, $\varepsilon_{exc}/A \simeq$ 3-4 MeV

II.10.4 Conclusions. In ^{22}Ne, Mg^{24} and Si^{28} + Em collisions at (4.1-4.5) A GeV/c, events having the total charge of PFs, Z* , equal to the beam charge, have been selected for studying the fragmentation of ^{22}Ne, Mg^{24} and Si^{28} in emulsion.

The inclusive charge distribution of fragments is a superposition of different mechanisms. The heavy fragments (Z= 8-14) as well as some of the light ones (Z=1,2) originate mainly from "gentle" peripheral collisions. They show a distribution characteristic for evaporation from the compound nucleus. This process is characterized by low exitation energy. These fragments are associated with a low multiplicity of target tracks. The medium mass fragments as well as the measurable part of Z=1 and 2 fragments are due to nonperipheral "violent" collisions characterized by associated large multiplicities of the target. The charge distribution of these fragments has a monotonously decreasing shape. Thus, the mechanisms

claiming one hot source at a certain excitation energy for explaining the inclusive charge distribution conflict with the present analysis.

The presented cascade-evaporation model does not reproduce the average multiplicities of projectile and target fragments in the selected class of extreme peripheral collisions.

II.11. Sideward flow of nuclear matter in nucleus-emulsion collisions at (.4.1-4.5) A GeV/c

II.11.1. Introduction. In recent years, many activites were devoted to the detection of a "collective sideward flow" predicted by hydrodynamical calculation of nucleus-nucleus collisions /22/ . The experimental investigations were basically directed to the observation of the collective flow of nuclear matter which appears in angular distributions of the fragments of colliding nuclei. Of particular interest was the dependence of the "flow angle" on the impact paramter. The sideward flow is usually called "bounce off" for projectile fragments and "side splach" for target ones . A collective flow of nuclear matter has been first reported in refrence /60/ using nuclear emulsion and AgCl nuclear track detectors. It has been shown that the angular distribution of alpha particle target fragments, emitted from central ^{12}C + ^{108}Ag collisions, peaks at an angle predicted by shock wave calculation . A series of subsequent experimental data has shown either less evidence for this peaking or its absence, e.g. /61/ A few years later another hint has been observed in a broad sideward maximum in the angular distribution of low and medium energy protons form 393 ^{40}Ar + ^{208}Pb collisions exhibited signatures of the "bounce off" effect. A 4π detector has been required. The exclusive data, obtained by the plastic ball have shown the "bounce off" of projectile fragments (PFs)

and the "side splash" of target fragments (TFs) in 400 A MeV ^{93}Nb + ^{93}Nb and ^{40}Ca + ^{40}Ca collisions. In the streamer chamber data the collective flow has been also seen in 1.8 A GeV ^{40}Ar + KCl and in 0.9 A GeV ^{238}U + ^{238}U collisions (see fig. 36 a,b)/62/. Recent results have been obtained by emulsion groups. The authors have studied the correlation between different secondary charged particles in the azimuthal plane of central ^{12}C +^{208}Pb collisions at 4.5 A GeV/c. They have pointed to a possible hydrodynamical collective effect. The transverse momentum data of projectile fragments have been analysed in interaction of Au and Xe with emulsions at energies form 0.5 to 1.2 A Gev/22/ . Evidence for the collective flow has been reported. Another group studied the angular distribution of projectile fragments and target fragments and correlations between them in high multiplicity preipheral collisions of 0.85 A GeV ^{238}U nuclei with Ag(Br) , the observations is consistent with the collective flow. The authors of /24/ analysed the azimuthal angles of secondary particles and the transverse momentum of projectile fragments. It has been shown that the residual of Ne nucleus receives a transverse momentum of $\approx$ 0.4 GeV/c in 4.1 A GeV/c ^{22}Ne + Ag(Br) collisions, the side flight of produced particles and target fragments has been observed. In reference /62/ we studied the collective flow of nuclear matter in central collisions of 4.5 A GeV/c Mg^{24} emulsion nuclei. The aim of the this study was to investigate the sideward flow of nuclear matter in heavy ion collisions. The reslts from this study shows that, the increase of projectile nucleus mass number leads to, the increase of the number of single-charged relativistic particles with $\beta >$ 0.75 and the increase of sideward emission of b-particle and the angular distribution of target fragments is not isotropic and the position of the maximum of the angle of flow (θ_F) distribution shifts to higher values with decreasing the impact

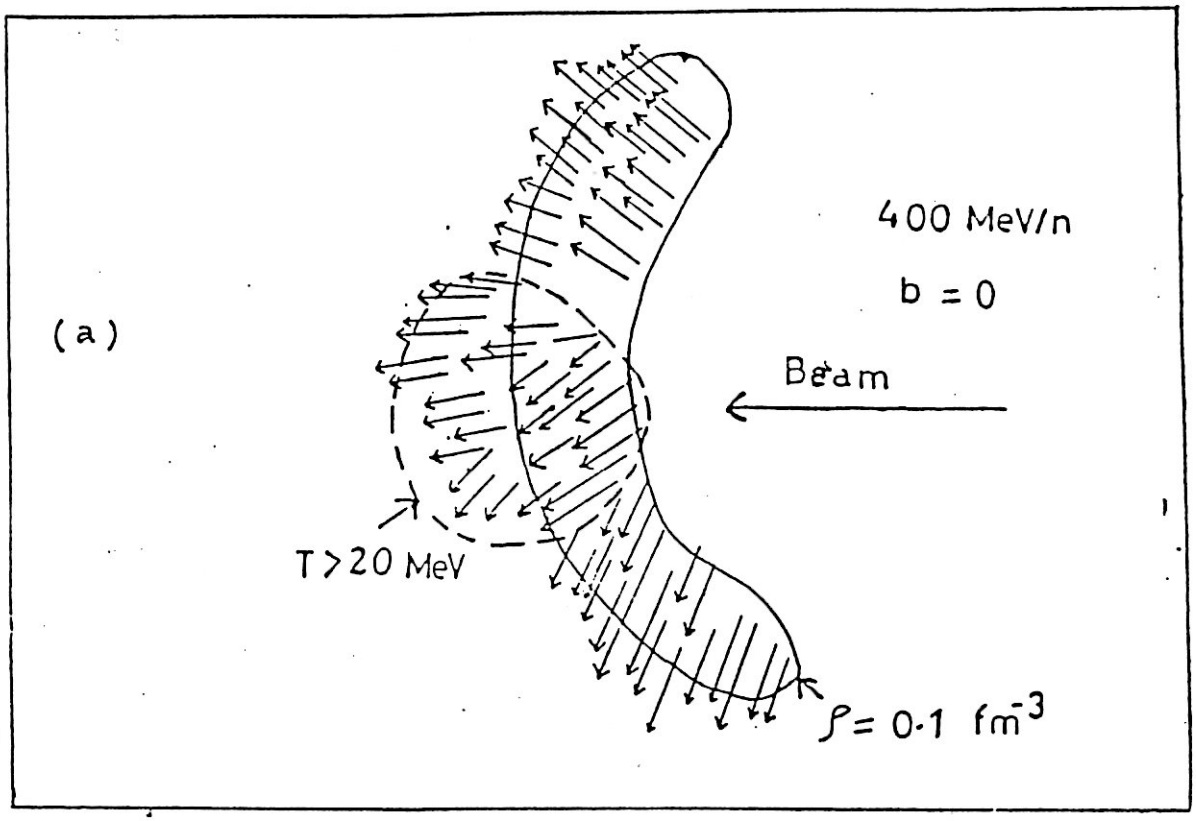

Fig.36 (a) Hydrodynamical side - splash effect expected at small impact parameter .

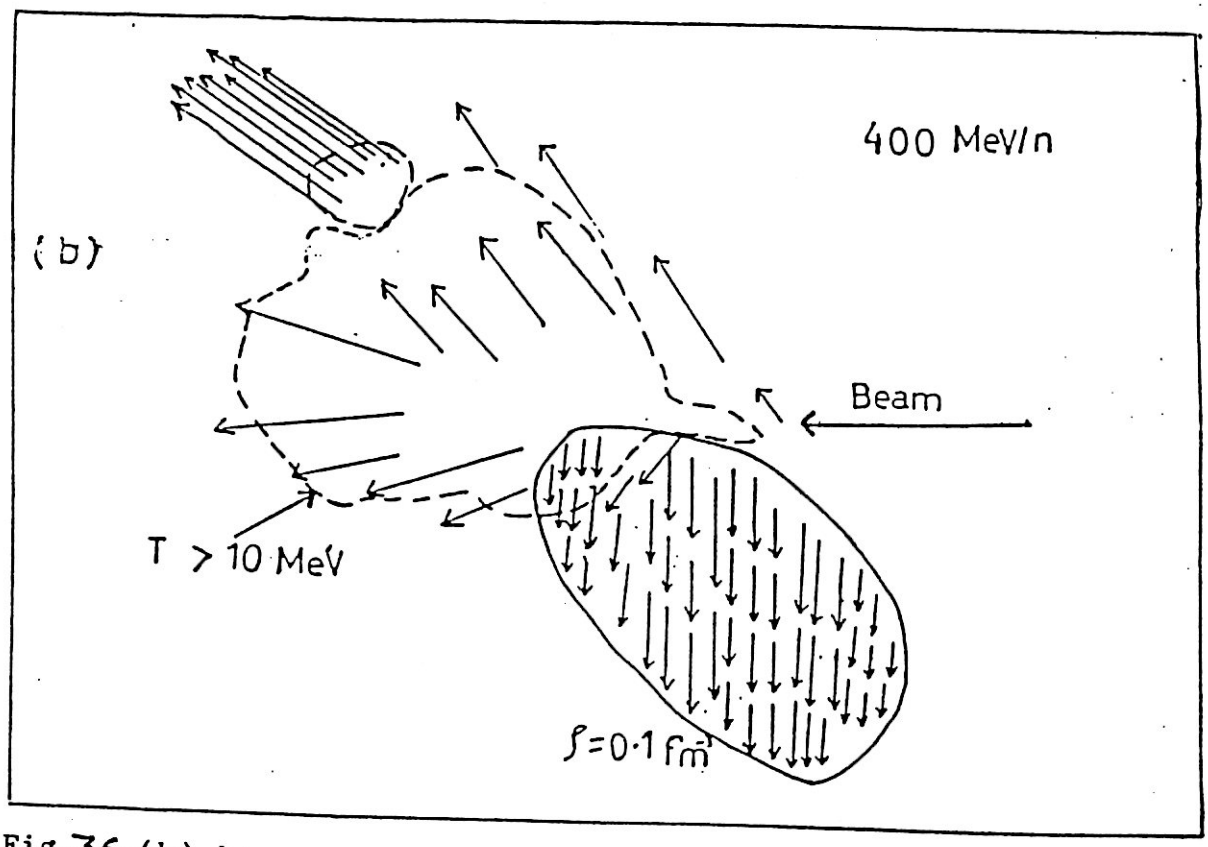

Fig.36.(b) bounce-off effect at large impact parameter .

shifts to higher values with decreasing the impact parameter which is consistant with the hydrodynamical calculations.

II.11.2 **Transverse momentum analysis.** We have chosen for the present analysis the events which fulfil the following criteria: (i) the number of projectile fragments $N_f>4$; (ii) the nubmer of target fragments $N_h>8$. In the following, the projectile fragments f are analysed.

In the present experiment, the momentum per nucleon of the incident nucleus P_L =4500 MeV/c. Assuming that after collision of the interacting nuclei the momentum per nucleon of a projectile fragment equals P_L, the transverse momentum per nucleon of an ith fragment P_i = P_L tan θ , where θ ,is the emission angle of the ith fragment. The vector P_i points in the azimuthal direction of this fragment.

According to the method used in the reaction plane is defined by the direction of the incident nucleus and the vector R_μ which is given by

$$R_\mu = \sum_{\substack{i=1 \\ i\neq\mu}}^{N_f} \omega_i M_i P_i \qquad \mu = 1, 2, \ldots, N_f$$

where

$$\omega_i = \begin{cases} 0 & \text{if } P_i > 240\ \text{MeV/}c \\ 1 & \text{if } P_i \leq 240\ \text{MeV/}c. \end{cases}$$

The coefficient ω_i is introduced to exclude fragments of very large transverse momentum. The quantity $M_i = \Sigma_k W_{i,k} A_{i,k}$ where $A_{i,k}$ is the mass number of the Kth isotope of the ith fragment and $W_{i,k}$ is the corresponding fractional yield of the isotope

The projection of P_i on the vector R_μ is given by $\overline{P_\mu^*} = P_\mu \cdot R_\mu / |R_\mu|$, $\mu = 1, 2, \ldots, N_f$. , The mean transverse momentum

per nucleon projected onto the reaction plane $\langle P^* \rangle$,is obtained by averaging P_μ^* over all fragments (each of weight M_μ) and over all the selected interactions. The $\langle P^* \rangle$ will be equal to zero if P_i is randomly distributed in the azimuthal plane and it will differ from zero if the energy flow of particles devites from the zero-angle direction,i.e. if bounce-off of projectile fragments takes place. If it is assumed that the residual projectile nucleus receives a transverse momentum during the collision process,the value of $\langle P^* \rangle$ will represent the transverse momentum transfer per nucleon.

Figure 37a shows the dependence of $\langle P^* \rangle$ on the emission angle θ of projectile fragments in Ne^{22} +Ag(Br) interactions at 4.1A GeV/c. Figure 37b represents the corresponding dependence for C^{12}+Ag(Br) collisions at 4.5A GeV/c. Each point of Figs.37a,b represents the average transverse momentum per nucleon projected onto the reaction plane. Averaging is taken over all projectile fragments in a given interval. The experimental data in Figs.37a,b show that $\langle P^* \rangle$ differs significantly from zero. This observation displays the bounce-off of projectile fragments.The shape of the dependence of $\langle P^* \rangle$ on θ,for CEM-simulated events in Figs.37a,b shows that the intranuclear cascade may make a small contribution to the effect.This contribution in the case of C^{12} data has insignificant role and is smaller than that of the Ne^{22} events. This is probably due to the smallness of the C^{12} nucleus.The experimental data in these figures show that $\langle P^* \rangle \neq 0$.

It is clear that the resultant vector $R=\Sigma_{i=1}^{N_\beta} \omega_i M_i P_i$ reconstructs the geometry of the collision with a certain

Fig. 37.

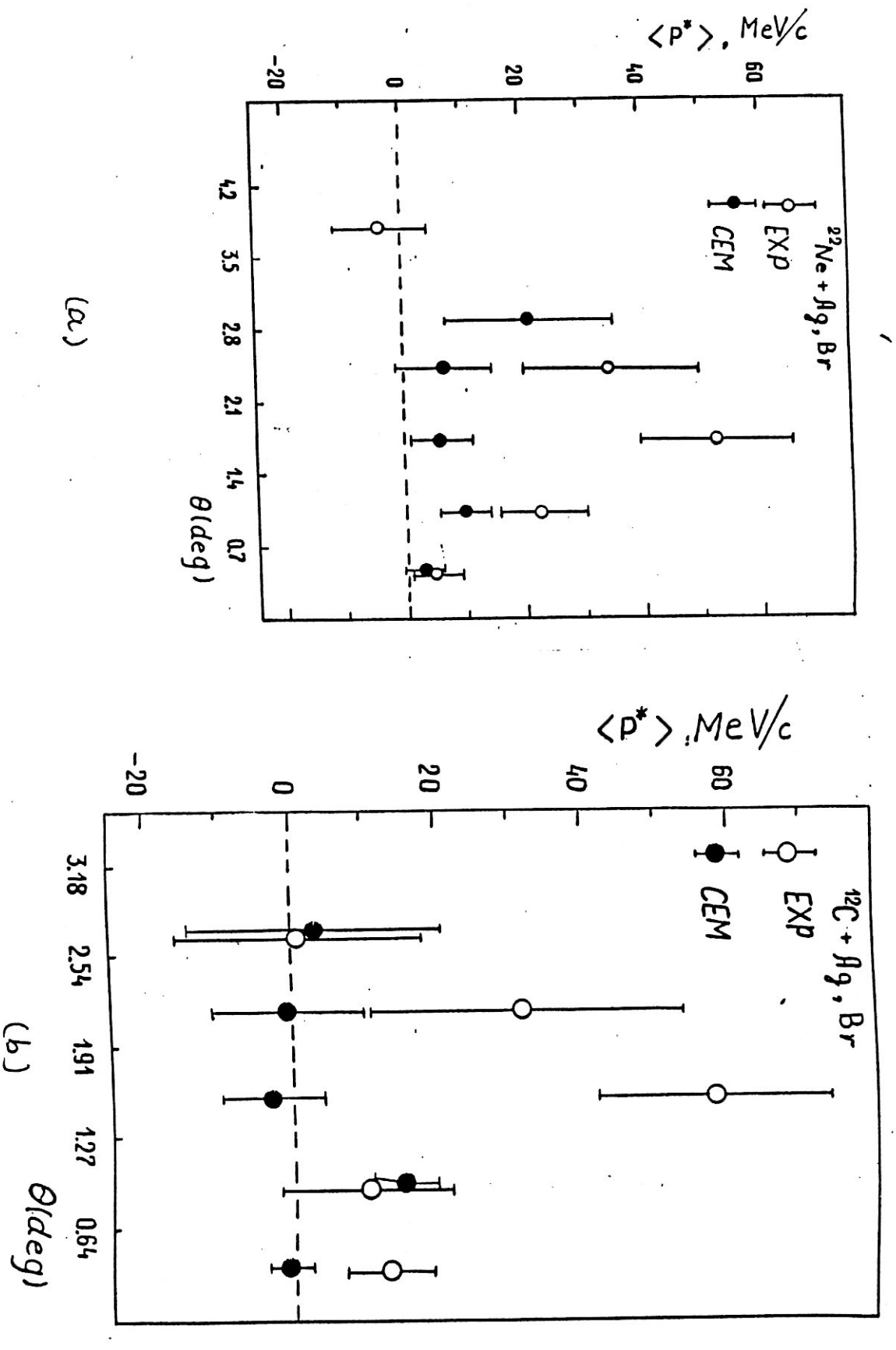
(a)
$^{22}Ne + Ag, Br$
EXP
CEM
$\langle p^* \rangle$, MeV/c
-20
0
20
40
60
4.2
3.5
2.8
2.1
1.4
0.7
θ(deg)
(b)
$^{12}C + Ag, Br$
EXP
CEM
$\langle p^* \rangle$, MeV/c
-20
0
20
40
60
3.18
2.54
1.91
1.27
0.64
θ(deg)

accuracy; it gives the reaction plane, which is determined by the direction of the incident nucleus and the line connecting the centres of the colliding nuclei. This commonly known fact can be useful in the setting up of experiemnts for which it is necessary to know the reaction plane. For example, in the case of studying emission of light fragments (deutrons, tritons and alpha particles) from reactions with relatively heavy nuclei, it is interesting to draw the distributions of fragments in the azimuthal plane as a function of their emission angles with respect to the vector R. Obviously, the side splash would increase the role of coalescence in the formation of fragments and consequently this would affect their angular distributions.

II.11.3. <u>The analysis of flow angle</u>. Insight into interactions can be gained by using event shape analysis. Event-by-event a tensor is constructed using the c.m. momenta of the all particles, essentially fitting an ellipsoid to the event. Each event can be characterized by the lengths of the axes, the angle of the major axis to the beam (θ_F) and the orientation with respect to a fixed plane (Φ). There are several ways of constructing such a tensor, depending on the weighting that is used:

$$Q = \overline{\sum_{\gamma}^{n_{tot}} P_i^{\gamma} P_j^{\gamma}} \quad \ldots\ldots\ldots\ldots\ldots\ldots \quad (32)$$

Energy Flow[55]

$$F_{ij} = \sum_{\gamma}^{n_{tot}} (P_i^{\gamma} P_j^{\gamma} / 2m_{\gamma}) \quad \ldots\ldots\ldots\ldots \quad (33)$$

Momentum Flow[56]

$$T_{ij} = \sum_{\gamma}^{n_{tot}} (P_i^{\gamma} P_j^{\gamma} / P^{\gamma}) \quad \ldots\ldots\ldots\ldots \quad (34)$$

Angular Emission[57]

$$A_{ij} = \sum_{\gamma}^{n_{tot}} (P_i^{\gamma} P_j^{\gamma} / P^{\gamma}) \quad \ldots\ldots\ldots\ldots \quad (35)$$

Thrust has also been used , where the thurst vector $\vec{n}$ is chosen such as to maximum ,

$$T(\vec{n}) = \sum_{\gamma=1}^{n_{tot}} \vec{P}.\vec{n} \quad \ldots\ldots\ldots\ldots\ldots\ldots \quad (36)$$

Because the thrust vector cannot be calculated analytically the sphericity method generally has been used. The sphericity tensor equation 35 is calculated from the momenta of all measured particles for each event. It is appropriate to choose the weight factor w (8) in such a way that composite particles have the same weight per nucleon as the individual mucleons of the composite particle at the same velocity. The sphericity tensor approximates the

event shape by an ellipsoid whose orienttion in space and whose aspect ratios can be calculated by diagonalization. The shapes predicted by hydrodynamical and intranuclear cascade calculations are quite different . The hydrodynamical model predicts prolate shapes along the beam axis for grazing collisions. With decreasing impact paramter the flow angle increase and reach 90 degree (with oblate shapes) for zero impact parameter events. This behaviour is independent of projectile and target mass. Cascade calculations on the other hand predict zero flow angle at all impact parameter. In the present experiment, the momenta of detected fragments were not measured. We adopte another method for the particle flow analysis. A unit vector in space is assumed in the direction of flight of each b-particle. These unit vectors were summed to give the resultant vector R. In the present case, the beam direction was taken as the X-axis, the perpendiculars to it are the Y-axis and Z-axis. Thus, we define the angle of flow θ_F such that

$$\theta_F = \cos \frac{X}{|R|}$$

where $\vec{R}=iX + jY + kZ$ and X, Y, Z are the components of R vector along the axis. The hydrodynamical calculations predict that the position of the maximum of θ_F distribution increases systematically with decreasing the impact parameter and consequently with increasing the multiplicity. So, it is interesting to investigate the dependence of θ_F distribution on the impact parameter. Since the impact parameter is difficult to measure accurately, we consider the multiplicity of target fragments N_h, as a measure of impact parameter. The higher the N_h is the lower the impact parameter b and vice versa. Qualitatively the events are divided into two intervals of (N_h). Thus, the θ_F -distribution are plotted for ($N_h < 7$) and for ($N_h \geq 7$). The peak position is shifted to

higher values of θ_F with increasing the multiplicity i.e. with decreasing the impact parameter. It has been shown in reference that the anglular distribution has less fluctuations if the flow angle θ_F is properly weighted by the Jacobian ($\sin\theta$). From the present analysis we see that there is a clear angle of flow of (side splash) of target fragments different from zero value. The dependence of θ_F on the impact parameter is seen in Figures 38-40. The θ_F distributions for $N_h < 7$ and $N_h \geq 7$ events from Mg^{24} and Si^{28} - Em interactions are shown in Figs. 38 and 39. We found that the average value of θ_F is

$$\langle \theta_F \rangle = 52.3 \pm 1.9 \quad \text{for } Mg^{24} + Em$$

and

$$\langle \theta_F \rangle = 50.0 \pm 0.5 \quad \text{for } Si^{28} + Em$$

while in the multiplicity of ($N_h > 7$) we found that the average value of θ_F is.

$$\langle \theta_F \rangle = 82.6 \pm 1.1 \quad \text{for } Mg^{24} + Ag(Br)$$

and ,

$$\langle \theta_F \rangle = 70.2 \pm 0.4 \quad \text{for } Si^{28} + Ag(Br)$$

Figure 40 shows the dependence of $dN/\cos\theta_F$ on θ_F for $N_h < 14$ and $N_h \geq 14$. The shift of peak position with increasing the multiplicity or with decreasing the impact parameter is clearly seen in Fig. 40 .

This agree with the observation of the side-splash of target fragments in plastic ball experiments and in streamer chamber. Also, it is consistent with the hydrodynamical calculaitons. From the present analysis we see that the hydrodynamical calculations predict that a maximum in flow angle distribution systematically increases with decreasing impact parameter and, consequently, with increasing multiplicity. The shift of the peak position with increasing multiplicity or decreasing impact parameter is clear in figures 38-40.

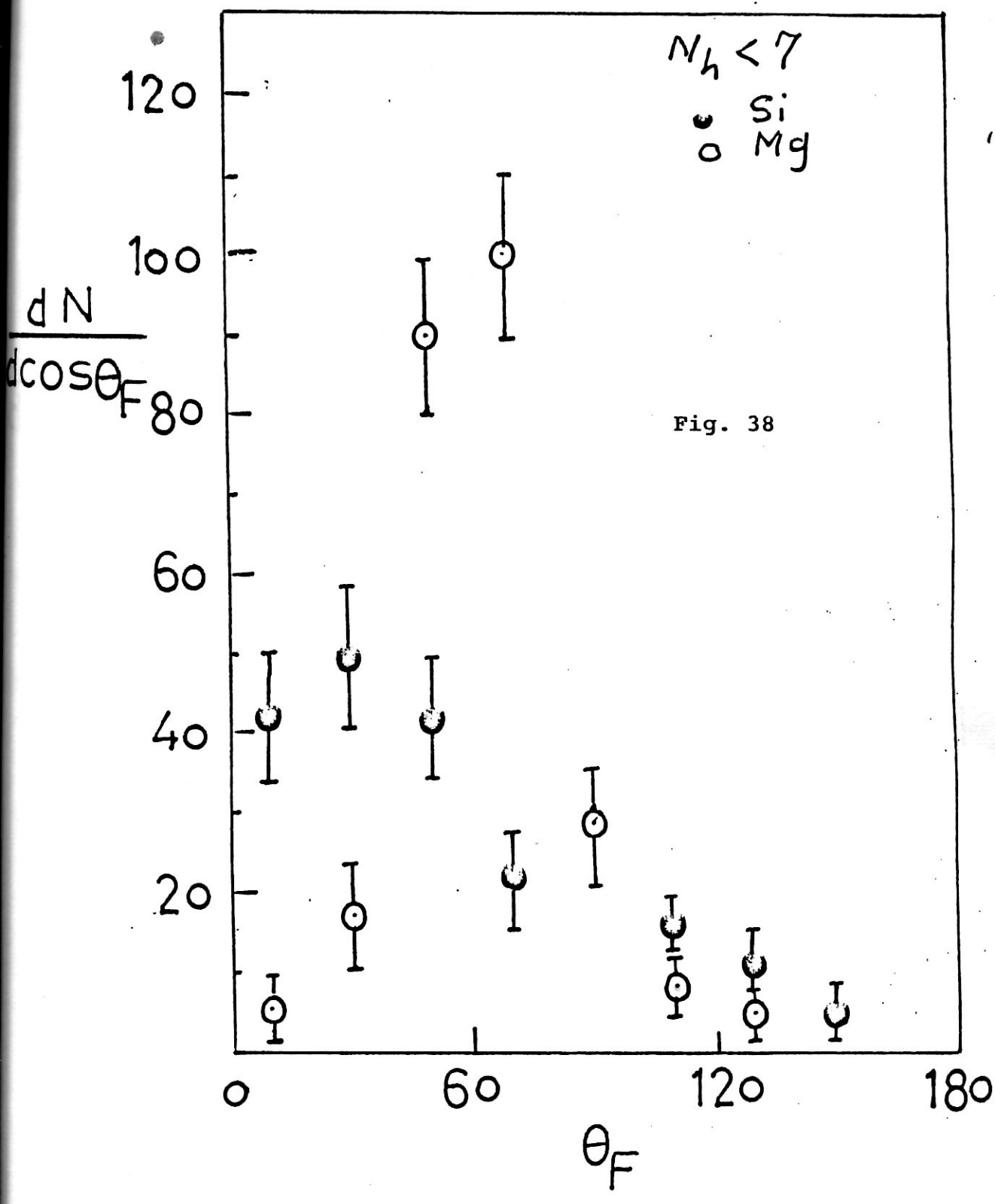
$N_h < 7$
Si
Mg
120
100
80
60
40
20
0
60
120
180
$\frac{dN}{d\cos\theta_F}$
θ_F

Fig. 38

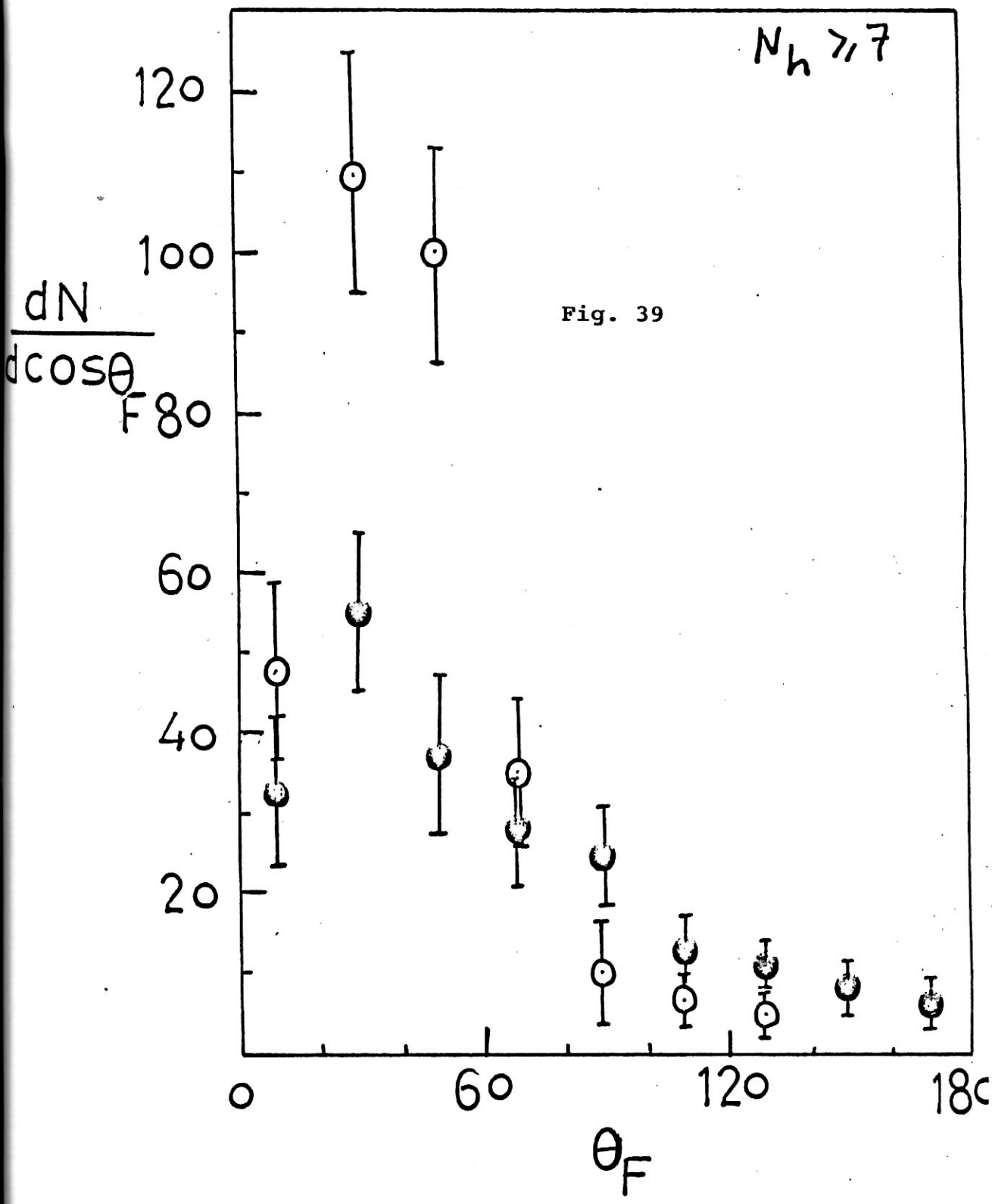
$N_h \geq 7$
120
100
80
60
40
20
$\frac{dN}{d\cos\theta_F}$
0
60
120
180
θ_F

Fig. 39

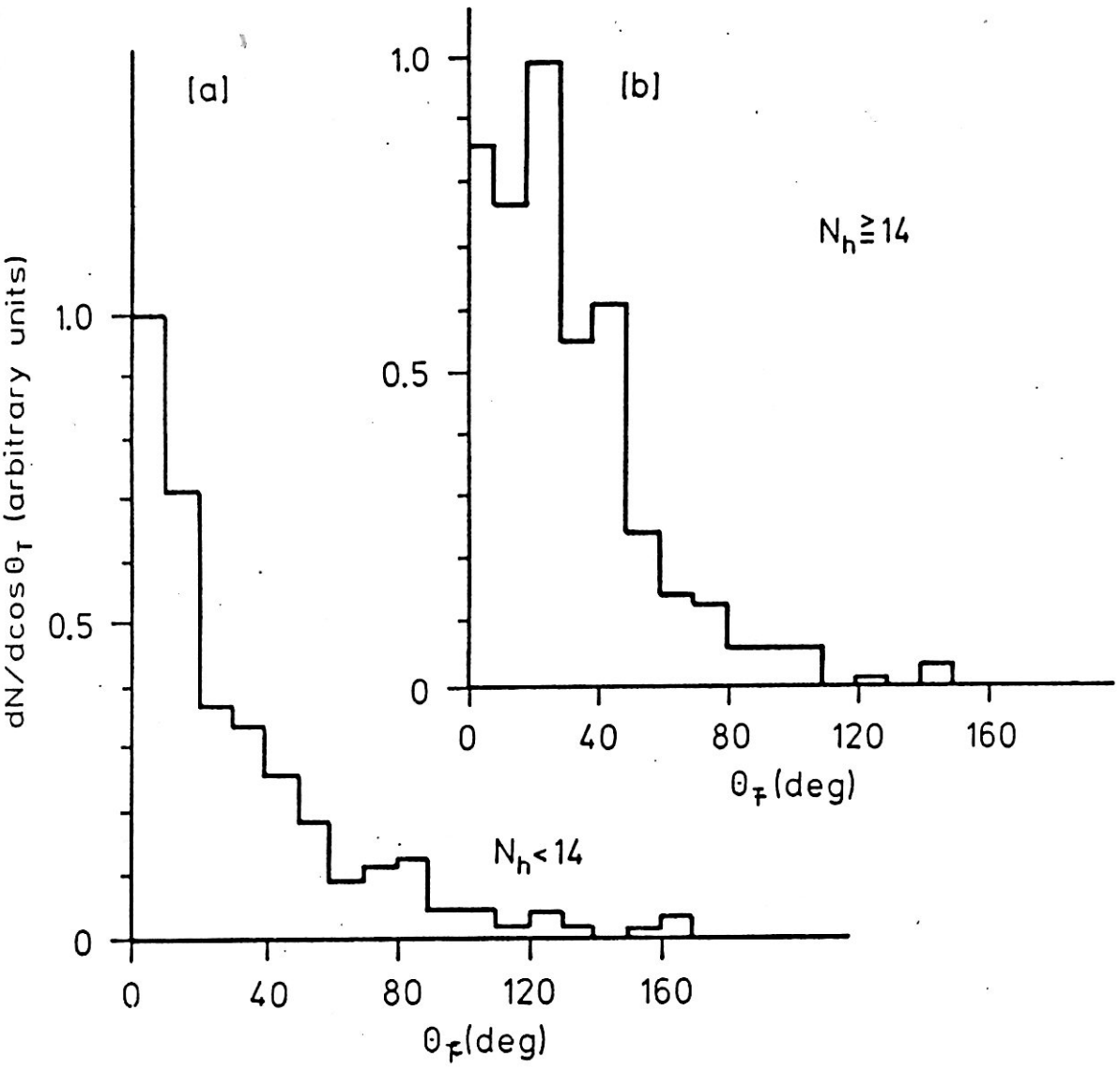

Fig. 4a and b. The dN/d cos θ_T distributions versus θ_T: **a** for $N_h < 14$ events and **b** for $N_h \geq 14$ events

II.11.4. **Azimuthal alignment**. The determination of the reaction plane allows us to obtain information on the azimuthal bounce-off of projectile fragments. It shows what the bounce-off looks like when it is projected onto the azimuthal plane. The azimuthal angular distribtion of particles should be isotropic in the absence of bouce-off. The bounce-off effect leads to deviation from isotropy. The degree of this deviation can be estimated from formula of P_i^* if P_i is replaced by its unit vector and the sum runs over i from 1 to N_f. Then $\langle P^* \rangle$ per nucleon is calculated. The possible values of $\langle P^* \rangle$ are from -1 to +1. In the case of isotropy, $\langle P^* \rangle = 0$. The azimuthal sideward flow can be measured by the azimuthal alignment which is defined here as $A = N(P^*)$, where N is the number of particles.

The azimuthal alignment, $A(\theta) = N_\theta \langle P^* \rangle_\theta$, is calculated as a function of the emission angle θ of fragment f, where N_θ and $\langle P^* \rangle_\theta$ are correspondingly the number of paricles and the mean $\langle P^* \rangle$ for fragments with angles of emission in the given interval of the angle . Figure represents the dependence of A on for projectile fragments.

Figure 41 shows that the azimuthal alignment of the projectile fragments in the experimental data is much more pronounced than that in the CEM-simulated events. This is expected from the dependeces in figures 37 , where it was shown that the cascade has a small opportunity to be developed in such small nuclei due to the limited nuclear matter. The flow of the projectile fragments is made mainly by the transverse momentum transferred to the projectile nucleus as a whole. The CEM provides an isotropic angular distribution for the projectile fragments in the azimuthal plane of the considered reactions. This leads to deviation between the CEM and the experiment. One may conclude from the analysis

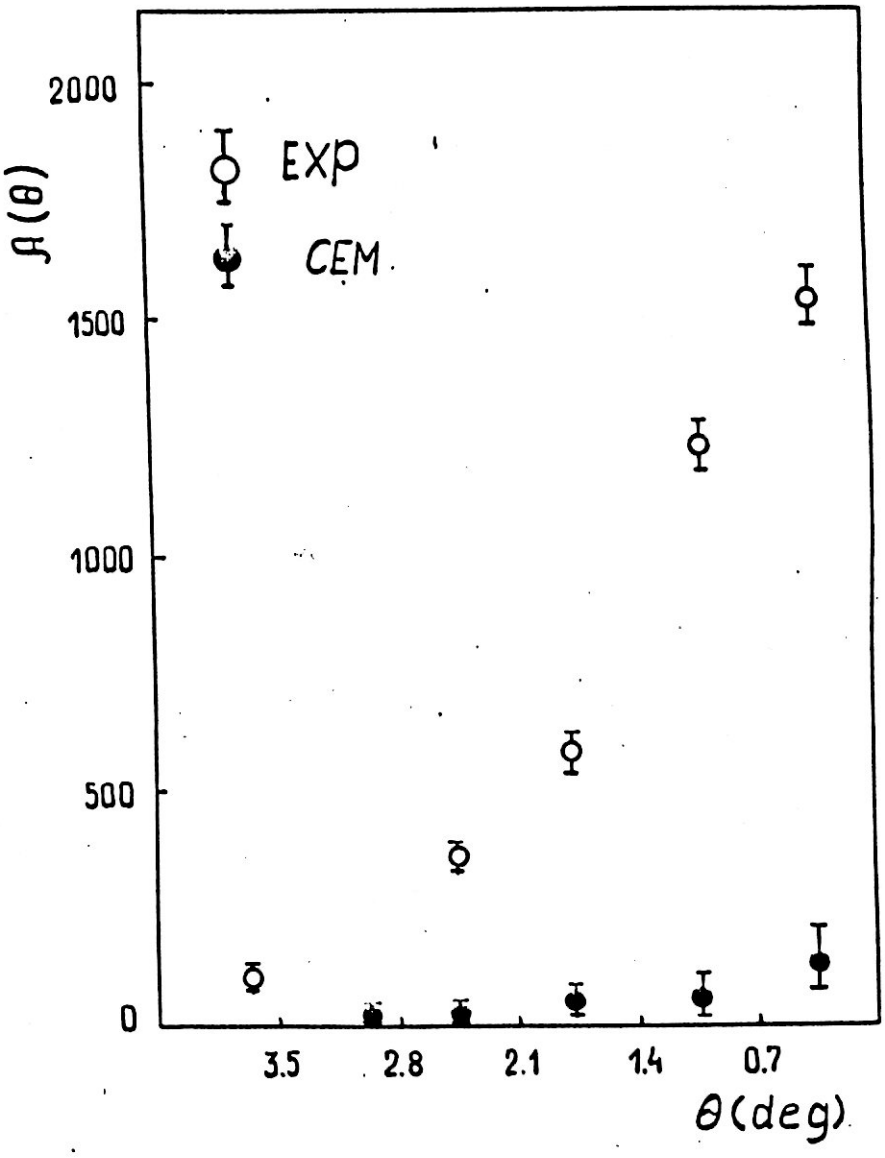

Fig. 41. The azimuthal alignment of PFs.

of figs 37,4 that the reflections of side splash on the angular distribution of target fragments are better seen if the reaction plane is considered. The CEM can describe the general behaviour of these experimental angular distributions.

By analogy, the azimuthal alignment of target fragments is studied. The value of $\langle P^* \rangle$ per particle is calculated for different intervals of θ. All $^{22}Ne+Ag(Br)$ inelastic collisions of $N_h \geq 7$ are used. They are divided into groups according to the value of Z^* and the type of fragment (h,b and g).

Table 23 represents the mean values of P^* for h particles; the averaging runs over all θ intervals. These values are calculated for the experimental and simulated data; the quantity $\Delta = \langle P^* \rangle_{Exp} - \langle P^* \rangle_{CEM}$. The values of $\langle P^* \rangle$ increase with increasing Z^*. This could have been expected because the increase of Z^* means the increase of the impact parameter. Then the amount of nuclear matter increases along the path of the secondary particles, inside the target nucleus, i.e. in the transverse direciton, opposite to that of the projectile nucleus. This leads to a correspondingly more developed intranuclear cascade.

Table 23 $\langle P^* \rangle$ per particle and $\Delta = \langle P^* \rangle_{Exp} - \langle P^* \rangle_{CEM}$ calculated for the h particles.

Z^*	Experiment $\langle P^* \rangle$	CEM $\langle P^* \rangle$	Δ
0-2	0.178±0.005	0.138±0.004	0.041±0.007
3-6	0.207±0.006	0.177±0.005	0.030±0.008
7-10	0.224±0.006	0.235±0.006	-0.011±0.011

The difference Δ reflects the effect of transverse momentum transferred to the target nucleus. Naturally, its value is small because the momentum transfer is distributed among a large number of the target nucleons.

Multiplying the value of $\langle P^* \rangle$ for the given θ interval, by the number of particles N_θ in this interval, the azimuthal alignment $A(\theta) = N_\theta \langle P^* \rangle_\theta$ is obtained. Figure 42 shows $A(\theta)$ as a function of cos for b particles (N_b=5969) from Z^*= 0,1 and 2 events. The azimuthal alignment $A\langle\theta\rangle$ for g particles (N_g = 12730) from the same events is shown in figure 43.

The azimuthal alignments of target fragments from CEM-simulated events are not presented in figures 42,43 and . This is due to the fact that figures 42 and 43, in addition to table 23, have shown that the flow of target fragments is mainly described by cascade processes. If the distributions from the CEM data corresponding to those presented in figures 42 and 43 are plotted, they will nearly reproduce the experimental data.

The analysis of figures 42,43 and table 23 shows the difference between the projectile and target fragments. In the case of projectile fragments, the flow of particles is conditioned by the transverse momentum transferred to the projectile nucleus, whereas the flow of nuclear matter is mainly (nearly all) conditioned by the cascade processes in the case of terget fragments .

A similar study of the collective azimuthal alignment of charged particles was reported in /24/, where data from the "plastic ball", for Ca + Ca, Nb + Nb and Au + Au collisions at energies from 0.4 to 1.05 GeV per nucleon, were analysed.

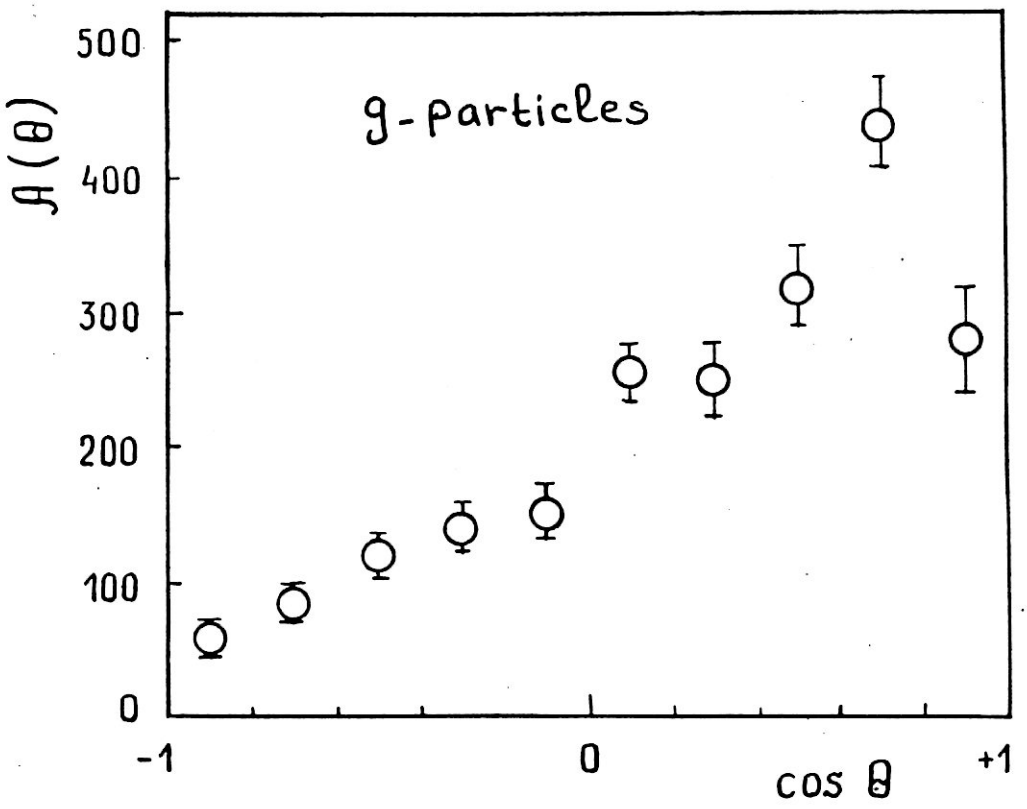
g-particles
A(θ)
500
400
300
200
100
0
-1
0
+1
cos θ

Fig. 42

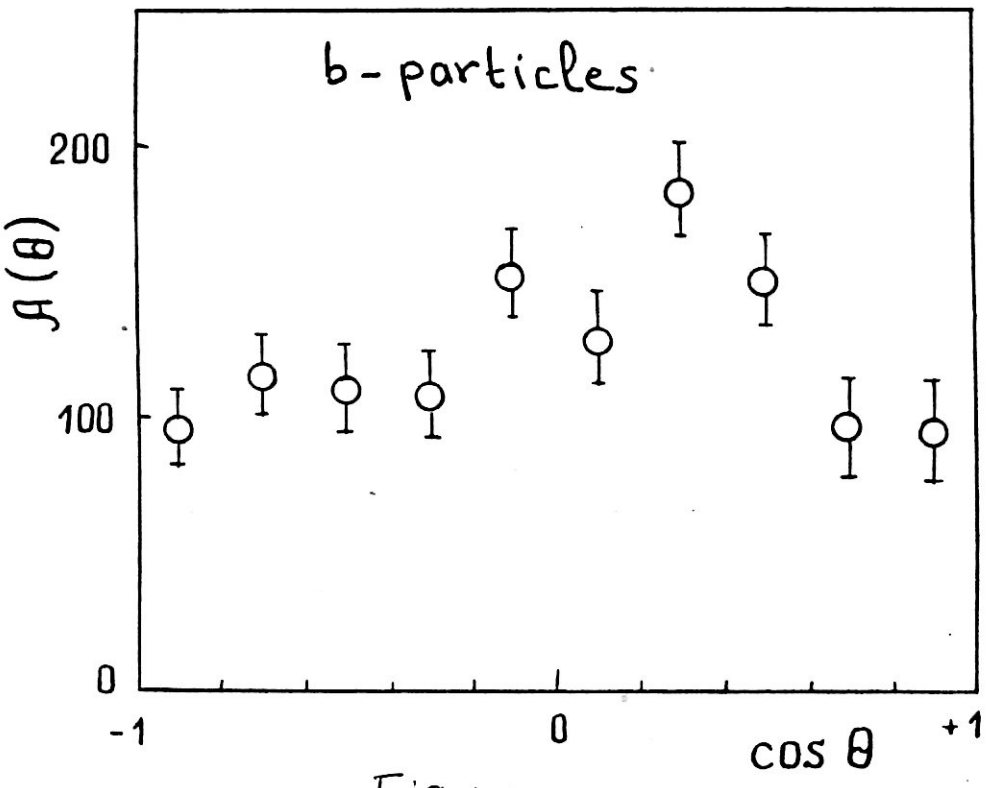
b-particles
A(θ)
200
100
0
-1
0
+1
cos θ

Fig. 43

II.11.5. Angular distribution of target fragments. As an illustrtion of the possibilities arising from the determination of the reaction plane, one can study the angular distribution of b particles of the target neucleus.

Using the $N_h \geq 7$ criteria, the collisions with heavy emulsion nuclei ^{22}Ne + Ag(Br) were selected from the total inelastic ^{22}Ne + emulsion interactions. The total charge of projectile fragments Z^* was determined in each event. The space angle θ and the azimuthal angle Φ were measured for each h particle.

The side-splash effect of slow fragments (b particles) of the target nucleus must be reflected in their distributions. The effect is clearer if one plots the angular distribution for those b particles which are emitted at small angles with respect to R (the reaction plane) in the azimuthal plane. Taking this into consideration, the resultant vector of the h particles, R, was found for each event by formula (1), where the coefficient $\omega_i=1, M_i=1$ and instead of P_i a unit vector in the azimuthal direction of Φ_i was considered. The sum runs over all h particles in the given event. A b particle is selected for the following distributions, only if its unit vector has an angle $\Phi \leq 30°$ with respect to R.

The distribution (1/N) dN/d cosθ for b particless (N=1418) from central (Z^* =0,1 and 2) ^{22}Ne + Ag(Br) collisions is shown in figure 44 (a). The total number of particles is normalised to 10. The distribution of CEM-simulated events (N=1340) is denoted by crosses. The error bars of the CEM data points are shown. Since the error bars of the experimental points are nearly equal to the corresponding ones in the CEM, they are not presented in the figure. A maximum which corresponds to the side splash of particles can be observed from the experimental data. The CEM reproduces the general

features of the distribution observed in the experiments.

For comparison, figure 44b, taken from our paper /24/, represents the angular distribution of b particles from central (Z*=0 and 1) ^{22}Ne+emusion interactions (without selecting events according to N_h). No reaction plane has been determined; consequently the selection of b particles according to the angle Φ was not used. The contrast between the experimental distributions (solid histograms) of the present work and that of 44b is clearly seen. The peaking in the angular distribution is more prononced when the reaction plane is taken into consideration.

The corresponding distributions from Z* =5,6 and 7 events are presented in figure 45a,b. The statistics in the experiment is N=1196 and N=1951 in CEM-simulated events. The difference between the experimental distribution, represented by solid histograms in figures 44(a) and 44(b) is obvious.

II.11.6. <u>Ranges of slow fragments</u>. In reference /24/, it was shown that the average tramsverse momentum transferred to a nucleon of the ^{22}Ne projectile nucleus, in ^{22}Ne+Ag(Br) collisions, equals about 50 MeV/c. Taking into consideraiton the difference in mass of Ne and Ag(Br) nuclei, one can expect that the average transverse momentum per nucleon is a few MeV/c; consequently for slow target fragments (b paarticles of range $L \lesssim 3$ mm) the corresponding difference in the range can be observed. A relative increase should be observed in the range of fragments emitted in the direction of the side splash.

The inelastic interactions of ^{22}Ne+Ag(Br) at small impact parameter (Z*=0,1 and 2) are used. For each event,

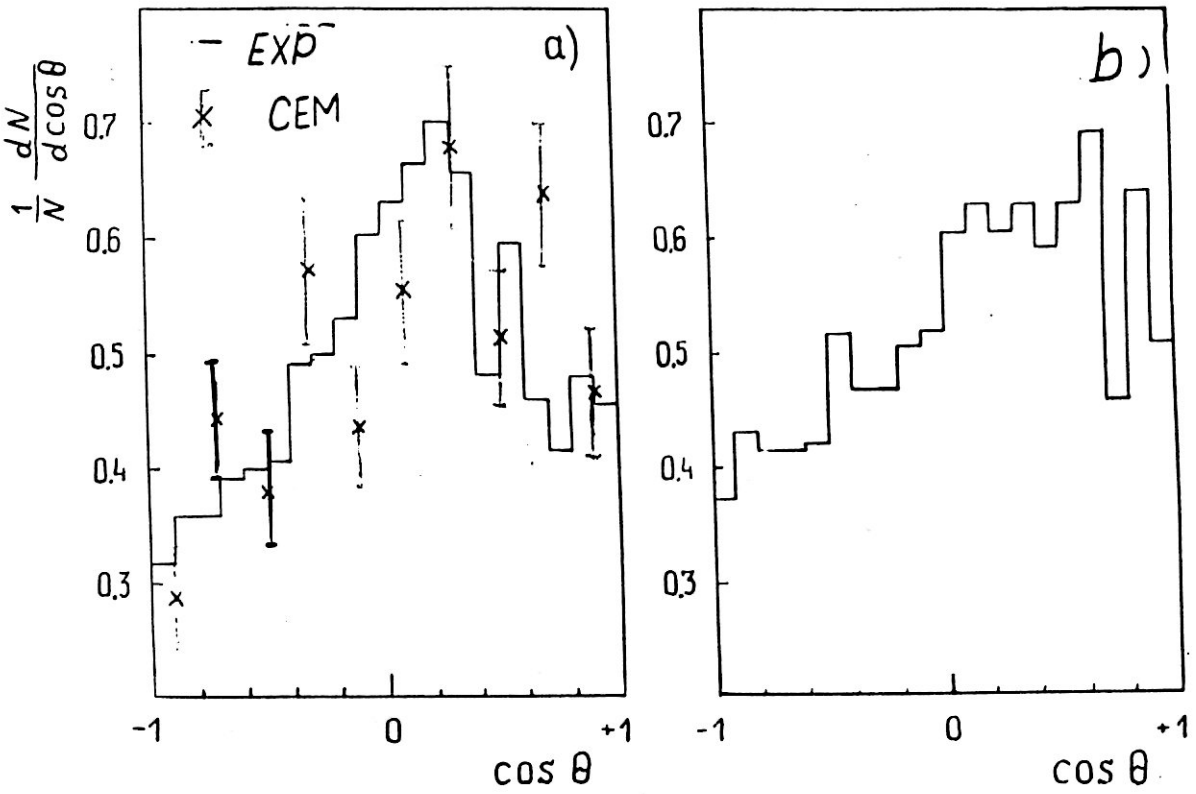
$\frac{1}{N}\frac{dN}{d\cos\theta}$
EXP
CEM
a)
b)
0.7
0.6
0.5
0.4
0.3
-1
0
+1
cos θ

Fig. 44

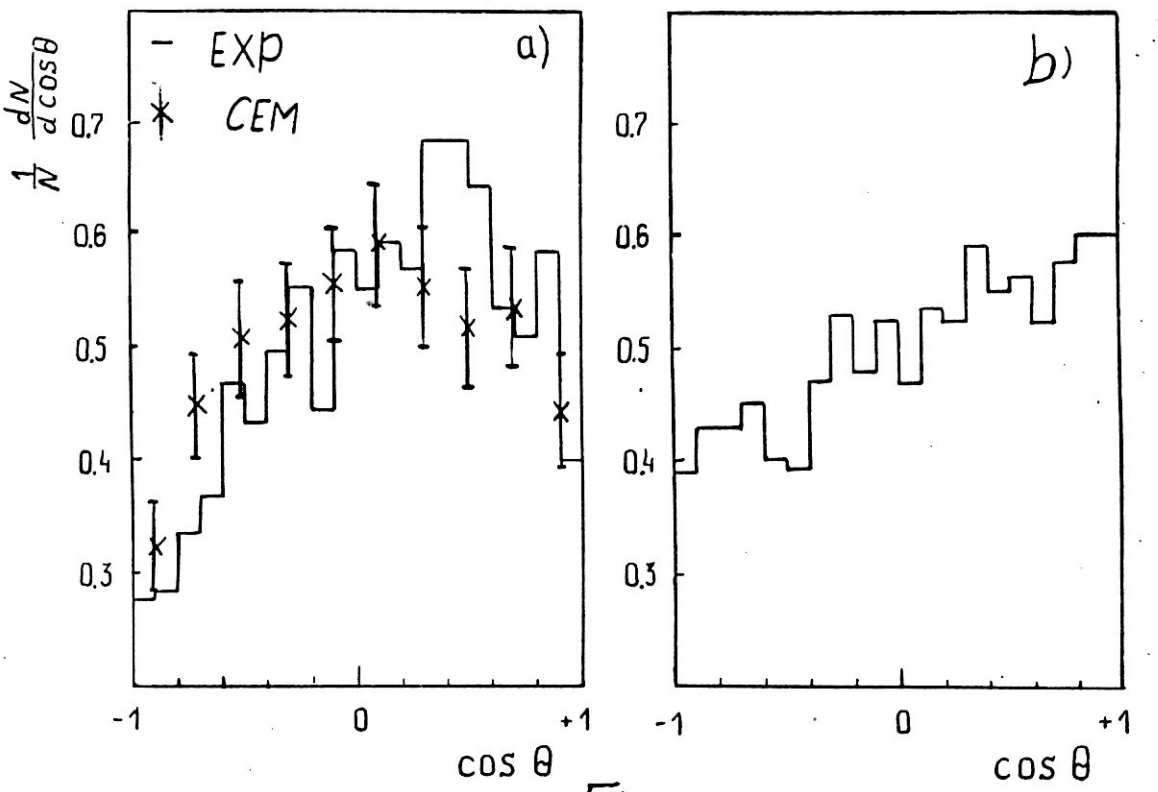
$\frac{1}{N}\frac{dN}{d\cos\theta}$
EXP
CEM
a)
b)
0.7
0.6
0.5
0.4
0.3
-1
0
+1
cos θ

Fig. 45

the resultant vector R which determines the reaction plane is found as described before. All b particles are divided into two groups. The first contains the unit vectors of particles which have angles in the azimuthal plane $<30°$ with respect to the vector R. In the second, $>150°$. In both groups, in order to strengthen the effect, only b particles within the interval of emission angle $-0.2<\cos\theta<0.4$ were considered. The mean ranges are $\langle L\rangle_{<30°}=77\pm28$ μm and $(L)_{>150°}=635\pm49$μm. The difference between the mean values is $\Delta_L=142+57$ μm. The deviation of Δ_L from the zero value may be due to the momentum transferred to the target nucleus in the direction of the side splash of the particles.

II.11.7. Angular distribution of Z=2 projectile fragments. Figure 46 shows the azimuthal angular distribution $dN/d\theta_\alpha$ of Z=2 fragments of the ^{22}Ne projectile nucleus. Here, θ_α denotes the angle between the vector R and the direction of the Z=2 projectile fragment in the azimuthal plane. The resultant vector R was determined using the h particles. The distribution $dN/d\theta_\alpha$ is plotted for ^{22}Ne+Ag(Br) inelastic collisions of $N_h>7$ and $Z^*=2,3$ and 4. The total number of Z=2 fragments in these events is N=197.

As a consequence of the sideward flow of particles, the angular distribution $dN/d\theta_\alpha$ shows an increase in the emission of Z=2 fragments at large values of θ_α i.e. back-to-back correlation between projectile and target fragments. Accordingly, one may think that the sideward flow creates suitable conditions to strengthen the role of coalescence in the formation of alpha fragments, i.e. due to the concentration of particles in small angular intervals. This can partially explain the observed large yield of alpha particles in the fragmentation on ^{22}Ne in emulsion .

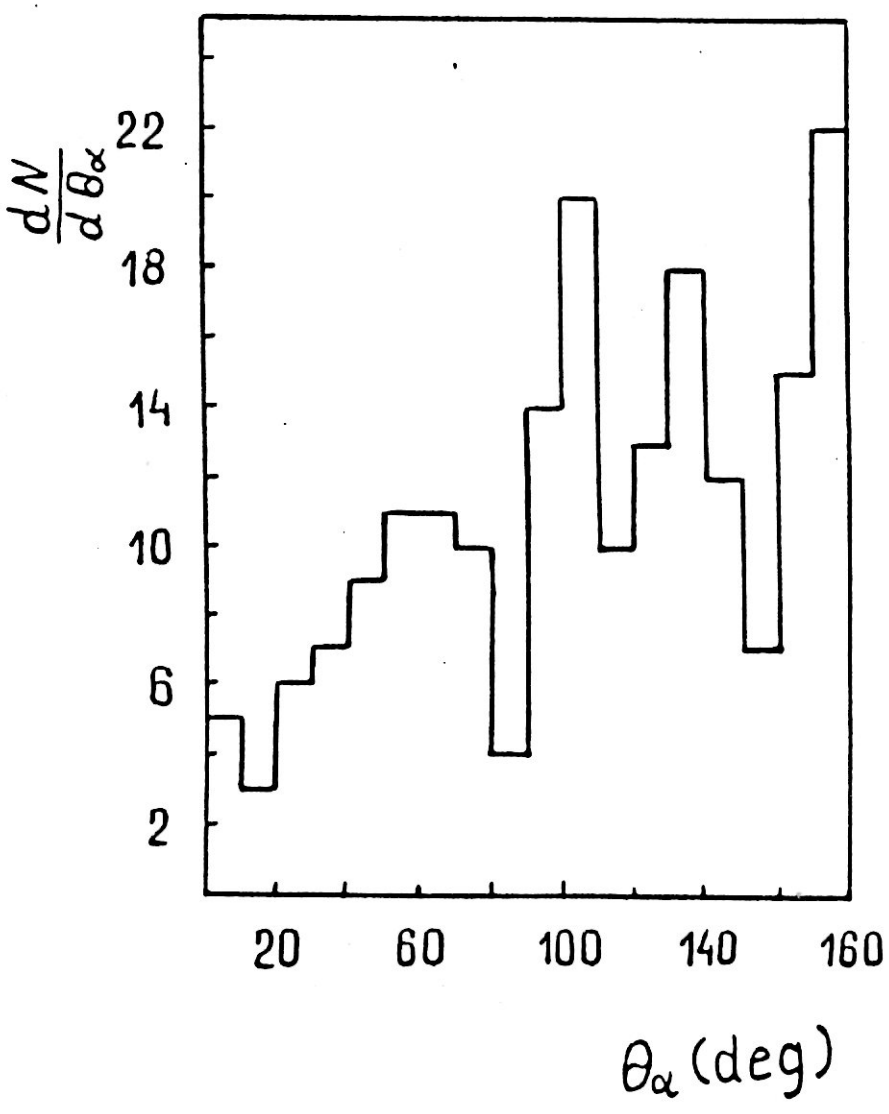

Fig. 46. Azimuthal angular distribution of Z=2 fragments.

II.11.8. Distribution of Pseudorapidity Intervals of Shower Particles

Another method of searching for sideward flow of nuclear matter is the method of pseudorapidity intervals $\Delta\eta$. For this purpose the pseudorapidity $\eta = -\ln \tan(\theta/2)$ was calculated for each shower particle in C^{12} + Pb, Mg^{24} +Pb, Ne^{22} + Ag(Br) and Si^{28} + Ag(Br) central collisions. For the validity of the $\Delta\eta$ method ,the η - distribution was found to be flat,within experimental errors, in the range of η = 1 - 2 . This enables us to use the quantitative method of $\Delta\eta$, in the given range,where

$$\Delta\eta^{k}_{ij} = \eta_i - \eta_j$$

The quantity $\Delta\eta^{k}_{ij}$ means the pseudorapidity interval between the ith and jth particles such that k-particles are lying between them.The value of η were rescaled in each event such that $\eta_i=(\eta_i - \eta_j)/(\eta_{max} - \eta_1)$ takes values from 0 to unity, where η_1 and η_{max} are the minimum and maximum values of η. The histogram is the experimental data while the curve is due to independent particle emission (IPE) and its form is given by

$$dN^{n}_{k}/d\Delta = n\, C^{k}_{n-1}\, \Delta^{k}(1 - \Delta)^{n-k-1}$$

where $C^{k}_{n-1} = (n-1)!/k!\,(n-k-1)!$. The IPE distribution has a maximum at $\Delta_{max} = k/(n-1)$. It is seen that in Fig.47,the experimental $\Delta\eta$ distribution is shifted to the left with respect to the IPE one. The same procedure was repeated for g-particles using the azimuthal angle Φ as variable instead of η. Fig a,b shows the normalized azimuthal angular interval $\Delta\Phi$ - distributions, for Mg^{24} + Ag(Br) collisions respectively. It is seen from these two figures that there is a shift of experimental $\Delta\Phi_g$-disribution to the left from that of the IPE one.

The above mentioned method was used by many physicists to search for clusters in nuclear interactions. The nature of these clusters were not explained, in the present work such correlations are recognized as due to sideward flow of nuclear matter. This was more confirmed in Fig . This figure shows the Φ_{s-g} - distributions for the given reactions, where Φ_{s-g} is the angle between the resultant vectors of s and g particles in the azimuthal plane. A peak is clearly observed at $\Phi_{s-g} \sim 180^{\circ}$,which means a back to back emission. This kind of distribution is characteristic for sideward flow of nuclear matter /22-24/.

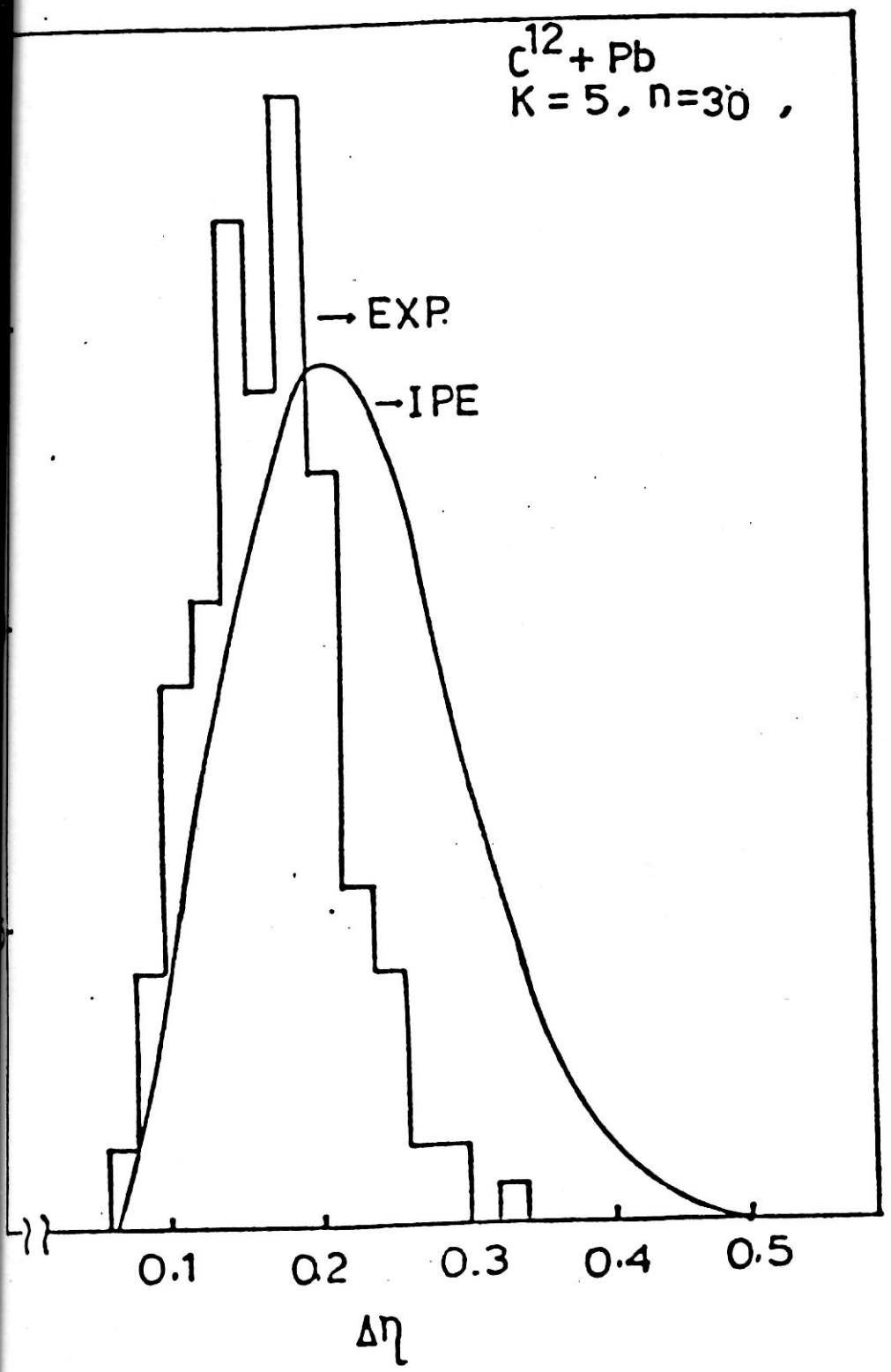

FIG. 47(a)

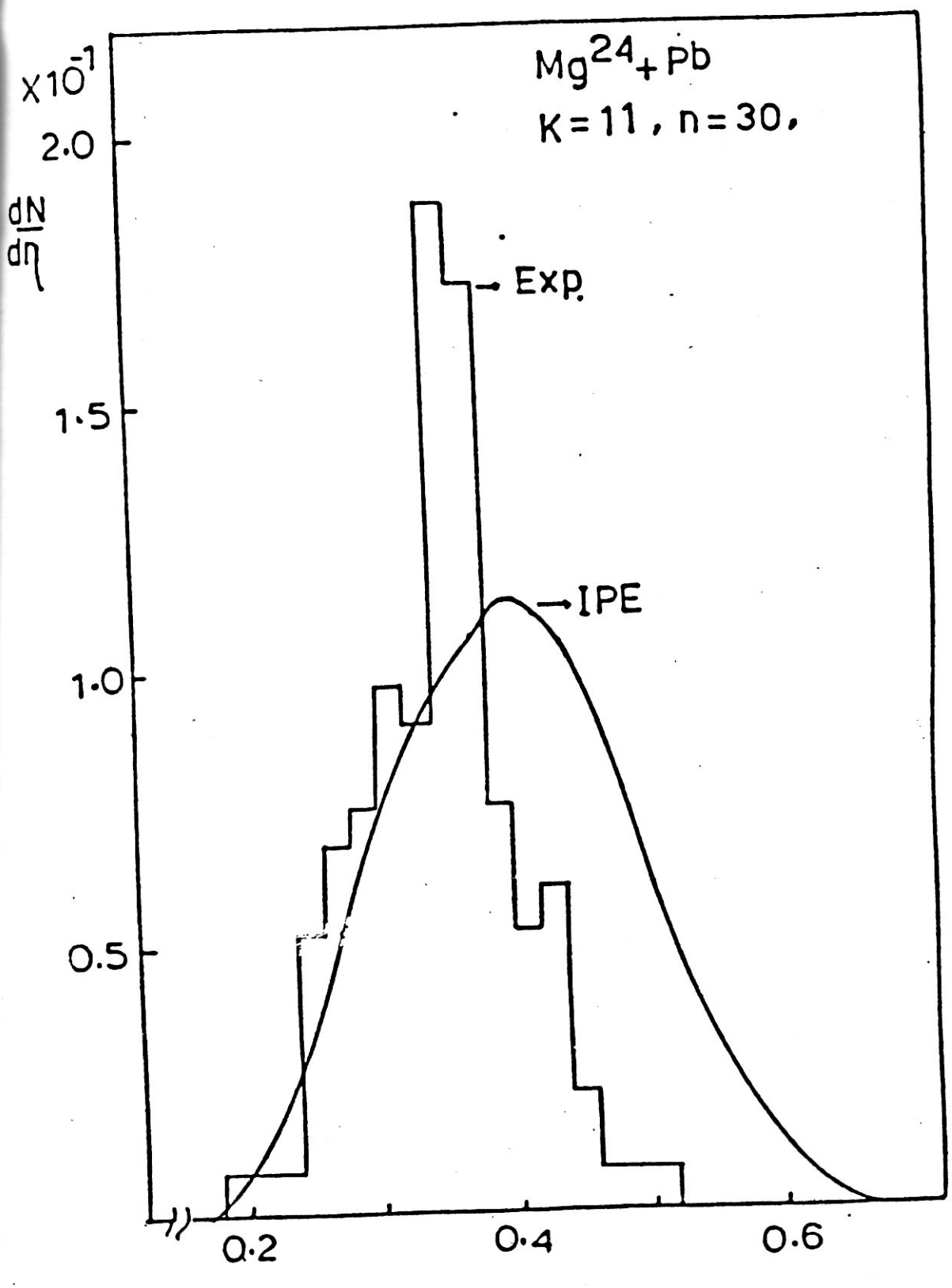
$Mg^{24}+Pb$
K=11, n=30,
$\times 10^{-1}$
2.0
$\frac{dN}{d\eta}$
Exp.
1.5
IPE
1.0
0.5
0.2
0.4
0.6
$\Delta\eta$

FIG.47(b)

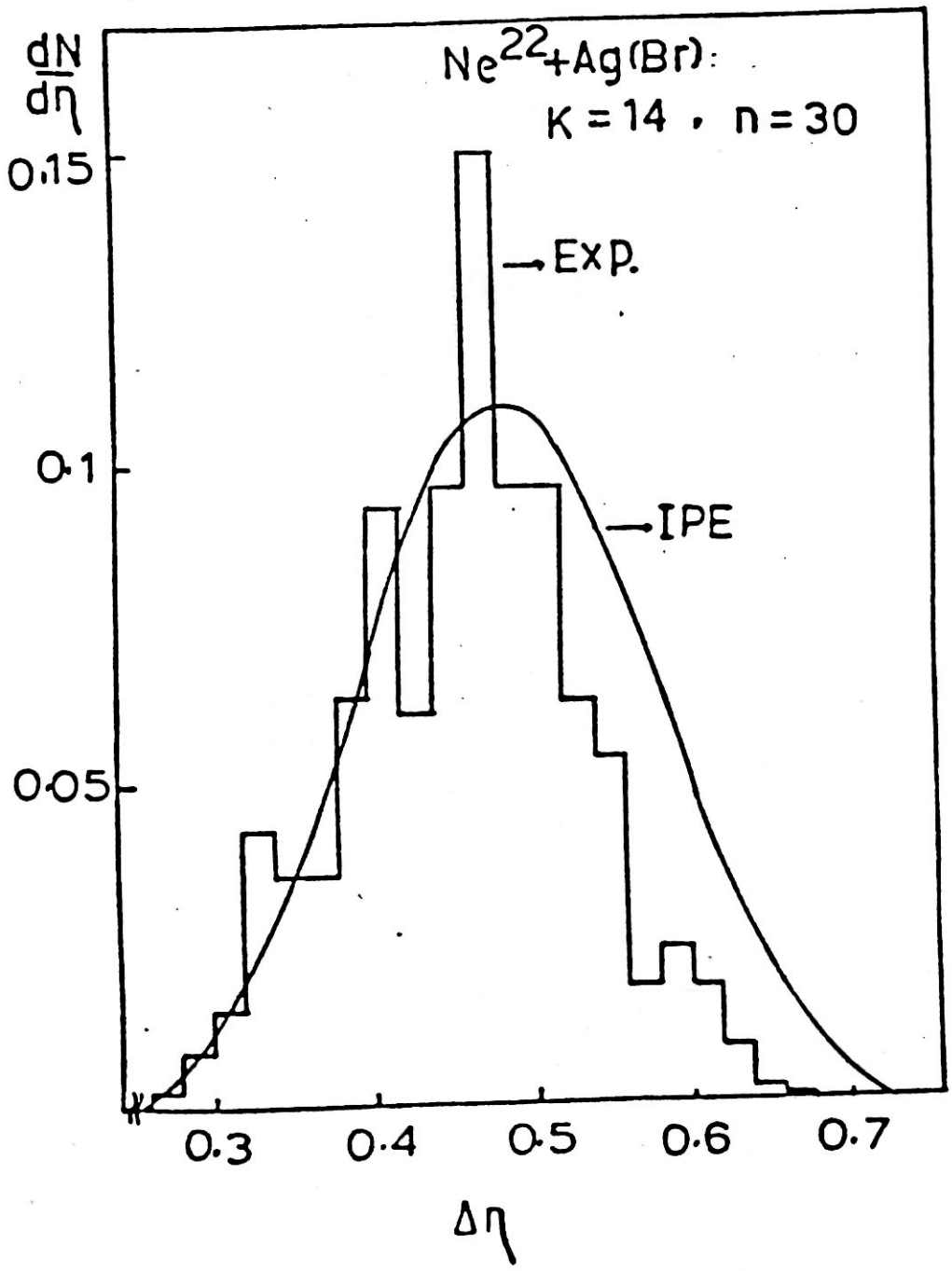

FIG. 47(C)

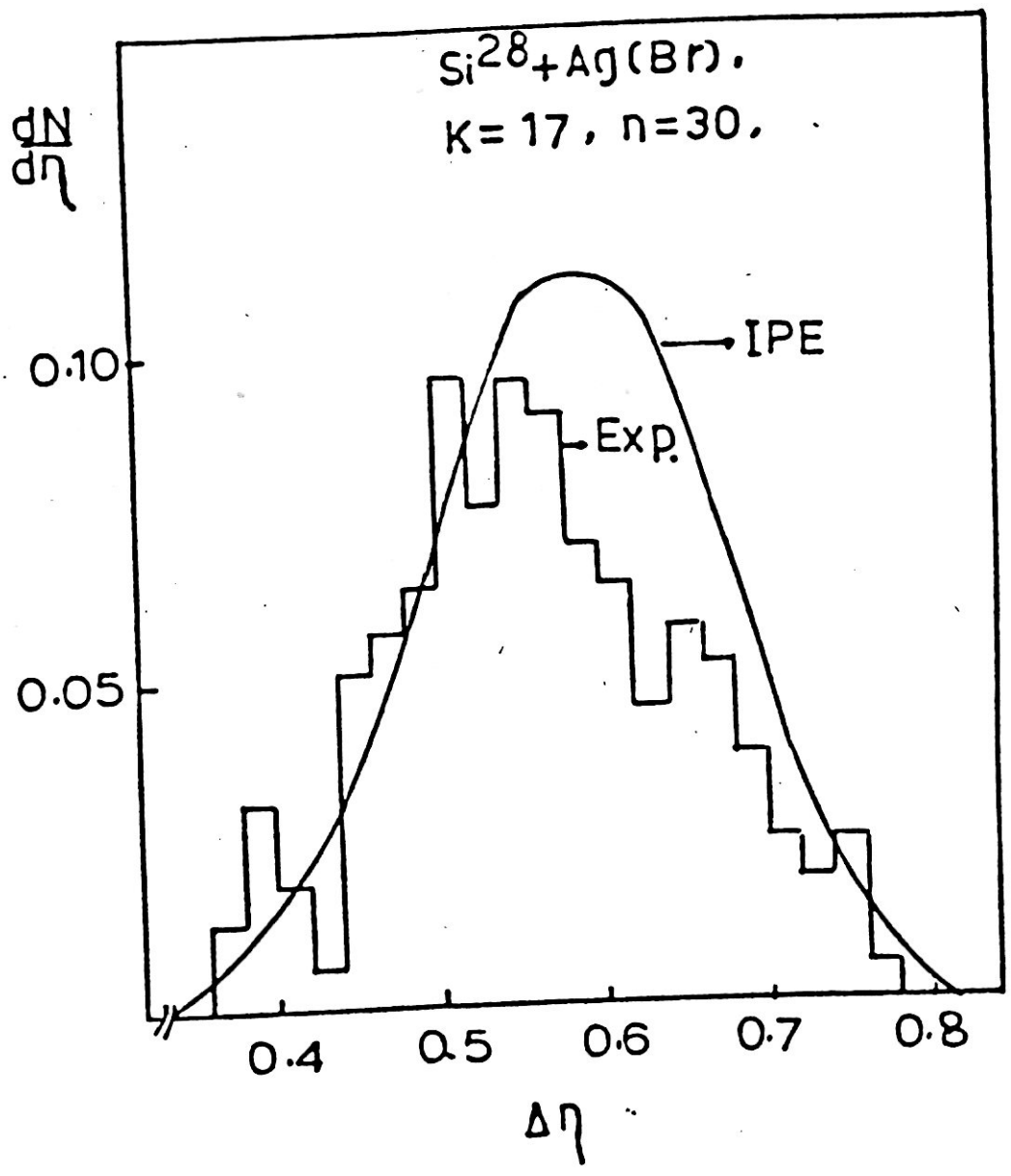
$Si^{28}+Ag(Br)$.
K=17, n=30.
$\frac{dN_p}{d\eta}$
0.10
0.05
IPE
Exp.
0.4
0.5
0.6
0.7
0.8
$\Delta\eta$

FIG.47(d)

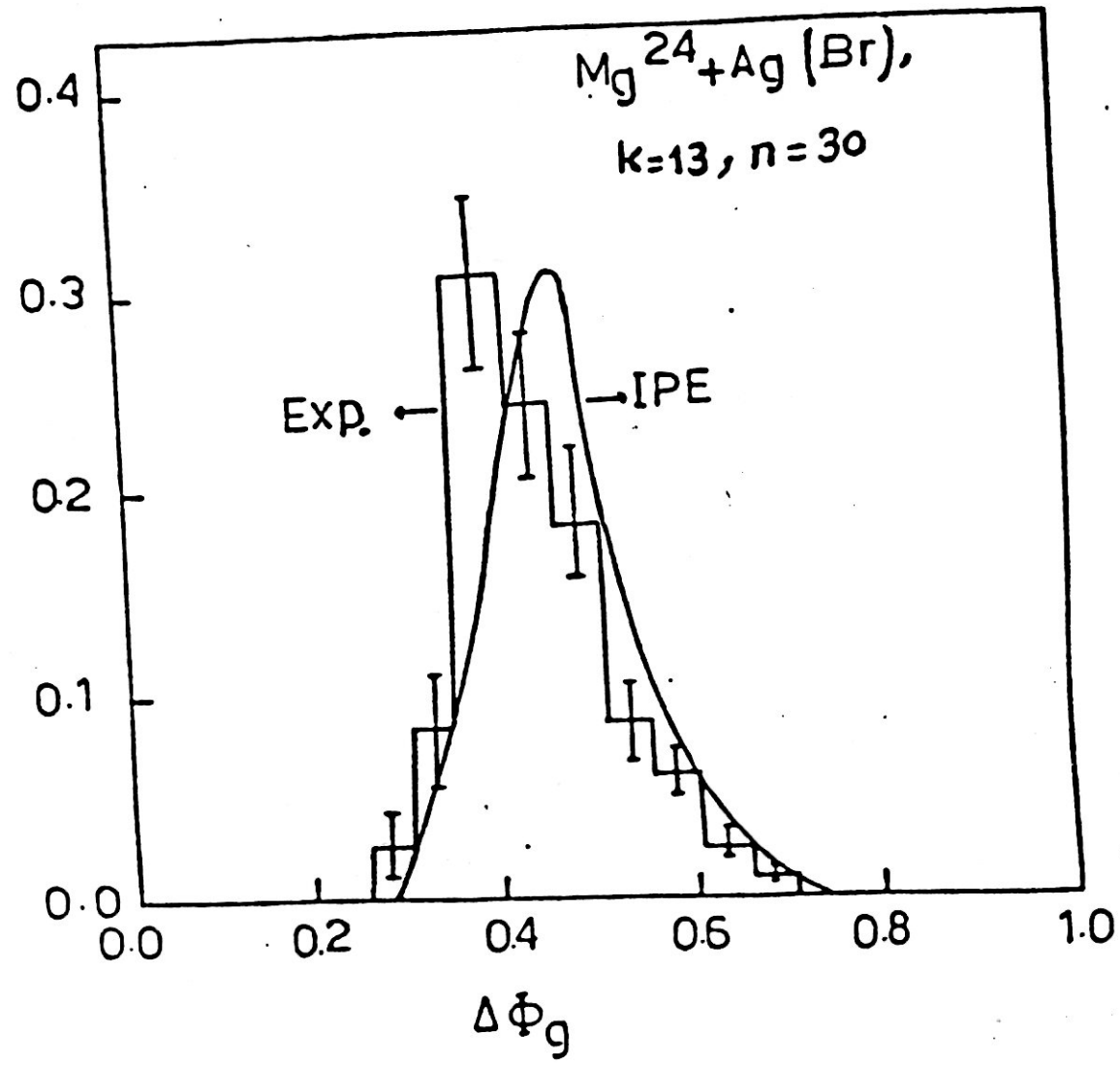
Mg 24 + Ag (Br),
k=13, n=30
Exp.
IPE
0.4
0.3
0.2
0.1
0.0
0.0
0.2
0.4
0.6
0.8
1.0
dN/dΔΦg
ΔΦg

FIG. 4 (a)

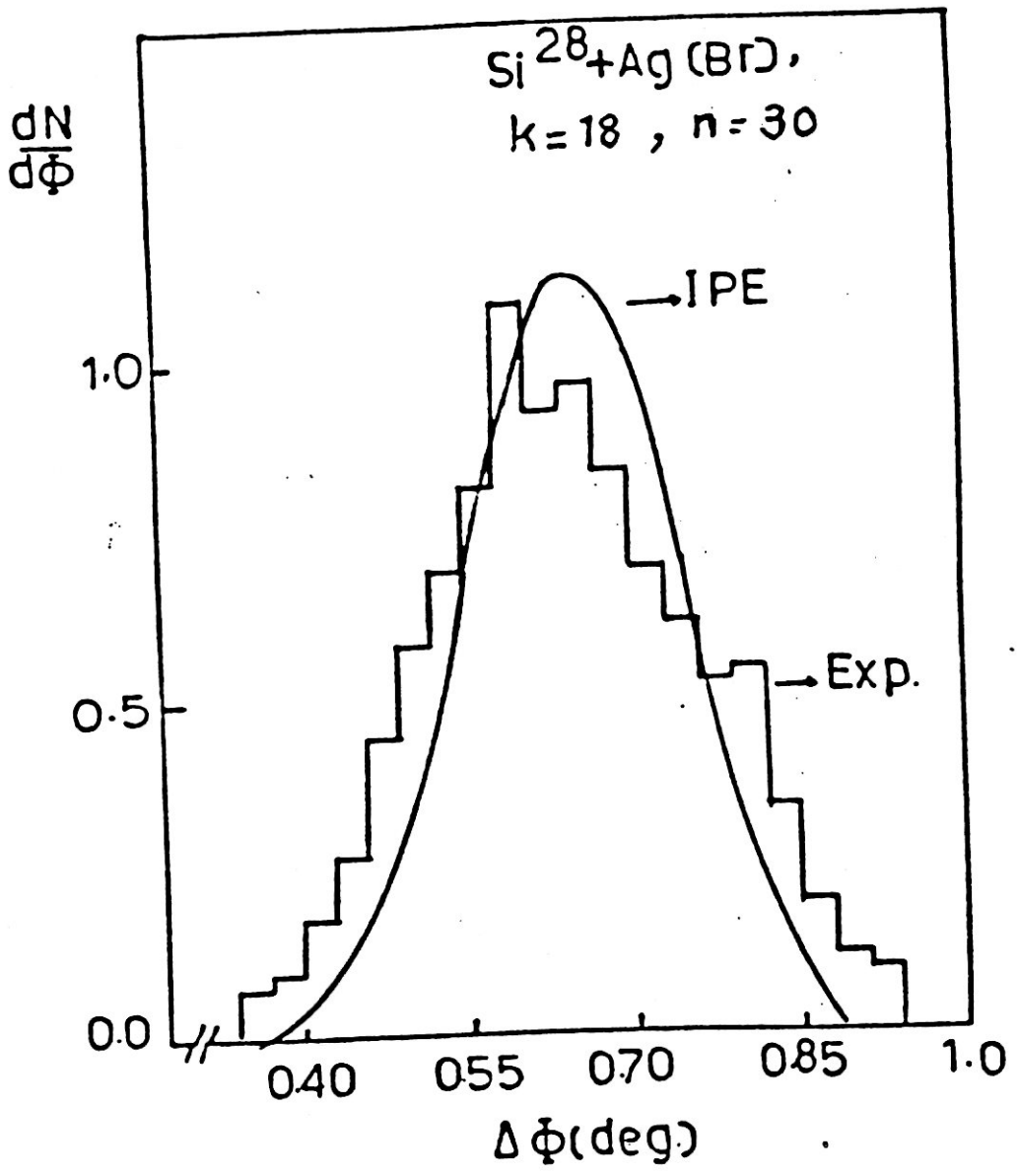

FIG. 48 (b)

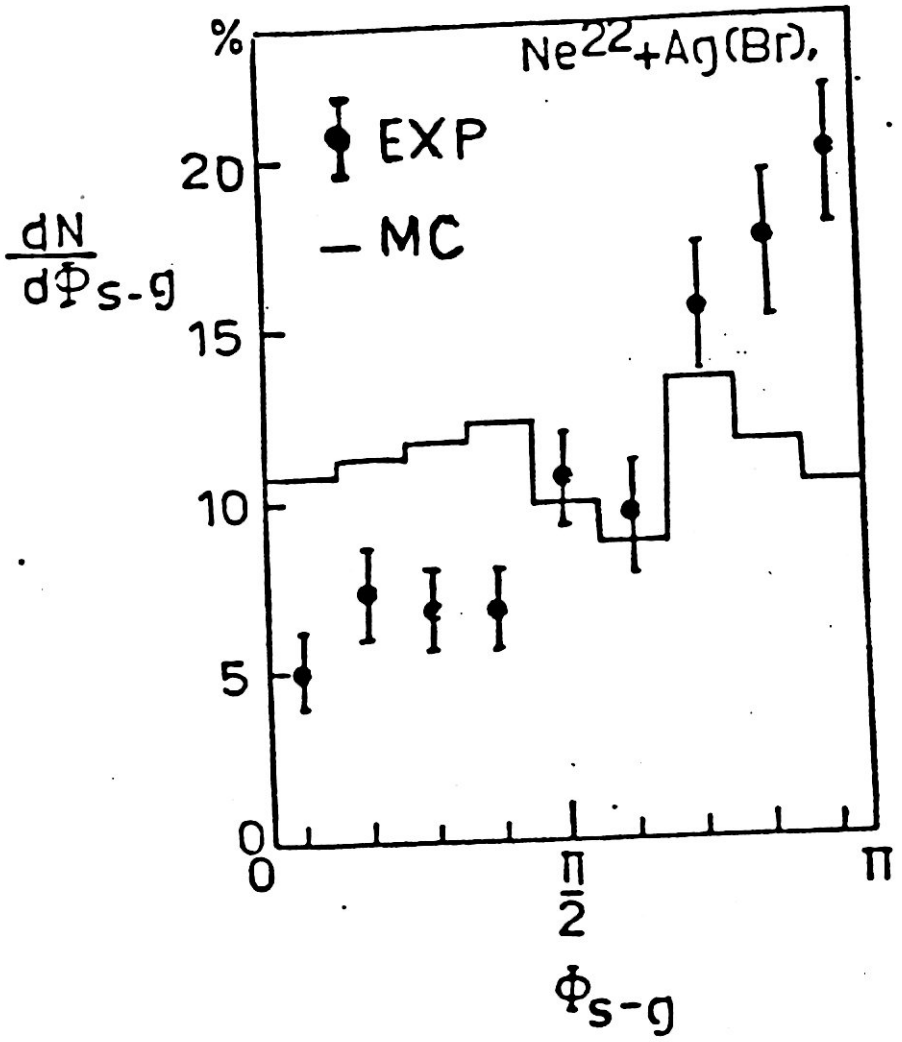

FIG. 4(a)

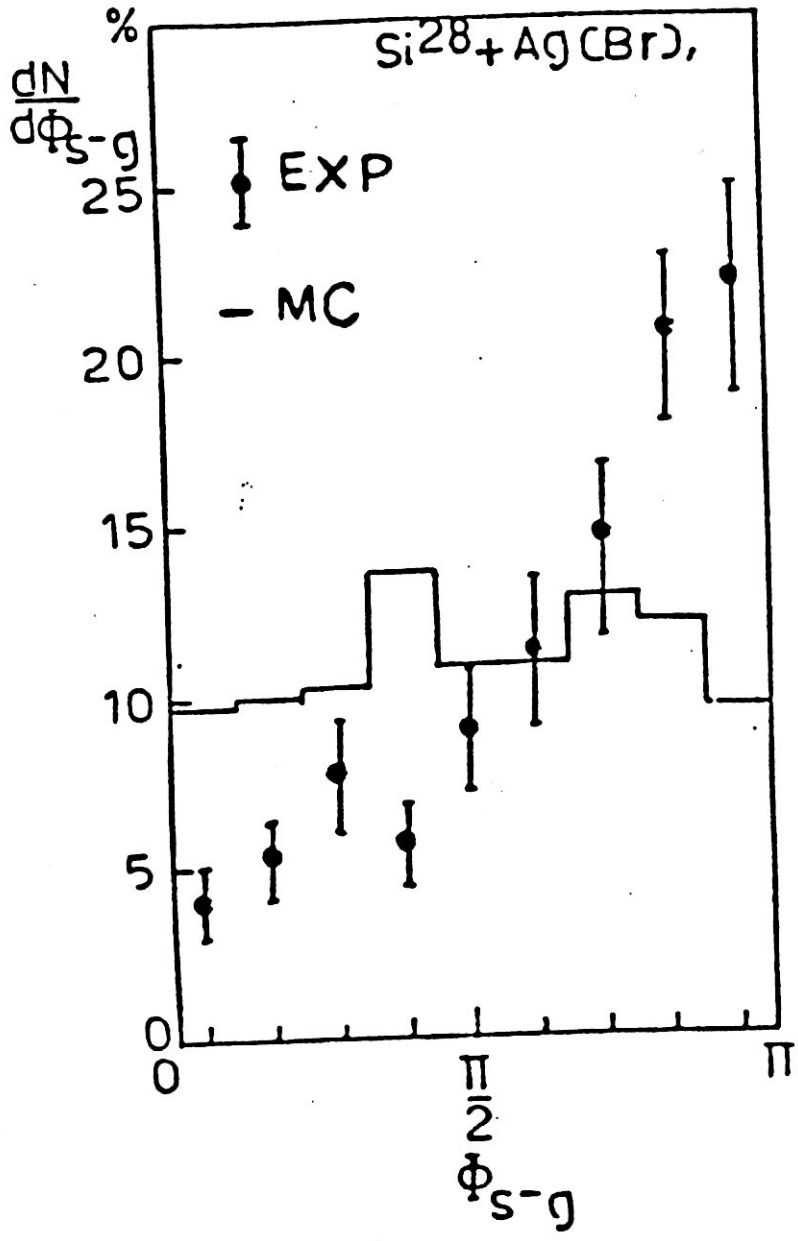

FIG.49(b)

II.1 . THE CHERENKOV HADRONIC LIKE JETS

II.1`.1 INTRODUCTION

An electron moving in a medium with velocity greater than the velocity of light in this medium,radiates light (Cherenkov effect) at a definite angle given by the relation

$$\cos\theta = 1/\beta n \qquad (37)$$

where $n>1$ is the refraction index of light in the medium and β is the electron velocity, in units of c. In a plane perpendicular to the axis of motion of the electron,one observes an illuminated ring whose radius is determined from equation (37). A new idea of multiparticle production at high energies was first proposed in/63/ This idea implies that when a hadron passing through nuclear active medium(a nucleus or a nucleon) may emit coherent hadronic radiation (pions) when its velocity is greater than the velocity of emission in the medium. Later,a series of papers appeared/64/. These papers were devoted to the study of hadronic Cherenkov radiation.These studies faced some troubles : first,it was assumed, not proved yet that the hadronic refractive index of nuclear-active medium can exceed unity;secondly,the strong interactions were treated in terms of perturbation theory;thirdly,an infinite hadronic medium was considered,whereas the

range of the nuclear forces was finite. These troubles were surmounted in/65,66/,where it was proved that the hadronic refractive index of nuclear-active medium can exceed unity and the concept of a hadron as a medium consisting of quarks and gluons was taken into account. In this case the problem is reduced to the passage of a point constituent(a quark or gluon carrying color charge) through a quark-gluon medium of finite dimensions. Radiation of gluons analogous to Cherenkov radiation becomes possible. Then each of the radiated gluons,evolved according to QCD and subject to the confinement mechanism, is converted into hadronic jet.

Collisions between nuclei at high energy may create a finite volume of high density hadronic matter. The lattice gauge theory of strong interactions/67/,suggests that above a critical temperature of about 250 MeV,the hadronic state of matter is channged into a new phase consisting of deconfined quarks and gluons with energy density

$$\varepsilon > \varepsilon \simeq 1\text{-}3\,\mathrm{GeV/fm}^3 \qquad (38).$$

Such conditions could be reached in central nucleus-nucleus collisions at high energy. The energy density ε is linearly related to the rapidity/68/ ρ ,by the relation

$$\varepsilon \approx m_T \rho, \qquad (39)$$

where: $\rho = dn/dy$ and m is the transverse mass of the emitted secondary particle (in most cases a pion).At high energies, the rapidity y is approximated by the pseudorapidity, η,

$$y = \eta = -\ln \tan (\theta/2) \qquad (40)$$

where θ is the emission angle in the laboratory system.

The mechanism of hadronic Cherenkov radiation,predicts typical features for such process that is the appearance of secondary particles with almost coincident polar angles i.e to lie within narrow rings on the target diagram (ring-like events) The pseudorapidity distribution for event of such type usually exhibit spikes higher than the overall distribution for the events of the same multiplicity.In /69/ the existence of the Cherenkov hadronic radiation was proved by analyzing experimental data in heavy ion collisions at high energies. In /70/ a systematic and statistically significant study of the phenomenon,its dependence on the projectile mass number and its probability, were presented.The hadron formation length was estimated from the determination of the ring radius or Cherenkov emission angle.

II.13.2. Analysis of experimental data

The investigated interactions were picked up from emulsion plates by along the track scanning. The plates

of 600μm thickness were exposed to 4.1A GeV/c Ne^{22} and others to 4.5A GeV/c Si^{28} beams at the Dubna synchrophasotron. The total numbers of inelastic interactions of these beams with emulsion are 1100 and 1360 respectively. The space angle θ and the azimuthal angle ϕ were measured for each secondary track. The details of the exposure, scanning and measurements may be found in/71,72/. For the present study, we have chosen events without any observable projectile fragment and with number of target fragments larger than seven. These events are central collisions of the given beams with Ag(Br) nuclei. Moreover, we began with the highest value of multiplicity of charged secondaries (almost pions), n_{ch}, descending to lower ones. Thus 27 Ne^{22}+Ag(Br) events of n_{ch} >38 and 48 Si^{28}+Ag(Br) events of n_{ch} >39 were analyzed.

To select unusual events (candidates) for investigation, we adopted a Monte Carlo (MC) procedure/73/. For each experimental event, a ν MC events were produced with the same multiplicity and pseudorapidity density. This amounts to shuffling, for each multiplicity, the tracks from different events, conserving the mean distribution but removing any correlation between tracks. The η-distribution of one of Ne^{22}+Ag(Br) and Si^{28}+Ag(Br) events are shown as

histograms in Fig.50a,b. Where η is the normalized pseudorapidity

$$\eta = (\eta - \eta_{min})/(\eta_{max} - \eta_{min}), \qquad (41)$$

which takes values from zero to unity. The η_{max} and η_{min} are the maximum and minimum pseudorapidity for individual events. The available η-range is divided into 10 equal bins.The smooth curve is the corresponding distribution from MC events. A spike is considered to be significant, if the differencee between the experimental peak and the corresponding MC value is greater than five standard deviations.This has been carried out to increase the level of significance and the ratio of effect to background. Thus,only 13 events,three from Ne^{22} and ten from Si^{28} have passed the above criteria. Statistically significant narrow spike are seen in the Fig.50a,b. The numbers of particles within the spike,n_{sp},equal 15 and 17 respectively. Correspondingly,the rapidity densities,ρ,at the spike are 38 and 29. These values are large enough to satisfy the equation (38). Then particles which lie within the spike are plotted on η - ϕ target diagram. The angle ϕ is the azimuthal angle i.e. the angle of the secondary track in the plane normal to the beam,measured in anticlockwise direction and it takes values from 0^{o} to 360^{o}. Fig.51 displays

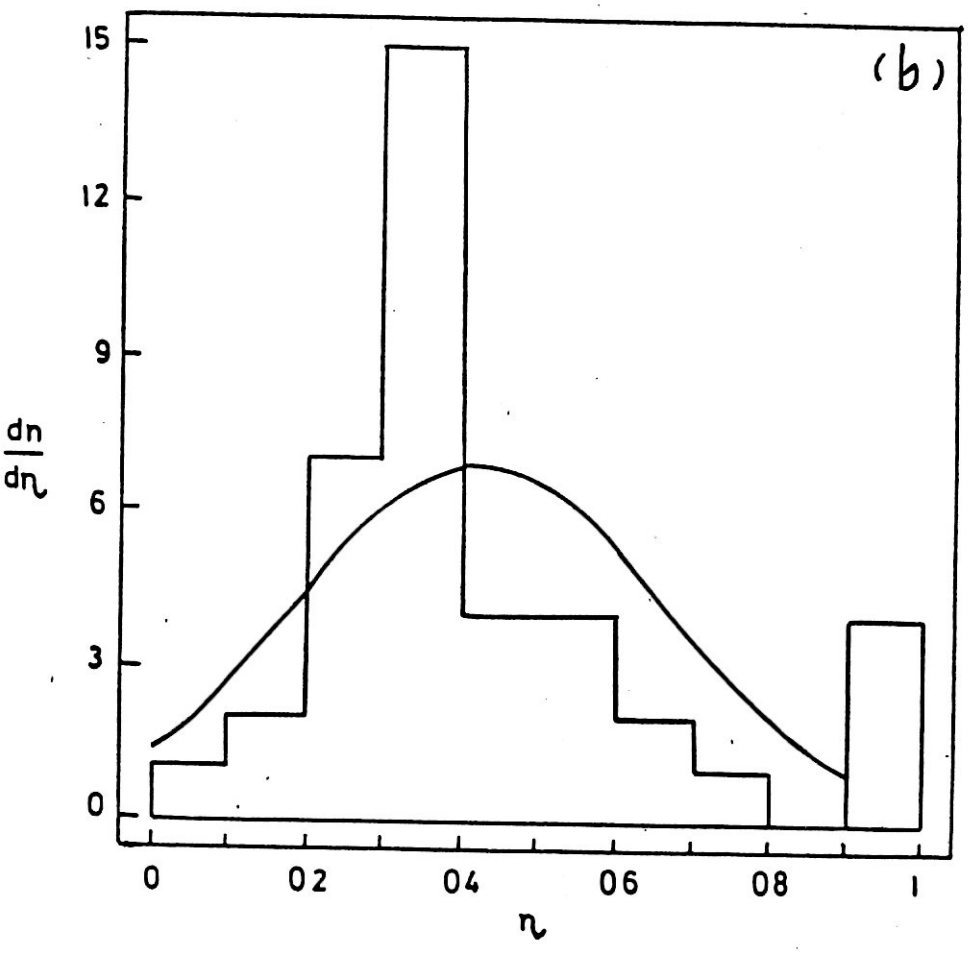

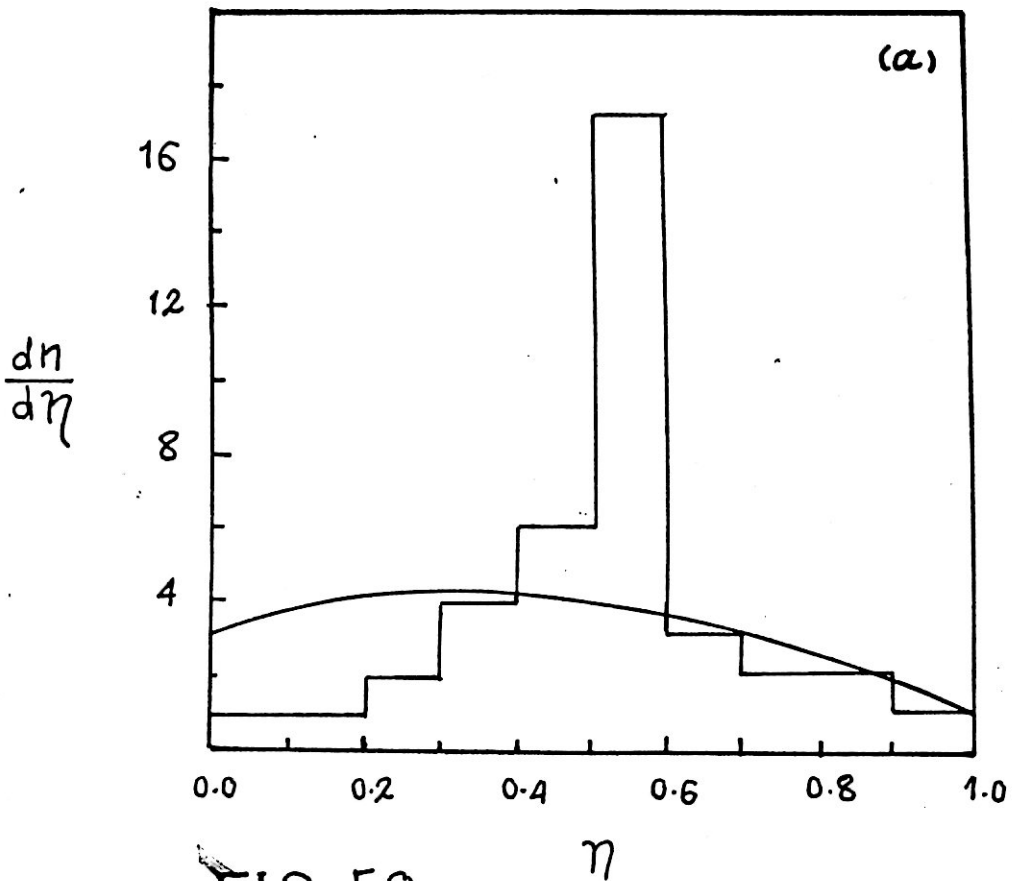

FIG. 50

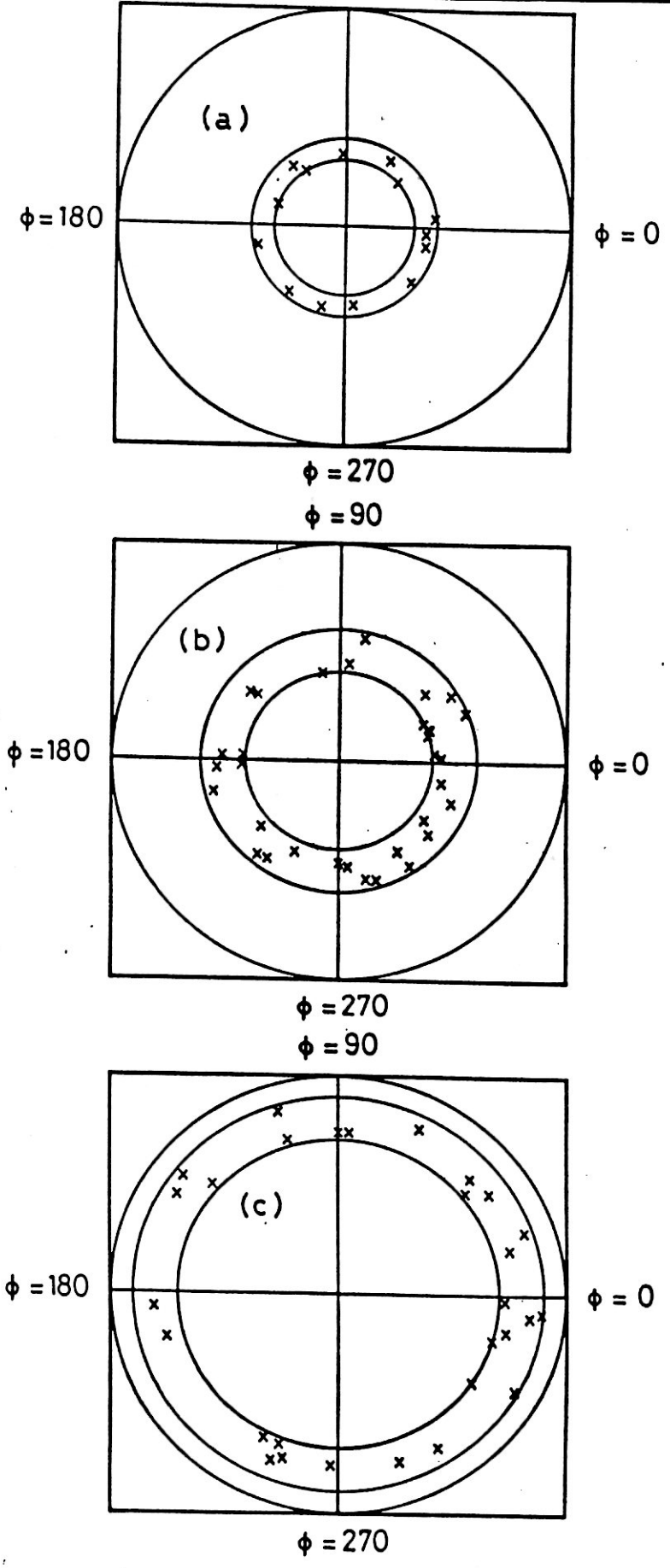

FIG. 51

three events of total multiplicities n_{ch}=65,70 and 39 respectively from Si^{28}+Ag(Br) interactions. The rapidity density,at the spike,ρ is 30,41,and 29 respectively. These values give energy density ε consistent with conditions necessary to phase transition to quark-gluon plasma.Fig.52 shows three ring-like events from Ne^{22}+Ag(Br) collisions. The multiplicity of charged secondaries in any of these three events is greater than 39. The general characteristics of the 13 ring-like events are given in table 23. The first column presents the multiplicity of the event,the second one gives the number of particles within the spike , the third column is the rapidity density ρ and the last one represents the Cherenkov angle of emission of hadrons. It is cleary seen that if we substitute m_T by 0.14 GeV, which is less than the actual value in our case,the condition (38) is satisfied.

II.13.3. Discussions and Conclusions

The most probable interpretation for the features of the ring-like events is that the particles within the ring are produced by some process of a formation length which is rather short. Actually,the large emission angles of Cherenkov gluon radiation were predicted in/65/, as a result of the thinness of hadronic

Table .23

n_{ch}	n_{sp}	ρ	θ_{Lab}
54	17	18.6	13.9
44	17	26.9	41.9
41	15	37.8	40.5
70	29	41.4	37.1
65	31	31.4	24.2
63	24	35.5	20.3
56	19	32.0	27.3
54	17	30.1	21.7
52	18	29.4	35.5
49	15	32.1	27.5
44	11	21.0	14.8
44	14	32.3	14.8
39	17	29.0	23.6

targets. Later,it was shown/66/ that the deconfinement of quarks within the hadronic targets can provide stronger effect at the same emission angles. The maximum of forward (in CMS) emission of gluon jets appears in the Laboratory System at angle

$$\theta_{Lab} = (2\pi / \omega\ell)^{1/2} \qquad (42)$$

where ω is the energy of a gluon jet(i.e. of a group of particles) and ℓ is the formation length which is close to the length of deconfinement. From the previous relation and the target plots shown in Figs.51,and 52,the angle of emission $\theta_{Lab} = 35^{o} - 60^{o}$. If the values of θ_{Lab}, deduced from Figs.51 and 52 are interpreted as ones due to gluon emission by deconfined quarks,and considering the mean transverse momentum equals to 0.4 GeV/c, one can calculate ω from the angles of emission of particles,then from(42) one can get ℓ = 1fm. The probability of this phenomena is about 1% of total inelastic events of Si^{28} and Ne^{22} with emulsion nuclei at 4.1-4.5A GeV/c. This probability increases with the mass number of the projectile nucleus.

References

1- Cocconi G. "The Role of complexity in nature" in "Evolution of particle physics" ed. M. Conversi, Academic Press N.Y. (1970), P.81.

2- BWDKLMT collaboration, Communication of JINR (Preprint) E1-10838, Dubna, 1977.

3- Bakaev V.A. et al. 15th ICRC, Plovdiv, 1977, Vol. 11. P. 532.

4- Bannik B.P. et al Z. phys. A284, 283, 1978.

5- Akhrorov O. et al, Communication of JINR P1-9963, Dubna, 1976. (in Russian)

6- El-Naghy A. et al. 16th ICRC, Kyoto (Japan), 1979, Vol. 6, p. 148.

7- El-Naghy A. et al. Z.Phys. A298, 55, 1980.

8- El-Naghy A 19th Int. Conf. for high energy Phys., Tokyo, 1978, Paper No. 996, p. 1023 of the Conf. proceedings.

9- El-Naghy A Z.Phys. A302, 201, 1981.

10- El-Naghy A Nuovo cimento, 71A, 245, 1982.

11- El-Naghy A et al. Izv. Akad. Nauk, USSR, 45, 1198, 1981 (in Russian)

12- El-Nadi M et al. Z.Phys. 310A, 301, 1983.

13- Marin A et al. Yaderniya Fizikia (in Russion) 32, 1379, 1980. and Sov. J. Nucl. Phys. 32, 711, 1980.

14- El-Naghy A et al. 18th ICRC, Bangalore (India), August 1983, Vol. 5, P. 207.

15- El-Naghy A et al 18th ICRC, Bangalore (India), August 1983, Vol.5, p. 208.

16- El-Naghy A. et al. 20th ICRC, MOSCOW, 1987.

17- El-Naghy A et al. 20th ICRC, Moscow, 1987, Vol. 5, p. 76.

18- El-Naghy A et al. 20th ICRC, MOSCOW 1987, Vol. 5, P. 78.

19- El-Naghy A et al 20th ICRC, MOSCOW 1987, Vol. 5, P. 81.

20- El-Naghy A. et al. 20th ICRC, MOSCOW 1987, Vol.5, p. 85.

21- El-Naghy A. et al. JINR Preprint E1-87-472, Dubna, 1987.

22- Bannik B.P. et al. Z. Phys. 329A, 341, 1988.

23- El-Naghy A et al. J. Phys. G. 14, 1125, 1988.

24- Bannik B.P. et al. J. Phys. G14, 949, 1988.

25- El-Naghy A. et al. CLUSTER' 88 Int. Conf. on clustering Aspects in Nucl. and Subnucl. Systems. Kyoto (JAPAN) July 1988 paper V-2 p. 262.

26- Baranik A.T. and El-Naghy A et al. CLUSTER' 88 paper V-3 p. 264.

27- El-Naghy A CLUSTER' 88 Paper V-7, p. 272.

28- Krasnov S.A. Communication of JINR, P1-88-389, Bubna, 1986.

29- El-Naghy A. et al. J. Phys. Soc. of JAPAN 58, (1989), Suppl. P. 741.

30- El-Naghy A. et al. J.Sc. of Cairo Univ., (Egypt) 1989.

31- Ghoniem M.T. and El-Naghy A.22nd ICRC Dublin(1991)paper HE 1.1-11.

32- Ghoniem M.T. and El-Naghy A. 22nd ICRC Dublin(1991) paper HE 1.1-12

33- El-Naghy A. et al, A 22nd ICRC Dublin (1991) paper HE 1.1-13.

34- El-Naghy A. et al A22nd ICRC Dublin (1991) paper HE 1.1-14

35- El-Naghy A et al 22nd ICRC Dublin (1991) paper HE 1.1-15

36- Bokova L.N. et al., Communicaiton of JINR PI-9364, Dubna (1980)

37- Jakobson B et al., Phys. Scripta, 13, 327, (1976)

38- Sayed M.M., Thesis for M.Sc., Cairo Univ. (1991).

39- Tolstov K.D. et al., Preprint JINR, PI-8313, Dubna (1974).

40- Westfall G.D. et al, Phys. Rev. C19, 1309 (1979).

41- Heckman H.H. et al, Phys. Rev. C17, 1735, 1978.

42-Bannik B.P. et al, Sov. J. Nucl. Phys., 52-982,(1984)

43- Abd El-Daim A.M., Thesis for Ph.D, Assiut University (1991).

44- Mangotra L.K. et al., IL NUOVO Cim., 87A, 279 (1985)

45- Bials et al., Nucl. Phys. B111 461(1976)

46- Wosiek et al., reprint of INP Kratov 26A, 30-055 Poland (1985)

47- Bials A. et al., Nucl. Phys., B100, 103(1975)

48- Bogdanov V.G. et al., Sov. J. Nucl. Phys. 38(6), 910 (1983)

49- Krasnov S.A. et al, Preprint JINR, PI-87-348, Dubna (1987)

50- Abd El-Daim A.M., Thesis for M.Sc. Assiut University (1988)

51- Gosset J et al., Phys. Rev., C16, 629, (1977)

52- Westfall G.D. et al., Phys. Rev. Lett. 37, 1202 (1976)

53- Bowman J.D. et al, LBL Report No. LBL-2908, (1973)

54- Ander B. et al, Nucl. Phys. 42B, 1399, (1975)

55- Tolstov K.D. et al., Comm. of JINR P1-6897, Dubna (1973)

56- Ghoh Dipak J. et al., Phys. Rev. C35, 4, (1987)

57- Hüfner J., Phys. Rep, 125, 131, 1985.

58- Toneev V.D. et al., Fiz E.Ch. Atom. Yad., 17,1093,(1986)

59- Kaufman S.B., Phys. Rev. C14, 1121, (1976)

60- Baumgardt H.C. et al, Z. Phys., A273, 359 (1975)

61- Heckmann H.H. et al., Phys. Rev. C17, 1651 (1978)

62- Abd Alla N.N., Thesis of M.Sc., Assiut University,(1989)

63- Wada W.W., Phys.Rev., 75, 981 (1949); Ivanenko D.D. and Gurgenidze V.A. Dokl. Akad. Nauk SSSR 67, 997; Blokhintsev D.I. and Indenbom V.L. Zh.Eksp.Teor.Fiz. 20, 1123 (1950).

64- Yekutieli G., Nuovo Cimento 13, 446 (1959); Czvz W., Ericson T. and Glashow S.L. Nucl.Phys. 13, 516 (1959); Czvz W. and Glashow S.L. Nucl.Phys. 20, 309 (1960); Smrz P., Nucl.Phys.35, 165 (1962).

65- Dremin I.M., Pisma Zh.Eksp.Toer.Fiz., 30, 152 (1979); JETP Lett., 30, 140 (1979); Yad.Fiz., 33, 1357 (1981); Sov.J.Nucl.Phys. 33, 726 (1981).

66- Dremin I.M. Pisma Zh.Eksp.Teor.Fiz., 34, 617 (1981); JETP Lett. 34, 594 (1982); Yad.Fiz. 37, 649 (1983); Sov.J.Nucl.Phys. 37, 387 (1983).

67- Koguy J.B. Nucl.Phys., A418, 381C (1984); Satz H., ibid, A418, 447C, (1984).

68- Gyulassy M., LBL Report 15175 (1982).

69- El-Naghy A. and Abdel-Khalek K.S. Phys.Lett. B299, 370 (1993).

70- El-Naghy A. et al. ICTP internal report IC-93-148, Trieste (1993); submitted for Z.Phys.A. (atoms & nuclei).

71- El-Naghy A. et al., J.Phys. 14G, 1125 (1988).

72- El-Naghy A. et al., 5th Conf.Nucl.Sc. & Appl., Cairo, Egypt, vol. 2, pp. 744-751, 1992.

73- El-Naghy A. et al., Supplement to J.Phys.Soc.of Japan, 58, 741, (1989).

Chapter III

Neutrino charged current Interactions with Emulsion

This chapter is divided into two main parts. The first part deals with the characteristics of slow particles emitted in the charged current interactions of neutrinos with emulsion. In this part, we test whether there is a difference in the average multiplicities of grey particles produced in "charm" and "non-charm" events. These results were compared with the calculations of Suzuki/1-3/ which were carried out in the framework of the cascade model. In the second part we tried to estimate the hadron "formation time" within the framework of a modified intranuclear cascade model (ICM)/4-6/.

Part I

III.1. Characteristics of slow particles emitted in the charged current interactions of neutrinos with emulsion

III.1. Introduction.

The neutrino beams became available at CERN, Serpukhov and Fermilab/1/ charged hadron multiplicities have been studied in detail in neutrino-nucleon, antineutrino-nucleon, neutrino-nucleus and antineutrino-nucleus interactions/7-16/. It was found that many features of these kinds of interactions are very similar and depend only on the quark content of beam and target particles and on the hadronic center of mass energy W. No data have been presented yet about emission of slow particles in neutrino-nucleus interactions.

In neutrino induced reactions on nuclei, a quark hit by a virtual photon or a weak boson propagates inside the nucleus either singly or after immediate recombination into a meson. The quark or the meson, in this case, is called leading particle system (LPS) which may interact further with a nucleon inside the target nucleus with an effective cross section σ_0'. The value of σ_0' may depend on whether the LPS is composed only of a single quark or a meson. Moreover, it may depend on whether it is c quark, u quark, charmed meson or non-charmed meson. In each of these cases, the value of σ_0' is expected to be reflected in grey particle multiplicity distribution and its average value, observed in the final state.

In this part we mainly report, for the first time, on study of multiplicity and angular distributions of slow charged particles (target fragments) emitted in the charged current interactions of neutrinos with emulsion nuclei (ν-Em) at average incident energy $\langle E_\nu \rangle = 54 \pm 4$ GeV. These interactions are classified into: (I) events without charm production "noncharm" and (II) events with produced charmed particle "charm". Both are compared to each other and to a third class of events which is proton-emulsion (P-Em) at energy 22.5 GeV.

The aim of the present work is to test whether there is a difference in the value of average multiplicity of grey particles produced in "charm" and "non-charm" events and consequently the difference in σ_0' in both cases. Also, to shed light on the general characteristics of slow particles emitted in the different classes of events and their physical implications.

This part is organized such that in Sec. 2 a brief description, of the set up and experimental conditions,

is presented. Sec. 3 deals with multiplicities of secondary particles and Sec. 4 is devoted to their angular distributions. The energy distribution of g particles is discussed in Sec. 5. An account of theoretical calculations of average number of g-particles $\langle n_g \rangle$ and their multiplicity distribution in comparison with the present experimental data, is carried out, in Sec.6. The main conclusions of this part are presented, in Sec.7.

III.1.2. Experiment. The charged current interactions of neutrinos with emulsion nuclei were picked up from those observed in a hybrid emulsion spectrometer which was used in the Fermilab experiment E-531 to study charm particle and their production cross section /17-19/. The apparatus shown schematically in Fig. 1 was exposed to the Fermilab neutrino beam, produced upstream by 350 GeV/c (first run) and 400 GeV/c (second run) protons and is incident from the left of the figure. The apparatus, starting from the upstream end, consisted of veto counters, an emulsion target, a time-of-flight counter I, upstream drift chambers, a magnet, downstream drift chambers, time-of-flight counters II, lead glass shower detectors, a hadron calorimeter, and a muon identifier. The details of the performances of the apparatus and exposures were presented in references /17-19/.

Events were recorded on magnetic tape if no signal was seen in the veto upstream of the emulsion target, and two or more charged particles left the emulsion and registered in the TOF hodoscope downstream of the magnet. This trigger does not distinguish between neutral and charged current interactions. A charged particle in an event was identified as a muon if it penetrates the muon counters which consisted of two hodoscopes of scintillator counters behind 1.3 m and 2.3 m of steel, respectively.

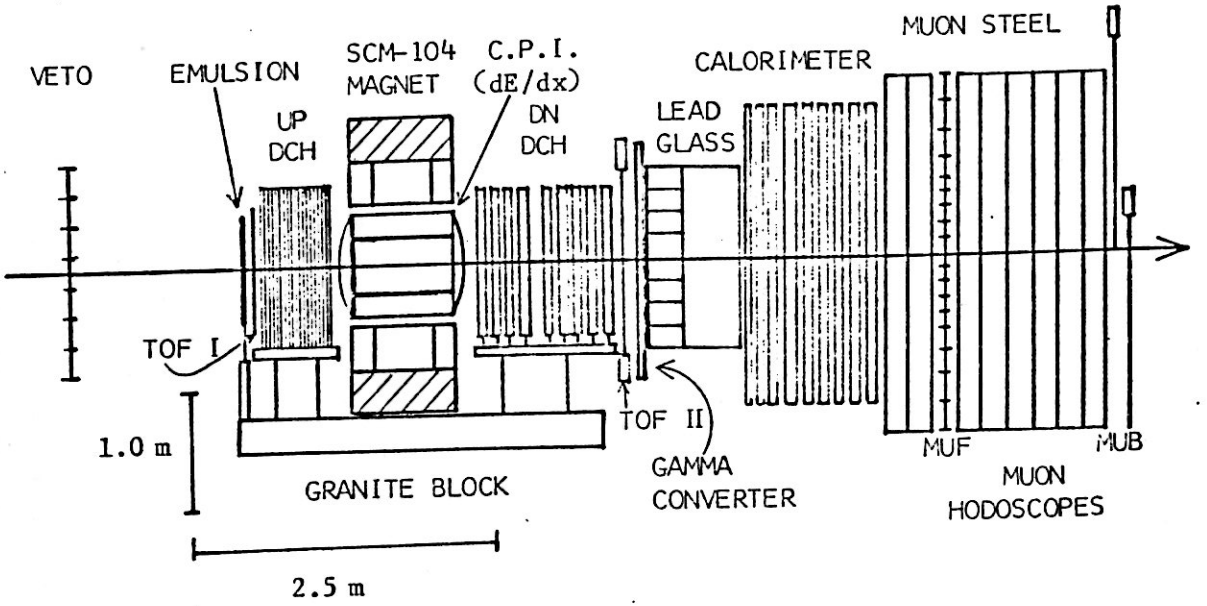

FiG. 1. Plan view of the experiment.

The energy required for a muon to reach the first hodoscope was 1.9 GeV and was 3.4 GeV for the second hodoscope. A net muon detection efficiency was 69 $\pm$ 5%. The incident energy of neutrino E_ν is calculated to be the total energy of an event visible in the calorimeters plus the energy of the identified muon. The uncertainty of E_ν is about 10% in the range from 0 to 30 GeV and increases with the increase in muon energy.

The 23 liter (35 liter in second run) emulsion target was contained in a volume 86 cm wide by 71 cm high by 5 cm (7 cm second run) deep. It was divided into two parts, the upper part with the emulsion surface parallel, and the lower part with the emulsion surface perpendicular to the incident neutrino beam. Neutrino and antinutrino interactions recorded in the downstream detectors have been located in this target. Only those events located in the lower part were used in the present study.

For the present study, the following selection criteria have been applied: (i) the event vertex must be at least 20 mm apart from the stack edges. (ii) the event should include identified negative muon. Applying the above mentioned criteria 260 events were selected, out of them 192 events with $N_h > 1$. It is appropriate to divide the secondary particles into: (i) relativistic particles or showers s of $\beta \geq 0.7$ or I^* ($=I/I_0$) < 1.4 where I is the particle track ionization and I_0 is the corresponding number for minimum ionizing particle track. These particles are almost charged pions of kinetic energy (K.E.) > 60 MeV and fast protons of K.E. > 400 MeV. (ii) grey track particles g are those of range in emulsion R > 3000 μm and I^* > 1.4. They are mainly protons in the energy range 27-400 MeV. (iii) Black track particles b of R < 3000 μm. These are low-energy singly and multiply charged fragments p,d,t ^{3}He and ^{4}He corresponding to proton energy E_p < 27 MeV emitted mainly due to evaporation. Altogether b and g particles are called heavy track particles h.

In each event, the number of showers n_s was counted. In the $N_h > 1$ event, for each h-track particle the space angle θ between the direction of the incident neutrino and that of the emitted h-track particle, the azimuthal angle ϕ between the projection of μ^- muon and that of the h-track particle in the plane perpendicular to the incident neutrino direction, and the range in emulsion R were measured accurately. Consequently the numbers: of heavy track particles N_h, of grey track particles n_g and of black track particles n_b were defined in each event.

The same measurements were carried out for 73 charm associated events/[17-19]/. These are events in which charmed particles were produced and μ^- was identified without applying the geometrical cut mentioned in the criterion (i). If this criterion were applied the main trends of physical results remained the same but charm events statistics are drastically minimized increasing the statistical errors. Thus, the following study considers two sets of data: (I) 260 events without charm production "non-charm" and (II) 73 events with charm production "charm". These two sets are compared to each other and to a third set (III) which is proton-emulsion (P-Em) collisions at 22.5 GeV /22/.

III.1.3. Multiplicities of secondary particles. It is interesting to study the dependence of average multiplicaties of differrent particles on the incident neutrino energy. Fig. 2 presents the dependence of $\langle n_s \rangle$, $\langle N_h \rangle$, $\langle n_g \rangle$, and $\langle n_b \rangle$ on incident neutrino energy E_ν for non-charm events. It shows that only $\langle n_s \rangle$ increases slowly with E_ν whereas the other average multiplicities are nearly constant. According to the cascade model, the leading particle system may further interact inside the target nucleus and n_g is a measure of the number of inranuclear collisions. Thus, the present data indicate

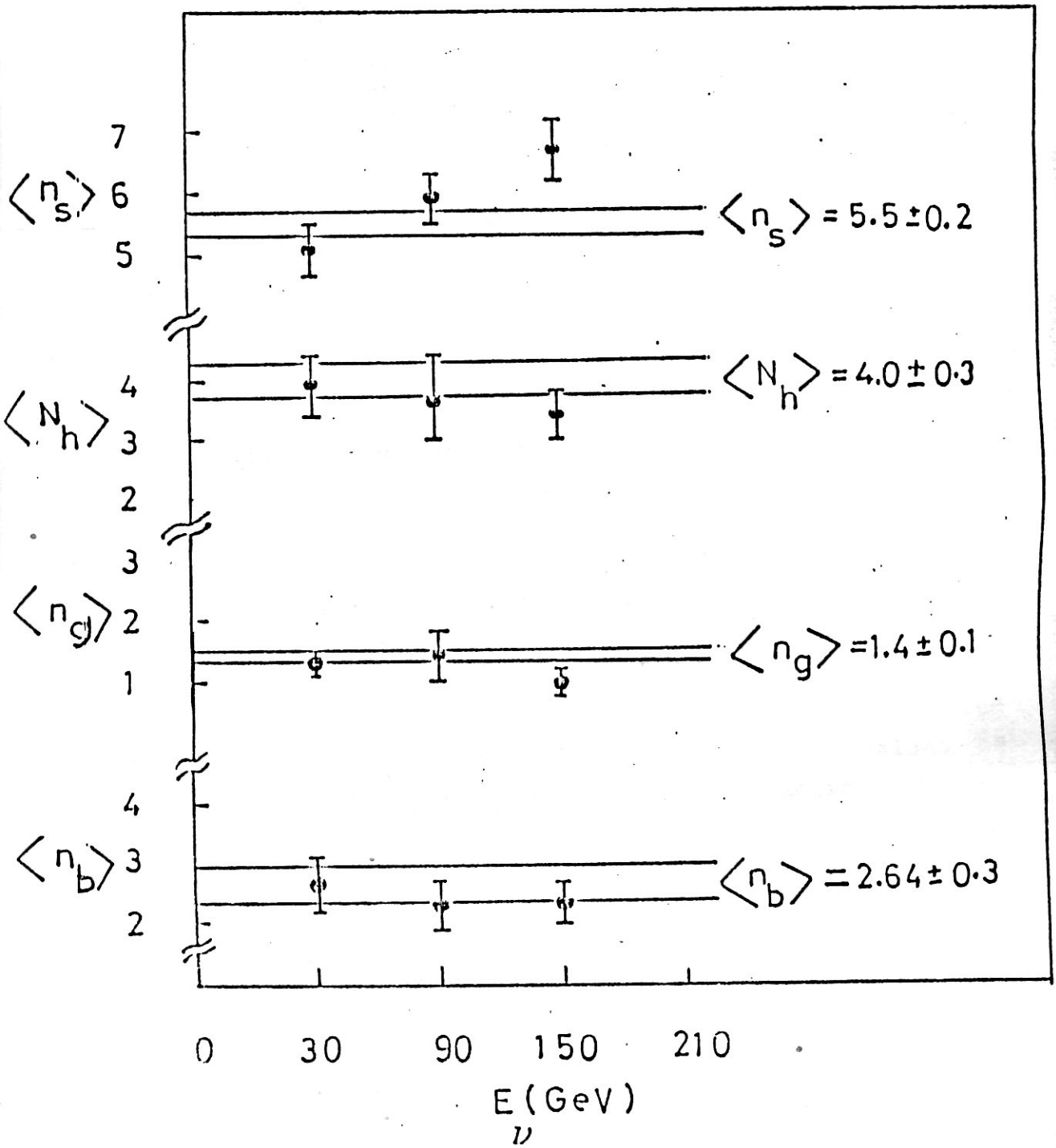

FiG. 2. The dependence of the average multiplicity of different particles on the incident neutrino energy for "non-charm" events, the two horizontal lines, in each relation, represent the upper and lower limit of the total average multiplicity.

that the number of showers produced per intranuclear collision increases with the incident energy.

Table 1 presents the average multiplicities of s,h,g and b particles emitted in "non-charm" ν -Em charged current inelastic interactions. These values are compared to the corresponding ones from P-Em collisions at 22.5 GeV, the nearest available hadron energy to the mean hadronic energy in ν -Em interactions which is about 25 GeV. The value of $\langle n_s \rangle$ for "charm" events is less than the corresponding one for "non-charm" events by about unity whereas $\langle N_h \rangle$, $\langle n_g \rangle$ and $\langle n_b \rangle$ for these two classes are consistent. This effect can be observed in Fig. 3, where a pronounced peak at $n_s=1$ exists only in "charm" events. The n_g and N_h-distributions for these two classes of events are consistent. This is attributed to the fact that charmed particles are heavy particles which are usually produced with a relatively high momentum and a small fraction of energy is remained for the production of other shower particles. Excluding the muon track, $\langle n_s \rangle$ for P-Em is higher than for ν Em "non-charm" interactions. It is to be noted that there is a measurable deviation in the values of $\langle N_h \rangle$, $\langle n_g \rangle$ and $\langle n_b \rangle$ for ν Em and P-Em interactions. Table 1 shows that for P-Em these values are about 1.5 times the corresponding ones from ν -Em events. Also, the n_g- and N_h-distributions Fig. 3 (b),(c) show that at low multiplicity ν -Em events are higher than P-Em ones whereas at high multiplicities there is no significant difference. This observation can be explained by the known fact that hadrons tend to interact as soon as they enter the hit nucleus and after the first collision, there is still a considerable nuclear matter for the leading particle to propagate through it. Neutrino can interact at any point inside the target nucleus and it usually penetrates for a measurable distance inside the nucleus. Thus, the degree of intranuclear cascading in case of hadrons is

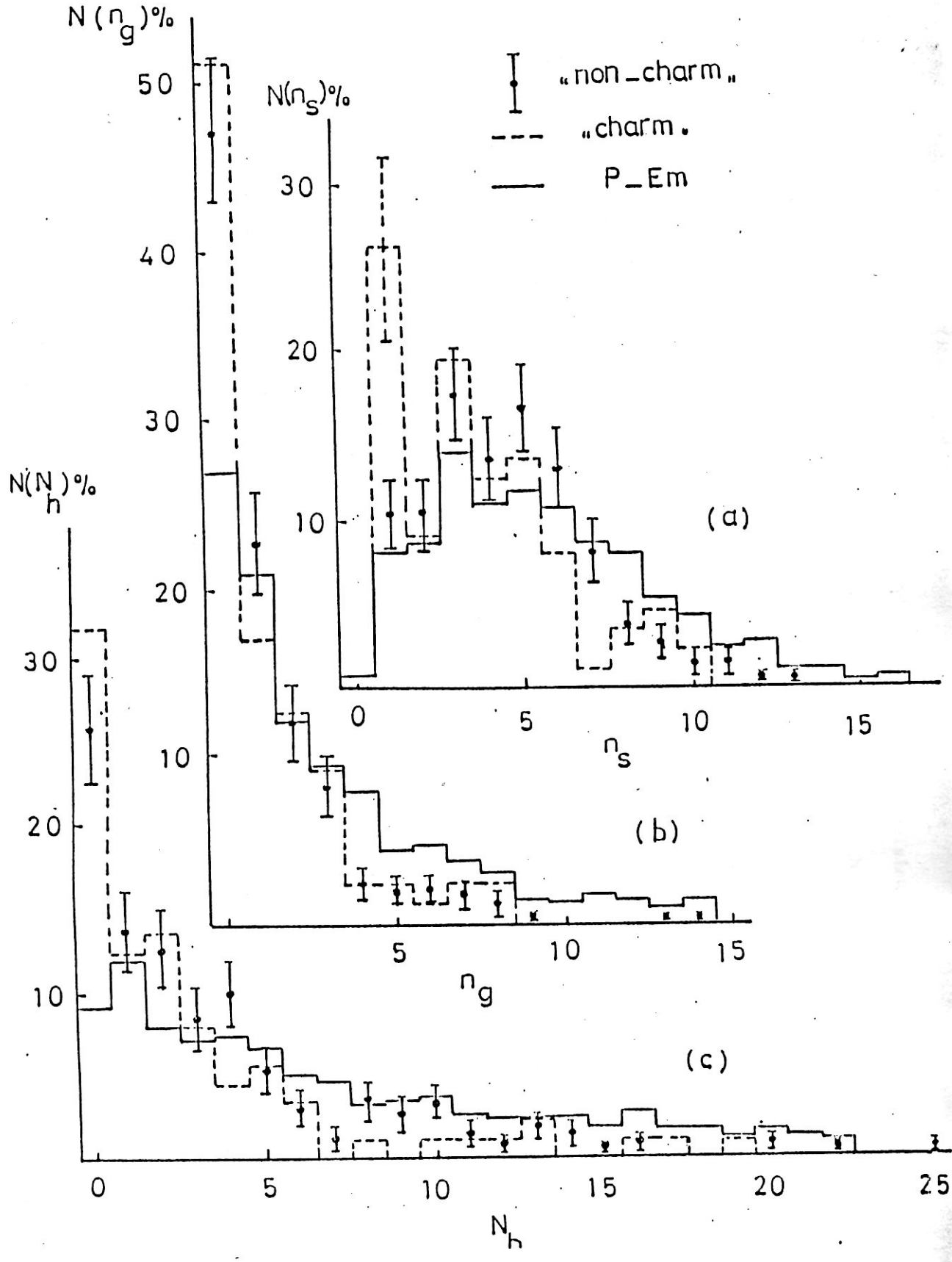

FiG.3. The multiplicity distributions for (a) s tracks (b) g tracks and (c) h tracks. All distributions are normalized to 100 events. The points with bar errors are "non-charm" events, the dashed histogram stands for charm events and the solid one represent proton-emulsion data at 22.5 GeV.

Table.1. The average multiplicities in the charged current neutrino emulsion interactions for "charm" and "non-charm" events in comparison with the corresponding values in P - Em collisions at 22.5 GeV.

Average multiplicity → / Class of events ↓	$\langle n_s \rangle$	$\langle N_h \rangle$	$\langle n_g \rangle$	$\langle n_b \rangle$	Number of events
"non charm"	5.52±0.15 *4.52±0.15	3.99±0.30	1.35±0.13	2.64±0.25	260
"charm"	4.67±0.26 *3.67±0.26	3.60±0.50	1.31±0.21	2.31±0.33	88
"P - Em" at 22.5 GeV	5.61±0.01	8.60±0.25	3.38±0.14	5.22±0.29	915

* excluding the muon track.

more than the neutrino one. In "charm" events, obviously, the LPS is either a c quark or a c meson whereas in "non-charm" ones, it is either a u quark or a non-charmed meson. For these different cases the cross section of LPS inside the nucleus σ_o' is expected to have different values correspondingly. This difference of σ_o' should be reflectd in $\langle n_g \rangle$ and consequently $\langle n_b \rangle$ and $\langle N_h \rangle$. The experimental data show consistency between values of $\langle N_h \rangle$, $\langle n_g \rangle$ for "charm" and "non-charm" events. Moreover, in Fig.3 (b), the ratio of $n_g = 0$ events can be calculated roughly from simple consideration of the quark theory, neglecting the cascading effects. It is known that nuetrino interacts with d-quark, so the neutrino -neutron cross-section is considered to be twice as large as the neutrino-proton one. In case of neutrino-neutron interaction the recoil particle is either a proton or a neutron with equal probability. Taking into consideration the emulsion composition, the ratio of events with recoil neutron is calculated to be 0.4 which agrees with the experimental value 0.5 ± 0.1.

These observations show that LPS, in ν Em interactions at $E_\nu = 54 \pm 4$ GeV, does not contribute significantly to the production of recoil nucleons. In P-Em collisions the n_g-distribution and the ratio of events with $n_g=0$, were successfully reproduced by theoretical calculations depending on internuclear cascading[1-3].

The correlations between multiplicities of different types of particles, for the considered three classes of events are presented in Fig.4. These correlations are fitted with straight line equation. The results of fitting are given in Table 2. It is seen that the correlation $\langle N_h \rangle$ -n_s has nearly the same slope for "charm" and P-Em events and this slope is about two times that of "non-charm" events. It is interesting to notice that in all

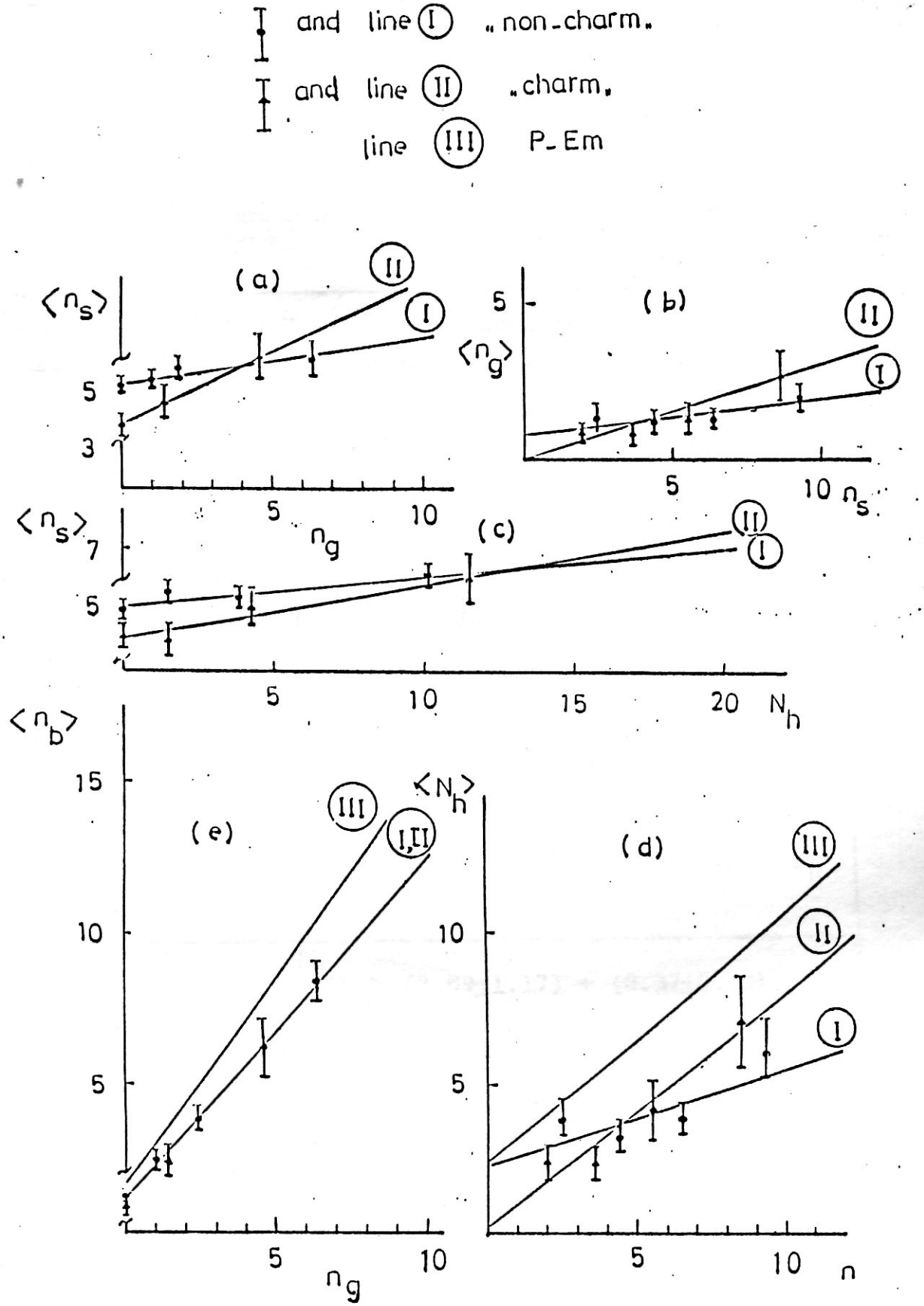

FiG.4. The correlation between different multiplicities (a) $n_g - \langle n_s \rangle$ (b) $n_s - \langle n_g \rangle$, (c) $N_h - \langle n_s \rangle$, (d) $n_s - \langle N_h \rangle$ and $n_g - \langle n_b \rangle$. The line I represents "non-charm" events, line II for "charm" events and line III for P - Em collisions . The equations describing these lines are given in table 2.

Table.2. Equations resulting from linear fitting of data, presented in FiG.4. Line I for "non-charm" events, II for "charm" ones and III for P - Em data/

Fig. Number	line No.	Equation
4-a	I	$\langle n_s \rangle = (5.33 \pm 0.06) + (0.15 \pm 0.02)\ n_g$
	II	$\langle n_s \rangle = (4.05 \pm 0.08) + (0.48 \pm 0.03)\ n_g$
4-b	I	$\langle n_g \rangle = (0.74 \pm 0.35) + (0.12 \pm 0.05)\ n_s$
	II	$\langle n_g \rangle = (-0.23 \pm 0.48) + (0.33 \pm 0.09)\ n_s$
4-c	I	$\langle n_s \rangle = (5.16 \pm 0.17) + (0.09 \pm 0.03)\ N_h$
	II	$\langle n_s \rangle = (4.02 \pm 0.16) + (0.18 \pm 0.03)\ N_h$
4-d	I	$\langle N_h \rangle = (2.09 \pm 1.17) + (0.37 \pm 0.19) n n_s$
	II	$\langle N_h \rangle = (0.05 \pm 0.78) + (0.78 \pm 0.14)\ n_s$
	III	$\langle N_h \rangle = 2.22 + 0.83\ n_s$
4-e	I,II	$\langle n_b \rangle = (0.94 \pm 0.08) + (1.16 \pm 0.09)\ n_g$
	III	$\langle n_b \rangle = 1.59 + 1.36\ n_g$

correlations including n_s the "charm" events have a slope greater than that of "non-charm" ones. The energy transfered to the target nucleus is usually measured by n_g or N_h. This energy transfer in "non-charm" events is more than that in case of "charm" events at low values of n_s, however the rate of its increase with n_s is much slower than in "charm" events and at high values of n_s the energy transfered to the hit nucleus in "charm" events is more than in "non-charm" events. Fig. 4(e) shows clearly the strong dependence of evaporation particles on the number of recoiling nucleons n_g, both in ν - Em and P-Em data. This means that the number of recoiling nucleons n_g in the hit target nucleus determines the excitation energy of the residual nucleus. The correlation in Fig. 4(e) is completely independent of the number of produced particles (pions or charmed particles) i.e. these produced particles do not transfer any significant energy to the target nucleus. In ν Em interactions, this correlation has a universal shape independent of being "charm" or "non-charm" events.

III.1.4. Angular Distribution. Grey track particles are mainly protons in the energy range 27-400 MeV. The angular distribution of these particles, in hA collisions, was found to exihibit a forward peak and a universal shape of the form $\frac{1}{N_{tot}} \frac{dn}{d\cos\theta_g} \simeq \exp(0.96 \cos\theta_g)$/20,21/. This distribution is nearly independent on the variaiton of projectile mass, primary energy and target mass. Fig.5 presents $\cos(\theta_g)$ distribution from neutrino-emulsion collisions in comparison with the corresponding one from hA interactions/20,21/. In this experiment, the $\cos(\theta_g)$ distribution is less peaked in the forward direction than in hA collisions. It is a remarkable feature that grey track particles from "charm" and "non-charm" events have

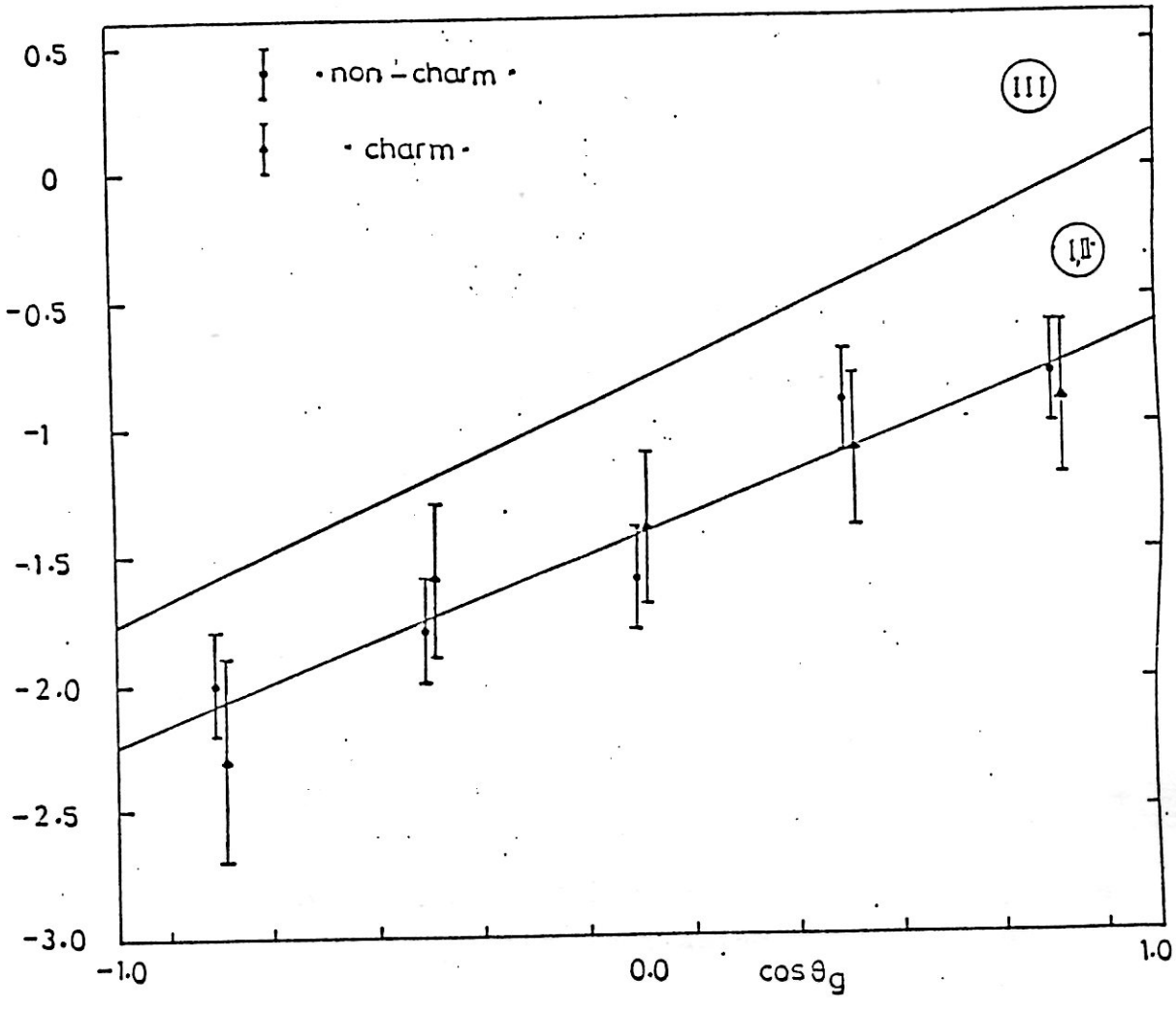

FiG.5. The angular distribution of grey track particles emitted in neutrino - emulsion interactions "charm" and "non-charm" events, line (I,II) has a shape of the form $\frac{1}{N_{tot}} \frac{dn}{d\cos\theta_g} \sim \exp(0.83+0.13)\cos\theta_g$ Line III stands for hA collisions in the energy range 6 - 400 GeV and it has the form $\frac{1}{N_{tot}} \frac{dn}{d\cos\theta_g} \sim \exp(0.96)\cos\theta_g$.

the same angular distribution and the universality, observed in hA collisions, has a corresponding one in ν- Em interactions in a shape of the form

$$\frac{1}{N_{tot}} \frac{dn}{d\cos\theta_g} \approx \exp\ (0.83 \pm 0.13) \cos(\theta_g).$$

The forward-to-backward ratio F/B i.e. the number of such tracks emitted at angles <90° to those emitted at angles > 90°, in laboratory system, was calculated for g-tracks and found to be F/B = 2.39 ± 0.37 which is less than the corresponding value in hA interaction F/B = 3.37/21/.

It is interesting to study the dependence of F/B ratio on the range of grey tracks. In Table 3 only g tracks stopped in emulsion were used for the calculation of F/B ratio. Although the statistical errors included in these values are high, it is noticed that there is a systematic increase in the value of F/B with increasing the range of g-track particle. More direct evidence for this experimental fact can be seen in the same table in the relation between the average angle of emission $\bar{\theta}_g$ and the range of grey tracks. The average emission angle $\bar{\theta}_g$ decrease systematically with increasing the range of grey track particles. The forward peaked behaviour and the increase in the value of F/B with the increase in the range support the assumption that grey particles are knock-on recoils.

Black track particles, are low-energy singly and multiply charged fragments (P,d,t, ^{3}He and ^{4}He with energy corresponding to proton energy E_p < 27 MeV) emitted almost isotropically. Fig. 6 shows the angular distribution of black track particles in comparison with the coresponding distribution for P-Em interactions/21,22/. An agreement is observed between the distributions. The F/B ratio for

Table.3. The values of F/B ratio and average emission angle $\bar{\theta}$ as functions of the range of grey track particles.

The F/B Ratio	Range (mm)	The average emission angle $\bar{\theta}$	Range
1.12 ± 0.31	< 9 mm	84.2	R < 10 mm
1.40 ± 0.31	< 15 mm	80.2	< 20 mm
1.68 ± 0.36	< 18 mm	77.7	< 30 mm
1.72 ± 0.35	< 30 mm	76.9	< 69 mm
2.39 ± 0.37	all		

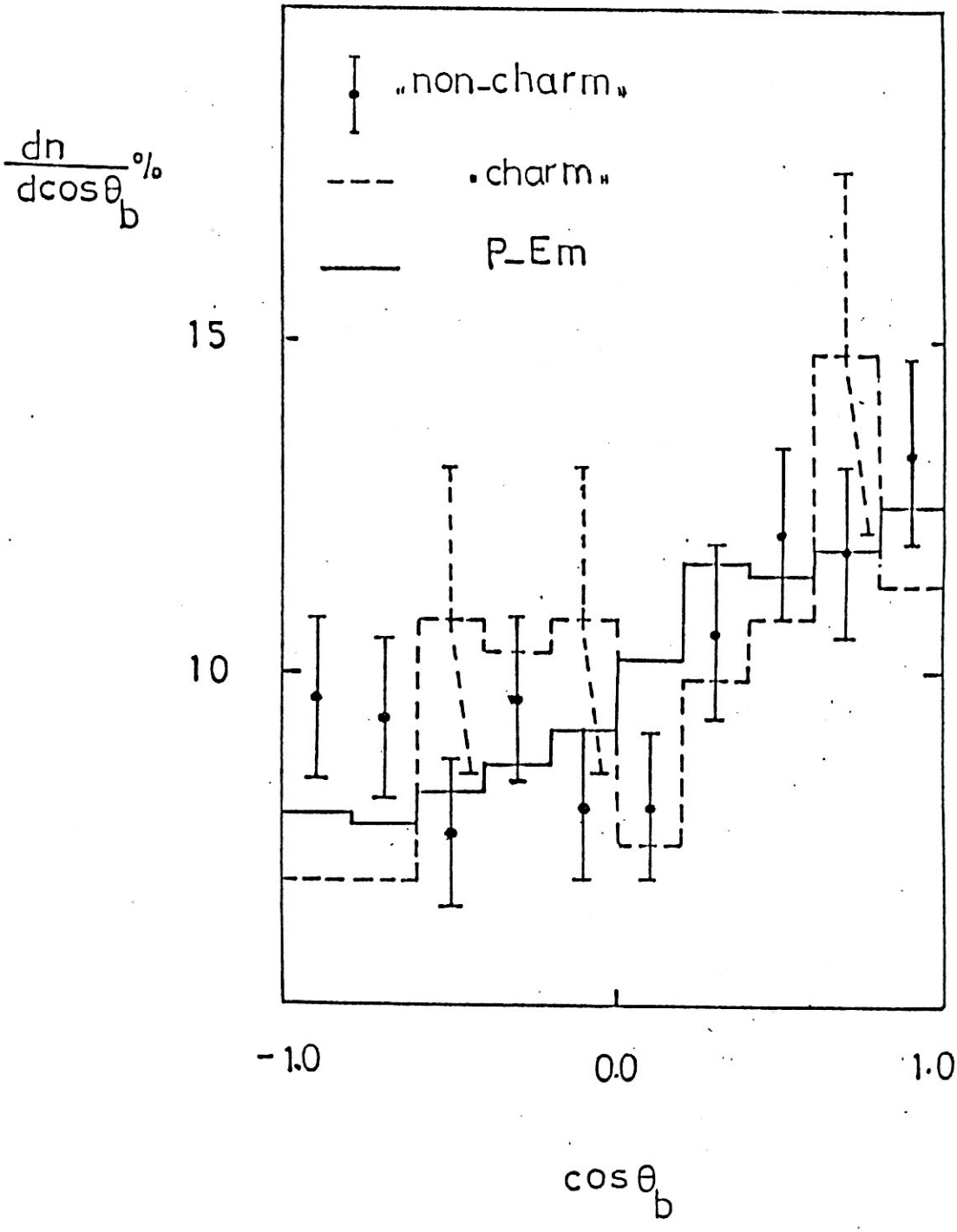

FiG.6. Black track particle angular distributions, points with bar errors represent"non-charm"events, dashed histogram represents"charm"events and solid histogram represents P- Em data . All distributions are normalized to 100 events.

ν-emulsion experimental data is 1.26 $\pm$ 0.13. As shown in Table 4 the value of F/B for black track particles is range independent. This confirms that b track particles, as defined in this paper, are emitted isotropically from a statistical equilibrium system. Table 4 shows that F/B values are very near to each other in neutrino-emulsion, proton-emulsion and nucleus-emulsion interactions.

Fig. 7 (a,b) shows the azimuthal angular distributions of g and b tracks measured relative to the projection of the μ^- track in the plane perpendicular to the incident neutrino direction. Both distributions are isotropic, within experimental errors. Within errors, the present data show that μ^- has no effect on the direction of grey and black particle emission.

III.1.5. Energy Distribution of grey track particles. In this experiment all h-track particles are followed either to the stop or to the exit of the stack. The g-track particles stopped in emulsion are almost protons of well defined measured range, so their energy could be determined from the energy-range relation for protons, e.g./22/. The energy distribution of these stopped g-track particles from non-charm events is shown in Fig.8. This distribution is fitted to a formula $N(E)\,dE \simeq E^{-\gamma}dE$ where $\gamma = -1.15 \pm 0.18$. This result agrees with the corresponding one in hA collisions/21/. It is worthwhile to mention that the data used in the fitting of Fig. 8 are unbiased ones i.e. all tracks of range < 3.5 cm could be picked up and measured completely. About 30% of g-tracks escaped the range measuring. This value is consistent with Fig. 8.

Table (4). The values of F/B ratio of black track perticles for different incident particles and energies.

Beam	<Ebeam> (GeV / A)	Target	Range	F/B
Neutrino	54 ± 4	emulsion	R < 3 mm	1.26 ± 0.13
Neutrino	54 ± 4	emulsion	R < 2 mm	1.30 ± 0.15
Neutrino	54 ± 4	emulsion	R < 1 mm	1.30 ± 0.16
P	2.2	emulsion	R < 3.5 mm	1.32 ± 0.05
P	2.0	emulsion	E_{He}<50 MeV	1.15 ± 0.09
P	5.0	Ag	<80 MeV	1.17
P	24.0	emulsion	emulsion	1.28 ± 0.09
^4He	2.1	AgBr	R < 4 mm	1.46 ± 0.04
^{16}O	2.1	AgBr	R < 4 mm	1.37 ± 0.05
^{14}N	2.1	emulsion	R < 3 mm	1.40 ± 0.06

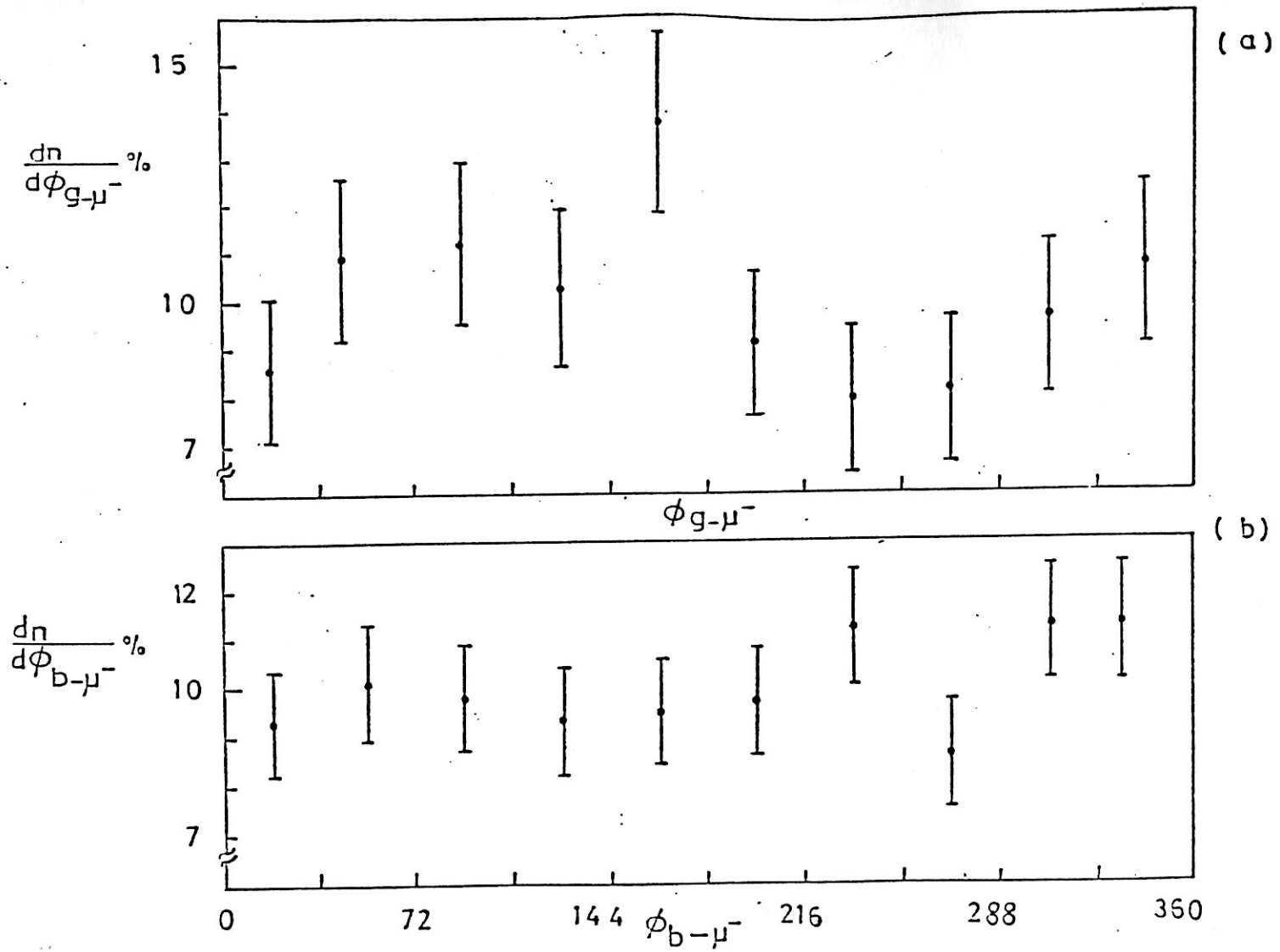

FIG.7. The azimuthal angular distributions (a) for g and (b) for b tracks measured relative to the muon direction in the plane perpendicular to the incident neutrino.

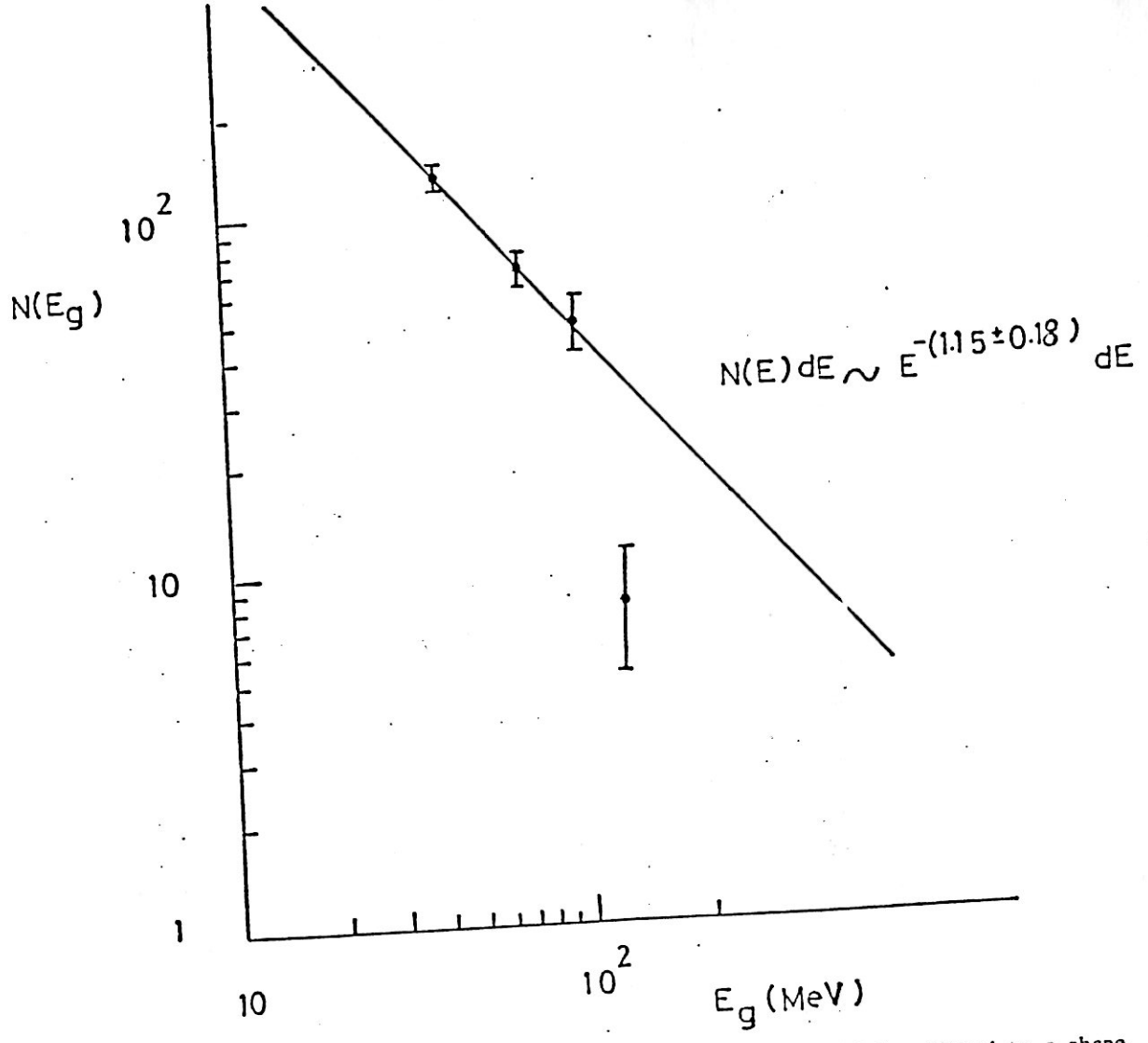

FIG.8. The energy distribution of grey track particles fitted to a shape of the form $N(E)\,dE \sim E^{-\gamma}\,dE$ where $\gamma = -1.15 + 0.18$.

III.1.6. Comparison with theoretical calculations.

In ref./2,3/, Suzuki studied the multiplicity distribution of grey track particles in the framework of the cascade model. He considered two types of the cascading models. The assumptions adopted in model I are:

(i) A primary particle incident on a nucleus at impact paramter b collides with a proton with a cross section σ_o or with a neutron with r σ_o. When the primary particle collides with a proton, a proton recoils with a probability a_1, and a neutron recoils with a_2. In the collision with a neutron, a proton recoils with a probability b_1 and a neutron recoils with b_2.

(ii) Charge exchange processes are taken into account only in the first collision of the primary particle with a nucleon.

(iii) The LPS formed in the first collision of the primary particle collides with a nucleon (proton or neutron) with a cross section σ'_o. The nucleon is considered to be a recoil nucleon of the FG.

(iv) Shower particles make a negligibly small contribution to the production of gray particles.

(v) A recoil nucleon hit by the primary particle collides with another nucleon, which is also counted in the recoil nucleons. The cross section of a recoil nucleon with a nucleon inside the nucleus is shown by σ .

(vi) Colliding with another nucleon, a recoil nucleon loses some portion of its kinetic energy. We denote by σ_a the cross section corresponding to the process that the kinetic energy of the recoil nucleon goes down below the threshold value of gray particles in the collision. This nucleon is excluded from the gray particles.

(vii) The recoil protons which come out from the target nucleus are considered to be gray particles.

In model II, assumptions (i)-(iv) are also adopted. Instead of assumptions (v)-(vii), he considered that only the recoil nucleons of the FG can produce other recoil nucleons. The ratio is designated by P that the recoil nucleons of the FG enter into the energy window of grey particles. Recoil nucleons of the second generation cannot produce other recoil nucleons.

Applying these two models for charged current interactions of neutrinos with emulsion nuclei, the author of ref./3/considered the diagrams given in Fig. 9 a,b,c and d, where a diquark in a nucleon, absoring a W^+ boson, changes into a u-quark or a c-quark, which forms a leading particle system (LPS). The remaining quark is assumed to recombine immediately into a nucleon, which is considered as the recoil nucleon of the first generation (FG).

In this process, σ_o denotes the neutrino-proton cross-section of the charged-current interactions and σ_o' indicates the cross-section of the LPS with a nucleon. From simple quark counting, r = 2. Other parameters are chosen as $a_1 = 1$, $a_2 = 1$, $b_1 = 0.5$ and $b_2 = 0.5$. Taking into consideration the emulsion composition, $\sigma = 28.0$ mb and $\sigma^a = 15.8$ mb for model I, for model II P=0.55 and $\sigma = 40.0$ mb the following relations were obtained.

$$\langle n_g \rangle_I = 0.0360\ \sigma_o' + 1.0251 \qquad (1)$$

$$\langle \nu \rangle = 0.0485\ \sigma_o' \qquad (2)$$

$$\langle n_g \rangle_{II} = 0.0369\ \sigma_o' + 0.9929 \qquad (3)$$

Moreover taking into consideration the additive quark model, he expected that one can distinguish from $\langle n_g \rangle$, whether the quark (u or c) produced in neutrino-nucleus collisions propagates singly inside the nucleus or in a state of meson. If the observed mean number $\langle n_g \rangle_c$ of grey particles per event with a charmed meson is about 1.0, the LPS is to be composed only of c quark. It propagates singly through the nucleus and then recombines into a meson. If the value

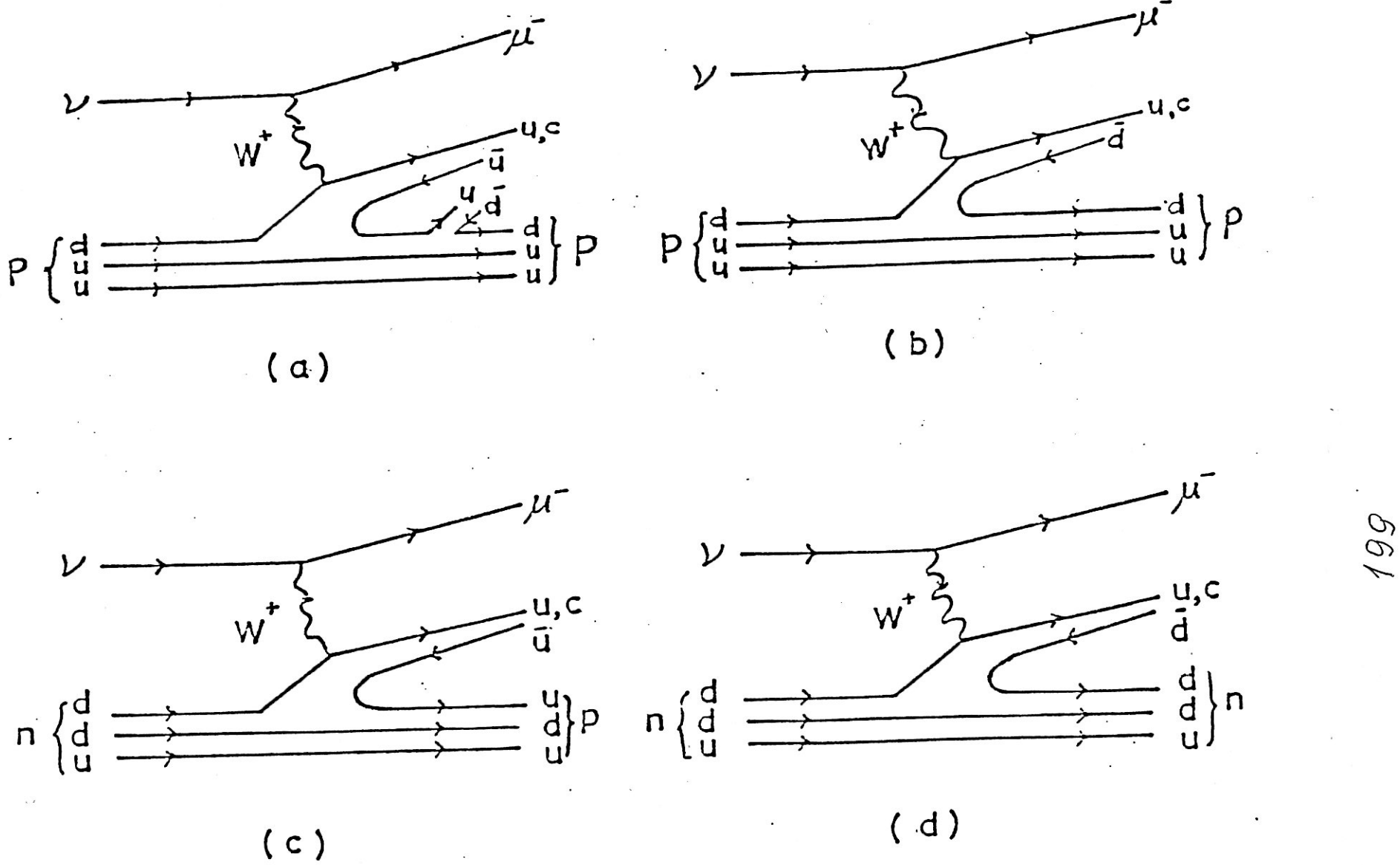

FIG. 9. Possible diagrams in the charged current neutrino - nucleon interactions.

of $\langle n_g \rangle_c$ is about 1.5 the c quark recombines into a meson at the instant of its production and propagates inside the nucleus in a state of a meson. As for the mean number $\langle n_g \rangle_o$ of grey particles per event without charm, the u quark propagates singly through the nucleus if the observed value of $\langle n_g \rangle$ is about 1.5. If the value of $\langle n_g \rangle_o$ is about 2.0, the u quark is to propagate inside the nucleus $\langle n_g \rangle_o$ is about 2.0, the u quark is to propagate inside in a state of meson.

To compare the present experimental data with the theoretical calculations of /3/, the $\langle n_g \rangle$ vlaues for "charm" and "non-charm" events, presented in table 1, were substituted in equations 1-3. The obtained values of leading particle system cross-section are tabulated in Table 5. The comparison of the experimental n_g-distributions with the predictions of model I and II, is given in fig. 10. (a,b) respectively. The analysis of Table 5 and fig. 10 shows that the cascading calculations of /3/ can not reproduce the experimental values. In the n_g-distributions the experimental points are scattered all over the set of given curves and no preferable value of σ_o' could be chosen. Moreover, there is no difference between the experimental values of $\langle n_g \rangle_c$ and $\langle n_g \rangle_o$ as predicted by the theoretical calculations. The experimental results are inconsistent with the theoretical calculations of /3/.

III.1.7. Conclusions. (i) In the charged curent interaction of neutrino with emulsion, the average numbers of grey and black track particles are nearly independent of the incident neutrino energy. The average multiplicity of showers increases slowly with energy. This indicates that the average number of intranuclear collisions is very small.

(ii) The average multiplicity of shower track particles associated with charm production is less by about unity than that with non-charm events and the n_s-distribution for charm events exihibit a statistically significant peak at $n_s=1$. These phenomena are explained by the fact that

Table (5). The values of cross section of leading particle system (LPS), σ_o , and the number of intranuclear collisions, $\langle \nu \rangle$, obtained substituting experimental <ng> in equations (1)-(3)

Class of events	Model No.	σ_o (mb)	$\langle \nu \rangle$
non-charm	I	9.0 ± 3.6	0.4 ± 0.2
	II	9.7 ± 3.5	0.5 ± 0.2
Charm	I	7.9 ± 5.8	0.4 ± 0.3
	II	8.6 ± 5.7	0.4 ± 0.3

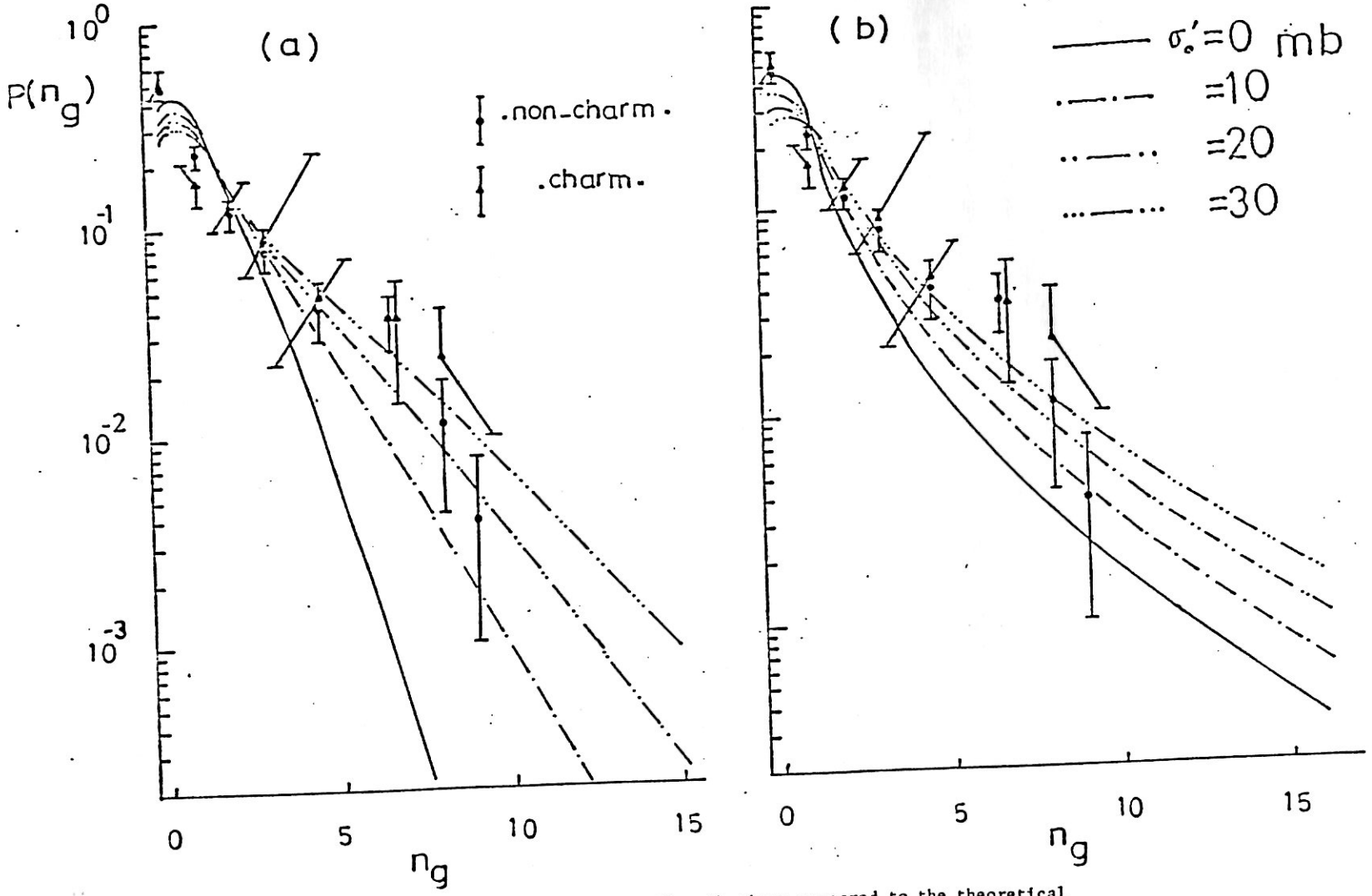

FiG. 10. The experimental n_g - distributions compared to the theoretical calculations of /3/,(a) for model I and (b) for model II . σ_0' is the cross - section of interaction of leading particle system inside the nucleus.

charmed particles are heavy and they are usually produced with a relatively high momenta. Thus the remaining energy for production is limited. The N_h, n_g and n_b-distributions as well as their average values for charm and non-charm events are completely consistent. This means that there is no measurable difference between a leading charmed or non-charmed particle.

(iii) Comparing the n_g-distributions for ν-Em and P-Em interactions, the ratio of events with $n_g = 0$ is 0.5 ± 0.1 and 0.27 ± 0.02 respectively. These two data are consistent with simple quark counting taking emulsion composition into consideration and neglecting cascading in ν-Em interactions.

(iv) Comparing the correlations between multiplicities of different particles the following conclusions could be drawn out: (a) in non-charm events, the energy transfered to the target nucleus, measured by(N_h), is higher than in the case of "charm" events at low n_s but the increase in it is much slower than "charm" events. (b) the degree of cascading, measured by (n_g), in ν-Em interactions is less than in P-Em ones. (c) the number of recoiling nucleons in the hit nucleus determines the average excitation energy of the target nucleus and this excitation is independent of the number and nature of produced particles.

(v) The angular distribution of grey track particles, emitted in charm and non-charm events, is the same and it is peaked in the forward direction as in case of hadron-emulsion interactions. It follows a formula $\frac{1}{N_{tot}} \frac{dn}{d\cos\theta_g} \simeq \exp (0.83 \pm 0.13) \cos \theta_g$. The average emission angle of grey track particles systematically decreases with energy. These observations indicate that grey track particles are knock on nucleons.

Black track particles, for charm, non-charm and P-Em events, are emitted isotropically from a slowly moving statistically equilibrium system.

(vi) The energy distribution of grey track particles, in ν Em interactions, is similar to that from hadron-nucleus collisions and it has a shape of the form $N(E)dE \simeq E^{-\gamma} dE$ where $\gamma = -1.15 \pm 0.18$.

(vii) The theoretical calculations based on the cascade model can not reproduce the experimental n_g-distribution in ν-Em interactions. The values of cross-section of leading particle system, for charm and non-charm events, obtained by substituting the experimental $\langle n_g \rangle$ in the theoretical calculations give a contradictory, result about the nature of this leading particle system.

Part 2

III.2. Neutrino charged current interactions with emulsion and an estimate of hadron formation time:

III.2.1. Introduction: In the absence of a reliable calculation scheme, phenomenological models have been built in order to incorporate the ideas of quantum chromodynamics (QCD) as far as possible. In QCD one finds a situation which formally resembles many aspects of cosmic ray electron-photon cascades. Since at the present time it is not possible to calculate accurately the space time characteristics according to "first principles" the parton evolution in QCD can be regarded as a cascading process in the leading log approximation/23/. In practice, the results of phenomenological models are usually used in multiparticle production processes.

In the present work, the experimental data obtained of charged current interactions of ν_μ with emulsion (Em) have been analysed using the version of the intranuclear cascade model (ICM)/4-6/. A trial was made to estimate quantitatively the value of the formation time (sometimes

called "formation zone"). The concept of a formation zone was considered by Landau and Pomeranchuk Goldhaber/25/ and Kikolaev/26/.

III.2. The intranuclear cascade model. In the ICM, the interactions of high-energy particles with nuclei are described in the following way. The incident primary particle interacts with a nucleon of the target nucleus. The particles, generated in these interactions, move inside the nucleus and scatter on separate nucleons. The process of generation of particles is simulated by the Monte Carlo (MC) method.

The cross section (CS) of the intranuclear cascade (IC) and the characteristics of secondary particles (multiplicities, angular and momentum distributions) at different energies are taken from experiments with free nucleon/4/. Elastic and inelastic interactions, charge exchange and absorption of slow pions, inside the nucleus, are taken into account. Nuclear effects such as Fermi motion and the Pauli principle are all taken into consideration as before/4/.

Since the interaction cross section of neutrino with nucleon is small, we assume that a neutrino can interact with any nucleon of the nucleus with equal probability, i.e.

$$\sigma(\nu + A) = \sum_{i=1}^{A} \sigma_i (\nu + N)$$

where $\sigma_i (\nu + N)$ is the interaction CS of a nuetrino with a separate nucleon. Following from experiments and from the quark parton model, we take into account that the interaction CS of neutrino with a neutron is twice that with a proton, i.e. $\sigma(\nu + n)/\sigma(\nu + p) = 2$.

The Fermi gas model of the nucleus is utilised. The nuclear density is taken from the Woods-Saxon expression.

$$\rho(r) = 1/(1 + e^{(r-c)/\alpha})$$

α = 0.54 fm and c = $1.19A^{1/3}-1.61A^{-1/3}$ fm. In practical calculations, the nucleus is divided into three zones. The nuclear density in each zone is supposed to be constant. It is calculated according to the Woods-Saxon expression, where r is the distance from the middle point of the zone to the centre of the nucleus. Moreover, three-dimensional geometry is used in our calculations.

According to emulsion composition, a nucleus (of mass number A) with which the neutrino would interact is drawn randomly. Then, knowing the density of nucleons in the spherical zones, we can place A nucleons inside the nucleus in a random way. For each simulation of A nucleons, we fix the coordinates of the centres of the intranuclear nucleons throughout the process of developing the IC. The characteristics of charged particles, produced in the first ν N interaction inside the nucleus, are taken from experimental data/4/. These data were obtained from reactions induced by the same neutrino beam used in the present work. The multiplicities of neutral particles (pions) are taken to be equal to the corresponding ones from the previous experiment/4/. These multiplicities are

$$\langle n_{\pi^0} \rangle = 0.72 + 0.22 n_{\pi^-} \quad \text{for } \nu n$$

and

$$\langle n_{\pi^0} \rangle = 0.14 + 0.73 n_{\pi^-} \quad \text{for } \nu p \text{ interactions,}$$

where, n_{π^-} is the multiplicity of negatively charged particles. The angular and momentum distributions of neutral particles are assumed to be the same as those of positively and negatively charged particles.

The calculations were carried out almost with the same program and assumptions of our previous work/4/. The space-time characteristics of particles produced in lepton-nucleon (LN) interactions inside the target nucleus were taken into consideration. After time τ from the LN intranuclear collision the interaction CS of a produced secondary particle with a nucleon inside the nucleus is given by

$$\sigma_{hN} = \sigma^{exp}_{hN} (1 - e^{-\tau/\tau_0}) \qquad (4)$$

where σ_{hN}^{exp} is the experimentally determined total interaction CS of a hadron with a free nucleon at the corresponding energy of the secondary particle produced. Thus, only after a relatively long time does the CS reach the value of σ_{hN}^{exp}. In equaiton (4), the parameter τ_o is a constant equal to $1/m_o$, where m_o is a certain characteristic mass corresponding to the formation time of the secondary generated hadron in its rest frame of reference. The time is equal to $L/\beta\gamma c$ where L is the secondary particle range inside the nucleus (the distance traversed by the secondary particle of velocity β (=v/c) from its generation point to the point of interaction with a nuclear nucleon). The Lorentz factor of the generated secondary particle is $\gamma = (1-\beta^2)^{-1/2}$. Equation (1) can be rewritten in the form

$$\sigma_{hN} = \sigma_{hN}^{exp} (1-e^{-moL/\beta\gamma c}). \qquad (5)$$

It is to be noted that when $m_o \to \infty$, this model will reduce to the old ICM in which secondary hadrons are produced instantly in the intranuclear interactions. In the present model, at a finite value of m_o, secondary particles (e.g. pions) are not formed instantly but after a certain time. According to equaiton (5), the CS of the IC is calculated as a function of the formation length L and the velocity . From (5), it is seen that slow secondary particles interact. inside the target nucleus more frequently than fast ones. The most rapid secondary particles may fly out without interacting with the nucleons inside the target nucleus.

III.2.3. <u>Results and discussion</u>. The average multiplicities of shower and grey particles, produced in the present experiment, compared with the corresponding quantities which were calculated according to the modified ICM at four values of $m_o = \infty$, 0.94 0.4 and 0.2 GeV are represented in table 6. One can see from this table that the

Table (6): The average multiplicities of s and g particles in ν_μ + Em interactions obtained in the present experiment compared with the corresponding values calculated according to modified ICM.

Present experimental data	Calculations of the modified ICM			
	$m_o = \infty$	$m_o = 0.94$	$m_o = 0.40$	$m_o = 0.2$
$\langle n_s \rangle$ 5.28±0.26	6.45±0.06	5.60±0.04	5.12±0.03	4.08±0.02
$\langle n_g \rangle$ 1.33±0.15	2.08±0.03	1.71±0.02	1.35±0.02	0.82±0.01

experimental and calculated data at m_o = 0.4 GeV are in good agreement. This indicates the existence of a finite formation time for the secondary hadrons produced in the intranuclear interactions. Eliseev et al pointed out/4,5/ that the formation time may differ for particles of different quark structure. El-Naghy/2,4/ showed that the formation time is different for the produced secondary charmed and uncharmed mesons. The agreement between the experiment and theoretical model, observed in the table is reproduced in figures 11 and 12. These figures present the n_s- and n_g -distributions, respectively. The curves are due to theoretical calculations. The points are the experimental data of the present ν_μ Em interactions. All distributions in figures 11 and 12 are normalised to unity.

The model predicts not only the multiplicity distributions but also angular distributions. Figure 13 shows the angular distribution of grey particles. The points are the experimental data while the histogram is the model calculation at m_o = 0.4 GeV. The agreement between the experiment and simulated data is also confirmed from figure 13

III.2.4. Conclusion. The present analysis shows that the experimental data of ν_μ Em interactions are reproduced by ICM which includes finite formation time of secondary hadrons produced inside the target nucleus.

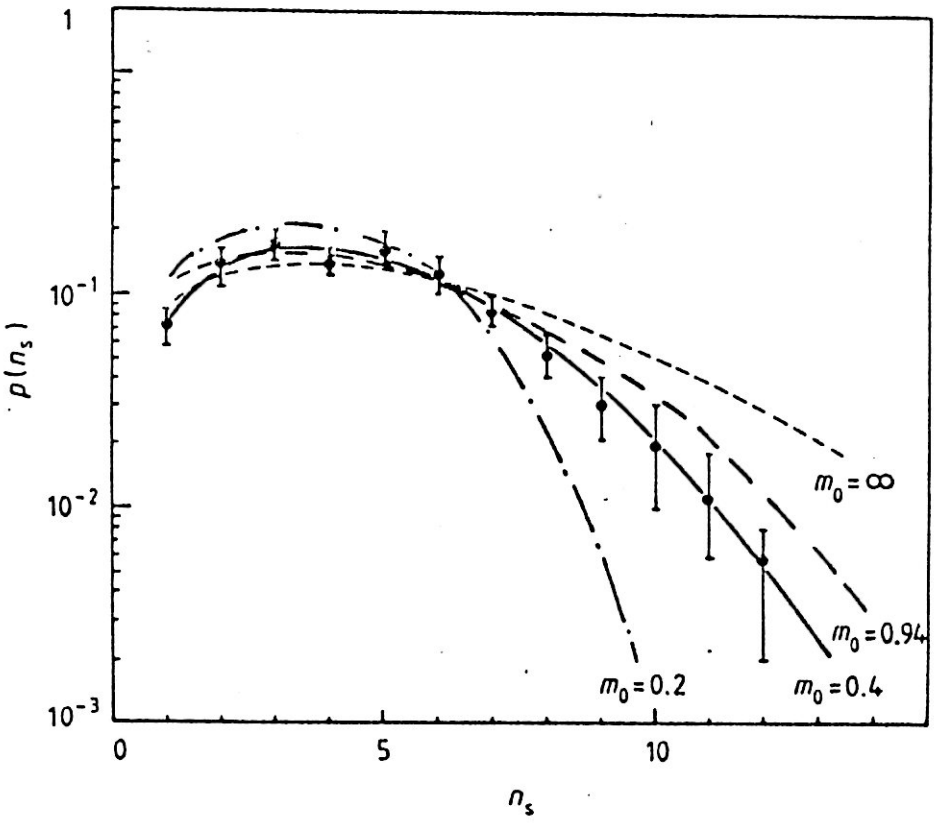

Figure 11. The n_s distribution in ν_μ + em interactions, the curves are due to the modifi
ICM.

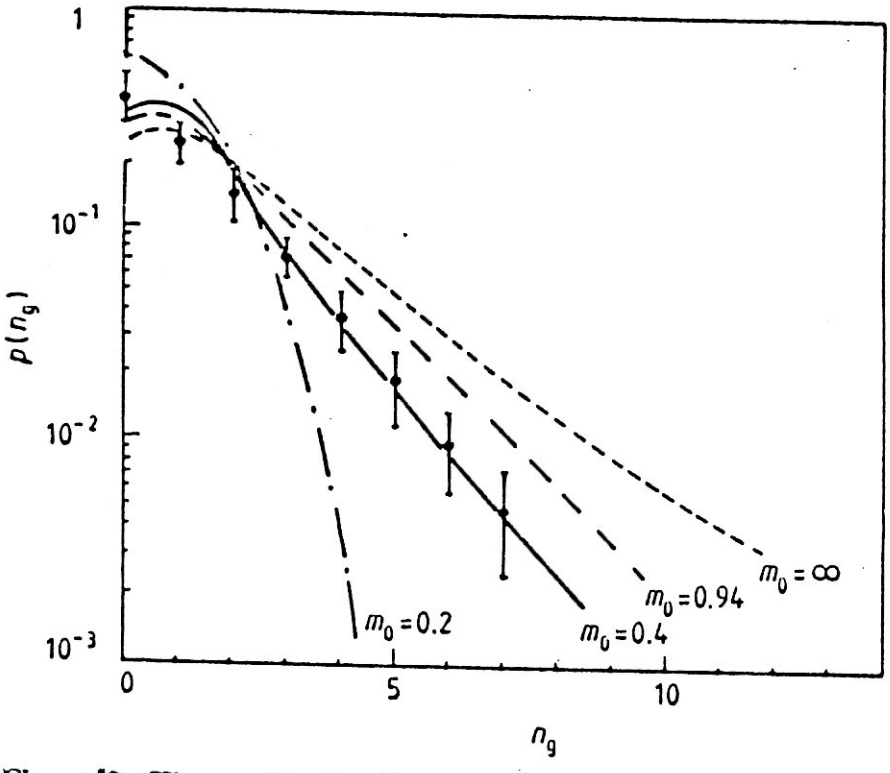

Figure 12. The n_g distribution.

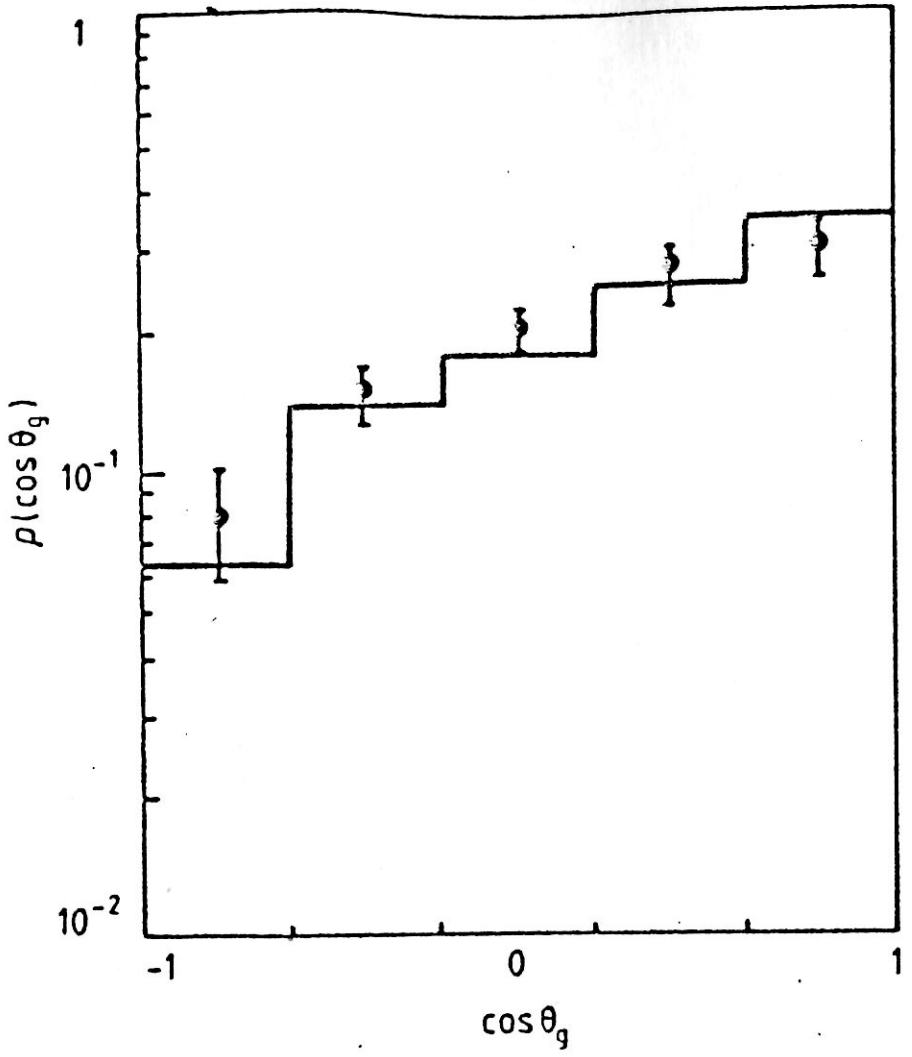

Figure 13. The angular distribution of g particles emitted in ν_μ + em interactions.

Iga and co-workers/27/noted the importance of introducing the concept of a formation zone in the ICM. Their characteristic values of formation zone are the formation length ℓ_f (=1 fm) and the parameter $m_o = \hbar c/\ell_f$ (0.2 GeV). These values agree, in order of magnitude, with our values m_o = 0.4 GeV ($\ell_f = \hbar c/m_o$=0.5 fm).

However, it is seen/27/ that the value of formation length is slightly larger. This may be due to the method of calculation for the leading particle effect. In our ν-Em interactions the leading particle is a muon which flys from the nucleus without interaction. In the case of hA interactions/27/, the leading particle is a hadron which carries an average of 50% of the primary energy. This hadron may colide further with nucleons of the target nucleus and may give an additional contribution in the nuclear reaction.

For a more accurate determination of the formation zone and for investigating the possible differrences in the mechanisms of LA and hA interactions, it is necessary and worthwhile to carry out further experiments using pure targets in LA interactions.

References

1. Suzuki N Prog. Theor. Phys. 1982, 67, 571.
2. Suzuki N Nucl. Phys. 1983, A403, 553.
3. Suzuki N Nucl. Phys. 1984, A414, 365.
4. Eliseev S M et al., Sov.J.Nucl. Phys.1984 40, 944 (In Russian).
5. Eliseev S M et al., Rapid Comm. of JINR(Dubna) 1988,6[32] (In Russian), P.11.
6. El-Naghy A. et al. J. Phys. G. 1990, 16, 39.
7. Berge JUP et al 1978 Phys. D 18 3905.
8. Bell J et al 1979 Phys. Rev. D 19 1.
9- Allen P et al 1981 Nucl. Phys. B 181 385.
10. Derrick M et al 1981 Phys. Rev. D 24 1071.
11- Barlag S et al 1982 Z. Phys. C 11 283.
12. Derrick M et al 1982 Phys. D 25 624.
13. Deden H et al 1982 Nucl. Phys. B 198 365.

14. Zieminsk D et al 1983 Phys. Rev. D 27 47.
15. Grassler H et al 1983 Nucl. Phys. B 223 269.
16. Baranov D S et al 1984 Z. Phys. C 21 189.
17. Ushida N et al 1984 Nucl. Inst. 224 50.
18. Ushida N et al. Phys. Lett. 1983, 121B, 287.
19. Ushida N et al. Phys. Lett. 1983, 121B, 292.
20. El-Naghy A 19th ICRC San Diego, USA, 1985, Vol.8,p.164.
21. El-Naghy A 20th ICRC Noscow, USSR, 1987, Vol.6, p. 313.
22. Winzler H Nucl. Phys. 1973, B56, 333.
23. Marchesini G, Trentadue L and Veneziano G 1981 Nucl. Phys. B 181 335.
24. Landau L and Pomeranchuk I 1953 Dok. Acad. Nauk SSSR 92 535.
25. Goldhaber A S 1975 Phys. Rev. Lett. 35 748.
26. Nikolaev N N1981 Sov. J. Part. 12 63.
27. Iga Y et al 1988 Z. Phys. C 38 557.

DISCUSSIONS

The study of hadron nucleon, hadron-nucleus. and nucleus--nucleus interactions have shown that the multiplicity characteristics and their regularities indicate the validity of the superposition models. The hadron nucleus and nucleus-nucleus interactions are considered as strings of hadron-nucleon collisions.

The insight of the dependence of the average multiplicity on the energy of centre-of-mass of nucleon-nucleon collisions, led to the following formula:

$$\langle n_{ch} \rangle = a + b \ln s + c \ln^2 s$$

The results of measuring the interaction mean free path and/or cross section in hadron-nucleus and nucleus-nucleus collisions show that the interaction cross-section of nuclei are essentially independent of the incident energy in the few GeV region. The interaction cross-section of nuclei are successfully explained by the geometrical cross-section including an overlapping parameter. This parameter depends on the size of the interacting nuclei.

From the angular distributions, one could naively expect that the pions produced with rapidities less than the beam rapidity could impose a difference when they travel through the target matter. Assuming the validity of the string picture one could explain why this is not the case: this is due to a finite formation time τ_o, fast particles are formed at

$$\tau = \tau_o \cosh(Y_{lab})$$

which exceeds the radius of the target for $Y_{lab} > 2$. The faster particles are thus produced outside of the target nucleus i.e. they can not rescatter.

From the above arguments, one may conclude that the energy

dependence of the target fragmentation gives experimental evidence that particles are not instanteously formed in a collision but, they require some "formation" time until they exist and can reinteract.

The analysis of ν_μ -emulsion interactions have shown that secondary particles inside the nucleus will have a cross-section

where τ_o is the formation time, which corresponds to a length about one fermi.

Thus, the whole data of hadron-nucleon, hadron-nucleus, and nucleus-nucleus, and neutrino-nucleus interactions have shown that particles are not produced instanteously inside thae nucleus but require some "formation" time untill they exist and can then reinteract.

In section (I.6.), from the study of the dependence of the associated multiplicities on the longitudinal rapidity of the given inclusive $\pi^{\pm}$ meson. Considerable correlation is indicated, different for the two regions ΔY (the rapidity interval between the two inclusive particles) < 1.2 and $\Delta Y > 1.2$ but qualitatively identical for $\pi^- N$ and $\pi^- A$ collisions.

From the study of analogous dependences in PP collisions it is known that there are strong constraints due to the conservation of longitudinal momentum and energy. In hA collisions these constrains can be strongly "suppressed" by a cascade mechanism of multiplication. The deep analysis of the dependence of $\langle n_{\pi^\pm} \rangle$ on the rapidity scale is of the same order as in an elementary act. This means that expected effects of multiplica-

tion by the cascade mechanism were not observed. This is another proof for the previous argument that fast particles may be produced outside the target nucleus. However, the slight increase in the multiplicity of shower particles in $\pi^- A$ relative to $\pi^- N$ shows that that target nucleus is not simply a spectator of the multiple production process. This is the subject of the next part of the discussions.

In section II.11, the study dealt with the flow of nuclear matter. It was found that the struck nucleus receives a transverse momentum as a whole. This fact was displayed in the angular distributions of projectile and target fragments, this is called "bounce-off" of projectile fragments and "side splash" of target ones. The determination of the reaction plane had proven to be a powerful tool for studying the collective effects such as the "bounce off" and the "squeeze out" of nucleons. The dependence of sideward effect on the impact parameter was studied and it was shown that the effect decreases with the decrease of the impact parameter while the flow angle increases. It was found that the average energy of slow target particles increases in the direction of "side-splash" which indicates the increase in the transverse momentum transfer during the collision process. The comparison with the cascade evaporation model (CEM) had shown the relative contribution of CEM to the sideward flow of nuclear matter. This enables one to assume that the sideward flow, in its general features. can be described as superposition of two mechanisms: momentum transfer to the struck nucleus as a whole and development of intra-nuclear cascade.

Fragmentation is one of the historical and fundamental ques-

tions in nuclear physics. Recently, the multifragmentation process acquired great attention. Many theoretical models have been devoted to the study of the multifragmentation process. In some models, the prefragment nucleus heats up and then condensates into droplets. In others, it simply evaporates the fragments sequentially. In certain models, the fragments are statistically emitted from an intermediate excited nuclear system. Other statistical approaches try to explain the multifragmentation without any reference to thermal equilibrium i.e. as shattering of the prefragment nucleus into many pieces. The correlation study carried out in section II.10. had excluded the models assuming one hot source at a certain excitation energy. The yield curve is a superposition of different mechanisms depending on the impact parameter of the collision.

In the neutrino induced reactions on nuclei, a quark hit by a virtual photon or a weak boson propagates inside the nucleus either singly or after immediate recombination into a meson. The quark or the meson, in this case, is called (conditionally) leading particle system (LPS) which may interact further with a nucleon inside the target nucleus with an effective cross section σ'. The value of σ' may depend on whether the LPS is composed only of a single quark or a meson. Moreover, it may depend on whether it is u quark, c quark, charmed meson or non-charmed meson. In each of these cases, the value of σ' is expected to be reflected in grey particle (most of them are recoil nucleons) multiplicity distribution and its average value, observed in the final state.

The analysis of the data cannot reveal the difference bet-

ween the values of the effective cross-section σ' for charmed and non-charmed mesons. Moreover the cascade calculations without the consideration of formation time could not reproduce the experimental distributions.

Another variant of the cascade model, assuming that the effective c.s. inside the nucleus changes with time according to the relation

$$\sigma_0' = \sigma_0 (1 - e^{-\tau/\tau_0}) \quad ,$$

reproduces the experimental distribution with a formation length ≈ 1 fm.

CONCLUSIONS

1. The average multiplicity of shower particles increases with the incident hadron energy. In nucleon-nucleon collisions, in a wide interval of energy, the dependence of the average multiplicity of shower particles $\langle n_{ch} \rangle$ on energy s, in the centre of mass system, agrees with the multiperipheral model and KNO scaling.

2. The average multiplicity, $\langle n_s \rangle$, in hadron-nucleus interactions follows the KNO scaling, and the experimental points lie on a universal curve fitted by the formula

$$\psi(z \equiv n_s/\langle n_s \rangle) = (3{\cdot}42z + 14{\cdot}34z^3 - 1{\cdot}06z^5 + 0{\cdot}09z^7) \exp(-3{\cdot}28z)$$

3. The normalized multiplicity $R = \langle n_s \rangle / \langle n_{ch} \rangle$, agrees with predictions of energy flux cascade model (EFCM) which gives the relation $R = \frac{2}{3} + \frac{1}{3}\langle \nu \rangle$ where $\langle \nu \rangle$ is the average number

of collisions of primary particle with nucleons inside the nucleas.

4. The asymmetry in the forward direction decreases with the increase of the multiplicity of hadron-nucleon interactions.

5. Studying the hammer-tracks in proton emulsion interactions at 69 GeV/c, the production ratio of ^{8}Li fragments was found to be 1.2%. The anisotropy in emission of ^{8}Li fragments is stronger than in angular distributions of slow fragments (b-particles) and cannot be explained by the motion of residual nucleus.

6. Studying the energy and angular characteristics of secondary charged particles from interactions of 50 GeV π^- mesons with emulsion one can observe the well-known effect of leading particle which is characteristic for hadron-nucleon collisions. The number of π^- mesons is greater than that of π^+ in the region of large rapidity.

7. The $P_\perp$ distribution of pions shows the validity of models of hadron-nucleus collisions where the production mechanism resembles an elementary act. The effects of multiplication by a cascade mechanism was not clearly observed. However, the slight increase in the multiplicity of shower particles in π^-A relative to π^-N shows that the target nucleus is not simply a spectator of the multiple production process.

9. The interaction cross-section of nuclei are essentially independent of the incident energy in the few GeV region.

10. The systematic study of the multiplicity characteristics and their regularities had proved the validity of the incoherent superposition models. This means that the nucleus-nucleus and nucleon-nucleus interactions are generally superposition of nucleon -nucleon- interactions.

11. From the study of complete destruction of Ag(Br) and Pb nuclei one may conclude that:

(a) The probablity of complete destruction is nearly independent of the incident energy and it increases linearly with A_B^{213} up to $A_B = 12$ where it becomes constant. Where A_B is the mass number of the beam nucleus.

(b) The $\langle n_s \rangle$ is proportional to A_B and A_T by the relation $\langle n_s \rangle \sim A_B^{0.63} \cdot A_T^{0.36}$ in case of proton-nucleus $\langle n_s \rangle \sim A_T^{0.11}$.

(c) The $\langle n_s \rangle$ is proportional to the number of interacting nucleons R_A from both nuclei by the relation
$\langle n_s \rangle = (2.45 \pm 0.22)\, R_A^{(0.78 \pm 0.07)}$.

(d) A simple model was put to explain the $\langle n_s \rangle$ values obtained in these events. It was found that $\langle n_s \rangle$ is proportional to the free energy in the C.M.S. of the interacting particles by the relation

$$\langle n_s \rangle = (-1.97 \pm 0.01) + (1.07 \pm 0.01) \ln E_f + (1.79 \pm 0.19) \ln^2 E_f$$

(e) The value of $\langle n_g \rangle$ follows the relation

$$\langle n_g \rangle = \text{const} \cdot A_B^{0.14 \pm 0.01},$$
$$\langle n_g \rangle = \text{const} \cdot R_A^{0.17 \pm 0.04}$$

in case of proton-nucleus $\langle n_g \rangle \sim A_T^{0.62}$.

12. The study of fragmentation of ^{22}Ne, ^{24}Mg and ^{28}Si in emulsion at (4.1 - 4.5) A GeV/c lead to the conclusion that, the inclusive charge distribution of fragments is a superposition of different mechanisms, depending on whether the process is "gentle" or "violent" collision. The study had shown that mechanisms claiming one hot source at certain excitation energy can not explain

the experimental yield distribution. The presented cascade-evaporation model does not describe the charge distribution of fragments.

13. The study of sideward flow of nuclear matter in nucleus--emulsion collisions at (4.1 - 4.5)A GeV/c have shown that:

(a) The bounce-off of projectile fragments and the side-splash of target fragments were observed by investigating their projections on the reaction plane and by other methods also.

(b) It is the first time, to attract the attention of scientific community to the importance of reaction plane determination for studying different aspects of AA interactions.

(c) The data obtained on sideward flow in the azimuthal plane reflect the relative contribution of the intranuclear cascade in the formation of the sideward flow. The relative increase of the ranges of slow target fragments emitted in the direction of the side splash can give evidence for the transverse momentum transferred to the target nucleus.

The sideward flow, in its general features, can be viewed as the superposition of two mechanisms: The transfer of momentum to the residual nuclei and the development of the intranuclear cascade.

14. The ring-like events were observed in interactions of Ne^{22} and Si^{28} with Ag(Br) emulsion nuclei. These events were interpreted as ones due to gluon emission by deconfined quarks. The formation length was determined and found to be $\simeq$ 1 fm. The probability of this phenomena is about 1% of total inelastic events.

15. The study of $\nu_\mu E_m$ interactions had shown no difference in the general characteristics of events associated with charmed particles production and those without. The Dubna cascade model

which includes finite formation time can reproduce the experimental data of multiplicity and angular characteristics of secondary charged particles. According to this calculation the formation length was estimated to be about 1 fm.

ACKNOWLEDGEMENT

The author of the disseration would like to express his gratitude to the authority of: Joint Institute for Nuclear Research (JINR), Cairo University, Japan Society for promotion of science (JSPS), International Center for theoretical physics (ICTP), National Institute of Nuclear physics in Italy (INFN), University of Califormia in San Diego (UC), for their valuable support to carry his research works.

The author would like to thank Academic A.M.Baldin for his interest in the work and his encouragement to him. The author thanks very much the members of emulsion collaboration especially, from LHE of JINR: prof. K.D.Tolstov, dr. B.P.Bannik, dr. G.S.Shabratova and S.A.Krasnov. The author appreciates the Collaboration he had with drs. S.M.Eliseev and V.D.Toneev. The author expresses his gratitude to his colleagues in Cairo University: drs. M.T.Ghoniem, M.T.Hussein, N.M.Sadek, N.N.Abdel-Allah, S.El-Sharkaway, A.Abd El-Daiem, M.Mohery and K.S.Abd El-Khalek.

The author is grateful to the staff of chemical group of LHE of JINR, the scanning and measuring team of the emulsion group of LHE of JINR, the staff of Dubna synchrophasotron and the staff of Fermilab accelerator.

The author thanks the directorate of JINR for giving him the possibility to work for a long period in LHE and thanks to international department staff who helped him in living and staying at Dubna.